Development of an Explosive Energy Distribution Optimization System

to accommodate drilling errors by adjusting blasthole charges

S. Klerkx

European Mining Course
Faculty of Civil Engineering and Geosciences
Delft University of Technology

Cover image courtesy of BHP.

Development of an Explosive Energy Distribution Optimization System

to accommodate drilling errors by adjusting blasthole charges

by

S. Klerkx

to obtain the degree of Master of Science at

Delft University of Technology
RWTH Aachen
Aalto University

to be defended publicly on March 23, 16:00 CET

Student number:	4369084	
Project duration:	March 1, 2020 – March 23, 2021	
Thesis committee:	Dr. M. Soleymani Shishvan,	TU Delft
	Dr. J. Sattarvand,	University of Nevada, Reno
	Ir. M. Keersemaker,	TU Delft
	Univ.-Prof. Dr. B. Lottermoser,	RWTH Aachen
	Dr. M. Rinne,	Aalto University

An electronic version of this thesis is available at http://repository.tudelft.nl/.

TU Delft

Acknowledgments

First of all, I would like to thank Masoud Soleymani Shishvan and Javad Sattarvand for giving me the opportunity to work on this project and for being of great help throughout this period. In the process of writing this thesis, I have gained a lot of knowledge about blasting and optimization and was able to improve my programming skills in Python. Thank you for your guidance and advice during the many meetings we had, which provided valuable input for solving the problems I encountered. Because the project quickly turned out to be more complex than expected, this led to interesting discussions about my experimental ideas that I will remember for a while. I would also like to thank Sam Berents, with whom I could brainstorm about these ideas sometimes. He helped me a lot by running a large share of the optimization scripts on his more powerful computer once mine could no longer handle it. Lastly, I want to thank my family and friends for always supporting me. At times when I felt a bit frustrated with my progress or other challenges, they offered the understanding and encouragement I needed to complete this work.

The author appreciates the US Center for Disease Control and Prevention (CDC) and the National Institute for Occupational Health and Safety (NIOSH) for supporting this research under the project contract number 75D30119C06044 with the title "Capacity Building in Artificially Intelligent Mining Systems (AIMS) for Safer and Healthier Automated Operations". Any opinions, findings, and conclusions, or recommendations expressed in this manuscript are those of the authors and do not necessarily reflect the views of the Center for Disease Control and Prevention and the National Institute for Occupational Health and Safety.

Sean Klerkx

Abstract

Open-pit mining blast patterns are designed to safely break rock mass at desired boundaries and to produce uniformly sized fragments that lead to the optimal performance of subsequent mining operations. An issue that is often overlooked, however, is the deviation of drillhole locations with respect to their coordinates as designed in the blasting plan. This causes changes in the spatial distribution of explosive energy; some areas of the blast may receive a surplus of explosive energy, while others see a reduction. This results in less uniform fragmentation, producing more fines and increasing chances of oversized boulders, which reduces the efficiency of loading, hauling, and crushing operations. Additionally, deviated drillholes can lead to slope stability issues, flyrock, and uneven benches. To mitigate these problems, this study attempts to reduce differences in the explosive energy distribution (EED) through an optimization approach that adjusts the height of explosive columns in blastholes. A case study combines planned drillhole coordinates of two blast patterns with both simulated deviations and actual deviated drillhole locations. The corresponding benches are discretized into block models, for which the explosive energy distribution is calculated from the planned drillhole configuration as well as the deviated holes. The optimization objective is then to minimize block-to-block differences in explosive energy by making discrete adjustments to the height of individual column charges. Since mathematical programming is not possible due to the complexity of the evaluated formula, solutions are generated by metaheuristic algorithms. Among the Genetic Algorithm (GA) and Tabu Search (TS), the latter is preferred for its local search neighborhood that gives superior computation times. An inconvenience of the block-to-block comparison is the introduction of very large differences in explosive energy in blocks nearest to deviated blastholes, which cannot be accounted for by any charge adjustments except reductions in the deviated hole itself. Because optimization should focus on manageable differences in lower-valued blocks, these high-valued blocks are discarded by applying a cap based on data percentiles. Obtained results show that optimized charging adjustments vary with the chosen percentile, which makes it challenging to define comprehensive truly optimal solutions. A bias for charge reductions at high percentiles gradually shifts towards a bias for charge increases at lower values. Because a bias-induced imbalance in the total amount of explosives (compared to the original charging) is undesirable, the setting closest to equilibrium is selected, which is the use of only the lower 50% of data. In this configuration, optimization of the case study blast patterns results in improvements of the objective value of 0.53-1.54%, or 2.14-3.94% when only the blocks affected by the recommended charge adjustments are considered. The block-to-block comparison handles any interchangement of block values as unwanted differences, which should not always be the case. Therefore, the true improvements to the explosive energy distribution might be better expressed using an alternative optimization objective. Computation times could be further reduced by expanding on the developed algorithm, and combination with prior research would be helpful to include any GPS-related inaccuracies in the actual drillhole locations.

Contents

List of Figures

List of Tables

1 Introduction

Because of the high strength of most ore-bearing rock masses, explosive substances have long been the dominant means for rock-breakage in the mining industry. Records of rock blasting go as far back as 1627 when Caspar Weindl first demonstrated the use of gunpowder as a rock-breaking mechanism in an underground mine in Hungary. Hand-drilled holes were filled with gunpowder and closed tightly using wooden plugs, as a replacement for the superseding firesetting technique [1]. By the 1650s, this technique was known and applied in most of Europe, until the rise of dynamite 250 years later [2].

Although the underlying principles can easily be traced to present-day applications, blasting in mining has naturally undergone many changes over time. Over the years it has evolved into much more than just an effective rock-breaking mechanism. These days, simply breaking the rock mass is not sufficient; subsequent processes in the mining cycle strongly depend on the properties of blasted material, and therefore it is crucial to ensure that every blast satisfies these needs as best as possible. According to Braden Lusk, Vice President of DynoConsult, *"decades of work have been put into this mine-to-mill study and practice, but the real focus in a modern context is to optimize blasting parameters and product selection in real-time with large amounts of data input"* [3]. Adding to work performed on the project at the University of Nevada, Reno, this thesis will present exactly such an approach to further improve blast performances.

1.1. Background

Rock blasting represents an important step in the mining process, because at this stage, the bulk material properties that can influence performance in many of the following tasks are determined. Blasted material should allow for efficient loading and hauling, and provide a consistent throughput to crushers and grinders. The result of a good blast should be a rock pile in which ore is separated from waste material, characterized by good diggability, with favorable average fragment size and size distribution, and as few boulders as possible. While also considering environmental factors like airblast, flyrock, noise, and ground vibrations, blasts are designed to break the rock mass such that all subsequent operations can be performed at maximum efficiency. Because rock breaking gets more expensive at later stages, blasting fragmentation has a major influence on downstream size-reduction costs [4].

However, due to the large differences in rock mass properties, the breaking behavior of rocks is often difficult to predict. This makes it challenging to blast rocks according to the desired specifications. Preliminary blast design still relies on empirical relations from decades ago, and must then be tuned by trial-and-error because of the varying rock conditions at each mining site. Although this eventually results in a blueprint for blasts that produce satisfactory fragmentation, it does not necessarily mean that every blast is performed in an optimal manner simply because it works.

Besides the variation in rock mass properties, fragmentation can also be affected by issues related to the blast setup like unfavorable detonation delays, degraded explosives, or detonation failures. In order to better understand blast performance and ensure optimal fragmentation, it is important to reduce these sources of error to a minimum. The subject of this thesis is another such cause of suboptimal blast performance, namely the deviation of drillholes with respect to their planned locations. The problem at hand will be described in more detail in Section 1.2

1.2. Problem Statement

In the process of creating optimal blast designs, blasting engineers have a variety of information available to base their decisions on. The foundation consists of course out of the geological models obtained from exploration data, performance of previous blasts at the mine, and personal experience. Once the blast holes have been drilled, cuttings may be analyzed to make adjustments to the blasting plan. An issue that is generally overlooked, however, is that the exact drillhole locations often differ from their position in the designed blasting pattern. Although most modern drill rigs are equipped with accurate GPS devices to guide them to the appropriate drilling positions, in practice, many drillholes deviate with respect to their planned coordinates. These deviations can be related to a number of causes like poor drill set-up, GPS-related inaccuracies, or operator inexperience.

Because determination of the exact coordinates of drillholes by means of surveying is a time-consuming task that can not be easily incorporated in a tightly scheduled mining operation, these deviations are often neglected, and blasts may not perform as expected as a result of this. Despite these differences in the blast pattern, drillholes are generally charged with explosives according to the designed specifications. As a consequence, the explosive energy distribution throughout blasted benches will differ from the designed values and lead to reduced blast performance. Appropriate blast design should produce optimal fragmentation, but this is unlikely to be achieved when the drillhole locations in reality do not match the designed configuration. Thus, in order to improve blasting results, blasting engineers would benefit from information regarding drillhole deviations.

The detection of drillhole deviations is the topic of parallel research performed on this project, described by [5]. A specially programmed Unmanned Aerial Vehicle (UAV) is used to gather images of a drilled blast site, which is processed by photogrammetry software to create an orthomosaic map and Digital Elevation Model (DEM). These models are then subjected to machine learning algorithms to automatically identify the drillhole locations. However, the drillhole deviation data by itself would not be very practical for consideration by blasting engineers. Therefore, the current thesis will focus on providing an optimization solution that uses drillhole deviation data to adjust charges in the blast design, such that an optimal distribution of explosive energy can be achieved for the altered, ‘real’ drillhole configuration.

1.3. Hypothesis

Due to deviations in the location of drillholes with respect to their coordinates as planned originally, the explosive energy distribution in blasted benches is likewise altered. Since the explosive energy delivered to the rock mass decreases with distance to charges, cases of both higher and lower explosive energy contributions are expected, depending on the direction of deviation for nearby drillholes; holes that have been drilled more closely together than designed will cause a higher supplied explosive energy in between them, whereas explosive energy will be reduced in places where they are spaced further apart.

Because drillhole deviations are still more a rule than an exception in open-pit mine blasting, the energy distribution throughout a bench can differ significantly from the planned blast design. This may lead to suboptimal blast performance and poor fragmentation, which increases downstream costs. In order to improve the blasting efficiency and promote the effective use of costly explosives, the proposed optimization program will make adjustments in the charging of drillholes to account for these deviations. By reducing charges in closely spaced holes, and increasing them in those further separated, the charging plan will be altered such that the overall explosive energy distribution will better match the designed configuration. If the drillholes are charged according to this adjusted plan, the blasted material should be characterized by a more uniform and desirable particle size distribution that benefits the efficiency of downstream operations.

The optimization system will produce modified charging instructions that could reasonably be followed by charging personnel without resulting in major changes to drill and blast scheduling and typical charging practices. Most importantly, the level of detail in charge height is practically achievable. The program will be used to demonstrate its effectiveness on a limited amount of data but can be easily applied to new drillhole deviation datasets by adjusting a small number of control parameters.

1.4. Research Questions and Objectives

The aim of this thesis is to examine the often neglected issue of drillhole deviations in rock blasting, increase understanding of its causes and consequences, and provide a mitigating solution to improve blast performance. In order to achieve this, the following research questions must be answered:

1. What are the sources of error that lead to drillhole deviations, and how does this affect blast performance and thereby subsequent steps in the mining process?

2. Can horizontal deviation in drillhole locations be compensated by allowing an optimization program to modify the length of explosive charges?

Additional objectives for the suggested solution are:

1. Demonstrate that adjustment of charge length leads to more effective use of explosives.

2. Alteration of the charging plan must be practically achievable according to typical charging practices, without requiring significant changes to drill and blast operations.

3. High computational efficiency and practical runtime.

1.5. Scope

Although the envisioned solution should be widely applicable and could be relevant for many mines' blasting operations, in this thesis the emphasis is on demonstrating its potential value using a limited amount of testing data, originating from an open-pit mine in Nevada, USA. Therefore, special attention shall be paid to drilling and blasting practices in this locale, which may not be applicable elsewhere. For a better understanding of the implications, fundamental considerations in blast design will be reviewed, as well as the causes and consequences of drillhole deviations. The explosive energy distribution corresponding to the designed blast pattern is assumed to result in optimal fragmentation, and blast performance of the deviated drillholes is described solely based on (dis)similarity to these values.

This leaves the following topics out of scope:

- Data collection and image processing of drillhole deviations; has already been performed in preceding research on this project.
- Detailed assessment of blast performance or fragmentation
- The effect of differing rock mass characteristics or original blast design
- Test application with real blasts or simulations

1.6. Report Outline

Completing the introduction, this section will give an overview of what is to come in the rest of this thesis report. Chapter 2 consists of a literature review on blasting in open-pit mining, drillhole deviations, explosive energy distribution, two metaheuristic optimization methods, and specific blasting practices in Nevada. It will provide the reader with a good understanding of the subjects discussed in the following chapters, while also supporting the relevance of this work. A description of the approach to the problem can be found in Chapter 3, alongside identification of the control parameters to be determined and pseudocode of the written Python program. The available datasets for the case study are presented in Chapter 4, with a particular focus on the blast design. These site-specific conditions play an important role in development of the optimization system. A sequential experimental design is included to summarize how this data is used to obtain the required results. Using images and statistics generated from the optimization output, Chapter 5 will present the results. Emphasis is placed on comparison with the designed drillhole configuration and the situation before optimization, to demonstrate the improvements attributed to the optimization program. In Chapter 6, these results will be discussed in a broader context. Special attention will be paid to the evaluation of the results in relation to the research objectives, as well as the potential for improvement. Finally, Chapter 7 contains the conclusions that can be drawn from this thesis. Answers will be given to the research questions, together with recommendations for usage of the optimization system and future research on the topic.

2

Literature Review

This chapter will be a composition of the available literature relevant to the topic of this thesis. It will provide a background to matters discussed in later chapters, should improve understanding, and give some context for the relevancy of this research. First of all, the design considerations and common practices of open-pit blasting will be discussed in Section 2.1. Section 2.2 will elaborate on the problem statement by defining the causes and consequences of drillhole deviations, followed by the various methods that can be used to describe the explosive energy around blast holes in Section 2.3. In Section 2.4 the principles of Genetic Algorithms and Tabu Search will be reviewed. Section 2.5 gives an overview of the particular conditions in Nevada mines regarding blast design, and Section 2.6 completes the chapter with a synthesis of this literature review.

2.1. Blasting in Open-pit Mining

In most open-pit mining operations, blasting of the rock mass is required to break the rock into appropriately sized pieces. How exactly this is done will have an effect on the properties of the extracted material, which in turn has a strong influence on subsequent steps in the mining process. Therefore, blasting plays an important role in creating the circumstances necessary for an efficient mining operation. In this section, an overview is given of the typical considerations for blasting that should lead to optimal performance.

2.1.1. Blast Design

The first topic that will be addressed is blast geometry. The design parameters that will be referred to are indicated in Figure 2.1. Bench height (H) is largely determined in conjunction with overall pit design and equipment selection, which generally does not leave much room for variation once these decisions have been made. If rows of blast holes are aligned parallel to the longest dimension of the bench, the burden (B) is defined as the distance between the rows. The distance between holes in the other direction is then the spacing (S). Hole length (L) is often larger than bench height because holes are drilled below the toe elevation; the function of this so-called sub-drill (J) is to provide more explosive energy to the toe region. Because the rock here is highly constrained, this extra energy is necessary to ensure adequate fragmentation in this area of the bench [4].

The top part of the blasthole is generally not filled with explosives, but with stemming material like drill cuttings. This results in lower explosive energy in the top of the bench to prevent broken material from being thrown too far. Furthermore, the stemming (T) acts as a plug and helps to direct the explosive energy into the rock mass. In case different explosive energy is required along the length of the explosive column, it can be divided into segments containing explosives with varying strength, separated by stemming material or air. This technique is called decking, but will not be discussed here, as it goes beyond the scope of this thesis. The dimensional characteristics for blast design are not determined individually but should be considered in close relation to each other. For instance, the selection of hole diameter (D) will have implications for many of the other parameters. They can be linked by the expressions listed in Table 2.1, with common associated ratio constants K for initial design, and similarly, the ratios as determined by [6], which used a hole depth ratio K^*_H instead of bench heigh ratio K_H.

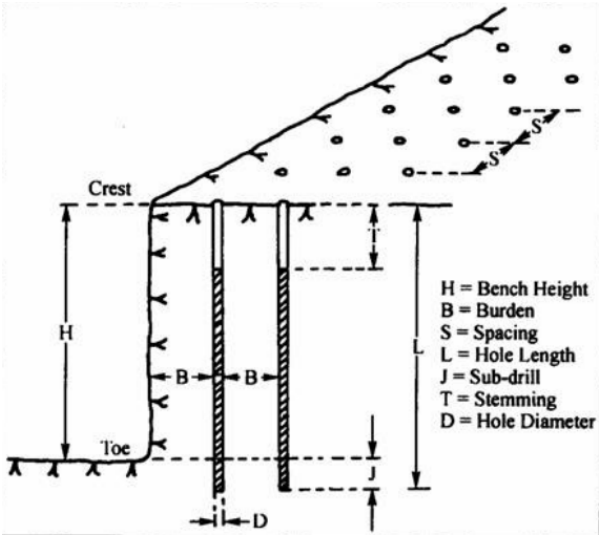

Figure 2.1: Blast geometry terminology [4].

Table 2.1: Ratios for initial blast design with associated K-values.

Ratio	**Common design constants [4]**	**Design constants suggested by [6]**
$S = K_s B$	$1.0 \geq K_S \geq 1.5$ Optimal for square pattern: $K_S = 1.0$ Optimal for staggered pattern: $K_S = 1.15$	$1.0 \geq K_S \geq 2.0$
$B = K_B D$	$K_B = 25\sqrt{\frac{\rho_{explosive} \times S_{ANFO}}{\rho_{ANFO}}}$ where S_{ANFO} is the explosive's weight strength relative to ANFO	Light explosives in dense rock: $K_B = 20$ Light explosives in average rock: $K_B = 25$ Heavy explosives in average rock: $K_B = 35$ Heavy explosives in light rock: $K_B = 40$
$J = K_J B$	Usually $K_J = 0.3$	Usually $K_J \geq 0.3$ For most conditions, never $K_J < 0.2$
$T = K_T B$	$K_T > 0.7$ Some suggest $K_T = 1.0$	$0.5\ K_T \geq 1.0$ (0.7 average)
$H = K_H B$	Generally $K = {}_H \geq 1.6$	$1.5\ K^*_H \geq 4.0$ (2.6 average)

Considerations regarding rock mass structure

The listed ratios are simply broad guidelines for initial blast design, and the actual parameters differ with each case. An important consideration for this is the structure of the blasted rock mass, and specifically its discontinuities. Radial cracks that develop around the blasthole resulting from the supplied explosive energy do not propagate across joints, which poses problems regarding fragmentation. Additionally, these existing cracks may provide less resistance to explosive gasses, and further reduce the fracturing effectiveness of the blast. In fractured rock masses, a larger number of small diameter holes located in between discontinuities should therefore be more effective than a couple of large diameter holes whose explosive energy spans across multiple blocks [4].

Burkle [7] defined another geological factor that influences blasting, namely the orientation of the geological units. Depending on the rock mass' dip direction or joint orientations with respect to the blast direction, one can either blast with the dip, against dip, or along strike. Each of these options comes with different performance characteristics; blasting along strike will typically result in the worst conditions, since it can lead to a 'sawtoothed' floor and irregular back break due to the intersection of the different rock types on the newly created surfaces. For blasting with the dip there is a tendency to get more back break. There would be more movement of rocks away from the face, and therefore one can expect a lower rock pile profile. When blasting against the dip, it is often more difficult to loosen the toe of the bench. Contrary to blasting with the dip, there is less movement away from the face, and the resulting rock pile is often higher.

Blast patterns and timing

Once the initial blast design dimensions have been determined, there are still more decisions to be made. While keeping the basic design parameters the same, the characteristics of a blast can still be adjusted by choosing either a square or staggered blast pattern, and by sequencing of the individual hole detonations. The difference between a square and staggered blast pattern lies in the alignment of subsequent blast hole rows. A square pattern is recognized by having the rows and columns of holes at right angles to each other, such that the rows are in-line (Figure 2.2a). If this is not the case, and instead rows are shifted from this alignment, the pattern is known as staggered (Figure 2.2b).

The largest difference between the two methods is the energy coverage of the blasted rock mass. When the spacing and burden are equal for both cases, and the energy coverage is represented as cylinders around each charge with surface area A, staggered patterns will lead to a higher percentage of covered area and less overlap than square patterns. This is illustrated in Figure 2.3. By allowing some overlap in energy coverage, a staggered pattern with a spacing/burden ratio of 1.15 can achieve a coverage of 100%. The optimal S/B ratio for square patterns is 1.0, resulting in a coverage of 77% [8].

Although their lower energy coverage makes square patterns look suboptimal, other factors exist that can justify using this method instead; grade control procedures are often the primary reason, since grades can simply be assigned to square areas based on blasthole assays [9]. Staggered patterns are sometimes also avoided when holes are drilled inclined because operators would be forced to realign the boom angle instead of simply driving perpendicular to the face. Square patterns are also more appropriate for confined blasts or for sinking cuts when developing a new level [10].

(a) Square (b) Staggered

Figure 2.2: Square and staggered blast pattern layout [4].

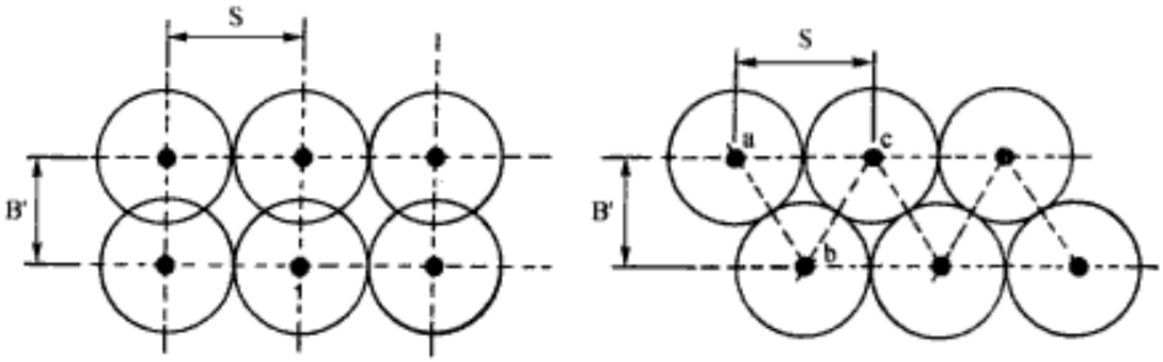

(a) Square (b) Staggered

Figure 2.3: Energy coverage in a square pattern and staggered pattern with S/B ratio of 1.155 [4].

Another important design characteristic is the sequencing of hole detonations. For a blast to result in optimal fragmentation, not all explosives are set off simultaneously. A number of commonly used timing delay patterns will be discussed here. The underlying principles of sequencing for efficient blasting were described by [11–13]; charges should be detonated in a sequence that maximizes the successive development of effective free faces. Each charge should be given just enough time to break and loosen its part of the rock mass before the next charge is detonated so that this one too is blasted towards a free surface.

For a single-row blast, this can be achieved by starting the initiation sequence at the center of the bench with delays between subsequent charges moving outward, as depicted in Figure 2.4a. Once the center hole is blasted, the successive blasts will have an additional free surface available, and therefore it will be easier to break the rock mass. For blasts consisting of multiple rows, a first improvement can be made by setting delays between rows, as shown in Figure 2.4b. However, better fragmentation can be accomplished by making use of so-called chevron firing patterns. These sequencing methods involve connecting holes 'diagonally', known as open chevron (Figure 2.5a), or in a V-shaped pattern, known as closed chevron (Figure 2.5b). Because of this, the spacing and burden 'as-shot' are no longer equal to the spacing and burden 'as-drilled', and are for that reason called the effective spacing and burden. This technique can be used to detonate holes that were drilled in a square pattern effectively staggered.

The main difference between open and closed chevron detonation sequences is the shape of the rock pile; a closed chevron pattern concentrates the blasted material in a central position, whereas an open chevron pattern spreads out the rocks more evenly. While discussing this topic, it should also be noted that the stemming height is often increased in the front row of blasts to compensate for the back break from the previous blast, to prevent rocks from being thrown too far away. This will result in a much better muck pile profile.

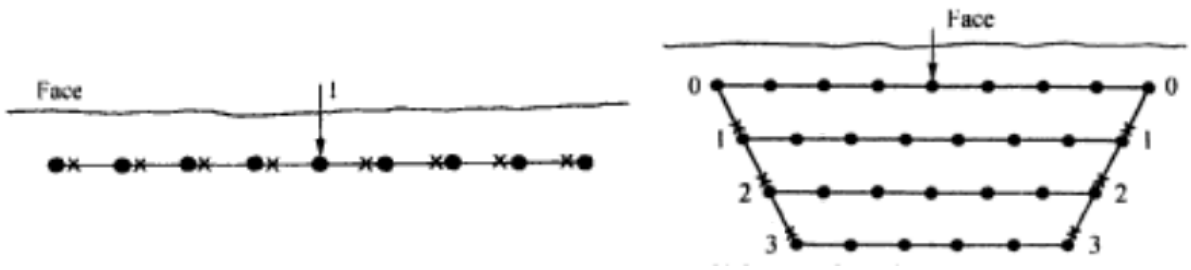

(a) Single row blast with center initiation (b) In-line delay pattern with delays between rows

Figure 2.4: Blast sequencing principles [14].

(a) Open chevron (b) Closed chevron

Figure 2.5: Open and closed chevron initiation patterns [8].

The final step is choosing the appropriate delay times. If the inter-row delay is too short, chances are the previous charge has not yet detached its part of the burden from the rock mass, the additional free surface to blast towards is not available for the next detonation, and blast quality will be poor. Conversely, if there is too much time between the detonation of subsequent rows, broken rocks from the first blast will have moved too far away. Because this material does not receive energy from the next blast, fragmentation is often poor and large boulders may be found. Furthermore, long delay times increase ground vibrations and the chances of flyrock. Thus, ideal delay times are long enough to allow the rock mass to be appropriately broken and loosened, resulting in sufficiently little confinement for the next blast, but also short enough to still make use of its explosive energy. The general consensus is that the 'sweet spot' for delay time between holes is 3 ms per meter of burden. When the number of rows is larger than 3, this timing should be increased [10].

Blast quality and shape

Generally speaking, blasts should be as large as possible since this leads to multiple positive effects. First of all, a blast pattern should be as long as practically possible; it should be at least 1.5 times the width to reduce the restraining effect from the confining rock mass to the sides. In order to optimally exploit this, a blast pattern should preferably be three to four times longer than it is wide [14]. Although the width of blasts is usually limited by the working width and bench width determined by pit design, multi-row blasts offer clear advantages over single-row blasts; multi-row blasts generally produce better fragmentation, which is largely due to creating fewer blast boundaries.

Fragmentation at blast boundaries is often worse than in the center of a blast because it is influenced by overbreak from the previous blast; explosion gases propagate through existing cracks, and large boulders that are already effectively detached do not receive the required energy to be broken sufficiently [11]. When a bench is blasted in one go by multiple rows, there will only be one new blast boundary, which is preferred over multiple single-row blasts that each create a new blast boundary. Large blasts increase productivity because the amount of unproductive back and forth movement of equipment is reduced. Finally, larger blasts translate to a lower frequency of environmental disturbances [12,13].

Nevertheless, there are also a couple of downsides to larger blasts. If the number of rows is too high, the rows detonated last may not produce acceptable fragmentation. If the rocks can not move forward to a free surface, charges may crater to the horizontal surface. This can result in high rock piles, toe problems, flyrock, overbreak, and 'tight' digging conditions. Besides, a higher number of rows will also lead to an increase in ground vibrations [12,13].

2.1.2. Explosives

An important consideration for blast design is the explosives selection. Because it does not fall under the geometric design factors, it will be discussed separately in this section. However, the choice of explosives can have a large influence on geometric blast design. Due to the different explosives available, and their varying properties, combination with the chosen geometric parameters should always be taken into account. The most common way to compare the strength of an explosive is through its weight strength or bulk strength, which are defined as the explosive energy per unit weight or volume respectively. The explosive energy is usually calculated as the theoretical heat of the explosion. Weight strength and bulk strength values are often compared to standard ANFO (Ammonium Nitrate Fuel Oil) values to obtain the relative weight strength S_{ANFO} and relative bulk strength B_{ANFO}. The absolute weight strength of ANFO is 912 kcal/kg (although this value can differ depending on assumptions of its composition), and its bulk strength can easily be calculated using the explosive's density [4]. This means that if another explosive would have an absolute weight strength of 875 kcal/kg, its relative weight strength S_{ANFO} would be 875/912 = 0.959.

But explosive strength is not all that matters, it is also essential to know how the explosive energy is used. This will be discussed in detail in Section 2.3, but for now a simplified division of explosive energy into shock and heave energy will be made. Two explosives can have the same weight strength, but a different distribution of shock/heave energy. Hard and massive rock types would benefit more from additional shock energy to create new cracks for improved fragmentation, whereas higher heave energy will be more useful in a soft and jointed formation to separate the existing blocks. This can be translated to the following physical characteristics of explosives; those with higher shock energy have a high peak pressure, which is related to high detonation velocity and high density. Explosives with higher heave energy can be recognized as having high gas pressure with expansion, which is found in explosives with lower detonation velocity and density [4].

In open-pit mining, blast holes are usually bulk loaded using a mix-pump truck instead of packaged products. Bulk explosives (or bulk blasting agents) by themselves are not explosive, despite their name, but must be detonated by a high explosive primer. In this literature review, only the various types of bulk explosives will be discussed, along with their advantages and disadvantages. They can be categorized into ANFO-types, watergels or slurries, and emulsions.

ANFO

ANFO consists of ammonium nitrate (AN) and fuel oil (FO), which are usually mixed in a 94/6 ratio by a bulk ANFO truck at the blast site. The maximum strength of the explosive occurs when about 5.5% of fuel oil is used, but this is a sensitive balance; adding either too little or too much fuel oil sharply reduces the explosive energy. In the case of insufficient fuel oil, nitrous oxides (NOx) may form, while a surplus leads to the formation of carbon monoxide (CO). Ammonium nitrate is usually supplied in the form of porous prills, making ANFO a dry and granular composition. Because the prills consist normally of around 50% air by volume, in addition to the voids between them, the density of ANFO as loaded into blast holes is much lower than just the density calculated from the ammonium nitrate and fuel oil (around 1.675 g/cm^3); in reality, it normally varies between 0.8 and 1.0 g/cm^3. The cost per unit of energy delivered is relatively low for ANFO, and because fuel oil is usually available at most mines, it is a popular and effective blasting agent. The initiation sensitivity decreases with increasing hole diameter, and a major disadvantage is its lack of resistance to water; ammonium nitrate is easily dissolved in water, and detonation will fail when ANFO contains more than 10% water [4].

The overall energy output of ANFO can be increased by adding aluminum powder as a fuel [15,16]. The amount of added aluminum normally lies between 5 and 15 weight percent, because the increments in explosive energy start to become smaller for values higher than these [14]. The addition of aluminum is a relatively simple adjustment to increase the explosive energy of ANFO where necessary, and can improve fragmentation in stronger rocks without alteration of the blast pattern. For the same reason, aluminized ANFO is often used as the toe load of a blast to ensure successful breakage in this part of the bench. Besides the higher explosive strength, its properties are the same as ordinary ANFO [4].

Under some circumstances, it may be desirable to use ANFO with lower bulk strength. This can be achieved by reducing the explosive's density and/or velocity of detonation. Wilson and Moxon [17] found that sawdust, polystyrene, and bagasse are suitable additives that accomplish this well. Because these materials act as a low-grade fuel that burns slower than fuel oil, they reduce the velocity of detonation of ANFO. Combined with the lower density, these mixtures effectively lower the detonation pressure. This can be favorable when more control of the blast is required, for example, to minimize back break. Because the ANFO is mixed with inexpensive products, there is also a cost-saving aspect to this method.

Watergels/slurries

A large problem with ANFO has always been its lack of resistance to water. By the late 1950s, a new type of blasting agent was introduced to deal with this problem. Slurries or watergels are especially suitable for blasting under wet conditions, because the substances themselves are water-based. Their composition was initially described as AN-TNT-H_2O, but these days a variety of suitable ingredients exist which are either dissolved or suspended in the water. This results in an aqueous ammonium nitrate solution with a fuel component. The water content ranges between 5 and 40% by weight, and the average is 15% [18]. Adding too much water will reduce the weight strength. A thickening substance like guar gum is usually added to obtain the required consistency so it can be easily pumped, and cross-linking additives provide cohesion and prevent leaching of the salts by water flowing through the hole [4].

An important characteristic of most slurries currently produced is the presence of small air or gas bubbles in the mixture. When the shock wave of a highly explosive primer or booster enters the slurry, the volume in these voids is believed to be compressed, instantly heating it to very high temperatures, and leading to explosive decomposition of the surrounding material [19]. Different types of fuel sensitizers may be added to produce large variations in bulk strength and weight strength, which allows for great customization. Aluminum powder is often an important ingredient. Slurries can be delivered in a number of forms; they can be supplied separately and mixed either on-site or directly in the blast hole, as already mixed, or packaged as cartridges.

Emulsions

Whereas the previous types of blasting agents involved solid materials, emulsions consist only of liquids. They are mixtures of two types of fluids that do not dissolve in each other. For optimal reaction efficiency in explosives, the oxidizer and fuel must be in close proximity. Emulsion blasting agents take this to the next level by reducing the particle size of the oxidizer, typically ammonium nitrate or another salt solution, to microscopic proportions; droplets of salt solution with a diameter between 2 and 10 microns are surrounded by a thin layer of fuel of near molecular thickness. Because of this scale, their intimacy approximates the molecular interaction in explosives such as TNT as closely as possible, which improves reaction efficiency and leads to a high velocity of detonation [4].

Just like watergels, emulsions require additional sensitization in the form of air bubbles. However, because there is no cross-linked gel network in place, emulsions have trouble holding the bubbles. To combat this issue, glass spheres with a diameter in the order of a couple of 10s of microns are often added [19]. Another similarity is the high customizability of emulsions; different types of oils and waxes can be used as fuel to vary the consistency and weight strength. Because fuel only represents about 10% of its volume, this will not have large effects on the density of emulsions. Unlike slurries, the mixing of emulsions is not done in a mix-pump truck, but instead at a central location close to the mine site.

Emulsions can also be used in combination with ANFO to create so-called heavy ANFO. The idea behind this is to fill the voids in between the AN prills with emulsion. By varying the amount of emulsion added, the properties of the mixture can be adjusted as required. The overall density and relative bulk strength vary depending on how much emulsion is added. Between 35 and 40% of emulsion is needed to fill all the voids, so below this value the density and strength will increase as more emulsion is added. At higher percentages, however, this relationship may change depending on the properties of both blasting agents. The water resistance is only significantly improved at weight percentages above 30%, and at least 50% is required for good water resistance [20].

Powder factor

The power factor of a blast is a figure that denotes the amount of explosives used per volume of blasted rock, usually expressed in kg/m^3. Naturally, it is dependent on both the selection of explosives and geometric blast design, which have been discussed here previously. Although some relationships exist between the powder factor and blast performance, it should not be used as a primary tool for blast design. Blast performance is influenced by a variety of factors that would not be adequately represented by a single value; changes in blast pattern, type of explosive, delay times, bench height and rock characteristics can all have a large influence on a blast, while the powder factor remains constant. These days, the powder factor is mostly a valuable property for cost analysis of blasting [21].

Nevertheless, some ranges of typical powder factors can be given as an indication of the blasting requirements. As can be seen in Table 2.2, less explosives are needed in softer rock. Although generally less explosives are used in large hole diameter patterns, fragmentation is often coarser than for patterns with a larger number of small holes. The powder factor can also be lowered as the number of free faces of a blast increases, or when the rock mass is very fractured [22].

Table 2.2: Typical powder factors used in mass blasts [23].

Rock strength	Powder factor (kg/m^3)
Very soft	0.15 - 0.25
Soft	0.25 - 0.35
Medium	0.40 - 0.50
Hard	0.70 - 0.80

2.1.3. Drilling and Charging Practices

Although the exact procedures for drilling and charging vary from mine to mine, certain generalizations can be made about common practices. This is necessary both from a safety and regulation point of view but also follows from the use of often similar equipment. This section aims to give an overview of how drilling and charging operations are in general performed, without going into detail on site-specific differences in methodology.

Positioning

Drillhole patterns are traditionally laid out by the surveying crew of a mining operation. Manual staking of patterns to mark the appropriate drilling locations is a time-consuming process, which could take up to 50% of a survey department's man-hours. In order to reduce this workload, surveyors at some mines would only place control pegs, leaving the marking of individual holes to the drilling crew [24]. Even if the drillholes were staked with the highest accuracy, this method would still lead to errors during the drilling process; operators used to position on the stake by looking through a *"one-foot square"* on the floor, which became even more challenging under circumstances like darkness, rain, snow or fog [25].

With the onset of technological advancements, specifically the implementation of GPS systems, drillhole positioning was significantly changed. By equipping drill rigs with GPS receivers, the need for manual staking of drillhole patterns has been eliminated. Using the GPS location in combination with a drillhole design file on the on-board computer, operators can easily navigate the drill rig over the designed collar positions by obtaining its relative location from a display. As the drill rig is moved closer towards the collar position, a *"crosshairs and bull's eye effect"* will be visible on the screen to guide the drill bit towards the target, representing the desired hole location [24]. An additional benefit is finding the elevation once the drill rig is in position for drilling. Together with other technology, this allows for more accurate determination of hole depth. Because this can be synchronized with the specified hole depth in the design file, it makes manual tape measurements redundant. Once drilling of a hole is completed, the planned and actual collar coordinates are recorded. These deviations will be discussed in more detail in the next section. Overall, the implementation of GPS technology on drill rigs has led to more accurate drill patterns and has improved surveying efficiency by up to 80% [24,25].

Drilling

The actual method of drilling the holes can be divided into two classes based on the equipment used; percussive and rotary drilling. Percussive drilling makes use of the rotation of the drill bit in combination with high-frequency percussive impacts delivered through hydraulic pressure to break the rock. A differentiation can be made between a top hammer and down-the-hole percussive drilling, depending on the location of the hammering parts. Percussive drill bits consist usually of chisel/cross-shaped or 'button' tungsten carbide inserts. Rotary drilling, on the other hand, cuts small rock chips at the bottom of the hole through rotation of the drill bit, by applying torque at the end of the drill string. These machines are diesel or electrically driven. The most common type of drill bits in use is so-called tricone bits.

The difference in penetration mechanism also leads to a difference in the application of these methods. Percussive drilling is mainly used in harder rocks for small to medium-sized holes of up to 200 mm in diameter, because of its high penetration rate under these conditions. The top hammer variation is generally limited to holes smaller than 150 mm, or even 125 mm [10,26]. Down-the hole percussive drilling can also be used in larger hole sizes. Having the hammering part closer to the drill bit allows drilling of straight and deep holes with minimum deviation, and good hole wall stability. Rotary drills work best for holes with a diameter of 6 inches (152 mm) or larger and is the main technique for holes larger than 230 mm [26,27].

According to [26], good drilling practices include *"carefully monitoring drill-rig operating parameters, taking notes of the changes in geology during drilling, and effectively communicating to the blasting crew any unusual conditions encountered during drilling that may affect blasting results or require changes in hole-loading practices"*. These tasks are often supported by data obtained from Measurement-While-Drilling (MWD) technology. By logging drilling parameters such as hole depth, rotation pressure, percussion and penetration rate, rock properties are derived. This information can be helpful to locate geological boundaries and may be used to adjust blasthole loading or detonation delays [28].

Charging

Before drillholes are charged, they must be checked. First, the depth must be measured with a weighted measuring tape or cord. The depth is measured from the bottom of the hole to the collar at the surface, disregarding the height of any drill cuttings, and recorded on a hole-by-hole basis. If the hole has been drilled too deep, it must be filled with stemming until the bottom of the hole is at the designed depth. Holes that are less deep than planned should be cleaned out with a drill or compressed air, or be redrilled. It is also advised to measure the water depth in the hole, for example with the weighted tape, check for wet sidewalls, and look for evidence of hole collapse.

In case of a wet hole, it may need to be pumped dry, and the choice of bulk explosive should be evaluated. Due to its lack of water resistance, ANFO should not be loaded into a wet hole without the use of a waterproof liner. Communication with the drill crew is important, especially regarding conditions where weak rocks are encountered that can result in hole collapse. Should a drillhole pass through or bottom into an opening, such voids must be filled. If this can not be achieved with stemming material, it may be necessary to plug the hole with gas bags, stemming plugs, or other air-decking devices. In some cases, a hole may need to be redrilled. To prevent venting from the faulty hole when the new hole is detonated, it must also be properly sealed with stemming or a gas bag.

Furthermore, stemming height, primer location, and amount of bulk explosive may be adjusted if there is broken ground around the collar, reduced free face burdens, excessive toe burdens, or reduced distance from the broken ground. This is especially troublesome if there is much variation in front row burden, due to flyrock or overpressure risk. Measurement of face geometry and drillhole deviation may be necessary, and increased stemming heights, adjusted charge quantities, or gravel decking could be required to combat these issues. In case of excessive toe burdens or adjacent presence of short holes, bulk explosive density and charge mass may be increased to achieve a higher localized powder factor. Conversely, it may need to be reduced in holes with too little burden at a free face. If blast holes have been undercharged, additional bulk explosives may be added within design charging and stemming height guidelines. However, the designed stemming height of a hole should not be reduced to accommodate the charges. Overcharged holes may require removal of the excess bulk explosives, which can be performed with an approved scoop or vacuum equipment, or by displacing it by pumping water [29,30].

Once it has been established that the drillhole conditions are suitable for loading, the procedure starts by lowering the primer. It is good practice to load a small quantity of explosives beforehand, to protect the primer from puncture and is also well coupled at the bottom of the hole. To prevent damaging or loss of the downline, they are preferably hand-held during charging and stemming, or otherwise secured at the collar. While continuing to load the bulk explosive, it is important to regularly check the rise of the column using a weighted tape, to identify any problems. If the hole is filling up slower than expected, this can indicate the presence of cavities or an oversized hole, which can both lead to overcharges. Furthermore, it helps to assess whether there is still enough room available at the top of the hole for the appropriate amount of stemming [29,30].

ANFO is usually augured into the holes at rates ranging from 100 to 500 kg/minute or can be blown using a pneumatic system with a discharge hose that is typically 10 meters long. With the charging truck driving between two rows of large diameter holes, usually, four to six holes can be charged from each position of the truck. Augured delivery is aided by a boom that has a typical length of five to six meters, which can normally reach two or three drillholes from one position. Watergels and emulsions are pumped at rates up to 350 kg/minute [4]. Emulsions may need to be gassed during loading, which may require additional time before the hole is stemmed [30]. Emulsions can be loaded even in holes containing water if the hose is lowered to the bottom of the hole and pulled up slowly as the hole is being filled. This is to make sure the water is displaced properly and does not become trapped within the explosive column [4,29].

Stemming should be loaded according to design depths, and to ensure this, the height of the explosive column must be checked after charging. In case there is broken ground at the collar, or when face burdens are reduced, stemming needs to be increased. Stemming heights must be recorded to a specified accuracy, which should be consistent with a safe and environmentally acceptable blast design. Another consideration is the sequence in which the holes are charged, which must be done systematically. For large blasts, this means that large sections could be shot in case unfavorable conditions might prevent firing of the whole blast within the required timeframe. Moreover, it should be taken into account that water displaced from wet holes can run into previously dry, loaded holes. This can be prevented by appropriate sequencing of hole charging, by considering the effect of treatment of wet holes on other holes nearby, and anticipation of rainfall-runoff and water accumulation in low areas [29].

2.2. Drillhole Deviations

The main problem addressed in this thesis is the deviation of drillholes relative to their planned configuration. In order to understand what these deviations mean for the drilling and blasting process, this section will elaborate on the problem statement by providing some important background information. First of all, the various types and causes of drillhole deviations are discussed. This will give insight into the complexity of the problem, and show why it is so difficult to eliminate it. Next, the importance of drillhole deviations will be demonstrated by presenting the possible consequences for blast performance, safety, and mining operations as a whole.

2.2.1. Sources of Error

Although drillhole deviations may seem like a straightforward problem, in reality, it can be difficult to deal with due to the variety of underlying causes. Many different sources of error can be identified, and each of these can contribute to the overall deviation. Modernization of the drill and blast cycle has improved drilling accuracy tremendously, most importantly by eliminating the need to manually stake drillhole patterns. Despite all the technological advancements in this area, however, there are still some challenges to overcome to facilitate further improvements.

The causes of drillhole deviations can be categorized in a number of ways. Almgren and Klippmark, for example, made a distinction between external errors and internal errors. External errors include incorrect surveying, marking errors, poor collaring practice, error in drill setup, incorrect boom alignment, and operator errors. Physical limitations of the drilling equipment, poor drill operation, poor condition of the equipment, and geology of the rock mass are internal errors [31]. A more common classification is made by the following types of drillhole deviation [32]:

- Collaring deviations
- Alignment deviations
- Trajectory deviations
- Depth deviations

Collaring and alignment deviations generally fall under Almgren and Klippmark's classification of external errors, whereas trajectory and depth deviations belong to the internal errors [31]. Collaring deviations can be described as the horizontal displacement of a drillhole with respect to its planned starting location at the surface. The most important factors that contribute to this type of deviation are poor drill setup, the topography of the drill site, and problems with holding the boom and feed beam in a fixed position, for example, due to worn parts. Alignment deviations take place in the process of turning the feed boom to set it in the planned direction of vertical inclination and can be caused by instabilities of the drill rig, misalignment of the feed beam, lack of precision in positioning equipment, topography at the collaring point, and structural geology. Trajectory deviations occur when the drill is deflected from its designed path during drilling, which is influenced by the hole design (length, diameter, inclination), rock properties (hardness, structures), drill parameters, and equipment. Similarly, depth deviations are also a consequence of these internal factors in combination with the accuracy of measure while drilling techniques and precision in positioning equipment [26,32,33].

For internal sources of error, it was found that small diameter holes more often deviate than large diameter ones. Deviations also increase with drillhole length and are more likely in inclined holes than for vertical drilling. Regarding the equipment, the characteristics and conditions of the drill string are of great importance, because the deviation is proportional to its flexibility [32].

Many of the causes that have been discussed thus far can be traced back to either equipment-related issues, some of which can be mitigated by proper maintenance, or geological conditions beyond the driller's control. However, this thesis will primarily address lateral deviations in drillhole location, and will therefore focus on the external sources of error (collaring and alignment deviations). A typical requirement for drilling accuracy is that the horizontal deviation is not larger than the hole diameter [34]. However, a blast optimization study conducted at Kriel Colliery, for example, found that this was only achieved for 8-19% of the holes, as well as for 33% and 47% at the Kleinkopje and New Vaal mines respectively, shown in Figure 2.6. It also shows that many deviations exceed even twice the hole diameter. This is problematic because the explosive power at a certain point could be reduced by 35% if a drillhole is moved by 0.5 m [35]. Two factors that have been understated up until this point, and especially relevant for these external errors, are the influence of operator (in)experience or human error, and the accuracy of GPS measurements in a mining environment.

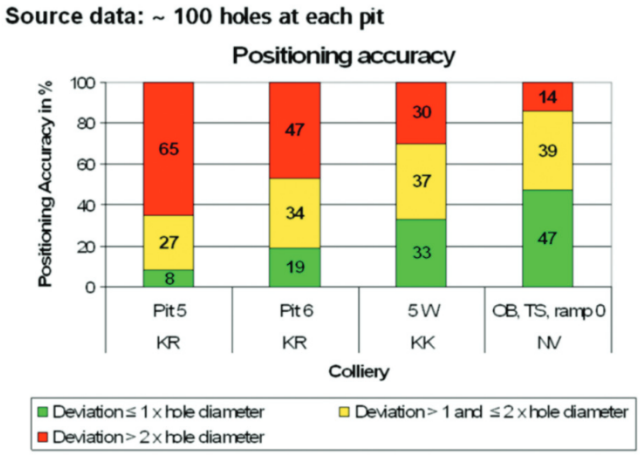

Figure 2.6: Example of drillhole deviations at Kriel, Kleinkopje, and New Vaal Collieries [35]

Human error

In order to understand the influence of the skills of a drill rig operator on drillhole deviations, it is important to first examine the tasks that must be performed, together with the typical instrumentation used in doing so. These days, most drill rigs are equipped with high-precision GPS positioning units, which serve as the basis for maneuvering these machines to the appropriate locations for drilling. Such a satellite positioning receiver is complemented by precision sensors on the boom that compute their orientation using forward kinematics. By combining the measurements of these sensors with the GPS position of the vehicle, the position and attitude of the boom can be compared to the values found in the drilling plan. This data is used to generate a visualization of the rig's position relative to the planned drillholes, which is presented on a display to the operator. In this manner, the operator is guided towards the appropriate drill setup by moving closer and closer towards the planned blasthole location. When the drill bit gets in close range of the collar position, the screen will zoom to a 'cross-hairs and bullseye' configuration to allow for optimal precision [24,34].

This process of maneuvering the drill rig in accordance with the drilling plan can be divided into two distinct tasks, namely the positioning (or collaring) and alignment. Naturally, these tasks correspond to the previously defined sources of errors, but a more detailed description will be given here.

Positioning is the operation of moving the drill bit, located at the bottom of the drill feed boom, such that it coincides with the projected hole line above-ground. If the drill would be lowered towards the ground, the drill bit would connect to the desired starting point of the hole, also known as the collar. To prevent unnecessary damages to the lower part of the feed boom by collisions due to an uneven surface, rocks, or other obstacles, the boom is lifted from the ground during positioning.

Alignment is the process of rotating the feed boom such that it coincides with the extension of the hole line above the surface, allowing the hole to be drilled in the direction as defined in the drilling plan. Although the positioning and alignment tasks are independent operations, in practice they are interdependent. Because of the structure of the boom and the mechanical movements it allows, positioning adjustments can have an influence on alignment, as well as the other way around.

A typical drill rig is equipped with hydraulic control of the boom that allows for six degrees of freedom. Six two-directional joints are required to perform the 12 distinct movements necessary for positioning and alignment, which can be bound to different control configurations like joysticks, levers or buttons, and are generally controlled individually. Because adjustment of one of these joints can change both the positioning and alignment, corrective movements may be required to maintain, for instance, the appropriate alignment when adjusting for positioning. Maneuvering the feed boom into the correct configuration is a challenging three-dimensional process that requires a lot of attention from the operator. The order in which the two tasks are performed can vary depending on the situation and operator, or can also be done simultaneously. This interdependency between positioning and alignment makes it difficult to achieve perfect hole placement, especially for inexperienced operators. In practice, there are always some differences between the planned and drilled hole locations [34].

In an attempt to reduce drillhole deviation by removing (or decreasing) the effect of human errors, much attention has gone out to automated or even autonomous drilling in recent years. Equipment manufacturer Caterpillar, for example, is well underway with its so-called ‘journey to autonomous drilling’. With the CAT Terrain for Drilling system as a basis, progress is made from ‘auto drill assist’ features, including automatic leveling and drilling of a single hole, towards semi-autonomous drilling of single rows under distanced supervision of the operator, and finally, fully autonomous drilling of an entire blast pattern [36,37]. With the latest release of its new MD6250 drill rig, Caterpillar has already brought the semi-autonomous drilling of single rows to the market [38]. Another frontrunner in this area is the mining company Rio Tinto, which has already observed great benefits from autonomous drilling in Australia. Rio has supposedly been the first company to achieve fully automated hole-pattern drilling and is expanding its remotely operated autonomous drilling fleet thanks to the impressive results, helping the company to *“drill more safely, accurately and consistently”* [39,40]. An early trial by Sandvik found that an automatic positioning mode for their surface drill rigs, as a replacement for traditional manual control, reduced the mean drillhole deviation from 11.5 cm to 5.5 cm [34].

GPS accuracy

Automatic positioning figures by Sandvik indicate that the problem of drillhole deviations is still not completely solved after eliminating the human errors. Of course, there are also mechanical limitations for the level of detail of the machines, but a more deep-rooted problem lies in the use of GPS positioning as the main source for relating a drill rig's location to that of the planned drillholes. Even though high precision receivers have become the standard on modern drilling equipment, boasting theoretical accuracies of 10 to 20 mm, there are many factors that can impair the quality of GPS measurements, particularly in a mining environment [34,36].

The most accurate GPS technique currently available is Real-Time Kinematic (RTK) GPS. Similar to differential GPS, this method makes use of a reference point with known coordinates that acts as a reference station. Combined with a variety of sophisticated techniques, the locations of nearby receivers on vehicles can be calculated from the distance to satellites and corrected using this reference station [24]. At least three factors can be identified that may reduce the accuracy of GPS measurements:

- Tropospheric delay
- Position Dilution of Precision (PDOP)
- Multipath

Tropospheric delay is normally incorporated when the distance between a GPS receiver and satellites is calculated. It is computed by empirical models that consider temperature, relative humidity, and pressure. While these models are able to predict the tropospheric delay with high accuracy, there can still be a difference with the true value, resulting in residual delays that are not accounted for. These effects are generally unimportant, but in case there is a large difference in elevation between the base station and a mobile GPS receiver, a common situation in open-pit mines, it may cause noticeable inaccuracies. This is especially true if there are differences in meteorological conditions [41].

Position Dilution of Precision is a number that represents a confidence factor for satellite availability at a certain point in time. On one hand, this depends on the number of satellites orbiting the earth, but it is also a geometrical problem. Because open-pit mines are generally characterized by steep, deep pit walls, a GPS receiver at the bottom of a pit will have a smaller angle of access to the open sky. Although Modular Mining Systems claims that the addition of other GNSS constellations like GLONASS, BeiDou, and Galileo to their network of available satellites leads to *"more dependable and accurate positioning"*, positioning technology provider Applanix reports that *"the large increase in the number of GNSS satellites over the past decade has not significantly ameliorated this problem"* [42,43]. Although there is software available to predict the PDOP for a given time of the day, a lack of optimal satellite coverage can still present a problem for deep open-pit mines and lead to inaccurate GPS positioning [24]. Fully operational time of satellite constellations, requiring at least 4 satellites in view, can be reduced to as little as 20% inside open-pit mines [44].

A mitigating measure for the PDOP problem is the use of so-called pseudolites. Pseudolites can be described as either GPS receivers or transceivers. In addition to receiving signals, a pseudolite transceiver also transmits them. Therefore, a pseudolite can act as a satellite to augment the conventional constellations. This is especially helpful in areas with poor satellite coverage, like deep mines with steep pit walls; pseudolites transceivers positioned at known coordinates along the pit perimeter

essentially improve the coverage for GPS receivers inside the pit. By providing an additional measurement point that is generally within line of sight, fewer satellites are required to triangulate the position of a receiver [44]. It was not only demonstrated that the PDOP is reduced by the addition of a pseudolite, but also that a larger number of pseudolites will have a positive effect on further decreases, especially in the vertical direction [45]. Although there is no question whether pseudolites improve the positioning geometry, the issues of tropospheric delay and multipath prevail, and additional differences could be introduced by potential pseudolite position errors [46].

Finally, multipath encompasses the situation where satellite signals are reflected off surfaces near a GPS receiver. This causes the signal to travel between satellite and receiver along different paths, leading to multiple possible distance calculations, and ultimately causing inaccurate positioning. Multipath is not a problem reserved for mining environments only. Methods exist to account for this effect, but they are generally not suitable for applications in mining because GPS receivers deep inside a pit are surrounded by many reflective surfaces, most importantly the pit walls. Multipath can be detected and canceled by double-differencing if it shows an apparent daily correlation as a result of repeating geometry of satellite, receiver, and reflecting object. However, this correlation only occurs with a specular reflection on smooth surfaces. In open-pit mines, reflection instead mostly occurs as diffraction (reflection from edges or corners of reflective objects) or diffusion (reflection from rough surfaces), making this method unsuitable and thus leaving the positioning subject to more inaccuracies [24,41].

2.2.2. Consequences

After having touched upon the different types and causes of drillhole deviations, this section will give an overview of their effects on blast performance. Furthermore, these consequences will be placed in a much broader perspective. Because drilling and blasting represent the first major step in a mining operation's bulk material handling of ore and waste rocks, discrepancies in blast performance can have tremendous cascade effects on many downstream operations. In order to recognize the significance of blast performance altering drillhole deviations, it is essential to consider the complications they introduce at subsequent stages of the production process as well.

Energy distribution & fragmentation

When focussing on collaring deviations, the most direct consequence is alteration of the spacing and burden between blastholes; a mispositioned hole reduces the effective spacing or burden in one area, and increase it in another [47]. When the realized spacing or burden is different from the planned blast design, this naturally causes local variation in specific charge, often known as the powder factor [34]. As a result, the explosive energy distribution will not match the designed specifications that were carefully decided on in the blasting plan. The purpose of a well-designed blasting plan is to achieve optimal blast performance. However, when the blast design is altered, blast performance will also be affected.

An important factor to assess blast performance is the resulting fragmentation of the rock mass, which can be quantified using size distributions. Because of the local differences in explosive energy, fragmentation across the blast pattern will vary more than intended and change the size distribution; the median fragment size (X_{50}) was found to be reduced in blasts characterized by greater drillhole deviations [47]. However, this does not tell the whole story; the resulting muck pile is likely to consist of more unevenly sized rocks, containing both oversized boulders (due to areas of reduced explosive energy) and a larger amount of fines (due to areas of increased explosive energy) [34].

Costs & productivity

Because of this relationship between drillhole deviations and poor fragmentation, a large number of extra costs incurred due to fragmentation issues can now be linked to inaccurate drilling. First of all, more drilling and blasting can be necessary to blast all of the intended rock mass. The presence of very large boulders can also require additional breakage or blasting. This results in higher secondary breakage costs, including increased explosive consumption and potential delays in the chain of production operations [32–34]. It was demonstrated that the additional drilling and blasting costs increase with the extent of drillhole deviation [47].

Although poor fragmentation has some implications for drilling and blasting itself, this is also the stage at which the consequences for subsequent operations become apparent. Evidently, any production delays can quickly propagate to consecutive operations, but there are also more direct influences on their performance. Especially the presence of large boulders is troublesome; this complicates excavation, loading, and hauling of the material. The efficiency of these operations is also reduced due to lower fill factors of both excavator buckets and haul trucks. Finally, disproportionate boulders can lead to excessive wear of equipment and higher crushing costs [32,34]. Because the amount of explosive energy in each area of a blast is altered, some control on ore loss and dilution may be lost. These are important properties that can have a significant effect on the performance of the processing plant and consequently the end-product quality, making this a major economic factor [34].

Safety & secondary effects

Besides the effects on production chain operations, there are a couple of other negative influences of drillhole deviation that are worth consideration. First of all, the safety implications; as discussed before, some areas in the blast pattern will receive more explosive energy than intended whenever a number of holes are spaced more closely than planned. Although the blast is designed to only loosen the rock mass, certain parts may receive a surplus in energy, which can lead to increased risk of flyrock. This is supported by the fact that blasts with deviated drillholes are characterized by lower median fragment size, and therefore contain more fragments that require little kinetic energy to be thrown far away [34,47].

Another factor for assessment of blast performance is often found in the loosening of the rock mass along the planned boundaries of the blast pattern. Fragmentation in these areas should be sufficient to loosen the rock such that a clean separation with adjacent rock mass occurs. When drillholes are displaced from their planned locations, this becomes an increasingly relevant issue. Once again, because the spatial energy distribution is altered, performance in this area may be reduced. In case there is too little or too much explosive energy to sufficiently loosen all the rocks, slope stability problems may cause dangerous situations [26,34]. At another boundary, namely at the bottom of the blasted rock mass, poor distribution of explosive energy can lead to an uneven bench floor or ground control problems [32]. In turn, this can complicate operations on such a bench; a very uneven surface may require filling or can cause higher equipment maintenance costs. Furthermore, blockage or collapse of drillholes may occur in a subsequent blast due to fractured areas in the remaining bench [34,48].

2.3. Explosive Energy Distribution

The topic of explosive energy distribution (EED) was already touched upon in Section 2.2 to explain the connection between drillhole deviations and blast performance. Although this relationship is closely linked to the spatial energy distribution, the significance of explosive energy partitioning should not be underestimated either. A lot of effort is put into the quantification of the various types of energy that result from the detonation of explosive charges. Although the theoretical energy contained in the explosives can be easily calculated, it remains challenging to find clear fundamental relations to the utilization of this energy when the charges are detonated. Although the principle of attenuation provides some theoretical starting points for the behavior of explosive energy in a spatial sense, reality often presents a different situation. Various empirical methods have been developed for the quantification of physical properties around blastholes. Unfortunately, most of these are focused on effects further away from the explosive charges. Since this research is only interested in the explosive energy distribution close to the blasthole, the formula developed by [49] will play an important role.

2.3.1. Explosive Energy Partitioning

The fundamental blast design principles presented in Section 2.1 have mostly been established by trial and error, leading to the described empirical relations. This was necessary because the connection between explosive charges and fragmentation is poorly understood. This will of course partly depend on the rock mass characteristics, which greatly complicate research, but a better understanding of this relationship could be quite valuable. An important step in this is to consider the conversion of energy stored in explosives to the other forms of energy resulting from its detonation. Numerous investigations have been performed on this topic, of which this section will provide a brief overview.

With the chemical composition of the explosive and its reaction products known, the heat of the reaction can be calculated, which represents the difference in internal energy associated with this state change. It then follows that the detonation energy, or heat of detonation, is defined as the portion of the explosive's heat of reaction that is going towards its reaction products. Notably, the heat of any secondary reactions of the explosive or its products (e.g. with air) are excluded. Although these thermodynamic calculations provide a good estimate of the energy from a detonation, in reality, it can be quite different due to the dependency on temperature, volume, and pressure during the reaction, which are influenced by the properties of both the explosive and the surrounding rock mass. The main principle behind the detonation of an explosive is to use the resulting energy to perform expansion work on the borehole wall, which ideally should be close to equal to the detonation energy. It was found that the expansion work is positively correlated with the explosive's velocity of detonation, whereas a smaller hole diameter will cause a reduction [50].

These thermodynamic principles of explosive detonation are quite clear, but the real problem lies in determining how exactly the expansion work energy is transferred to the rock mass in order to break it up. An important differentiation can be made between shock energy and heave energy; the former is mostly aimed at creating new fractures in the rock mass, and benefits from explosives providing high peak pressures, while the latter is used to extend fractures and move the rock mass by maintaining higher gas pressure. Furthermore, some energy is lost to undesirable effects like flyrock, noise, ground vibrations, air blast, and heat [4].

The inability to measure certain types of energy makes it challenging to quantify the different factors in the energy balance. Nevertheless, this makes it a contested research topic. Spathis [51] first defined the energy balance of a blast as follows:

$$E_E = E_F + E_S + E_K + E_{NM} \tag{2.1}$$

with E_E as the explosive energy, E_F as fragmentation energy, E_S as seismic energy, E_K as kinetic energy, and E_{NM} as non-measured energy. The percentage of heat of explosion this total energy represents ranges from 12 to 40% after conversion [51,52]. Sanchidrián et al. [52] mimic this approach, but incorporate fragmentation energy calculations based on the surface area of the fragments, estimated from particle-size distributions according to [53], and calculate seismic energy from seismograph readings and kinetic energy from initial velocity captured by high-speed video cameras. They determined that the total measured energy amounts to 8-26% of the heat of the explosion, leaving at least 3/4th of the explosive energy unaccounted for. Although the ranges of figures found for the individual energy components are quite narrow for the fragmentation energy and seismic energy (2-6% and 1-3% respectively), the calculated kinetic energy varies significantly, ranging between 3 and 21% [52]. It should be noted that Spathis [51] reported even higher kinetic efficiencies, up to almost 40%.

Zhang [54] recently expanded the energy balance by adding rotation energy (E_R), internal fracture energy (E_{IF}), and gas energy vented to the atmosphere (E_{GE}) as factors that could technically be measured or reasonably estimated. Moreover, the remaining energy forms were identified as the energy used in borehole expansion (B_{BE}), heat consumed in heating the rock mass (E_{HR}), friction energy lost due to cracks influencing stress wave propagation (E_{FE}), and other forms of energy (E_{OF}), like radiation, plastic work, and acoustic energy, which were all grouped as E_O to produce Equation (2.2).

$$E_E = E_F + E_S + E_K + E_R + E_{IF} + E_{GE} + E_O \tag{2.2}$$

It was observed that fragments do not fly following a blast, but rotate instead. E_R could be calculated by making the assumption that all fragments are differently-sized spheres. Although E_{GE} technically includes energy loss due to escaping gas through joints, broken rock mass, and stemming, the method suggested by [54] only estimates the last-named situation by measuring gas pressure close to blasthole collars. A suitable technique to measure and calculate E_{IF} is not yet found, but it could technically be estimated by measuring the surface area or volume of internal cracks in rock fragments.

2.3.2. Spatial Energy Distribution

Similar to the intricacies of explosive energy partitioning, determination of the spatial energy distribution is also challenging. Naturally, this is partly due to the knowledge gaps discussed in Section 2.3.1, but even if the useful energy provided by explosives was known, its propagation through the surrounding rock mass poses another challenge. First of all, a theoretical basis for this will be given by reviewing the principle of attenuation, followed by a brief overview of empirical equations that can be used to characterize physical properties as a function of radius around blastholes. Finally, the explosive energy distribution formula that represents the main concentration of this research will be presented.

Attenuation encompasses the physical phenomenon of a signal being reduced in amplitude or intensity the further it moves away from the source. If the source is considered to be the explosive detonation, and the shock wave is the signal, it follows that the amplitude of the resulting pressure wave is reduced as it propagates through the surrounding rock mass. This has four major causes; geometric spreading, dispersion, reflection at acoustic boundaries, and damping.

Geometric spreading is the only factor that involves the geometry of the charge and relates amplitude to radius away from the source by a factor $1/R^n$. For homogeneous materials, n equals 2. In real rock masses, however, this assumption of homogeneity is invalid. This causes not only the amplitude to decrease as a wave propagates away from its source, but also the overall wave energy. According to the principle of dispersion, the velocity of a wave is proportional to its frequency. Since the high-frequency components of the amplitude peak travel slower than the low-frequency components, the wave becomes longer with lower peak amplitude. Because the energy contained in the wave is proportional to the amplitude squared, the energy pulse will be smaller. Due to joints and other discontinuities in a rock mass, waves are reflected at these boundaries. Although part of the wave's energy does not necessarily leave the system, it will not continue along the same path. The proportion of transmitted and reflected part of the wave depends on factors like the angle of incidence and properties of the media at either side of the interface. Finally, damping occurs as work performed by the shock wave as it moves through the rock mass. This may cause molecules and atoms within the material to move, most often simply producing heat. Furthermore, it can lead to elastic or plastic deformation, fragmentation, or ultimately, changes of state [55].

A number of empirical equations have been developed to express the effect of detonated blastholes on the surrounding rock mass. Unfortunately, most of these relationships are only applicable on intermediate distances with the purpose to prevent undesired damage. Because the focus of this thesis is on the energy distribution within a blast, these will be discussed only briefly. A very general method is the definition of blast damage transition zones. Depending on the rock strength, 'crushed', 'fractured', and 'influenced' damage zones can be assigned. For ANFO in medium strength rock, for example, the crushed zone is assumed to reach from the blasthole up to 6 times the hole diameter, followed by the fractured zone up to 15 times the hole diameter, and finally the influenced zone up to 60 times the hole diameter. These boundaries correspond to the peak particle velocities (PPV) of 20, 5, and 1.5 m/s respectively [4].

The PPV indicates how fast particles in the rock mass move, and it follows naturally that a higher value will cause more deformation or breakage. Many different methods have been developed to estimate the extent of the damage zone, considering the PPV (e.g. [56,57]). However, at small distances to the blasthole, these equations return extraordinarily high values that seem to have little relevance for determination of the explosive energy distribution within blasts, since their main purpose is to estimate the extent of damage or length of cracks. Furthermore, PPV can be related to the scaled distance, which is a factor obtained by multiplying the radius to the blast hole with the square root of the powder factor [58]. A different approach can be found in relating pressure to the distance to the blasthole. This takes its main input from the borehole pressure, which is assumed to be equal to the detonation pressure [59].

Although these empirical relationships can be valuable for a better understanding of physical properties in the vicinity of blastholes, they do not directly address spatial energy distribution. This will be calculated using the empirical equation for 3D explosive energy flux developed by [49]:

$$P = \int_{L_1}^{L_2} \frac{1000 \cdot \rho_e \cdot \pi \left(\frac{D}{2}\right)^2}{\rho_r \cdot \frac{4}{3}\pi \left(h^2 + l^2\right)^{\frac{2}{3}}} dl \tag{2.3}$$

This equation considers an infinitesimal charge segment dl and can be used to calculate the resulting explosive concentration, or powder factor, at any point P near a column charge. After integration, this equation can be rewritten to:

$$P = 187.5 \cdot \frac{\rho_e}{\rho_r} \cdot D \cdot \frac{1}{h^2}\left(\frac{L_2}{r_2} - \frac{L_1}{r_1}\right) \tag{2.4}$$

in which ρ_e and ρ_r represent the explosive density and rock density respectively, D is the drillhole diameter, and h the horizontal distance between P and the blasthole. L_1 and L_2 correspond to the extent of the explosive column that is above and below the elevation of point P, and the three-dimensional distances from P to the top and bottom of the column charge are identified as r_1 and r_2. A visual representation of these variables is given in Figure 2.7. To incorporate the effect of timing delays between the detonation of explosive decks, the following weighting factor may be added for every deck in the timing simulation:

$$e^{\frac{-|t_d - t_{nd}|}{t_c}} \tag{2.5}$$

in which t_d is the time the deck is detonated, t_{nd} is the time the nearest deck is detonated, and t_c is the cooperation time, a rock mass-specific factor [60].

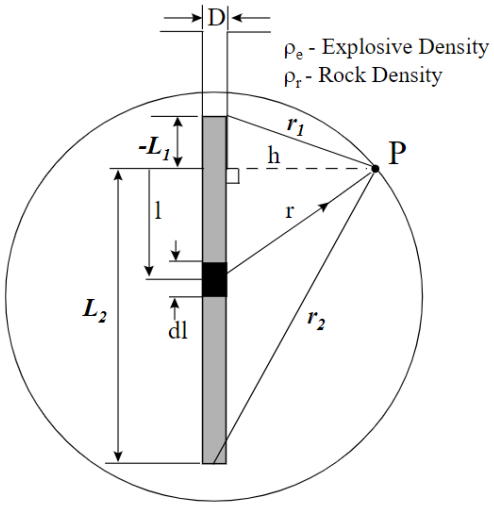

Figure 2.7: Variables for calculation of explosive energy concentration at point P [60].

2.4. Optimization

Optimization can be described as the evaluation of numerous elements with the goal of finding the best option available, according to a specified criterion. The possible alternatives are often solutions to complicated problems that are difficult to solve analytically. By choosing input values for variables that lie within set boundaries, different outcomes to a function that represents the optimization criterion are calculated. The most common goals are finding either the lowest or highest outcome of this objective function, known as the objective value, which can be described as minimization or maximization respectively. The configuration of the variable input values, or decision variables, that leads to the most suitable objective value is then identified as the optimal solution. A wide variety of optimization methods exist that each applies a different procedure or algorithm to find optimal solutions. Some of these can be applied universally, while others are specifically designed for a particular problem.

The two methods considered in this thesis are Genetic Algorithm (GA) and Tabu Search (TS), which are both parts of the metaheuristics group of optimization methods. Although metaheuristics do not necessarily find the very best solution, these are practical algorithms that are able to solve problems more quickly than pure mathematical optimization or provide approximate solutions when exact ones can not be achieved. By trading some optimality for speed, the solution search space is explored efficiently with the goal of finding near-optimal solutions. How exactly this is performed, depends on the selected algorithm. An important characteristic of metaheuristic methods is that they are not problem-specific, but instead can be easily applied to a wide range of optimization problems [61].

2.4.1. Genetic Algorithms

As with many metaheuristics, Genetic Algorithms take inspiration from a process observed in nature. Originally created to simulate biological evolution, Genetic Algorithms make use of a number of mechanics observed in the evolution of species. An iterative process is used to sample candidate solutions from an evolving ‘population’. Through recombination and/or mutation of the best-fitting solutions, succeeding evolutionary generations exploit the positive attributes of the various solutions while discarding the unfavorable ones. In line with Darwin’s theory of natural selection, the fittest individuals have increased chances of survival and reproduction, while the weaker portion is unlikely to endure the evolutionary process. In this analogy, the optimization problem represents the environmental factors to which the individuals must adjust. The individuals are often known as chromosomes and form an encoded representation (genotype) of the candidate solutions (phenotype). Their fitness is evaluated based on the objective criteria of the problem, which is then used to select individuals suitable for breeding. New individuals are created using recombination and/or mutation to form the next generation [62].

The initial population can be composed of randomly generated solutions, in which a bias might be included to ensure sufficient diversity, or heuristic solutions, in case there is some initial information available about the problem. In the evaluation process, a fitness value is assigned to each solution. This is often directly obtained from the objective function and will play an important role in deciding which solutions take part in evolution. Based on their fitness, the individuals suitable for reproduction are sampled from the population in a selection procedure. The most common selection operator methods include:

- Roulette-wheel; assigns selection probabilities, or roulette portions, proportional to the fitness of solutions. The roulette is performed as many times as necessary to obtain the required number of solutions.
- Stochastic universal selection; a modification of the roulette-wheel method. To reduce the chances of selecting the best individual too often, multiple spinners select the required number of solutions at once.
- Tournament selection; a number of individuals are randomly chosen from the population, and only the best is selected for reproduction.

The components responsible for the creation of new candidate solutions are the crossover and mutation operators. The solutions sampled by the selection operator are first subjected to crossover, which entails the combination of solution information stored in multiple individuals to produce offspring. With the encoded representation of a solution being a chromosome, this makes the elements of which it is built up the genes. Examples of the simplest crossover operators are listed in Table 2.3. Additional techniques exist for more complicated cases, but these will be left out of consideration here.

Table 2.3: Crossover operator examples with binary parent chromosomes P_1 = [0 1 1 0 1 0 0] and P_2 = [1 1 1 1 0 0] [62].

Name	**Intermediate steps**			**Result**
One point Crossover	Cut point 4	Heads [0 1 1 0 [1 1 1 1	Tails 1 0 0] 0 0 1]	Offspring [0 1 1 0 0 0 1] [1 1 1 1 1 0 0]
Uniform Crossover		Genes from P_1 1, 3, 5, 6	Genes from P_2 2, 4, 7	Offspring [0 1 1 1 1 0 1]
Half uniform Crossover	Differences 1, 4, 5, 6	Genes from P_1 4, 5	Genes from P_2 1, 6	Offspring [1 1 1 0 1 0 1]

After crossover, the individuals of the new generation may be mutated. Mutation operators are applied according to mutation probability, which can be evaluated at either the chromosome level or gene level. In the first case, each chromosome is only mutated once, the second case considers each gene individually and may thus result in multiple mutations per chromosome. The most common mutation operators include flipping of binary values, swapping of genes, reordering, insertion, or sublist inversion [62].

The next design consideration for Genetic Algorithms is the replacement strategy. Traditionally, Genetic Algorithms apply a generational evolution principle, which means that every subsequent population is entirely generated from the current one. In this configuration, it might occur that the new population is worse in terms of solution quality. To prevent this, the best solution from the current population can also be included, for a model called generational evolution with elitism. Another approach is the use of a steady-state strategy, in which new solutions, often just one, compete to enter the population according to set replacement strategies. Usually, the worst solution is discarded if the new one is better. Finally, a stop condition must be chosen. This is usually set by a maximum number of generations, processing time, or fitness criteria [62].

Genetic Algorithms are generally well-suited for finding good global solutions. An intricate balance exists between diversification (exploring the search space) and intensification (finding better solutions in a promising region). Although the diversification component of Genetic Algorithms can be very useful, and many techniques exist to augment this, they are quite inefficient at finding the absolute optimal solution in a small region based on mutations alone. Therefore, the combination of Genetic Algorithms with other optimization methods can be very effective.

2.4.2. Tabu Search

Tabu Search is a local or neighborhood search procedure that starts from a single initial solution. The solution space is explored by consideration of neighboring solutions corresponding to minor transformations of the initial solution. To increase efficiency, it may be worthwhile to consider only the value of the moves to neighboring solutions instead of computing the complete objective value for each. Tabu Search belongs to the family of single-solution searches as opposed to population-based methods like genetic algorithms. It differs from pure local search in the ability to accept worse solutions; in case none of the neighbors provide an improvement, a move to a solution of lower quality is permitted, which allows Tabu Search to depart from local optima.

The second mechanic that promotes this, is the introduction of restrictions on recently visited solutions. To avoid cycling between the same two neighboring solutions over and over, previously visited solutions are considered ‘tabu’ (The Tongan word for ‘prohibited’ or ‘forbidden’). Consequently, solutions that have been visited previously are considered tabu-active, and will not be part of subsequent solution neighborhoods. All tabu-active solutions or attributes are placed on the tabu list, usually with a predefined expiration time known as tabu tenure. After a sufficient number of iterations has passed, corresponding to this tabu tenure, the item will be removed from the tabu list and may be considered again as a suitable neighbor. Tabu tenure can be static or dynamic, and the tabu status of an item may be overwritten subject to aspiration criteria, e.g. when it would result in a better solution than the best so far [63].

The tabu list represents short-term memory, and although this alone can be sufficient to achieve good solutions, implementation of long-term memory can have beneficial effects on both intensification and diversification. High-valued attributes may for instance be identified by their occurrence in solutions of high quality, or how often they enter or leave the visited solutions. This information can then be used to introduce a bias towards promising regions of the solutions space, or to create a new initial solution. Similarly, attributes that deteriorate the solution quality could be penalized. Diversification rules may be applied in case the search becomes stuck in a local optimum. More advanced methods include strategic oscillation, which allows for small deviations from constraints by moving back and forth across the feasibility boundary, or path relinking, which makes use of guiding solutions to explore trajectories between e.g. high quality or diverse solutions [63].

2.5. Mining Activities in Nevada, USA

Before discussing the common blasting practices observed in Nevada, some general details about the current state of mining in this area will be helpful. Traditionally known as the 'Silver State' thanks to a rich history in the production of mineral commodities, Nevada represents an important mining region. The glory days of digging up enormous amounts of silver may be long gone, but the mining business is still booming thanks to the other precious metal found in the rocks below the dry deserts: gold. Largely thanks to the discovery of Carlin-type gold deposits, which were not exploited on a significant scale until the early 1960s, today Nevada gold mines are responsible for the lion's share of US gold production; in 2019, more than 4.8 million ounces of gold accounted for roughly 83% of the national output. The majority is supplied by Nevada Gold Mines, a joint venture between mining giants Barrick Gold and Newmont Corporation. Their 8 operations combined produced almost 3.7 million ounces last year, making up 75% of the state's total, and forming the world's largest gold mining complex. In terms of reserves, this region is only surpassed by South Africa's Witwatersrand deposits. Additionally, Nevada mines produced 6.3 million ounces of silver and over 64,000 tonnes of copper in 2019 [64–66].

It shall come as no surprise that the majority of gold in Nevada is mined from the aforementioned Carlin-type mineralizations. Named after settlements in the northeast, most gold is extracted from these deposits found in the northern half of the state, both as open-pit and underground operations. Carlin-type gold deposits are characterized by low grades of extremely fine-grained gold. Despite their low grade, large amounts of gold can be extracted thanks to the size of these deposits, which allows for large open-pit operations. Microscopic amounts are found in disseminated pyrite, or hematite when oxidized, hosted in limestones with significant clay content. The mineralization depends on both local fault structures that allowed hydrothermal fluids to move upwards, as well as the favorability of the various stratigraphic layers. Combined with displacement by new faults, this makes exploration very challenging [67].

The ore bodies in Nevada are generally characterized by a very discontinuous grade distribution. Because there is often no clear geological distinction between ore and waste, a lot of effort is put into grade control. The drilling and blasting operations also play an important role in this. Ore regions are defined using blasthole assays, and blast patterns are designed for optimal grade control by minimizing forward rock movement. This often differentiates blasting practices in Nevada from the standard open-pit blasting concepts laid out in Section 2.1.1.

A 2003 survey of 25 mines by the Mining Engineering department of the Mackay School of Mines, University of Nevada, Reno, found that mines in Nevada use relatively short and small benches, averaging only 7.3 m in height. Although a minimum bench height-to-burden ratio K_H of 1.6 is generally recommended, the average value found in Nevada is 1.44 [4]. Blast hole diameters range from 171 to 251 mm, with 171 mm as the most common size, and the average burden is 5.12 m. With the exception of only a single mine, the spacing is always equal to the burden. The stemming-to-burden ratio K_T averages 0.8, and the stemming material mostly consists of drill cuttings. Square blast patterns are strongly favored as opposed to staggered patterns, despite the fact that the staggered layout produces a more efficient energy distribution [8,9]. Because of the high requirements for grade control, simple assignment of grades to square areas corresponding to the blasthole assays is preferred.

Most mines use a relatively short row-to-row delay for sequencing, in order to minimize forward rock movement during the blast. For the same reason, most faces are choke- or buffer-blasted. The most popular explosive is ANFO, due to its low costs and favorable rock conditions; the rock mass is often very weathered and fractured, and therefore much use is found in the high proportion of gas energy offered by the low-density ANFO. These rock conditions play an important role in some of the blast design decisions. Because it is relatively easy to achieve good fragmentation, this allows for more emphasis on grade control. The techniques applied in Nevada can therefore not easily be carried over into circumstances that require more attention to good fragmentation. It should also be noted that most of the surveyed mines use heap-leaching processes instead of milling circuits, which may reduce the importance of good fragmentation. Another striking difference is that Nevada mines tend to fire blasts on a daily basis, compared to once or twice a week for many large operations elsewhere. Whereas most other mines stick to the principle of blasting with patterns as large as possible, the orebodies in Nevada seem to require more flexibility in material loading schedules for optimal grade control [9].

2.6. Synthesis

There is a long history in the design of production blasts in open-pit mining, which has led to numerous guidelines to achieve efficient blasting. The foundations of this, however, still rely on empirical relations that were established decades ago. Due to site-specific rock mass characteristics, blasting at each individual mining operation is then generally tweaked by trial-and-error. This may cause blasting engineers to stick with ‘what works’, which means blast performance can in fact be suboptimal. Blast designs in Nevada notably differ from the practices followed by most other mining operations in the rest of the world, in a number of ways.

A major reason for this is the relatively weak and fractured rock mass encountered, in combination with high grade control requirements. Although inconsistency in rock mass properties remains a challenge, it would be helpful to the industry to improve the process of blast design by using a more theoretical approach that also works in practice. A potential foundation for this is the understanding of the behavior of explosive energy in blasted rocks. Research into the area of explosive energy partitioning could provide valuable insights, but quantification of the various energy forms in a mining blast has proven to be highly challenging. Evaluation of the spatial energy distribution is generally focused on smaller effects far away from blastholes, e.g. for determination of the extent of the damage zone using peak particle velocities, rather than its behavior inside the blasted zone.

Besides the geometric considerations of a blast pattern, another design tool is the type of explosive used. Due to the infrastructure requirements and associated costs for using multiple different products, many mining operations are limited to using only one type of explosive, or perhaps a small selection. More flexibility in this area may be beneficial to tailor the requirements for each blast.

Although some procedures are in place to ensure that drilling and charging of blastholes are performed according to plan, a certain margin of error is accepted. Unless significantly reduced blast performance is observed, one must generally be satisfied with ‘good enough’. Because of similar standards used in the design of a blast, small margins of error could be seen as insignificant for overall blast performance. Deviation of drillholes from their planned location and trajectory has a wide variety of causes, most importantly human errors and GPS positioning accuracy.

Recent developments in drilling automation provide a mitigating solution, but these new technologies may not yet be affordable to all mining companies. Though the accuracy of GPS positioning has improved over the years, deep open-pit mines nevertheless remain a challenging environment. Despite technological advances, 100% accurate drilling is difficult to achieve, and collaring deviations are to be expected. Drilling accuracy is currently obtained by comparing GPS coordinates of the real drillhole locations with those in the drilling plan. While this method can be used to capture major components of drillhole deviation, errors in GPS positioning are still not included. MWD data is increasingly utilized to assess blasting requirements, but the available information on horizontal drillhole deviations is rarely used directly for this purpose.

Research into the consequences of drillhole deviation reveals that it can have a significant influence on operational costs of a mining operation, stressing the importance of recognizing and addressing this issue. In addition to its impact on safety, the effects of suboptimal blast performance can quickly propagate to subsequent steps in the mining process, decreasing overall efficiency and increasing costs in a variety of ways. The most desirable means to control these negative effects is of course the elimination or reduction of drillhole deviations. Because improvements in this area are costly or technologically challenging, it is worthwhile to consider alternative solutions that aim to mitigate this issue in a different way.

Although redrilling of strongly deviated drillholes is common practice and normally beneficial to blast performance, this is not possible in all cases and will lead to additional costs as well as potential production delays. However, further improvements might be achieved by instead focusing on other blasting variables like the loaded explosives. To achieve more consistent blast performance, it is essential to bring the characteristics of a real blast as close as possible to those of the planned configuration. A new method to assess this aspect is found in the comparison of spatial explosive energy distributions corresponding to both the planned and real drillhole locations, which can be obtained using the EED formula developed by [49].

By making adjustments to the height of the explosive column in drillholes, the explosive energy in the surrounding rock mass can be altered accordingly. In order to find the charging specifications that result in the largest improvement, a blast model can be subjected to optimization. Although the application of mathematical programming using e.g. the GUROBI solver is not possible due to the complexity of the EED formula, metaheuristic methods like Genetic Algorithm and Tabu Search are identified as potentially meaningful alternatives to achieve (near-)optimal solutions to this problem. An optimization program following such an approach could directly allow real blasts containing deviated drillholes to resemble the original blasting plans more closely. While the primary intent of this is to mitigate the adverse effects of deviated drillholes on blast performance, improved consistency in blasting may also be beneficial to future research on the discussed topics of blast design and energy partitioning.

3

Methodology

This chapter presents the details of the research approach by describing the specifications of the explosive energy distribution optimization system that is used to answer the research questions of this thesis, and how it can meet the additional objectives listed in Section 1.4. Besides offering the general characteristics of the constructed model in Section 3.1, a number of key control parameters are identified in Section 3.2. Following this, Section 3.3 delineates how the selected optimization methods are applied to this model, and Section 3.4 presents a simplified version of the written Python code.

3.1. Model Design

For an appropriate representation of the explosive energy distribution around blastholes, the surrounding area, corresponding to the rock mass of a bench, is discretized as a block model. Using the formula developed by [49], as presented in Section 2.3.2, the explosive energy distribution throughout the blast area is modeled. By evaluating this function for all blocks in the block model, each block is assigned a calculated EED value based on various geometric measures relative to the explosive column in the blasthole. Additional inputs for this formula are the explosive density, rock density, and drillhole diameter. For the rock density, a standard assumption of 2.65 g/cm^3 is made for limestone. The remaining parameters are dependent on the blast design and are assigned according to the datasets introduced in Chapter 4. The weighting factor for timing delays is not included, because the rock mass' cooperation time is unknown and delay timings are not provided in the datasets.

Evaluation of the EED formula across the block model is not limited to a single pass; in order to compare the influence of charge adjustments on the explosive energy distribution, it is necessary to recalculate it multiple times for different configurations of the blastholes and their charging instructions. Therefore, every block in the block model will contain the following data entries, that each corresponds to a distinct blasthole setup:

- Planned EED
- Real EED
- Optimized EED

The planned EED represents the explosive energy distribution calculated using the planned x-, y-, and z-coordinates of the drillholes, in combination with the planned charging instructions. The real EED denotes the explosive energy distribution that is computed from the blasthole configuration in which the drillholes have deviated, or more specifically, in which drillholes' x-, y-, and z-coordinates are different from their planned values. In this case, the blasthole charging remains unchanged. This captures the explosive energy distribution achieved if no charge adjustments are made, corresponding to the current reality of how a blast pattern with deviated holes is blasted, meaning without EED optimization. Naturally, it follows that calculation of the optimized EED makes use of the deviated drillholes too, but is contrarily characterized by adjustments of the explosive charges in blastholes to produce a more desirable, optimized result. Whereas the planned and real EED are only computed once for a given blast pattern, the optimized EED is recalculated numerous times during the optimization process. The details of this optimization are given in Section 3.3.

For adjustments of charges during the optimization procedure, every blasthole is also discretized according to the following specifications:

- The blastholes' x-, y-, and z-coordinates do not necessarily need to coincide with the discretization grid of the block model but are simply taken as provided in the data, meaning each hole is discretized on its own grid.
- The supplied z-coordinate is used to define the upper boundary of the hole, which is combined with the drilled hole depth to determine the lower boundary. Based on these limits, and together with the given stemming height, z-coordinates are set for both the bottom and top of the explosive column.
- During optimization, charge bottom and top coordinates may be adjusted to alter the height of the explosive column, and thereby change the amount of explosives in each hole individually.
- Charge increments or reductions are subject to discrete charge segments of a specified length, which control the number of possible adjustment choices in optimization.

The implications of the selected charge segment length are discussed in Section 3.2, along with various other control parameters.

3.2. Control Parameters

When taking in mind the model design as described in Section 3.1, a number of control parameters can be identified, which are expected to affect its appropriateness in relation to reality. Although *"all models are inherently wrong, some can be useful"* [68], and assigning suitable values to these parameters is essential to achieve at least a degree of consistency, as well as a more accurate representation of real blasts. A general overview will be given of the influence of these control parameters on the model, the optimization process, and its results. This is complemented by a listing of selected options for consideration, and the necessary steps going forward to determine the best choice for each parameter.

Block size

The explosive energy distribution formula used in this thesis is assumed to be the most important factor of accuracy in the approximation of reality, and the block size should be a close second. The small cubes that constitute the block model together cover the whole area of interest for the EED calculations.

Their size plays a critical role in the level of detail that is achieved since it determines the interval at which calculations are made. Ideally, the block size should therefore be as small as possible, to capture the continuous relationship between distance from a blasthole and the corresponding EED value with the highest accuracy. However, the available computational power is a highly constraining aspect to this, since the amount of required calculations increases rapidly; for every halving of block size in x-, y-, and z-direction, the total number of blocks, and therefore also the necessary calculations, increases by a factor $2^3 = 8$. This often means that concessions must be made in the balance between accuracy and computation time. For selection of the most suitable discretization of the block model, block sizes of 1.0, 0.5, 0.2, 0.1, and 0.05 m will be considered. By comparing the block models that result from a number of small-scale tests with these varying block sizes, a choice will be made for the option that combines modest differences with respect to smaller block sizes with acceptable computational requirements. It should be taken into account that the optimization process involves many recalculations of the EED, which will act as a multiplicative factor to computation times.

Search radius

The explosive energy distribution formula can be evaluated for all points, or blocks, at an arbitrary location relative to a blasthole. As the distance towards a blasthole increases, however, the calculated EED values will become smaller and smaller. The total number of calculations can be reduced by ignoring very low-valued blocks. Because the assigned EED values are proportional to distance away from a blasthole, this is achieved by setting radius limits based on the holes' coordinates. Thus, only the blocks that lie within this search radius around a blasthole are subjected to the EED calculation that takes the explosive column in that particular hole as input.

Since the Euclidean distance between each block and its nearby blastholes, in the horizontal plane, is already one of the geometric measures required for the EED calculation, this can be easily incorporated as a filtering operation before its corresponding value is determined by the EED formula. To reduce the computational requirements, a one-time minimum/maximum x- and y-coordinate filter is passed over the whole block model to ignore the blocks that are not within the range of any drillhole, before computation of the geometric distances is started. An appropriate search radius will be chosen by comparing values calculated at the radius around a single blasthole, which should be of insignificant magnitude compared to the highest values found in its vicinity. This ensures that blocks outside of the search radius represent a very small contribution to the overall explosive energy distribution, and can therefore be neglected to improve performance in terms of computation time.

Charge segment length

As explained in Section 3.1, the explosive column of every blasthole is divided into charge segments to define the possible adjustments that will be considered in the optimization. The length of these charge segments, therefore, influences the number of presented adjustment choices. However, it appears unlikely that adjustments towards either a blasthole entirely filled with explosives at the expense of stemming, or a completely uncharged blasthole would be beneficial for the explosive energy distribution. Instead, relatively small adjustments are expected that tweak the energy output. This makes the choice for a suitable charge segment length mainly a consideration about the desired level of detail; with smaller charge segment length, the resulting explosive energy distribution can be adjusted with more precision, which in turn facilitates the correction of smaller deviations in drillhole location.

The other side of this story is the practicality of charge adjustments. Corrections to the height of explosive columns must be practically achievable by the crew and machinery responsible for loading the blasthole. If they are unable to operate at the same level of detail as the selected charge segment length, the advantages of this optimization program would be limited. Moreover, alteration of charge height in a majority of the holes would also be undesirable. The objective is to choose a charge segment length that results in an appropriate amount of targeted adjustments. The investigated options are the 10 cm intervals from 0.1 to 0.5 m.

EED cap

The deviation of drillholes naturally causes the spatial energy distribution throughout a blast to be altered. The resulting differences between the real and optimized EED with respect to the planned EED should reflect this. However, when the EED values are compared on a block-to-block basis, this leads to disproportionately large differences in the blocks nearest to blastholes; a block within close vicinity in the planned configuration will receive a very high EED value, but is assigned a much lower value if the hole's real location is further away. Although the goal of the explosive energy distribution optimization is to reduce these differences, which will be further elaborated on in Section 3.3, some block-to-block variations may be too large and can not be compensated in a sensible manner. Instead of trying to account for extraordinarily high values, optimization should focus especially on the areas that receive relatively small amounts of explosive energy. To accomplish this, an EED cap is applied; the values of all blocks above a certain threshold will be ignored. For a more generalized approach, this threshold is determined by selecting a percentile of all planned EED values in the block model, instead of an arbitrary number specific to each blast. The most suitable percentile is chosen by evaluating the relationship between various charging adjustments and percentiles at 10% intervals.

3.3. Optimization

Once the explosive energy distribution model is constructed, optimization methods can be used to find the best solutions to the problem. What exactly differentiates a good solution from a poor one, is determined by the optimization objective. This is defined in the objective function, which may be subject to constraining requirements. Through repeated evaluation of these equations, following different adjustments of charge height in the blastholes, the solution that leads to the best objective value is identified as the optimal solution. Mathematical optimization using e.g. the GUROBI solver was quickly found to be unsuitable, because it is unable to deal with the required geometric calculations depending on the adjustable height of the explosive column. Instead, metaheuristic algorithms are applied. The selected methods, Genetic Algorithm and Tabu Search, were chosen for their straightforward representation and use of the charge height decision variables. Furthermore, these options facilitate comparison between either a more global or local search approach to this problem. The possibility of a hybrid method that combines Genetic Algorithm and Tabu Search will also be investigated.

Decision variables, objective function, and constraints

Optimization of the explosive energy distribution will be performed through adjustment of the explosive charges in drillholes. To accomplish this, the decision variables must represent the top and bottom z-coordinates of the explosive columns in all drillholes DH (Equation (3.1) and Equation (3.2)). Their initial values are assigned based on the equivalent z-coordinates of the charges in the real EED drillhole configuration, $z_{charges,\,i}^{top,\,real}$ and $z_{charges,\,i}^{bottom,\,real}$. During optimization, the decision variables are adjusted by increments of a discrete charge segment length, as discussed in Section 3.1 and Section 3.2.

$$x_i^{top} \text{ for } i = 1, 2, ..., n \in DH \tag{3.1}$$

$$x_i^{bottom} \text{ for } i = 1, 2, ..., n \in DH \tag{3.2}$$

The goal of this optimization is to bring the explosive energy distribution corresponding to the actual drillhole locations more in line with values produced by the planned configuration. This is achieved by minimizing the absolute block-to-block differences between the planned EED and optimized EED. The real EED represents the initial solution and remains stored in the block model for comparison with the optimized EED once optimization is completed. The planned EED and real EED values will not change throughout the optimization, but the optimized EED is updated every iteration by making adjustments to the charges in some of the blastholes. The EED calculations for each individual block use a variety of information specific to the drillholes for which it is located within the search radius. While the top and bottom z-coordinates of the explosive columns remain constant for the planned EED, calculation of the optimized EED takes the decision variables x_i^{top} and x_i^{bottom} as input instead. The objective function is then defined as Equation (3.3). For convenience, the retrieved objective values are expressed as the arithmetic mean of the differences, denoted by $\overline{Z}$.

$$min\ Z = \sum_{i=1}^{DH} \sum_{j=1}^{N_p} \left| E_j^{planned}\left(DH_i^{planned}\right) - E_j^{optimized}\left(DH_i^{real},\ x_i^{top},\ x_i^{bottom}\right) \right| \tag{3.3}$$

in which

N_p = All blocks in the block model within the lower p-th percentile of EED values

$E_j^{planned}$ = Planned EED value of block j, from EED formula taking $DH^{planned}$ as input

$E_j^{optimized}$ = Planned EED value of block j, from EED formula taking $DH^{optimized}$ as input

$DH_i^{planned}$ = All information regarding planned drillhole i
hole location x- and y-coordinates, bottom and top of hole z-coordinates,
bottom and top of explosive column z-coordinates, explosive density,
and hole diameter

DH_i^{real} = All information regarding real drillhole i;
hole location x- and y-coordinates, bottom and top of hole z-coordinates,
explosive density, and hole diameter

Equation (3.4) and Equation (3.5) ensure that no charge adjustments can be made beyond the boundaries of the drilled blasthole; because of simple physical restrictions, the explosive column must not be able to extend below the drilled hole depth or above the collar elevation. Equations (3.6) to (3.8) constrain the charge adjustments to reasonable alterations. In some cases, drastically reducing the explosive column height may be beneficial for the objective value. The limit for reasonable adjustments is

chosen as half the stemming height, in both the upward and downward direction relative to the original z-coordinates of the explosive column.

$$x_i^{top} \leq z_{drillhole,\,i}^{top,\,real} \text{ for } i = 1, 2, ..., n \in DH \tag{3.4}$$

$$x_i^{bottom} \geq z_{drillhole,\,i}^{bottom,\,real} \text{ for } i = 1, 2, ..., n \in DH \tag{3.5}$$

$$x_i^{top} \leq z_{charges,\,i}^{top,\,real} + \left(z_{drillhole,\,i}^{top,\,real} - z_{charges,\,i}^{top,\,real}\right)/c_{lim} \text{ for } i = 1, 2, ..., n \in DH \tag{3.6}$$

$$x_i^{top} \geq z_{charges,\,i}^{top,\,real} - \left(z_{drillhole,\,i}^{top,\,real} - z_{charges,\,i}^{top,\,real}\right)/c_{lim} \text{ for } i = 1, 2, ..., n \in DH \tag{3.7}$$

$$x_i^{bottom} \leq z_{charges,\,i}^{bottom,\,real} + \left(z_{drillhole,\,i}^{top,\,real} - z_{charges,\,i}^{top,\,real}\right)/c_{lim} \text{ for } i = 1, 2, ..., n \in DH \tag{3.8}$$

In the above equations, c_{lim} is a selected charge height limit constant, and z represent z-coordinates at various positions in the blastholes. Choosing $c_{lim} = 2$ restricts the maximum charge adjustment in a hole to half the stemming height, as previously specified. Taking this into account, Equation (3.4) becomes redundant. This constraint will only be applicable when a c_{lim} smaller than one is used. A 4th charge adjustment limit constraint addressing the maximum reduction of the bottom z-coordinate of the explosive column is not required; all holes are filled to the bottom of the hole in original charging plans, and therefore Equation (3.5) suffices. When optimization exclusively considers adjustments to the top of the explosive column, Equations (3.5) and (3.8) are no longer necessary.

The total amount of explosives used in the blast may be restricted by applying Equations (3.9) and (3.10), in which $c_{allowance}$ regulates the maximum oscillation around the planned quantity of explosives, $l_{segment}$ is the charge segment length, D the drillhole diameter, and ρ_e the explosive density. To ensure the amount of explosives remains equal to the planned quantity, $c_{allowance}$ must simply be set to zero. However, when this constraint is applied as such from the start of optimization, every individual charge adjustment will automatically be infeasible. In order to allow progression by making subsequent charge adjustments, the total explosives quantity should be allowed to deviate slightly from its planned value.

By setting $c_{allowance}$ initially to a value of three, and considering the planned explosives quantity as the perfect zero-balance, the explosives quantity balance is allowed to move between -3 and +3, corresponding to three excess reductions or increases by one charge segment length respectively. Although this balance is forced back to zero at the end of optimization to realize an equal amount of explosives as in the planned configuration, some freedom is necessary during optimization to obtain better solutions. Once optimization is finished, the forced zero-balance explosives quantity solution is compared to the best zero-balance solution encountered throughout the optimization process, and the best of the two is selected as the final solution.

$$\sum_{i=1}^{DH}\left(x_i^{top}-x_i^{bottom}\right)\times\pi\left(\frac{1}{2}D_i\right)^2\times\rho_{e,i}\leq\sum_{i=1}^{DH}\left(z_{charges,\,i}^{top,\,planned}-z_{charges,\,i}^{bottom,\,planned}+\left(c_{allowance}\times l_{segment}\right)\right)\times\pi\left(\frac{1}{2}D_i\right)^2\times\rho_{e,i}\ \text{for}\ i=1,2,\ldots,n\in DH \tag{3.9}$$

$$\sum_{i=1}^{DH}\left(x_i^{top}-x_i^{bottom}\right)\times\pi\left(\frac{1}{2}D_i\right)^2\times\rho_{e,i}\geq\sum_{i=1}^{DH}\left(z_{charges,\,i}^{top,\,planned}-z_{charges,\,i}^{bottom,\,planned}-\left(c_{allowance}\times l_{segment}\right)\right)\times\pi\left(\frac{1}{2}D_i\right)^2\times\rho_{e,i}\ \text{for}\ i=1,2,\ldots,n\in DH \tag{3.10}$$

A number of alternative optimization objectives were considered, but did not provide much perspective or advantage over the selected setup:

- Maximization of the mean block value
- Minimization of differences in EED frequency distribution
- Minimization of differences in EED frequency distribution, with a regional or global constraint for absolute block-to-block differences in EED
- Minimization of absolute block-to-block differences in EED, with a regional or global constraint for differences in EED frequency distribution

Genetic Algorithm

The Genetic Algorithm considered for the EED optimization problem makes use of generational evolution with elitism, in which alterations of blasthole charging instructions are the candidate solutions. This is encoded as lists of both the bottom and top z-coordinates of the explosive column, which together form the chromosomes. Individual hole charging specifications can then be seen as genes. Each generation consists of a population of a number of candidate solutions. The initial population includes the original charging instructions and is complemented by copies of this initial solution with randomized adjustments. For every gene, an arbitrary selection is made between a reduction or increase of one charge segment length or no adjustment at all.

The fitness of all candidate solutions is determined by evaluating the objective function for each of them, where the most suitable outcome will be saved as the best solution and is directly inserted in the next generation. The other candidate solutions for the next generation will be generated by crossovers and mutation of solutions in the current population. These parent solutions are chosen by tournament selection with three participants. Each offspring solution requires two parents, hence (population*2) - 2 tournaments are held every generation.

The cutting point for one point crossover is chosen randomly, with each parent providing opposite parts of the chromosome. Subsequently, individual genes of the offspring chromosomes are subjected to a mutation probability for a random increase or decrease by one charge segment length. This completes the advance to a new generation, which will be followed by the repetition of the described procedure until a set number of generations have passed without improvement of the best solution.

Tabu Search

Whereas the Genetic Algorithm is better suited for finding good global solutions, Tabu Search is more aimed towards a local search neighborhood to find the very best solution in a limited range. Candidate solutions are generated from direct neighbors of the current solution, which starts out with the original charging instructions as the initial one. Neighboring solutions are then obtained by the reduction or increase of one charge segment length to the explosive column of a single blasthole, for either the top or bottom z-coordinate of the charge. Repeating this for every blasthole gives all possible neighbors of the current solution.

Contrary to the Genetic Algorithm, the EED formula is not evaluated for the whole block model during optimization. Since every candidate solution only has a single charging difference compared to the current solution, the computation time is greatly reduced by considering just the altered blasthole. This is done by calculating the EED contribution of the unaltered explosive column and subtracting it from the block model, followed by the addition of the EED calculated from the adjusted charges. Once this substitution is performed for all neighboring solutions, the objective function is evaluated to determine the most suitable solution, and the current solution is moved accordingly.

The current solution is not necessarily the best solution encountered so far; if none of the neighboring solutions result in an improvement, the least deteriorating is chosen. To prevent the algorithm from immediately undoing this adjustment in the next iteration, there is a Tabu tenure of 3 iterations in place. This ensures that the Tabu Search does not quickly get stuck in a local optimum, and therefore leads to some diversification. In practice, this means that instead of undoing unfavorable adjustments, other options are explored that might produce yet a better solution, most importantly adjustments in the opposite direction in neighboring holes to account for newly introduced EED differences.

Tabu Search is stopped when a repetitive loop is detected in subsequent ‘current’ solutions, leading to no further improvements. The best solution up until this point is then taken as the result of optimization. In the rare occasion that a loop is not reached, a back-up stopping criterion is in place for 100 iterations without improvement of the best solution.

To further improve the computational efficiency, the algorithm is ‘boosted’ at the beginning by making the adjustments corresponding to the three best neighboring solutions instead of only the very best one, which greatly reduces the number of computations. This could have a minor effect on the optimization process, but adjusted holes are generally spaced far apart and therefore independent of each other. Any unfavorable adjustments are presumably corrected in subsequent iterations or once this boost is stopped, which occurs when it does not produce an overall improvement of the solution anymore.

3.4. Pseudocode

Having outlined both the characteristics of the constructed model as well as the selected optimization procedures applied to it, a general description of their implementation can be provided. The explosive energy distribution optimization system is programmed in Python 3, and this section presents a simplified representation of the written code. The first block in Figure 3.1 includes the assignment of initial design parameters derived from loaded drillhole data, construction of the block model based on planned drillhole locations, and calculation of the planned EED and real EED to find the original objective value.

```
charges_planned = load(planned_drillholes)
charges_real = load(real_drillholes)

for all drillholes in charges_planned:
    bottom_drillhole = z - depth
    bottom_charge = bottom_drillhole
    top_charge = z - stemming

create_bm(x, y, z, block_size)
select_blocks_in_range(bm, charges_planned, search_range)

planned_EED = calc_EED(bm, charges_planned, search_range)
apply_EED_cap(planned EED)

real_EED = calc_EED(bm, charges_real, search_range)
apply_EED_cap(real_EED)

best_difference = mean(|planned_EED - real_EED|)
best_solution = charges_real
```

Figure 3.1: Pseudocode for model initialization and setting the starting point of optimization.

```
initial_solution = charges_real
add initial_solution to population

add random_solutions(initial_solution, segment length) to population

for all solutions in population:
    solution_EED = calc_EED(bm, charges_solution, search_range)
    apply_EED_cap(solution_EED)
    solution_difference = mean(|planned_EED - solution_EED|)

best_difference = minimum(solution_difference)
best_solution = solution of best_difference

while not x iterations without improvement:
    start new generation
    add best_solution to population
    add offspring_solutions(crossover, mutation) to population

for all solutions in population:
    solution_EED = calc_EED(bm, charges_solution, search_range)
    apply_EED_cap(solution_EED)
    solution_difference = mean(|planned_EED - solution_EED|)

best_difference = minimum(solution_difference)
best_solution = solution of best_difference

optimized_EED = calc_EED(bm, best_solution, search_range)
apply_EED_cap(optimized_EED)
```

Figure 3.2: Pseudocode for Genetic Algorithm.

Following this, either one of the optimization methods is applied. The pseudocode corresponding to the Genetic Algorithm is summarized in Figure 3.2, and the Tabu Search method is presented in Figure 3.3. For a more convenient representation, the 'boosting' mechanism is not included here.

```
current_solution = charges_real
optimized_EED = real_EED

while not in solution loop:
    charges_up = current_solution + segment_length
    charges_down = current_solution - segment_length

    for all drillholes in current_solution:
        add charges_up to charges_neighbors
        add charges_down to charges_neighbors

    for all drillholes in charges_neighbors, not in tabu_list:
        dh_EED = calc_EED(bm, charges_neighbors, search_range)
        neighbor_EED = replace_EED(optimized_EED, dh_EED)
        apply_EED_cap(neighbor_EED)
        neighbor_difference = mean(|planned_EED - neighbor_EED)

    best_neighbor = minimum(neighbors_difference)
    current_solution = solution of best_neighbor

    update_tabu_list(adjusted_drillhole, tabu_list, tabu_tenure)

    if best_neighbor < best_difference:
        best_difference = best_neighbor
        best_solution = current_solution

    optimized_EED = replace_EED(optimized_EED, adjusted_drillhole_EED)

optimized_EED = calc_EED(bm, best_solution, search_range)
apply_EED_cap(optimized_EED)
```

Figure 3.3: Pseudocode for Tabu Search algorithm.

4

Case Study

The aim of this chapter is to describe the available datasets and how these are used in a stepwise procedure to obtain the required results to demonstrate the benefits of the explosive energy distribution optimization system. The data consists of blasting plans provided by mining operations in Nevada and therefore represents real-life blast pattern designs that can later be used in combination with drillhole deviations to assess the optimization tool's effectiveness on a realistic scale. A first challenge is found in the varying structure of the drillhole data files; different mining companies, or even different mines operated by the same company, often take a distinct approach to archiving blast designs. The type of information included in such files can differ widely, as well as the naming convention of the various data columns, imperial or metric units, and even file type. Because this is all very specific to internal agreements at the companies that provide the data, it is difficult to write a general, straightforward program that can directly take the blasting plans as input. Therefore, the provided blasthole data first requires some generalization into .csv files containing the following columns:

Table 4.1: Generalization of data files.

Column name	**Significance**
BHID	Blasthole/borehole ID or drillhole number
x	x-coordinate or easting of collar
y	y-coordinate or northing of collar
z	z-coordinate or elevation of collar
Depth	Total depth of the drillhole, in meters
Diameter	Diameter of the drillhole, in meters
Stemming	Height of the stemming column, in meters
Density	Density of the explosive, in g/cm^3

4.1. Dataset Nevada 1

The first dataset, hereafter referred to as Nevada 1, consists of 243 drillholes. The coordinates of their planned locations are given by northing, easting, and elevation in metric units, with two decimal figures precision. A top-down schematic overview of the blast pattern, drawn from these coordinates, is provided in Figure 4.1. Since blasts are always shot such that the rock mass can move towards as much open space as possible, the bench's free face is most likely on the south-eastern side of the blast. This implies a more or less square blast pattern, slightly focused towards the center for a less dispersed muckpile. Calculation of the average distances between these drillholes gives an average burden of 6.00 m and spacing of 5.00 m.

The remaining data columns contain the same values for each drillhole; the total hole depth is 11.5 m, of which the upper 1.8 m is taken up by stemming. The hole diameter is 0.125 m, and the loaded explosive is regular ANFO with a density of 0.9 g/cm^3. Additional information includes a subdrilling length of 1.5 m, to achieve an excavation depth of 10 m, and 2 kg primer is placed at the bottom of every hole. Moreover, dips of -90 degrees and azimuths of 0 degrees are specified, indicating that all holes are to be drilled vertically. This extraneous information will not be considered directly in the optimization program but may be helpful to provide some perspective on the resulting explosive energy distribution later on.

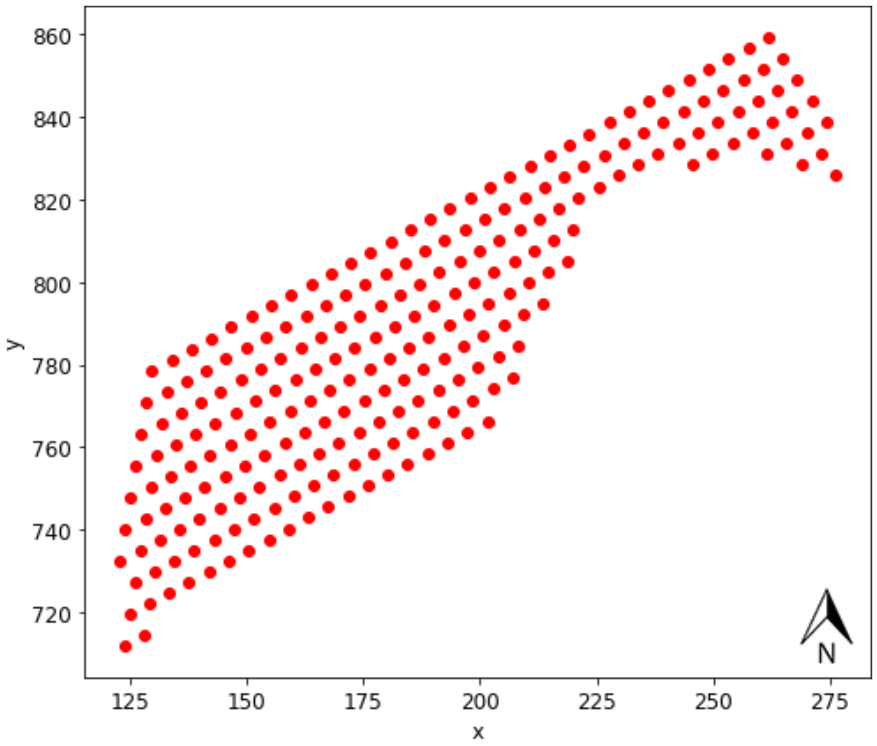

Figure 4.1: Planned drillhole locations of Nevada 1 blast pattern, with collars at z = 960 m.

4.2. Dataset Nevada 2

The second dataset in this case study, hereafter referred to as Nevada 2, consists of multiple sources of information detailing up to 407 drillholes. The x-, y-, and z-coordinates of their planned locations are again specified with two decimals precision. A top-down view of the planned blast pattern is given in Figure 4.2. Besides the drillhole coordinates, a number is assigned to every hole, in addition to two fixed columns that denote the blast number. Because there is no need to differentiate between blasts here, these last columns are omitted and only the drillhole numbers are taken as BHID. The other required information is derived from a schematic shot plan that accompanies this data, indicating a 14 x 16 (7 7/8“) blast design with 14 feet stemming and powder factor of 1.067 lbs/ton, for a 218,866-ton blast. Conversion from imperial to metric units by dividing by 0.3048 gives a designed burden of 4.88 m and spacing of 4.27 m. Cross-referencing with the drillhole locations learns that the coordinate system is originally given in imperial units as well, meaning all coordinate data must be converted to metric units. The corresponding sequencing to the blast indicates this pattern is initiated in the bottom-right corner, at the wall side of the pattern. Calculations based on the drillhole coordinates result in a mean burden of 4.81 m and spacing of 4.27 m for this staggered pattern. The slightly smaller burden is mainly due to a small section of more closely spaced drillholes in the lower-right corner of the blast, where breakage of the rock mass is started. Conversion of the other blast design parameters yields a stemming height of 4.27 m and drillhole diameter of 0.200 m.

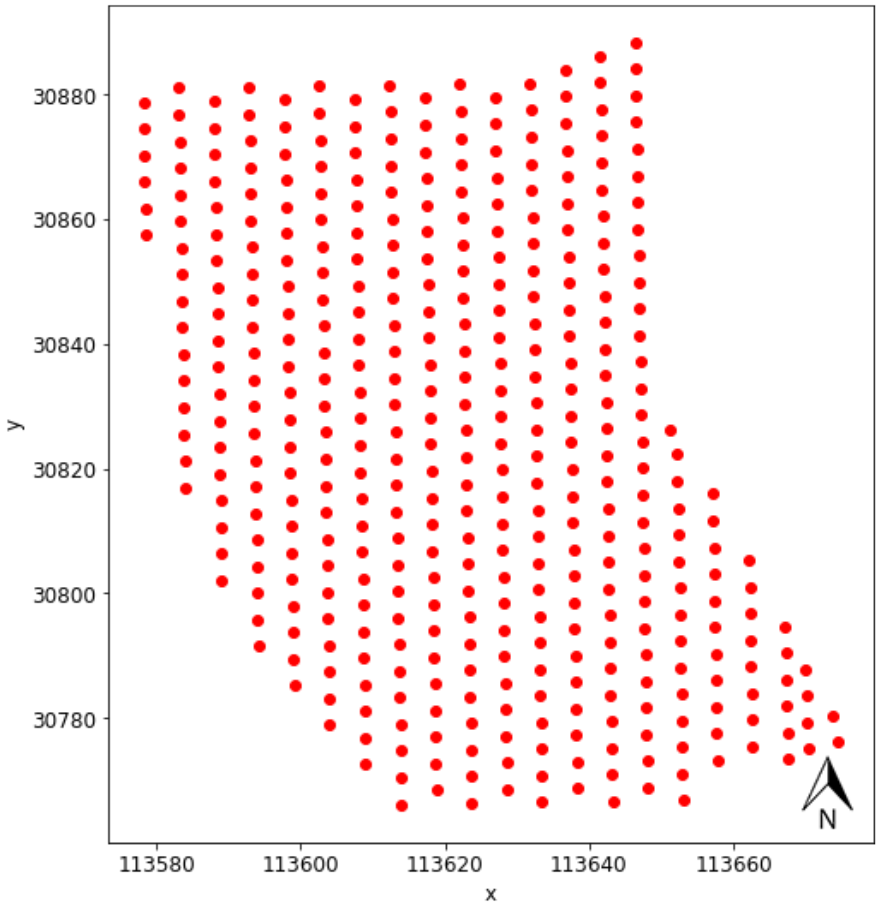

Figure 4.2: Planned drillhole locations of Nevada 2 blast pattern, with collars at z = 1633.73 m.

In addition to the planned drillhole locations, the Nevada 2 dataset also comes with data logged by the drill rigs. For each hole drilled, the actual coordinates, as well as hole depths, were registered with two decimal precision, along with the mean penetration rate for each hole. The latter gives blasting engineers some guidance on the rock strength of the material to be blasted. However, since consideration of rock mass properties is not within the scope of this study, it will not be utilized in explosive energy distribution optimization. Although the planned hole depth was not provided in the information available for the original blast design, using these actual z-coordinates and hole depths it can now be reasonably assumed as 45 ft or 13.72 m. From this hole depth, combined with the powder factor and mass of blasted material as noted before, an explosive density of approximately 0.9 g/cm^3 can be derived. The explosive type is not given, but given its density, it is assumed to be ANFO.

The actual, real drillhole locations are displayed in a top-down view in Figure 4.3. It should immediately be evident that, besides some clear deviations of individual holes, the drilled blast pattern varies significantly from the planned design. Instead of 407 drillholes, it consists of only 317. The core of the pattern remains roughly the same as the planned configuration, but the blast is reduced in size mainly on the left side, where a number of alternative holes are drilled. This can be explained by the fact that the pit edge to which the blast was designed, is in reality somewhat shifted, or leaves a part of the bench inaccessible for drill rigs.

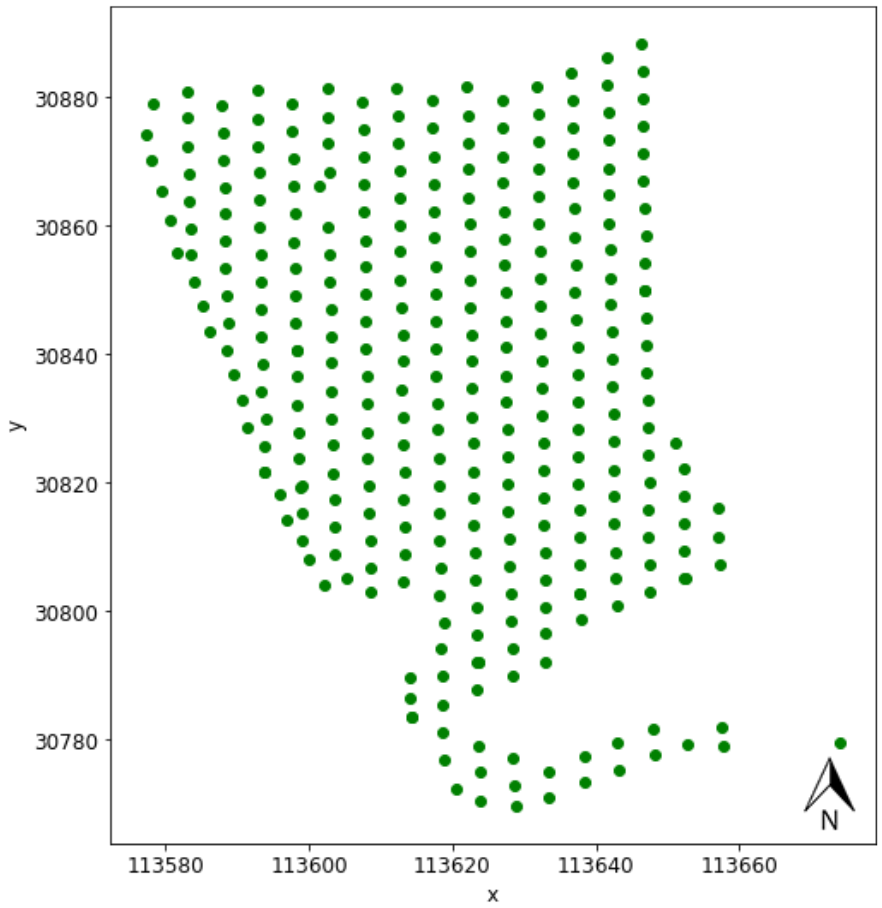

Figure 4.3: Real drillhole locations of Nevada 2 blast pattern, with collars at z = 1633.73 m.

Another zone of missing drillholes is found in the lower-right corner of the blast. Contrary to the previously discussed area, this does not seem to be an intentionally made adjustment; it breaks up the blast pattern, and thereby reduces the cooperating effect of neighboring blastholes. Since most drillhole patterns are drilled row by row, it is unlikely to point towards incomplete drilling of the pattern. It may be caused by failure to report information by the drill rig, perhaps caused by insufficient GPS coverage in this particular area.

In order to allow an unbiased comparison between the planned and real drillhole locations of the Nevada 2 dataset, and later on their corresponding explosive energy distribution, only drillholes that are part of both sets will be considered. A top-down view of the resulting pattern is given in Figure 4.4. It should be noted that a small amount of duplicate BHIDs was encountered in the real drillholes, namely holes 6025, 6059, 6130 (3), 6183, 6266, 6271, 6288, and 6934. After investigating their corresponding coordinates and depth, it was found that all duplicates were registered in very close proximity to each other, too close to justify the assumption of redrills. These errors may have been caused by multiple attempts to accurately position the drill bit on the collar or could be due to variance in the determined GPS position during drilling.

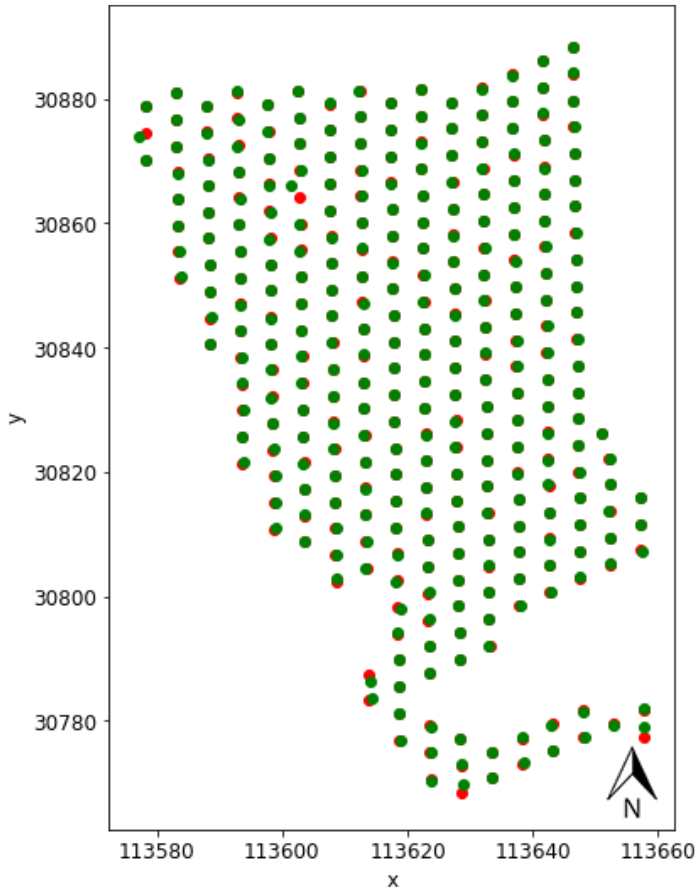

Figure 4.4: Overlap of planned (red) and real (green) drillhole locations of Nevada 2 blast pattern, with collars at z = 1633.73 m.

All duplicate holes registered normal, expected depths, except hole 6934; one of the drillholes marked by this hole number reached a depth of only 4.46 m instead of the expected 13.72 m. The positions and depths of all duplicates were considered, and only the best ones with respect to the planned hole locations were kept. After this adjustment, the Nevada 2 dataset consists of 292 drillholes. Due to discarding the area of more closely spaced holes in the lower-right corner, the average burden of the planned layout has been increased slightly to 4.87 m, and now resembles the provided design specifications more closely. The average spacing remains unchanged at 4.27 m.

Another discrepancy between the two sets of drillholes was spotted in the assignment of the drillhole numbers. Likely due to the use of two drilling rigs, BHIDs of the planned configuration did not match with the real ones. To allow for a simple comparison between the sets, the real BHIDs were mapped to their planned equivalents based on proximity calculations. Now the drillhole locations can be compared hole-to-hole, drillhole deviations can be calculated.

A number of key statistics are presented below in Table 4.2, and frequency distributions corresponding to the deviations can be found in Figure 4.5, along with a drilling precision map. For a more convenient representation, outliers are excluded from the frequency distribution figures. The first number that stands out in Table 4.2 is the minimum deviation in the xy-plane of 0.01 m, which corresponds to the theoretical precision of the latest GPS receivers. Nevertheless, this shows that out of 292 holes, not a single one was drilled exactly in its planned location.

The mean and median of deviation in both x- and y-direction are very close to zero, which indicates low chances of systematic errors. The absolute mean and median of the deviation in y-direction are slightly larger than their equivalents in the x-direction. However, due to their small size, the magnitude of the y-direction median is twice that of the x-direction. In Figure 4.5a and Figure 4.5b is shown that they are both characterized by approximately normal distributions, but the y-direction deviation is slightly more skewed. This difference between deviation in the x- and y-direction can be associated with the blast design. Drillholes are usually drilled row by row, which means drill rigs move in straight lines across the bench, along the y-axis for the Nevada 2 dataset. Through the examination of the BHIDs, this was indeed confirmed to be the case. If the x-coordinate is accurately determined at the start of such a row, its variation will be minimal for all holes, since the drill rig will only drive straight ahead. The appropriate y-coordinate, however, must be determined for each hole individually, leaving it more vulnerable to random errors.

Table 4.2: Drillhole deviation statistics overview of Nevada 2 dataset, all figures in m.

	Deviation in x-direction	**Deviation in y-direction**	**Deviation in xy-plane**	**Deviation in z-direction**	**Deviation in hole depth**
Minimum	-1.32	-1.14	0.01	-1.08	-0.90
Mean	0.01	-0.01	0.13	-0.34	-0.17
Mean (abs)	0.08	0.09	0.13	0.41	0.31
Median	0.01	-0.02	0.10	-0.36	-0.20
Maximum	0.62	1.96	2.36	0.50	1.24

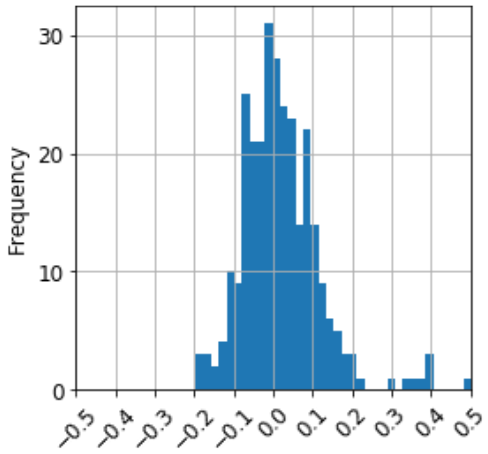

(a) Deviation in x-direction [m]

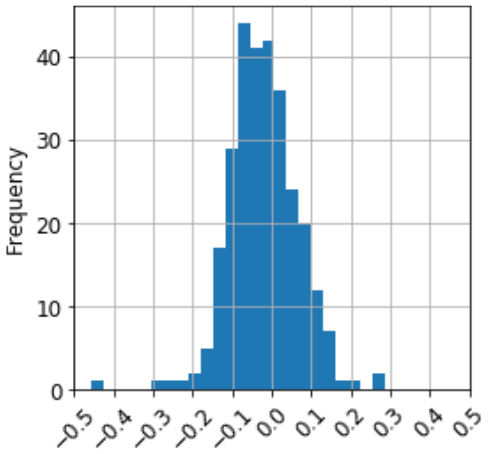

(b) Deviation in x-direction [m]

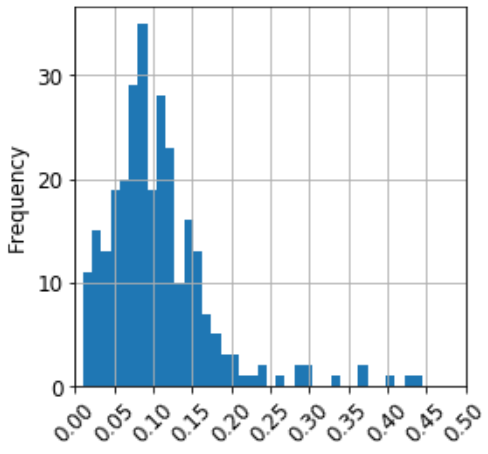

(c) Deviation in xy-plane [m]

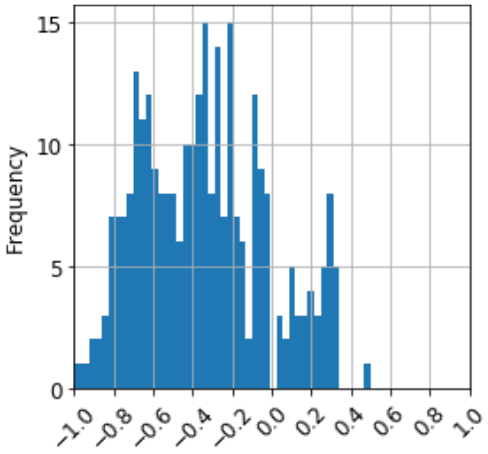

(d) Deviation in z-direction [m]

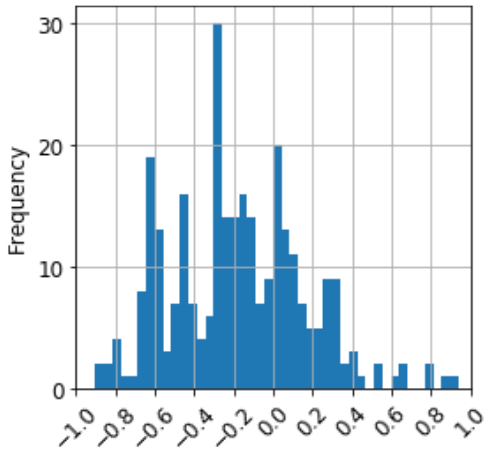

(e) Deviation in hole depth [m]

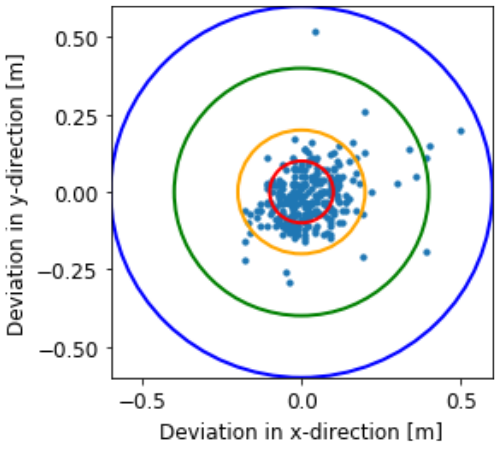

(f) Drilling precision map

Figure 4.5: Deviation frequency distributions (a-e) and precision map (f) for deviations obtained from Nevada 2 dataset. The colored circles in (f) correspond to 1/2, 1, 2, and 3 time the hole diameter.

Both the deviation in z-direction and drilled hole depth are characterized by a clear bias towards negative values. For the z-direction, this can be attributed to irregularities in the bench surface, which seem to be more common as depressions rather than elevations. Its corresponding frequency distribution (Figure 4.5d) is multimodal, and this translates, to some degree, to deviations in drilled hole depth (Figure 4.5e). While these properties tell a lot about the background of the data by connecting the deviations to their underlying causes, the most important figures for the explosive energy distribution optimization program are the overall deviations in the xy-plane.

The frequency distribution of this parameter is displayed in Figure 4.5c, and Figure 4.5f gives a schematic overview of the geometric spread, excluding the 6 drillholes with deviations larger than three times the hole diameter. Although the median deviation in the xy-plane of 0.10 m is a magnitude larger than the theoretical precision of the latest GPS receivers, the majority of holes is considered accurately drilled; 91.10% lies within one hole diameter (0.200 m) of its planned location, and 51.37% is even less deviated than half this distance. Nonetheless, 26 holes do not satisfy this requirement and are considered inaccurate. Special attention will be paid to this set, as charge adjustments should be expected mainly in or around these holes to adjust the explosive energy distribution in their vicinity accordingly. An overview of the drillholes with deviation in the xy-plane larger than one hole diameter is given below in Table 4.3.

Table 4.3: BHIDs of holes with deviation in the xy-plane larger than one, two, and three times the hole diameter.

> 1 hole diameter	**> 2 hole diameter**	**> 3 hole diameter**
6019	6159	6010
6028	6214	6097
6052	6265	6183
6125	6290	6184
6160	6330	6253
6196		6342
6197		
6202		
6264		
6266		
6275		
6288		
6300		
6313		
6341		

4.3. Sequential Experimental Design

The previous sections of this chapter have described the available datasets for application of the developed optimization program. The role of the current section is to combine this information with the methodology presented in Chapter 3 to put forward the proposed path to obtain all necessary control parameter settings as identified in Section 3.2, and subsequently, the particular results that are required to answer the research questions of this thesis. An overview of this stepwise approach is displayed in Figure 4.6, along with the objectives at every stage. By increasing the scale and resemblance to real blasthole data from one step to the next, early testing can be done more efficiently. This leads to a better understanding of the variables involved before proceeding to the application on full-scale. In the end, this procedure should result in more consistent performance with the chosen control parameters and optimization settings, as well as facilitate confirmation of findings in previous stages.

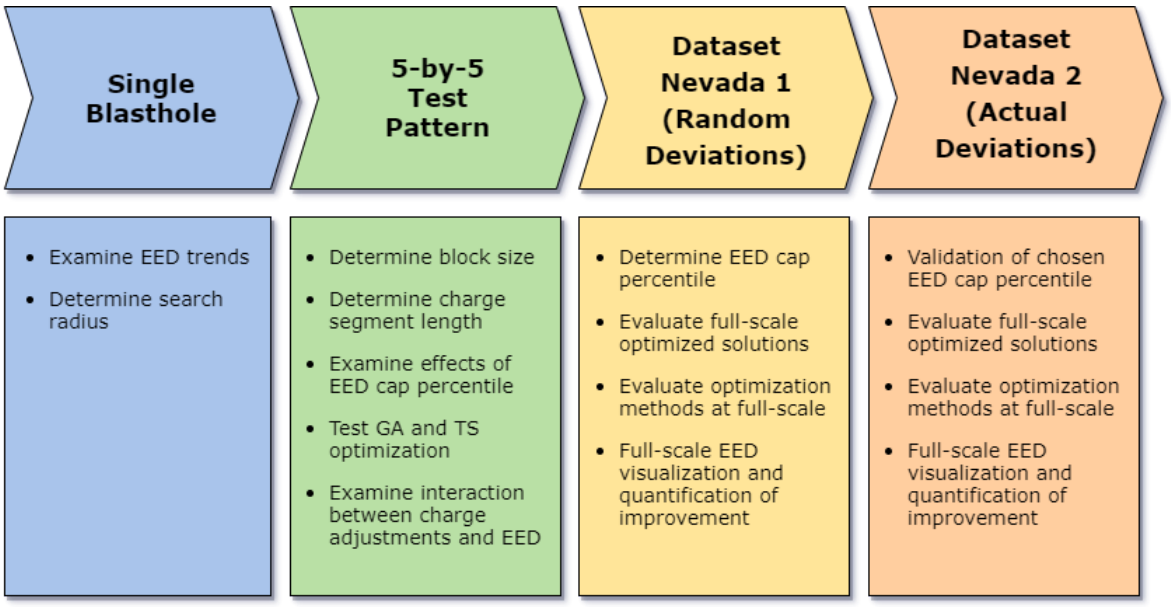

Figure 4.6: Sequential Experimental Design flowchart and objectives at each stage.

Single blasthole

For a better assessment of what happens to the explosive energy distribution in the rock mass surrounding a blasthole when the height of its explosive column is adjusted, it is important to first get an idea of its general behavior before any adjustments are made. EED values for each block in the block model are calculated through the EED formula by [49], but how exactly do these values change depending on a block's location relative to the explosive column? The answer to this question is required to select an appropriate search radius. In a normal blast pattern, the area of influence of neighboring blastholes is naturally overlapping, as their combined input delivers sufficient energy to break the rock mass. Although this cooperation effect between (deviated) blastholes is an important consideration for blast design and optimization, it will blur the EED contribution of individual holes. Therefore, this first test will feature only a single blasthole to produce a clearer picture of the relevant trends in EED around it, and most importantly, determine the meaningful limits of the calculation range.

The first step in this, is the visualization of the EED around a single blasthole with the characteristics of the Nevada 1 dataset, in a 20 by 20 m block model centered around the hole. In addition to complete heat maps of the explosive energy distribution, depth profiles of the EED values encountered at different radii around the blasthole may be helpful to illustrate any trends in more detail. Based on these findings, a number of potential search radii are selected. By comparing the EED values found at these radii, the point at which the computational requirements presumably start to outweigh their statistical significance can be identified as a suitable search radius. An identical approach is then applied to a single blasthole with the characteristics of the Nevada 2 dataset.

5 by 5 test pattern

The next part of the results chapter will focus on the interaction between multiple blastholes and the EED values found in the block model. It includes idealized drillhole deviations that are implemented to study the effects of charge adjustments on the explosive energy distribution. Using this small test case, both the appropriate block size and charge segment length can be identified effectively, forgoing the long computation times of the full-scale datasets. It also allows for early testing of the GA and TS optimization algorithms, as well as experimenting with different settings to improve their performance. Although these results might not be entirely representative for the full-scale datasets, its purpose is also to find relationships that will likely be useful for the examination of the full-scale configurations.

The test setup involves 25 drillholes with a diameter of 0.125 m, positioned in a 5 by 5 pattern with both spacing and burden of 3.0 m in the planned configuration (Figure 4.7a). In order to investigate the effect of charge adjustments in deviated holes with varying control parameter settings, the location of 12 of these holes is adjusted by 0.25 m to produce an idealized 'real' configuration of deviated drillholes Figure 4.7b). In this idealized case, the holes that are expected to have their explosive column adjusted are easily identified, which allows for a straightforward assessment of optimization performance. By moving holes number 1, 5, 7, 11, 13, 17, 19, and 23 closer together, charge decreases are expected in holes 6 and 18 to compensate for the increased explosive energy. Conversely, charge reductions are anticipated in holes 8 and 16, because holes 3, 7, 9, 11, 15, 17, and 21 are spaced further apart than before, and the explosive energy is therefore reduced in the area in between.

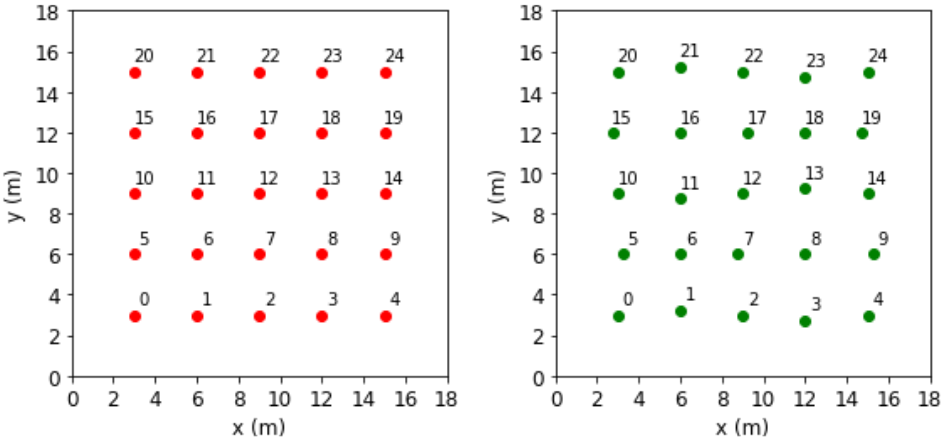

(a) Planned drillhole locations

(b) Real drillhole locations

Figure 4.7: 5 by 5 test setup drillhole locations in the planned and real configuration.

It is important to realize that simple comparisons of the planned EED or real EED for different block sizes, to determine the most suitable option, may not reflect its impact on the optimization. Although the most accurate representation of the planned EED and real EED is of course desirable, the block model should in the end be sufficiently accurate for optimization to result in the same charge adjustment solutions as obtained by the smallest block size. This approach should reduce computational requirements, and thereby lead to shorter optimization times. In order to evaluate this before diving into the actual optimization using the GA en TS algorithms, the expected charge adjustments in blastholes 6, 8, 16, and 18 are performed manually to create a first 'optimized' charging configuration. By calculating its corresponding explosive energy distribution, the resulting EED difference with the planned EED (the 'optimized' objective value) can be compared to the EED difference between the real EED and planned EED (the initial objective value) to obtain the realized improvement. These percentage improvements of the objective value will be calculated for each of the considered block sizes, and appropriate block size is chosen accordingly. It should be noted that both the EED cap and charge segment length are not yet defined. Because these variables might influence the suitability of the different block sizes, all possible configurations will be considered for a final choice.

The effect of charge adjustments on the overall improvement of the objective value is strongly influenced by both the magnitude of the adjustments as well as the EED cap. For a better understanding of how the choice of these control parameters will change the outcome of optimization, the effects of charge reductions are compared to charge increases. This is investigated using three manual charge adjustment cases, displayed in Figure 4.8; the expected adjustments as listed previously, adjustments in a selection of the deviated drillholes, and a setup combining the two. In the first place, this will highlight the variability of the EED difference improvement with different EED cap percentiles. Furthermore, it will demonstrate the complexity of the relationship between charge adjustments in neighboring blastholes and their effect on the EED differences.

The choice for an appropriate charge segment length will be based on optimized charge adjustment solutions of the 5 by 5 test pattern, for each of the 10 investigated EED cap percentiles. By performing these optimizations for every charge segment length between 0.1 m and 0.5 m, the overall sensitivity of the explosive energy distribution throughout the block model can be evaluated with respect to the magnitude of the charge adjustments. The selected charge segment length should then be small enough to lead to adjustments; choosing a charge segment length that is too large might not result in any adjustments, because its effect on the explosive energy distribution is too great. On the other hand, the charge segment length must not be too small either; this can cause an excessive amount of charge adjustments, which increases the duration of optimization and would be impractical for real-life explosives loading. Furthermore, the increased level of detail that is provided by a small charge segment length likely makes the optimization more susceptible to the variability in adjustments that comes with the different EED cap percentiles. Hence, a suitable charge segment length should ensure that optimization results in only a couple of highly effective charge adjustments, while minimizing differences in the solutions for each EED cap percentile.

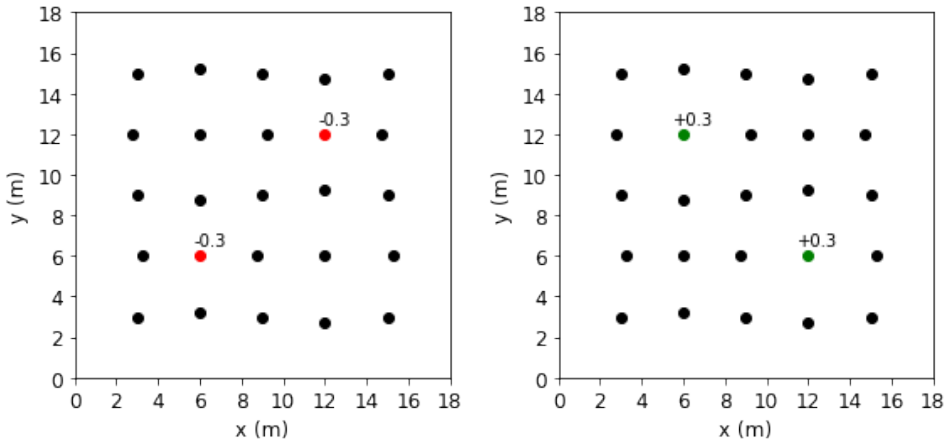

(a) Test case 1 (reductions)

(b) Test case 1 (increases)

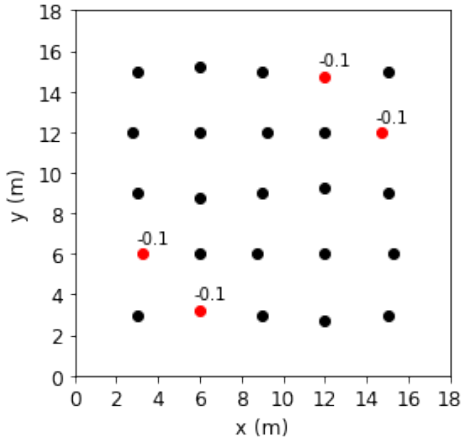

(c) Test case 2 (reductions)

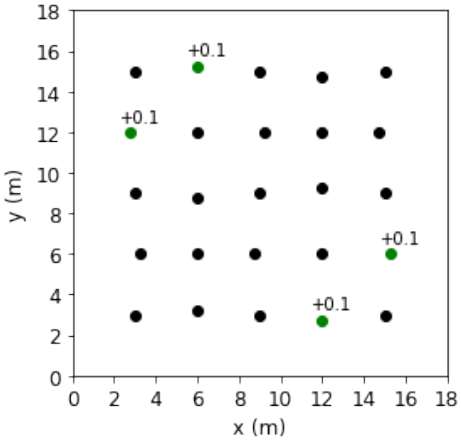

(d) Test case 2 (increases)

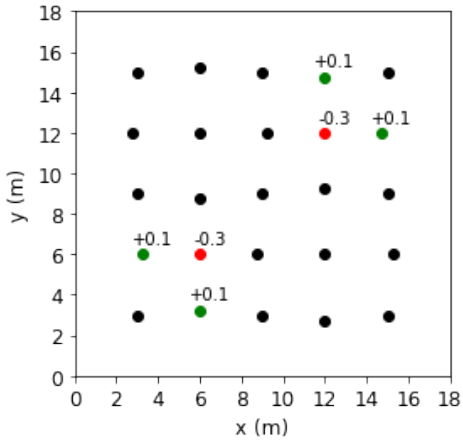

(e) Test case 3 (reductions with compensation)

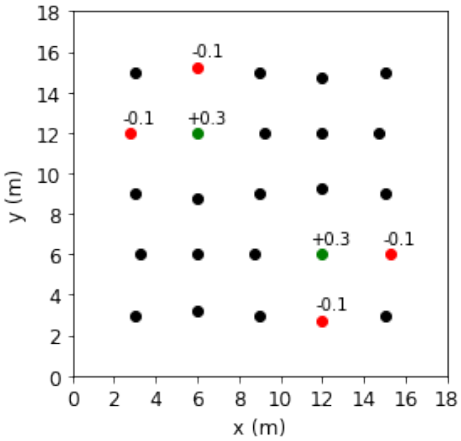

(f) Test case 3 (increases with compensation)

Figure 4.8: Three manual adjustment test cases to compare the effect of charge reductions and increases on EED differences.

With the first control parameters selected based on the findings in the previous tests, the GA and TS algorithms are then applied to the 5 by 5 test pattern for evaluation of their performance, by plotting the progress of the objective value during optimization. The settings of these algorithms can be altered to demonstrate their effect on the optimization paths. For practicality reasons, only adjustments to the top of the explosive column are considered, which will be the case for all optimizations performed, including those with the Nevada 1 and Nevada 2 datasets. The TS starting boost and explosives quantity constraint are not applied to the 5 by 5 test pattern optimization.

Finally, a detailed look into the distribution of EED values is provided. Visual representations of the explosive energy distribution throughout the block model include cross-sections as well as top-down views of the planned EED, real EED, optimized EED, initial EED difference, optimized EED difference, and improvement of the EED difference. These should paint a clear picture of the explosive energy distribution for the various drillhole and charging configurations in a more spatial sense. The goal of these visualizations is to show how the explosive energy distribution in the blasted area is influenced by the charge adjustments. Additionally, frequency distributions are generated for the various EED configurations to evaluate whether optimization leads to any major shifts in EED values.

Dataset Nevada 1 (random deviations)
The knowledge obtained from the 5 by 5 test pattern results, most importantly the best settings of the discussed control parameters and optimization algorithms, will now be used with the Nevada 1 dataset to verify some of these findings for a full-scale blast pattern. Besides the scale of the blast pattern, the nature of the drillhole deviations is also changed from an idealized test setup to randomized. Two scenarios are investigated; scenario 1 features drillhole deviations randomly picked from a uniform distribution ranging from -0.5 to 0.5 m, while scenario 2 implements the deviations drawn from a uniform distribution ranging from -0.25 to 0.25 m.

Special attention goes out to the determination of the most suitable EED cap percentile. Since this has shown to have a major effect on the overall number of charge increases and charge decreases, selection of this control parameter will be primarily based on the balance of the total explosives quantity. Because the overall powder factor of the blast is generally not tempered with to respect the initial blast design, it is assumed that the total amount of explosives in the optimized charging configuration must be equal to the planned quantity. Although this will later be enforced by the explosives quantity constraint described in Section 3.3, the charge adjustment solutions obtained through optimization without this constraint should aim to keep the total number of charge reductions and increases as closely in equilibrium as possible. The EED cap percentile that achieves this the best, is chosen as the most suitable option.

To ensure that the outcome of this is not influenced by any particular bias in the random drillhole deviations, the most promising EED cap percentiles are investigated using multiple randomizations of the drillhole deviation. For each scenario, five different randomizations are tested, for which some key characteristics are listed in Table 4.4. The EED cap percentile that gives the best results overall in terms of the balance between charge reductions and increases, is chosen as the most suitable option. For the remainder of the Nevada 1 dataset results section, only the first randomization of scenario 1 and scenario 2 will be used (R1).

Table 4.4: Properties of deviation (m) in the xy-plane for various randomizations of scenarios 1 and 2.

	Scenario 1				Scenario 2			
	Min.	**Mean**	**Median**	**Max.**	**Min.**	**Mean**	**Median**	**Max.**
R1	0.0362	0.3743	0.3885	0.6548	0.0064	0.1882	0.1957	0.3443
R2	0.0280	0.3888	0.4096	0.6769	0.0122	0.1920	0.2012	0.3505
R3	0.0700	0.3762	0.3901	0.6835	0.0052	0.1925	0.1978	0.3497
R4	0.0144	0.3678	0.3698	0.6834	0.0151	0.1961	0.2064	0.3437
R5	0.0410	0.3561	0.3735	0.6662	0.0138	0.1976	0.2088	0.3441

After selection of the most appropriate EED cap percentile, a similar approach to the 5 by 5 test pattern results will be taken. Investigation of these results is an important step because it will show how well the previous findings translate to full-scale optimization and might indicate if the approach should be changed. Contrary to the 5 by 5 test pattern that features manually implemented deviations for an idealized test setup, the random deviations applied to the Nevada 1 dataset make the outcome of optimization unpredictable. It is therefore important to examine the charge adjustment solutions obtained by the explosives quantity constrained optimization with random deviations of both scenario 1 and scenario 2, to check whether the suggested adjustments are reasonable. Comparing the optimal charging solutions for both scenarios will also give an idea about the sensitivity of charge adjustments with respect to the magnitude of the drillhole deviation, given the selected charge segment length.

Following this, the performance of the GA and TS algorithms is evaluated. The increased scale of the blast pattern will likely have some effect on their optimization paths; because the total number of drillholes is much larger than the 25 holes of the 5 by 5 test pattern, the number of blastholes that may have the height of their explosive column adjusted also becomes much larger. While the genetic algorithm would likely benefit from a large number of charge adjustments thanks to its more global approach, the performance of the Tabu Search may worsen due to the many individual steps required. The performance of both methods will thus be assessed to determine which one is more efficient for optimization of full-scale datasets and to address the potential of a hybrid option.

Lastly, visualizations of the explosive energy distribution throughout the block model will be provided for the various drillhole and charging configurations, similar to the 5 by 5 test pattern. Although the improvements of the objective value are also calculated for the previous test setup, the significance of these values for full-scale non-idealized optimizations is clearly much greater. After all, these are the most important figures to quantify the beneficial effects of optimization to the explosive energy distribution.

Dataset Nevada 2 (actual deviations)

With the last control parameters and optimization settings selected using the Nevada 1 results, the main purpose of optimization of the Nevada 2 dataset is to demonstrate the validity of the implemented approach on a different blast pattern with fully realistic drillhole deviations. If optimization with the settings as previously determined leads to results with characteristics that are similar to the Nevada 1 results, this will show a certain degree of consistency of the developed optimization program, instead of it being tailored to one particular dataset. Important indications for this are of course reasonable charge adjustments, and optimization actually leading to improvement of the objective value. Because of its variability with the chosen EED cap percentile, special attention is paid to the number of charge reductions and increases to ensure the explosives quantity does not differ too much from the planned amount. This will be done by running the optimization, once again, without the explosives quantity constraint at first.

The remainder of the results section for the Nevada 2 dataset will follow a similar approach as previously for the Nevada 1 dataset (and 5 by 5 test pattern), except using the actual drillhole deviations instead of two randomized scenarios, and considering only the most effective optimization method; based on optimization with the explosives quantity constraint activated, the optimal charge adjustment solution is reviewed. This is followed by an inspection of the corresponding optimization path, visualizations of the explosive energy distribution throughout the block model, EED frequency distributions, and of course the calculated improvements of the EED difference.

It should be noted that the actual drillhole locations of the Nevada 2 dataset also include the real z-coordinates for the collars, which are often different from the values in the planned layout due to irregularities in the bench surface. When this is translated to the constructed model, however, it would inadvertently place drillhole collars above or below the surface of the block model. To prevent optimization from making excessive charge adjustments to account for these ‘misplaced’ collars, the z-coordinates of the actual drillholes are shifted such that they coincide with the planned z-coordinate, and thus with the surface of the block model.

5

Results

This chapter presents the results of the developed explosive energy distribution optimization program. Because the obtained solutions are strongly dependent on the control parameters identified in Section 3.2, much attention will go out to the determination of the appropriate settings. Due to the size of the Nevada datasets and the resulting lengthy computation times, it is not convenient to use these for the testing of many different control parameter configurations. Instead, most of this is done using a number of small-scale tests described in Section 5.1. Although this gives a good idea of what can be expected from optimization of the larger datasets, it remains a simplification, and might therefore not entirely capture the full-scale behavior. After narrowing down the selection of control parameters, the most promising options are investigated in Section 5.2 using the Nevada 1 dataset in combination with randomized drillhole deviations. Finally, Section 5.3 offers the results of optimization of the Nevada 2 dataset consisting of both planned and actual drillhole locations, by using the most suitable settings as defined in the preceding sections to assess whether the developed program performs as expected with real data.

5.1. Small-scale Tests

For more efficient and in-depth testing of the various control parameters, a number of small-scale tests are performed to explore the different settings. First of all, an appropriate search radius is chosen in Section 5.1.1 by examining EED values around a single blasthole. In the remaining sections, the 5 by 5 test pattern as described in Section 4.3 will be used. By comparing the results of both manual and optimization-derived adjustments for different configurations of control parameters, their positive as well as negative effects can be identified. This information is then used to reduce the number of options to consider in subsequent steps of the process. The test blast pattern is used directly in Section 5.1.2 to determine a suitable block size, followed by selection of appropriate charge segment length in Section 5.1.3, which also includes a detailed investigation into the effects of the chosen EED cap. Section 5.1.4 focuses mainly on performance of the Genetic Algorithm and Tabu Search optimization methods for a selection of interesting settings, followed in Section 5.1.5 by an overview of the explosive energy distributions resulting from the optimized charge adjustments.

5.1.1. Search Radius

In order to select an appropriate search radius around blastholes, it is important to consider how the explosive energy diminishes with distance. This is of course dependent on the explosive energy distribution formula by [49], as well as the characteristics of a blast. This section investigates how the EED values change around a single blasthole and uses this information to choose an appropriate search radius that balances the quality of the model with computational efficiency.

The reviewed test blasthole follows the characteristics of blastholes in the Nevada 1 dataset, which means a hole diameter of 0.125 m, total hole depth of 11.5 m, and 1.5 m stemming. The loaded explosive is ANFO with a density of 0.9 g/cm^3. The EED is calculated for a square block model with sides of 20 m, centered around a blasthole with a search radius of r = 10 m. A cross-sectional view of this block model, visualizing the explosive energy distribution with a block size of 0.05 m, can be found in Figure 5.1. It should be clear from the logarithmic scale that EED values increase dramatically in close vicinity to the explosive column, and rapidly decline when moving away from it. Evidently, the EED values do not approximate a normal distribution, and therefore the extent of statistically significant values can not be determined from the three-sigma rule of thumb, using the mean and standard deviation. Instead, EED values at various radii around the blasthole are compared to the highest numbers found closeby, to evaluate at which point the explosive energy is sufficiently diminished to neglect the values outside of this range. Because the smallest possible distance to the explosive column is largely determined by the block size, so is the magnitude of the highest EED values. To produce figures that are applicable to other block sizes as well, the EED values will therefore be compared to the ones found at radius r = 0.5 m.

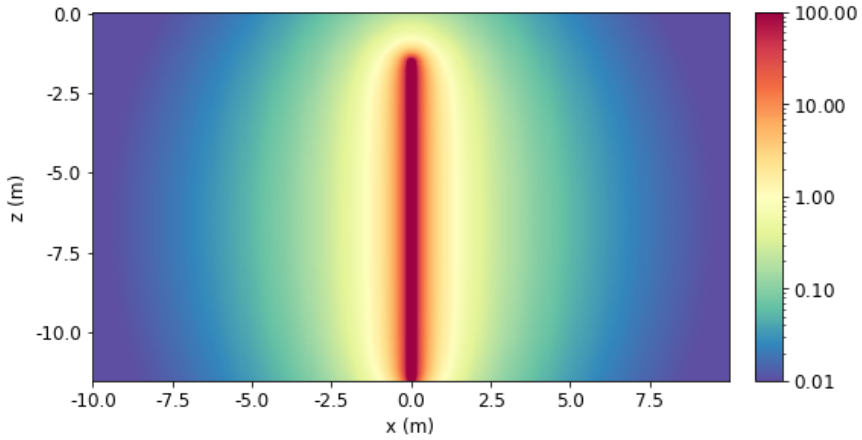

Figure 5.1: Vertical cross-section of the explosive energy distribution around a single blasthole.

Another variable component in this is the z-coordinate of the chosen block values. By plotting the EED values along the z-axis for various radii in the xy-plane, Figure 5.2 illustrates how the stemming in the upper 1.5 m of the blasthole affects the explosive energy distribution along the z-coordinate. It should be noted that the vertical differences for blocks located at radius r = 0.5 around the blasthole are much larger than at the greater radii. Variation in the upper part of the block model extends beyond the stemmed part of the blasthole; EED values at the top of the explosive column (z = -1.5 m) are still about half of those at z = -4.0 m. At the middle section of the explosive column, the explosive energy distribution remains relatively constant, with the maximum found around z = -7.0m. Below z = -9.0 m, the EED is more strongly reduced again as the bottom of the explosive charges is approached.

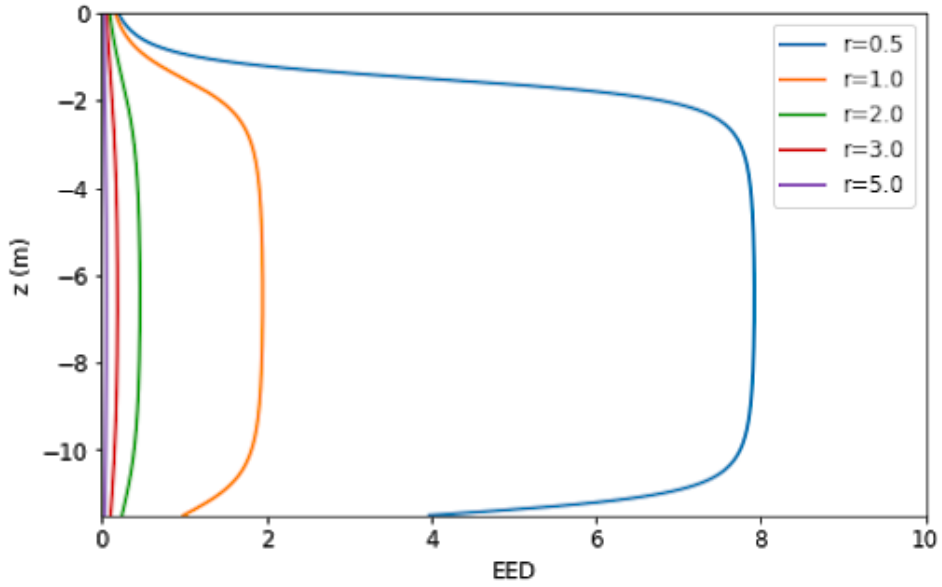

Figure 5.2: Change in EED with depth for various radii around a single blasthole.

In Figure 5.3 a plan view of the block model slice at z = 7.0 m is displayed, which will be used moving forward. The EED changes with distance from the blasthole are visualized in Figure 5.4, and Table 5.1 lists the corresponding EED values found at various radii. A block size of 0.1 m was used to generate Figure 5.3 and Figure 5.4. Since smaller block sizes lead to a small number of blocks located more closely to the blasthole, the maximum value of the observed EED peak is highly dependent on the chosen block size. A block size of 0.2 m, for example, doubles the smallest distance and produces a maximum EED value of only 49.7.

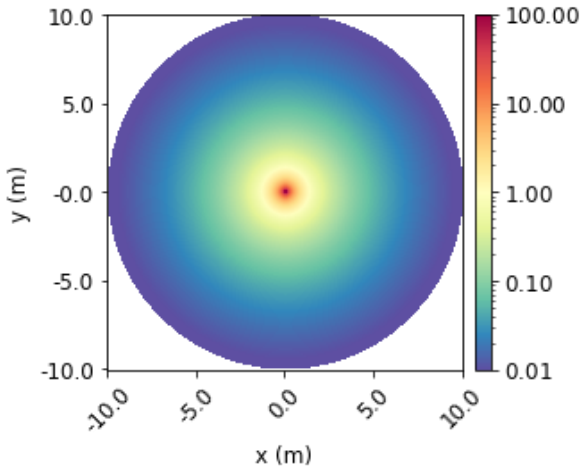

Figure 5.3: Plan view of the explosive energy distribution at z = -7.0 m around a single blasthole.

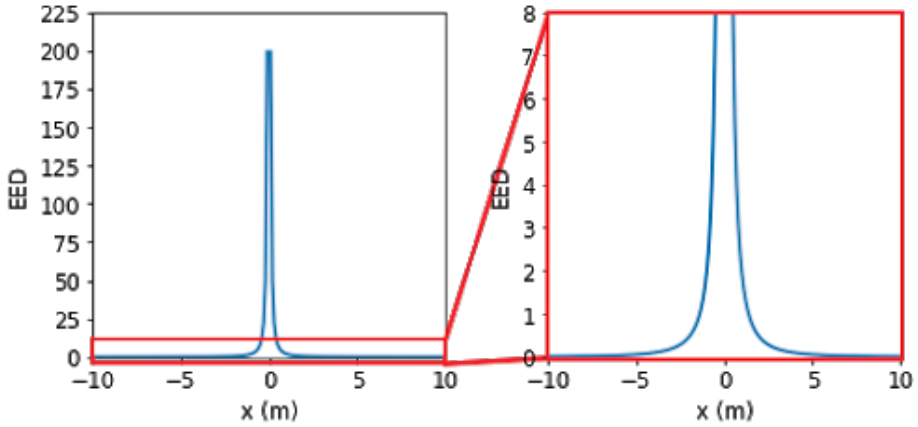

Figure 5.4: Explosive energy distribution around a single blasthole as a function of the x-coordinate.

Because of the exponential relationship between distance to the blasthole and the corresponding EED values, there is a thin line between cutting off too much useful data by selecting a search radius that is too small and using data with little significance by picking one that is too large. In Figure 5.4 it can be observed that the curve starts to flatten out around 5.0 m away from the blasthole. The figures in Table 5.1 indicate that, at this point, there is less than one percent of the explosive energy remaining, relative to the value found at a distance of 0.5 m. The search radius must be significantly increased to result in meaningful reductions to this, which will drastically increase computation times. Therefore, a search radius of 5.0 m is an appropriate choice.

Table 5.1: EED values at various radii around a single blasthole similar to those in dataset Nevada 1.

Radius (m)	EED at radius	Percentage of EED at r = 0.5 m
0.5	7.9192	100.00%
1.0	1.9502	24.63%
2.0	0.4610	5.82%
3.0	0.1890	2.39%
4.0	0.0968	1.22%
5.0	0.0560	0.71%
7.5	0.0196	0.25%
10.0	0.0089	0.11%

An identical approach is applied to a single blasthole with characteristics of the Nevada 2 dataset blastholes (0.200 m hole diameter, 13.72 m total hole depth, 4.27 m stemming, 0.9 g/cm^3 ANFO explosive). The resulting EED values at various radii, at a depth of z = 9.0 m, are displayed in Table 5.2. Clearly, the encountered values are higher compared to the smaller Nevada 1 blasthole. Percentage-wise, however, the two cases are very similar. A search radius of 5.0 m will therefore also suffice for this blasthole, and presumably for most blasthole designs.

Table 5.2: EED values at various radii around a single blasthole similar to those in dataset Nevada 2.

Radius (m)	EED at radius	Percentage of EED at r = 0.5 m
0.5	20.1826	100.00%
1.0	4.9112	24.33%
2.0	1.1240	5.57%
3.0	0.4489	2.22%
4.0	0.2265	1.12%
5.0	0.1306	0.65%
7.5	0.0457	0.23%
10.0	0.0209	0.10%

5.1.2. Block Size

For the remainder of Section 5.1, the 5 by 5 test pattern will be used. To reduce computation times especially for the smaller block sizes, the hole depth in these tests is taken as only 6.0 m. Because the explosive energy distribution is relatively constant around the middle part of the explosive column, as indicated in Figure 5.2, this should be a reasonable simplification without too much influence on the results. Charge adjustments will only be made at the top of the explosive column, and their effect on lower parts of the block model is already limited. For the selection of appropriate block size, the expected charge adjustments in blastholes number 6, 8, 16, and 18 (as in Figure 4.7) are made manually. Direct comparison of the planned or real EED statistics for the various block sizes is unreliable because the mean is inherently increased for smaller block sizes, as shown in Table 5.3. Instead, the absolute differences between the manually generated 'optimized' EED and planned EED will be compared with the differences between the real and planned EED, to assess the resulting improvements. After all, the block model doesn't necessarily need to reflect the exact same statistics for various block sizes, but they should result in the same charge adjustments. If the improvements produced by manual adjustments are similar for different block sizes, this is a good indication that they represent the explosive energy distribution in sufficient detail for the purpose of this optimization problem.

Table 5.3: Mean EED values and differences increase with block size.

Block size (m)	Mean planned EED	Mean difference with real EED
1.0	1.3982	0.1442
0.5	1.5533	0.2012
0.2	2.8531	0.6410
0.1	2.9155	0.9031
0.05	3.4982	1.4961

In order to assess these improvements for the various block sizes, the expected charge adjustments for the test setup are performed manually to represent the 'optimized' configuration; the height of the top of the explosive column is reduced by one charge segment length in holes 6 and 18, and increased by one charge segment length in holes 8 and 16. As defined in Section 3.3, the optimization objective is the minimization of the differences in EED with respect to the planned setup, so the numbers listed in Table 5.4 represent the achieved percentage changes of this objective value. Because the appropriate charge segment length is yet to be determined in Section 5.1.3, all options are investigated.

Table 5.4: Improvements in mean EED difference for selected manual charge adjustments.

Block size (m)	**Charge segment length (m)**				
	0.1	**0.2**	**0.3**	**0.4**	**0.5**
1.0	1.21%	0.56%	-0.08%	-1.17%	-2.61%
0.5	0.74%	0.47%	-0.28%	-1.20%	-2.33%
0.2	-0.40%	-1.18%	-2.09%	-3.07%	-4.10%
0.1	-0.29%	-0.86%	-1.53%	-2.24%	-2.99%
0.05	-0.31%	-0.79%	-1.39%	-2.01%	-2.60%

Although the block sizes of 1.0 m and 0.5 m result in positive improvements for charge segment length 0.1 m and 0.2 m, all other cases are actually resulting in negative changes, indicating deterioration of the objective value. When the level of detail is increased with smaller block sizes, none of the adjustments produce a satisfying result anymore. Because this is an idealized setup for which improvements are expected after these adjustments, the results are peculiar. The fact that these adjustments do not lead to positive improvements can likely be attributed to the block-by-block comparison, which causes disproportionally large EED differences in blocks close to the blastholes. This also explains why even the initially positive values turn negative at smaller block sizes. The selection of the appropriate EED cap to combat this issue will be discussed in Section 5.1.3, so all options are still considered here. The block size will therefore be evaluated with both a varying charge segment length and EED cap.

The effect of block size can then be illustrated using graphs like Figure 5.5. Similar graphs for charge segment lengths 0.1, 0.2, 0.4, and 0.5 m are included in Appendix A. To ensure a block size represents the explosive energy distribution with sufficient accuracy, the corresponding improvements should follow the values of the smallest block sizes as closely as possible for each EED cap percentile; greater differences affect the favorability of these charge adjustments in relation to others, increasing the likelihood of alternative optimization results later on. Because their differences with graphs of smaller block sizes are relatively large, block sizes 1.0 m and 0.5 m seem too inaccurate. The calculated improvements in block sizes 0.2, 0.1, and 0.05 m, however, are very similar. It can thus be expected that optimization will produce similar charge adjustments for each of these.

The mean differences in the calculated improvements between each subsequent reduction in block size are listed in Table 5.5. It shows that the differences between block size 0.2 m and 0.1 m are quite small and more or less equal to those between 0.1 m and 0.05 m, which means the benefits of using a block size smaller than 0.2 m are limited. Because block size 0.2 m will naturally have lower computation times than 0.1 and 0.05 m, this is chosen as the most suitable option. The figures in Table 5.5 also indicate that differences between block sizes increase with the charge segment length.

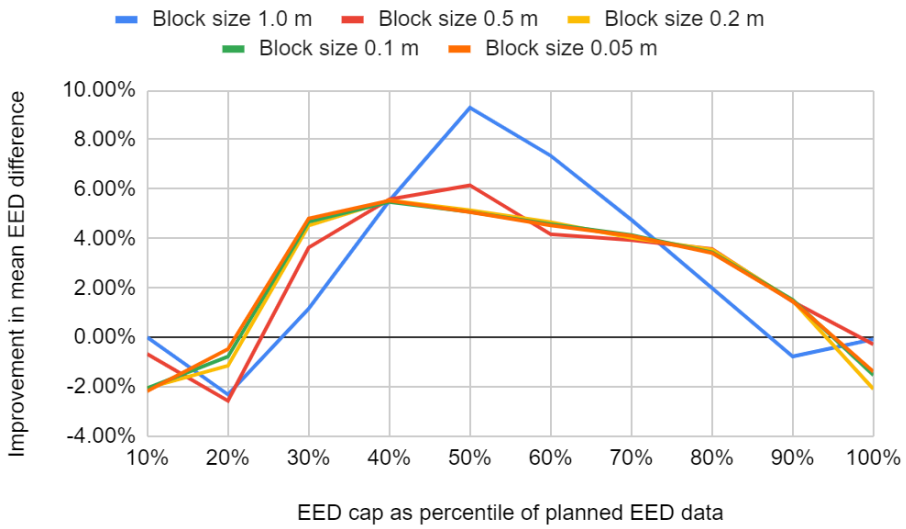

Figure 5.5: Comparison of improvement in EED difference for different block sizes, for manual adjustments to the explosive column by charge segment length 0.3 m.

Table 5.5: Mean differences between improvements for subsequent smaller block sizes (all EED cap percentiles averaged).

Charge segment length (m)	Block size 1.0 m –> 0.5 m	Block size 0.5 m –> 0.2 m	Block size 0.2 m –> 0.1 m	Block size 0.1 m –> 0.05 m
0.1	± 0.71%	± 0.46%	± 0.04%	± 0.05%
0.2	± 0.98%	± 0.57%	± 0.07%	± 0.08%
0.3	± 1.46%	± 0.72%	± 0.10%	± 0.09%
0.4	± 1.93%	± 1.01%	± 0.12%	± 0.11%
0.5	± 2.31%	± 1.00%	± 0.16%	± 0.17%

5.1.3. EED Cap Percentile & Charge Segment Length

As shown in Table 5.4, none of the expected adjustments result in an improvement of the objective value for block sizes of 0.2 m and smaller. The underlying reasons for this will be illustrated through a number of examples derived from the 5 by 5 test pattern setup. Additionally, it will be demonstrated how the application of an EED cap can be used to deal with this issue. However, the selection of an appropriate EED cap is challenging. The charge adjustment solutions for the 5 by 5 test pattern corresponding to different EED cap percentiles are examined to determine which configuration produces the most sensible results. Because of the simplicity of the test setup, Tabu Search can be used to quickly reach obvious optimal solutions. The optimization itself will be discussed in more detail in Section 5.1.4. Solutions are obtained for every charge segment length since the choice for this variable also affects the performance with different EED cap percentiles. To explain the reasoning behind the application of an EED cap, a cross-section of the 5 by 5 pattern's block model is taken to visualize various explosive energy distributions corresponding to the different drillhole and charging setups. This cross-section is taken at y = 6.1 m, directly next to the second row of drillholes (number 5-9, as displayed in Figure 4.7). First, the configuration without any EED cap is illustrated; Figure 5.6 shows the planned EED, and Figure 5.7 the real EED. The block-to-block differences between these two resemble the starting point of optimization before any charge adjustments, and are shown in Figure 5.8.

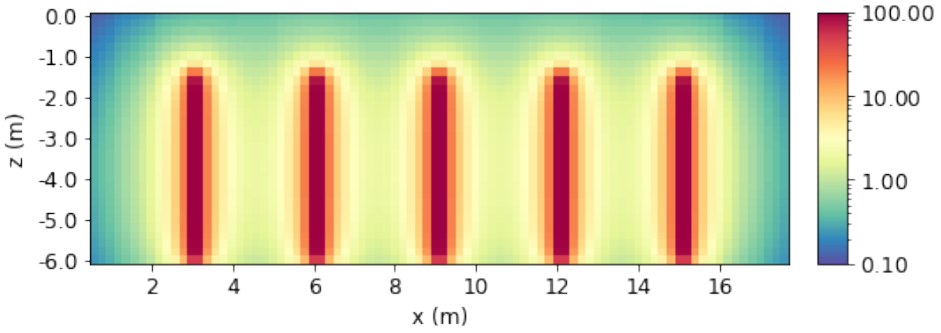

Figure 5.6: 5 by 5 pattern planned EED cross-section at y = 6.1 m.

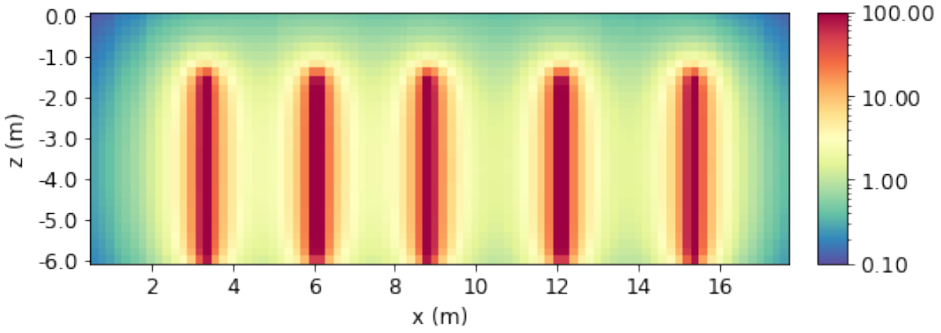

Figure 5.7: 5 by 5 pattern real EED cross-section at y = 6.1 m.

In the real configuration, the drillholes are deviated according to the description of the 5 by 5 pattern in Section 4.3, meaning they are spaced more closely to hole 6 (second from the left) and further away from hole 8 (second from the right). In Figure 5.8 it can be clearly observed that this causes very large EED differences in the blocks nearest to both the planned and real drillhole locations. These disproportionally large differences can not be accounted for by the expected charge adjustments in blasthole 6 and 8. The effect of these adjustments is shown in Figure 5.9 and Figure 5.10, which illustrate the 'expected adjustments' optimized EED and its resulting difference with the planned EED respectively. Not only is the EED difference in blocks near the deviated drillholes not significantly reduced by making the expected adjustments, they actually introduce more differences in their direct neighborhood. Therefore, the resulting improvement in this cross-section alone is -3.39%.

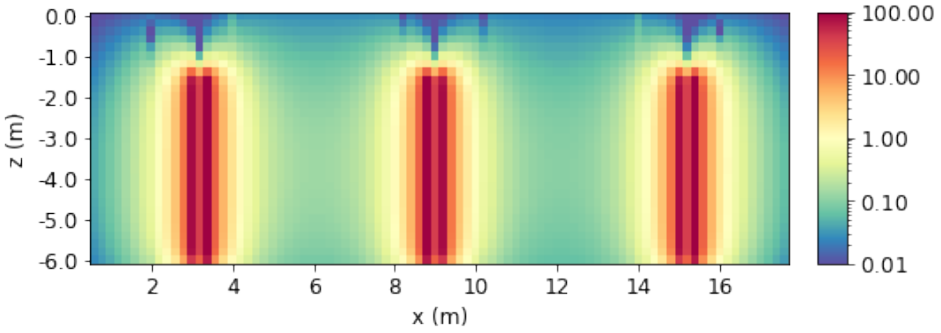

Figure 5.8: 5 by 5 pattern EED difference (planned - real) cross-section at y = 6.1 m.

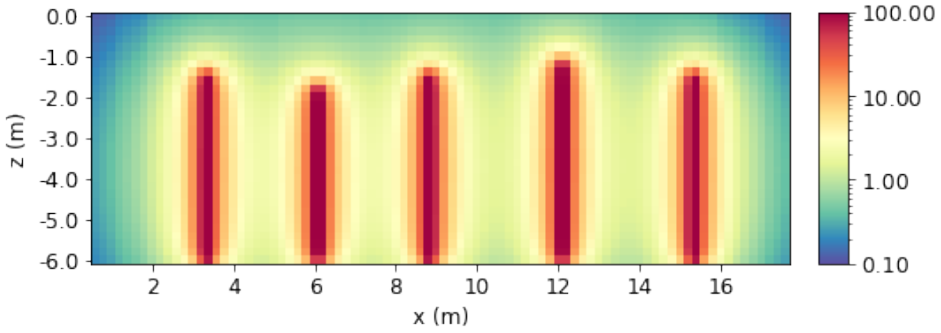

Figure 5.9: 5 by 5 pattern 'expected adjustments' optimized EED cross-section at y = 6.1 m.

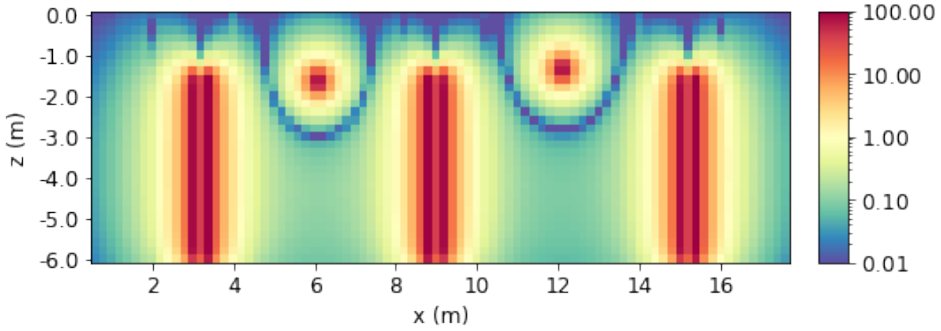

Figure 5.10: 5 by 5 pattern EED difference (planned - 'expected adjustments') cross-section at y = 6.1 m.

When comparing the expected charge increase to the expected charge reduction, it becomes clear that their effects on the EED differences are not equal; lowering the top of the explosive column by 0.3 m in blasthole 6 accounts for an improvement of -1.67%, while the opposite increase in blasthole 8 improves the mean EED difference by -1.72%.

The only adjustments that lead to positive improvements in this setup are reductions of charges in the deviated blastholes because this reduces the differences introduced by the explosive column in the real drillhole locations. This is problematic because this effect would cause optimization to reduce the charge height in deviated blastholes only with the purpose of attempting to compensate for the large differences found in nearby blocks. To demonstrate this, Figure 5.11 shows the EED corresponding to excessive reductions of 3.0 m to the top of the explosive column in the deviated drillholes.

The resulting differences with the planned EED are shown in Figure 5.12. At the cost of small increased differences further away, some of the highest values near the upper part of the blasthole are reduced, to produce an overall improvement of 10.08% in this cross-section, which is of course highly undesired. In the three-dimensional setup, the number of small differences that are located further away will naturally be much larger, which will likely reduce the effectiveness of excessive charge reductions. Nevertheless, it is important to realize that the block-to-block comparison may cause a bias towards charge reductions in deviated drillholes, simply because they introduce less differences into the block model compared to charge increases.

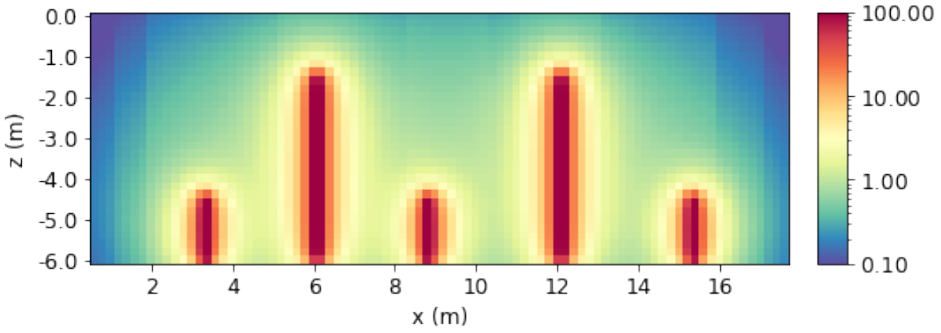

Figure 5.11: 5 by 5 pattern 'excessive reductions' optimized EED cross-section at y = 6.1 m.

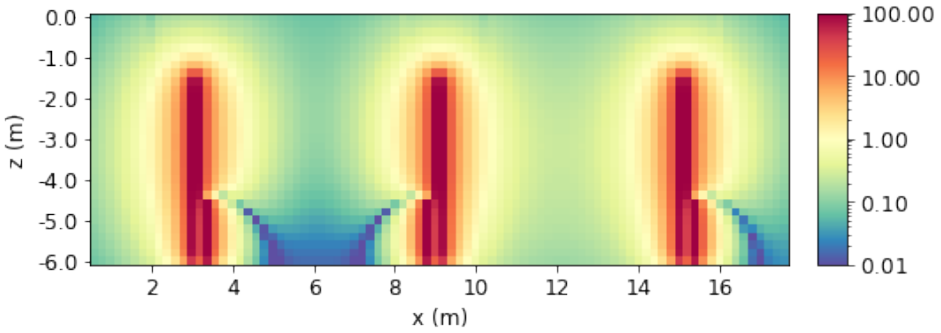

Figure 5.12: 5 by 5 pattern EED difference (planned - 'excessive reductions') cross-section at y = 6.1 m.

From the EED cross-sections, it is clear that disproportionately large values are found in the direct vicinity of the blastholes, while the rest of the block model contains much lower values. When considering this from a practical point of view, the rock mass further away from the blastholes should already receive sufficient energy for the desired fragmentation, at least in the planned drillhole configuration, while the rocks close to blastholes receive an enormous surplus. Realistically, it should not matter exactly which part of a bench receives this surplus in energy, and what its magnitude is. Instead, optimization should focus especially on larger, low-valued parts of the block model which receive just enough energy for appropriate breakage in the planned drillhole setup, but receive a little less or more in the real case due to drillhole deviations. When the spacing between two drillholes in the real configuration is for example larger than in the planned configuration, the relatively low-valued blocks in the middle of these holes receive even less energy.

The goal of adjusting the height of the explosive column in these drillholes must then be to compensate for such differences, instead of the much larger ones introduced very close to the planned and real drillhole locations. To achieve this, the highest EED values in the block model are eliminated by applying an EED cap. Because the exact EED values will change with both blast design and block size, a more general approach is taken by defining the cap value based on EED value percentiles. By removing all values above the 80% percentile, for example, results in the planned EED cross-section of Figure 5.13. After the expected charge adjustments to the real drillhole configuration, the 'expected adjustments' optimized EED becomes as in Figure 5.14, and Figure 5.15 displays the differences between the two.

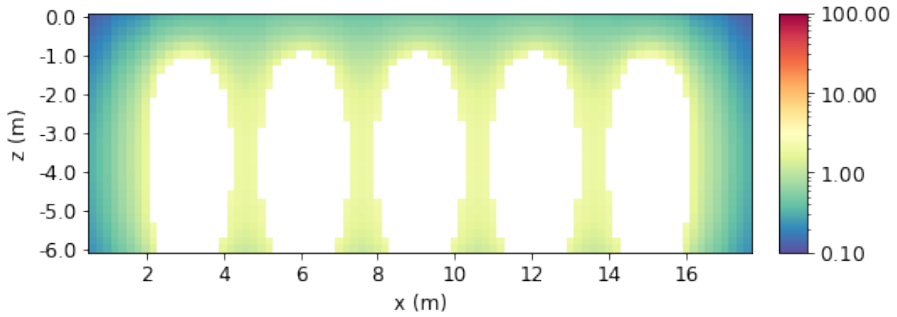

Figure 5.13: 5 by 5 pattern planned EED cross-section at y = 6.1 m, with 80% percentile EED cap.

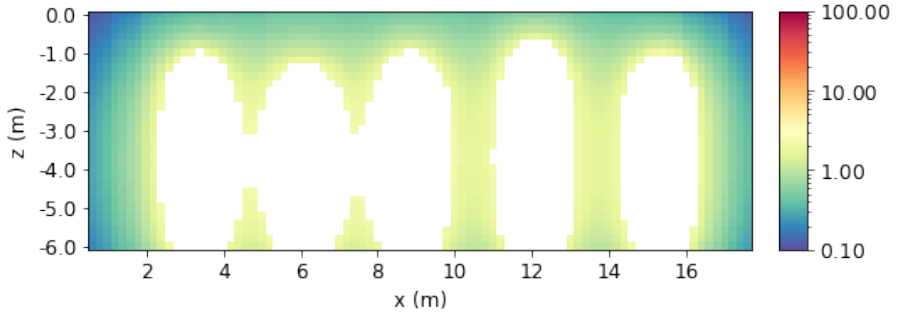

Figure 5.14: 5 by 5 pattern 'expected adjustments' EED cross-section at y = 6.1 m, with 80% percentile EED cap.

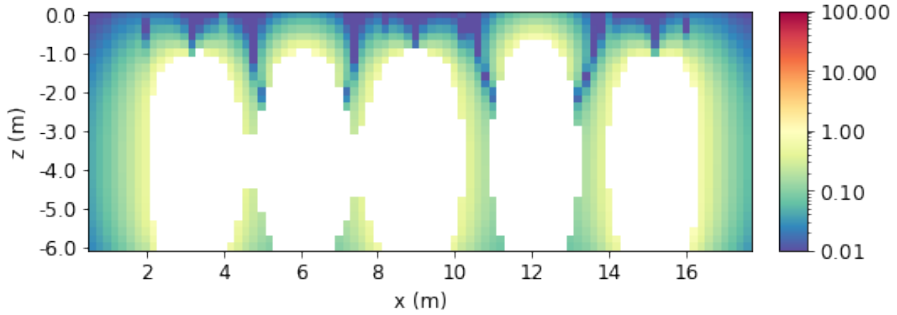

Figure 5.15: 5 by 5 pattern EED difference (planned - 'expected adjustments') cross-section at y = 6.1 m, with 80% percentile EED cap.

Determination of the appropriate EED cap percentile will be continued later on. First, the difference in the effect of charge reductions and increases is further examined by calculating the improvements resulting from the manual charge adjustment cases introduced in Figure 4.8, this time using the full 3D block model of the 5 by 5 test pattern. In the first case, the expected adjustments (reduction in holes 6 and 18, increase in hole 8 and 16, displayed in Figure 4.8a and Figure 4.8b) are made using a charge segment length of 0.3 m. The resulting improvements to the EED difference are then calculated for each EED cap percentile and plotted in Figure 5.16. Evidently, the negative improvement found at 100% would never lead to this adjustment being made by optimization. At lower percentiles, however, both the expected charge reductions and increases produce a positive improvement, as desired, except at the 10% and 20% percentile. This graph also shows that the relationship between the effect of these charge adjustments changes with EED cap percentile; the reductions are favored at 80% and higher, while increases are favored in all other cases.

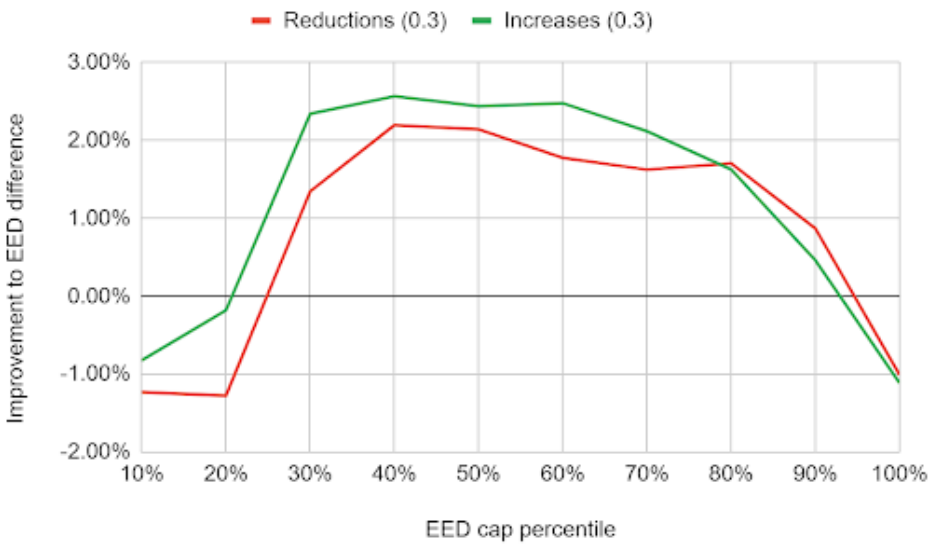

Figure 5.16: Comparison of improvements from expected charge reductions and increases.

The second manual charge adjustment that is examined, is the adjustment of deviated holes (Figure 4.8c and Figure 4.8d). Here the top of the explosive column is lowered by a charge segment length of 0.1 m in holes 1, 5, 19, and 23, and elevated in holes 3, 9, 15, and 21 (numbers as in Figure 4.7). The resulting improvements are displayed in Figure 5.17. Although it is clear that these adjustments by themselves would not result in a positive improvement to the EED difference, it does indicate there is a bias for charge reductions in deviated blastholes; reducing the charge height has a more positive impact than increasing it, for holes deviated an equal amount in opposite directions. Clearly, more differences are introduced by increasing the height of the explosive column compared to decreasing it, similar to what was observed in the two-dimensional setup.

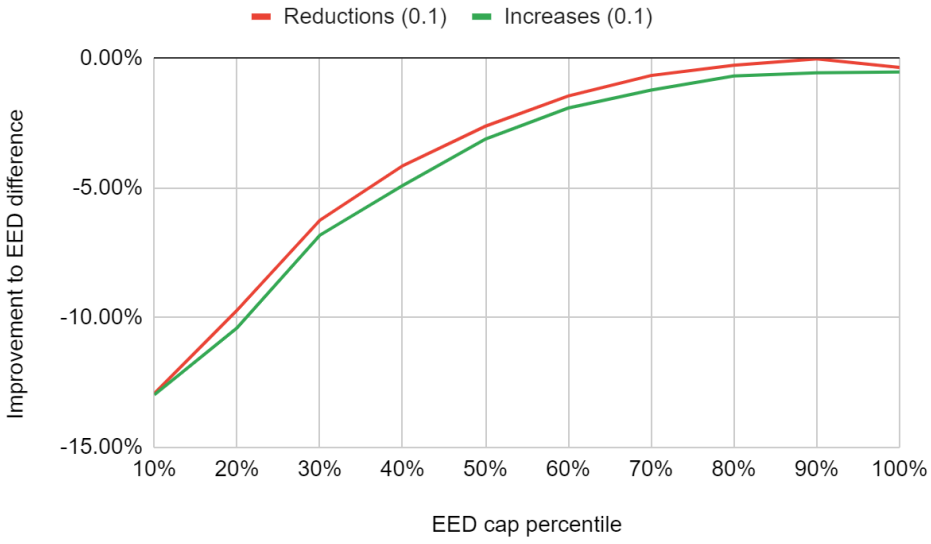

Figure 5.17: Comparison of improvements from charge reductions and increases in deviated holes.

When small charge adjustments in deviated holes are combined with the expected adjustments in holes 6, 8, 16, and 18, this does result in positive improvements; Figure 5.18 shows the results generated by combining the expected charge adjustments by a charge segment length of 0.3 m with adjustments in the deviated holes in the opposite direction as previous, according to Figure 4.8e and Figure 4.8f. This is done to compensate for some of the effects of the expected adjustments. Evidently, this is beneficial to the improvements when compared to those in Figure 5.16, especially at the percentiles of 50% and lower. Although the expected charge increases in holes 8 and 16 alone are more beneficial than similar decreases in holes 6 and 18, below EED cap percentiles of 80%, the effect of reducing charge height in deviated holes 3, 9, 15, and 21 to compensate for some of its excessive or lacking EED contribution leads to a greater improvement than the opposite charge increase in holes 1, 5, 19, and 23. This indicates that even though there is a bias towards charge increases in stationary holes surrounded by deviated holes, the bias towards charge reductions in deviated holes themselves is still stronger. The relationships between charge adjustments and improvement in EED difference do somewhat change with charge segment length since larger adjustments naturally lead to larger effects on EED values.

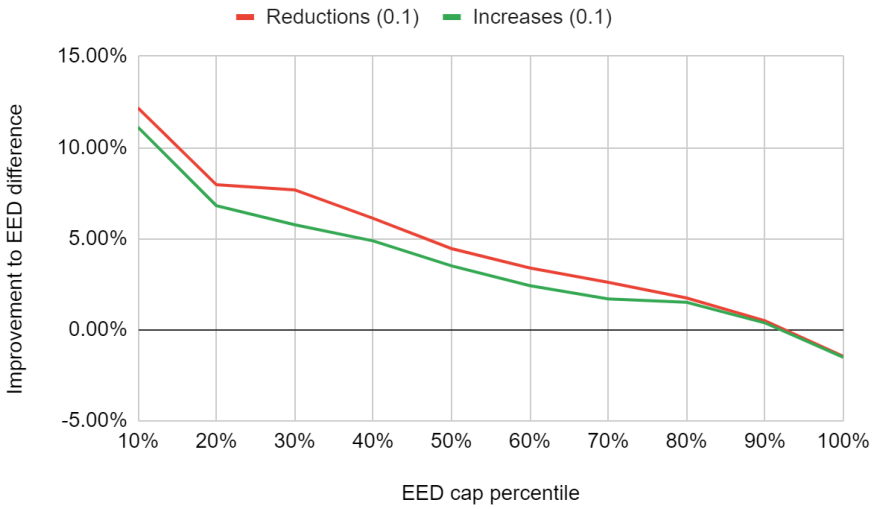

Figure 5.18: Comparison of improvements from opposite charge reductions and increases in deviated holes 1, 3, 5, 9, 15, 19, 21, 23 in combination with the expected adjustments in holes 6, 8, 16, 18 (numbers as in Figure 4.7).

These three examples provide meaningful insights in dissimilarity between the effects of charge reductions and increases, but can of course not cover the complete mechanics of their interaction in a blast pattern during optimization, which considers all possible charge adjustments instead of a few idealized ones. Therefore, the optimization results obtained by using different EED cap percentiles will now be examined to select the most appropriate option, as well as a suitable charge segment length. Solutions are obtained using Tabu Search with tabu tenure set to 3.

The greatest level of detail is desired for evaluation of the various EED cap percentiles, to check whether any bias is found in the obtained charge adjustment solutions. Therefore, a charge segment length of 0.1 m is used initially. Assuming that the total amount of explosive charges should remain equal to the amount used in the planned drillhole configuration, an unbalanced number of charge reductions and increases would indicate a bias. The solutions for all ten percentiles, using charge segment length 0.1 m, block size 0.2 m and search radius 5 m, are visualized in Figure 5.19 and Figure 5.20. The corresponding number of charge reductions and increases for each solution are listed in Table 5.6.

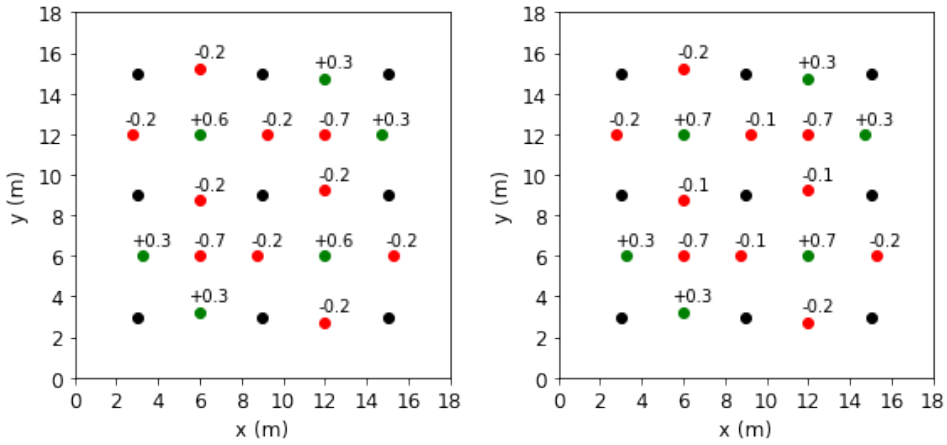

(a) Solution for 10% percentile.

(b) Solution for 20% percentile.

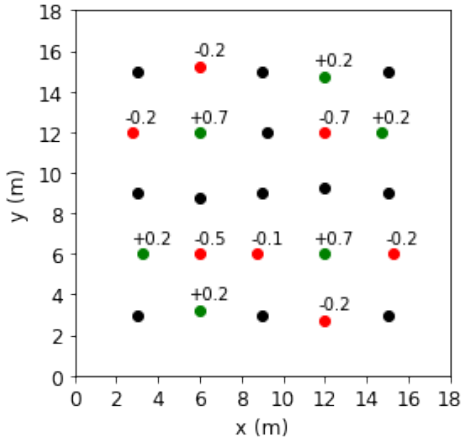

(c) Solution for 30% percentile.

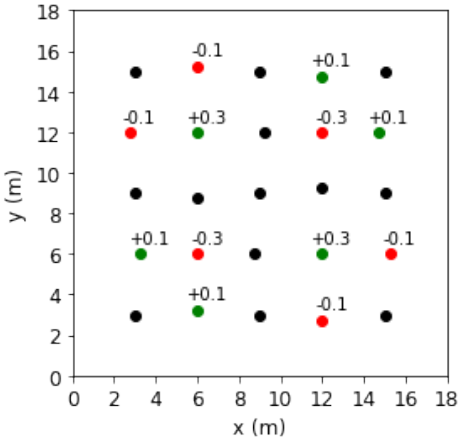

(d) Solution for 40% percentile.

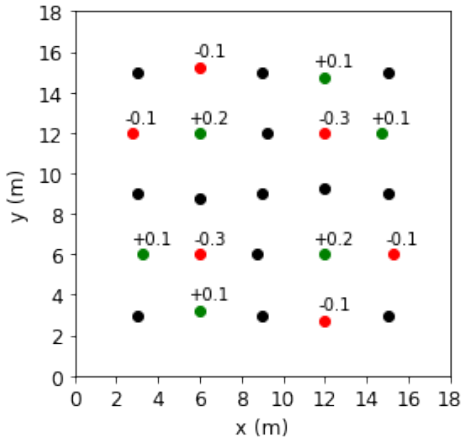

(e) Solution for 50% percentile.

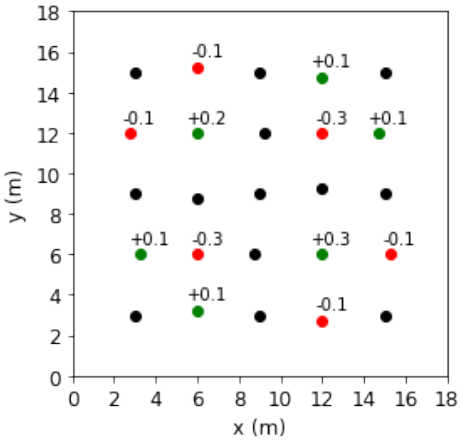

(f) Solution for 60% percentile.

Figure 5.19: Charging adjustment solutions obtained using charge segment length 0.1 m, for 10-60% percentiles.

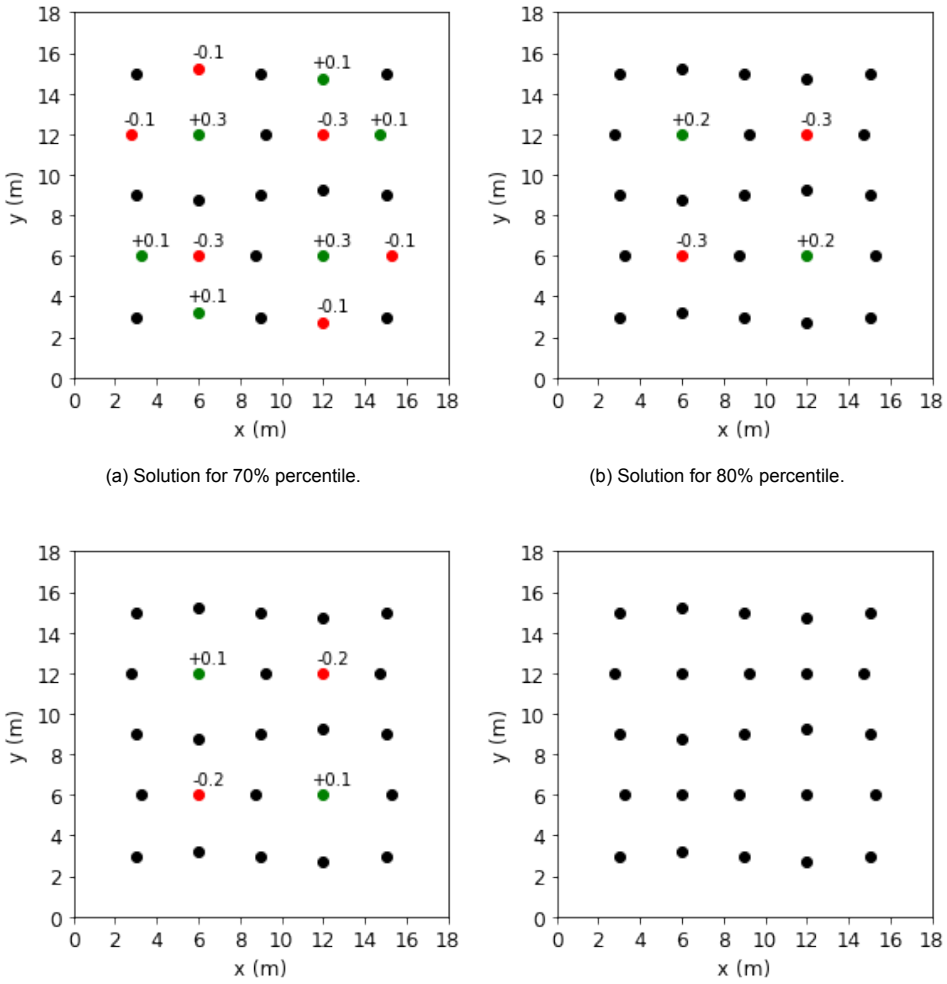

(a) Solution for 70% percentile.

(b) Solution for 80% percentile.

(c) Solution for 90% percentile.

(d) Solution for 100% percentile.

Figure 5.20: Charging adjustment solutions obtained using charge segment length 0.1 m, for 70-100% percentiles.

Table 5.6: Number of charge reductions and increases by segment length 0.1 m corresponding to solutions displayed in Figure 5.19 and Figure 5.20.

EED cap percentile	Charge reductions	Charge increases	Balance
10%	30	24	-6
20%	26	26	0
30%	21	22	+1
40%	10	10	0
50%	10	8	-2
60%	10	9	-1
70%	10	10	0
80%	6	4	-2
90%	4	2	-2
100%	0	0	0

Examination of the charging adjustment solutions learns that there is a clear trend; with lower EED cap percentiles, the number of charge adjustments increases. At the 100th percentile, effectively meaning that no EED cap is applied, not a single adjustment of the height of explosive columns in the blastholes leads to an improvement of the objective value, while at the 10% percentile the best result is achieved by making 54 adjustments of charge segment length 0.1 m. For the 80% and 90% EED cap percentiles, charge adjustments are only made in the blastholes where they would be expected (number 6, 8, 16, and 18). However, in both cases, more charge reductions than improvements are made, which of course points to a bias like explained before.

When using lower percentiles, some of the excess or lacking EED resulting from charge increases and decreases in holes 6, 8, 16, and 18 is compensated by making opposite adjustments in the nearby deviated blastholes, similar to the example of Figure 5.18. More imbalances in the number of charge reductions and increases are occurring with EED cap percentiles of 10%, 30%, 50%, and 60%. The ones for 30% and 60% are notably caused by slight asymmetry in the charge adjustments, as can be observed in Figure 5.19c and Figure 5.19f. This may be due to Tabu Search not reaching the very best solution here. Even without this, though, the imbalance between charge reductions and increases in these tests indicates that results are affected by a bias which behavior might change with the used EED cap percentile.

The effect of this could perhaps be reduced by choosing a larger charge segment length since this makes the optimization less sensitive to small differences in EED; when larger differences in EED are required to make charge adjustments, the dissimilarity between increases and reductions may be less of an issue. In Figure 5.21 the charging adjustment solutions obtained with a charge segment length of 0.3 m are displayed, and an overview of the number of adjustments is given in Table 5.7. Because there are no imbalances in the amount of charge reductions and increases any more, using a charge segment length of 0.3 m indeed seems to do a better job at circumventing any biases, as the expected adjustments are found in holes 6, 8, 16, and 18.

Table 5.7: Number of charge reductions and increases by charge segment length 0.3 m corresponding to solutions displayed in Figure 5.21.

EED cap percentile	Charge reductions	Charge increases	Balance
10%	8	8	0
20%	8	8	0
30%	8	8	0
40%	4	3	-1
50%	2	2	0
60%	2	2	0
70%	2	2	0
80%	2	2	0
90%	2	2	0
100%	0	0	0

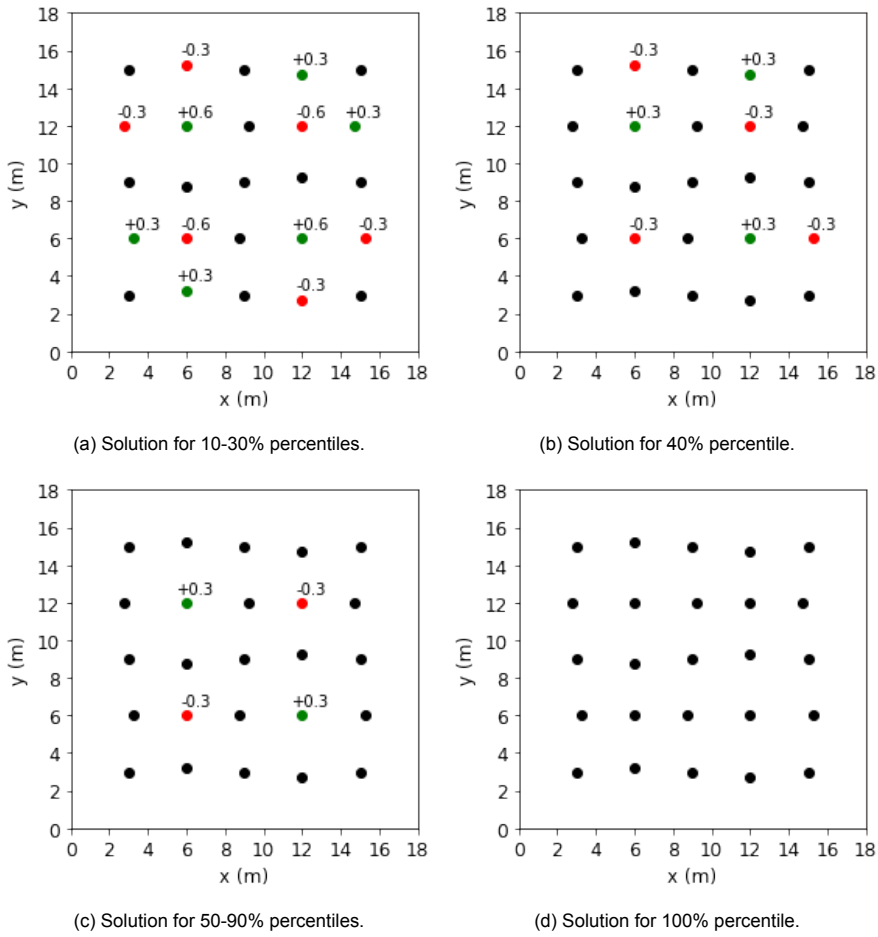

(a) Solution for 10-30% percentiles.

(b) Solution for 40% percentile.

(c) Solution for 50-90% percentiles.

(d) Solution for 100% percentile.

Figure 5.21: Charging adjustment solutions obtained using charge segment length 0.3 m.

Thanks to the greater charge segment length, the compensating effect of opposite adjustments in the nearby deviated holes is only present with EED cap percentiles of 30% and lower. The solution corresponding to the 40% percentile of EED data can be seen as an interstitial case, for which optimization perhaps also did not reach the very best solution. Between 50% and 90%, only the expected adjustments are made. This is preferred over the situation in the lower percentiles, because it improves the practicality of the optimization program, as the focus should be on a small amount of the most effective charge adjustments. The practicality is of course also improved by using the larger segment size 0.3 m compared to 0.1 m, because the level of detail corresponding to the latter might be difficult to achieve when loading drillholes with explosives.

Considering the observed benefits, using a charge segment length of 0.3 m seems to be the appropriate choice. Although the arguments of both the enhanced robustness regarding biases between charge reductions and increases as well as the improved practicality apply similarly to charge segment lengths of 0.4 m and 0.5 m, the required EED difference threshold for charge adjustments is also further increased. This may be applicable to situations with many large drillhole deviations, but generally, such a setup would result in the loss of too much detail and only lead to a very small number of charge adjustments. In this 5 by 5 test pattern, the expected charge adjustments by 0.4 or 0.5 m are still found in the optimization solutions, but their resulting improvement to the EED difference is smaller than the same adjustments by 0.3 m. This can be observed in the corresponding graphs included in Appendix B.

Additionally, this effect can also be observed in some of the charging adjustment solutions in Figure 5.21; excess and lacking EED resulting from 0.3 m adjustments in holes 6, 8, 16, and 18 are already compensated by opposite adjustments in nearby deviated holes to reach optimal solutions. When the expected adjustments in holes 6, 8, 16, and 18 are increased to 0.4 or 0.5 m, more opposite adjustments would be required in nearby deviated holes to achieve the best improvements to the EED difference. The individual charging adjustment solutions obtained using charge segment lengths 0.2, 0.4, and 0.5 m can be found in Appendix C.

Although the performance at all EED cap percentiles is a lot more stable when using charge segment length 0.3 m, the tests with segment length 0.1 m do indicate there is a bias that likely varies with the used percentile of EED data. Although an equal amount of charge increases and decreases is not necessarily required for the optimization of the explosive energy distribution, the fact that this is not achieved in a simplified test setup is worrisome. Using charge segment length 0.3 m might be an effective way to suppress any biases in this idealized configuration, but it is important to also evaluate whether this is also the case for blast patterns on a true scale. Based on the 5 by 5 test pattern results, the most promising percentiles are those between 50% and 90%, but additional testing on full-scale blast patterns is required to make a selection with greater confidence.

5.1.4. Optimization

The solutions displayed in Section 5.1.3 indicate that only a small number of charge adjustments are required to achieve the optimal configuration. With a maximum of eight changes to the top of the explosive columns, at most two in the same blasthole, this will likely favor optimization methods that focus especially on exploring the solution space by searching locally. Therefore, Tabu Search is expected to outperform the more globally oriented Genetic Algorithm. Nevertheless, GA may have useful applications in blast patterns that require more charge adjustments. Two scenarios will be examined using both optimization methods. Scenario 1 uses the selected charge segment length of 0.3 m and an EED cap percentile of 50%, which should result in the expected charge adjustments in holes 6, 8, 16, and 18 only. To compare the performance of the Genetic Algorithm for blast patterns with more adjustments, the charge segment length is changed to 0.1 m for scenario 2. Having already provided the optimal solutions in Section 5.1.3, here the focus will be on how these solutions are reached by examining the optimization paths of the two methods, and how this is influenced by the optimization parameters.

Tabu Search is initially performed using a tabu tenure of 3 iterations. For the Genetic Algorithm, the best results for the 5 by 5 test pattern are obtained by setting the population size to 20, and the mutation probability to 0.025. The resulting optimization paths for both scenarios are displayed in Figure 5.22, in which the red dots represent the first encounter of the lowest objective value found. The greater level of detail using charge segment length = 0.1 m naturally results in better (lower) objective values, but evidently, this causes greater computation times as well. The computation time is also the most obvious difference between the two optimization methods, caused by their varying approaches. It should be noted that the implemented Tabu Search method uses a more heuristic procedure, making individual adjustments based on their effect on the objective value, while the Genetic Algorithm is more random due to arbitrary cutting points for crossover and probability-controlled mutation. As a result, the optimization path for a given blast pattern will always be the same when using Tabu Search, but the ones obtained by multiple runs of a particular Genetic Algorithm are not necessarily identical.

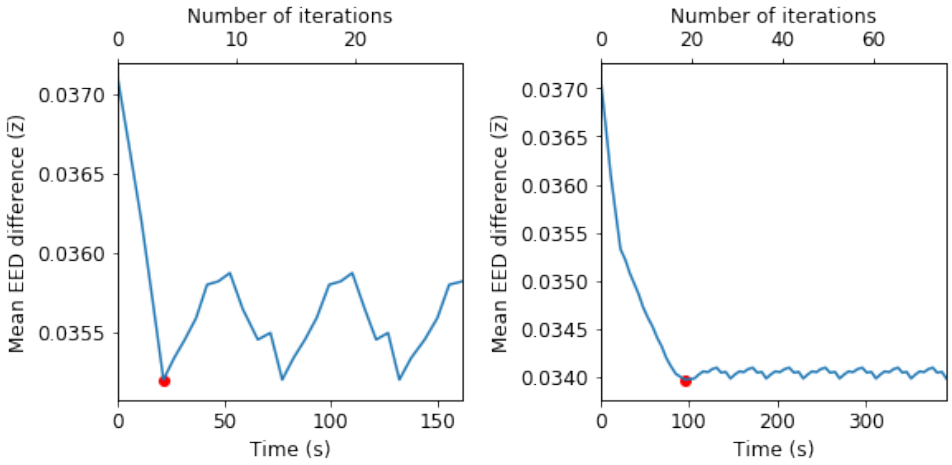

(a) TS scenario 1.

(b) TS scenario 2.

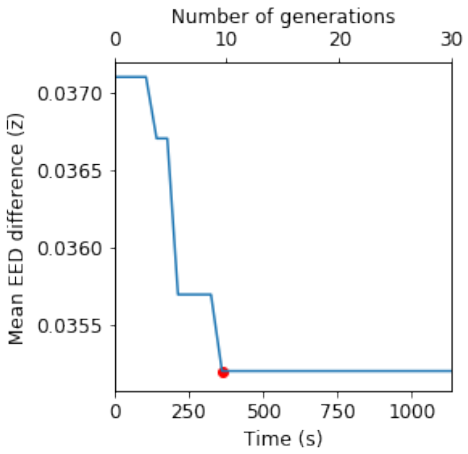

(c) GA scenario 1.

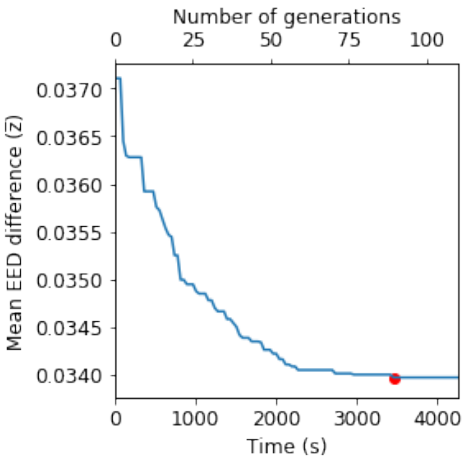

(d) GA scenario 2.

Figure 5.22: TS and GA optimization paths for scenarios 1 and 2.

For Tabu Search, the ‘current solution’ of each iteration is plotted, which illustrates how the procedure attempts to depart from local optima by briefly allowing deterioration of the objective value, which is controlled by the tabu tenure. Clearly, a better solution than the initial optimum is not found in this configuration for the 5 by 5 test pattern. Tabu Search is stopped once a clear loop of identical values is detected (when the last 10 solutions have already been visited before), which indicates that no further improvements will be achieved.

Although populations in the Genetic Algorithm naturally contain solutions of varying quality, only the very best solution of every generation is plotted. Because of the implemented generational elitism, this best solution will never worsen and the objective value only decreases as optimization progresses. As indicated by the step-like pattern, a couple of generations might pass in which none of the offspring produces a better solution than the best one from a previous generation. The stopping criterion for the Genetic Algorithm is set to 20 generations without any improvement of the objective value.

Although the GA's computation time is significantly longer than the TS's, even for the second scenario with more adjustments, it may be more useful when applied to larger datasets. Especially the first couple of GA generations are generally quite effective, and could perhaps be used to provide a better starting point for TS in case many adjustments must be made. As indicated by the gently sloped second half of the optimization path in Figure 5.22d, it takes GA a lot of effort to reach the very best solution.
The first optimization parameter that will be discussed is the tabu tenure. Since this variable effectively controls how much the Tabu Search optimization can depart from a local optimum, a lower tabu tenure leads to less diversification. In the most extreme case, that is with a tabu tenure of 0, an unfavorable adjustment can be directly undone. This instantly leads to a loop in the Tabu Search, as this single adjustment will simply be repeated over and over, as illustrated by the optimization path in Figure 5.23a. In Figure 5.23b, the resulting changes to the objective value are too small to be recognized, but the same process applies. With a tabu tenure of 0, Tabu Search in this configuration effectively becomes a hill-climbing algorithm, and moving away from a local optimum becomes impossible.

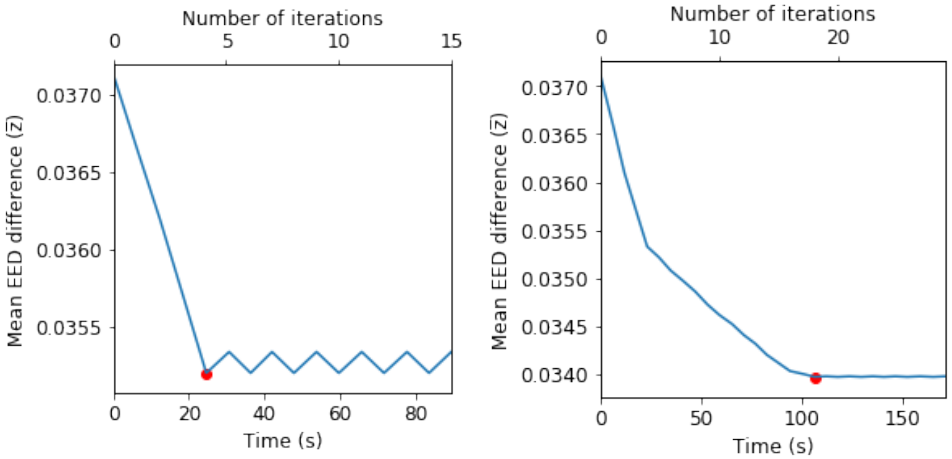

(a) TS scenario 1, tabu tenure = 0.

(b) TS scenario 2, tabu tenure = 0.

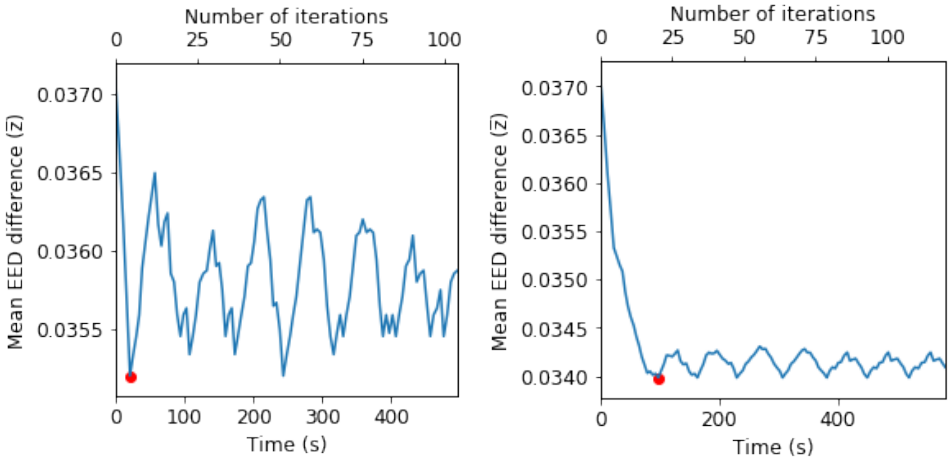

(c) TS scenario 1, tabu tenure = 6.

(d) TS scenario 2, tabu tenure = 6.

Figure 5.23: Influence of tabu tenure on TS optimization paths for scenarios 1 and 2.

Increasing the tabu tenure, on the other hand, forces Tabu Search to look for solutions further away from the local optimum by preventing the undoing of adjustments for a larger number of iterations. In Figure 5.23c and Figure 5.23d it can be observed that this causes a lot more variation in the current solution. The obvious downside is that it takes a lot longer to reach a solution loop to verify that no improvements will follow. In both cases, this solution loop is not reached within 100 iterations marked by no improvement. Because scenario 2 uses the more detailed charge segment length of 0.1 m, multiple charge adjustments in the same drillholes are required. In combination with the longer tabu tenure, this causes optimization to take more iterations to find the optimal solution (21 iterations compared to 19 for tabu tenure = 3). Moreover, using a tabu tenure of 6 results in a slightly worse 'optimal solution' for scenario 2 compared to using a tabu tenure of 3; the required combination of charge adjustments can apparently not be achieved within a reasonable time.

Due to the implemented search radius of 5 m, the area of the block model that is affected by a single charge adjustment is relatively small; only a small number of blastholes will influence part of a particular hole's area. This means that, except for directly neighboring holes, charge adjustments in various blastholes do not impact each other. Restricting the undoing or direct further adjustment in a single hole is therefore valuable only to consider the effect of potential adjustments in neighboring holes. In this manner, multiple charge adjustments in neighboring holes may be considered before e.g. undoing an unfavorable adjustment, which could ultimately result in a net improvement. Because only the directly neighboring blastholes are relevant, there is likely not much benefit in using a very high tabu tenure. Although a tabu tenure of one or two iterations shorter or longer can lead to some differences in optimization, the best performance is generally achieved with a tabu tenure of 3 iterations, which thus permits charge adjustments in three neighboring blastholes to compensate for an unfavorable one, before allowing its reversal.

For the implemented Genetic Algorithm, the relevant optimization variables are the population size and the mutation probability. The tournament size could also be altered, but this is left out of consideration. When the population size is reduced to 10, more generations may pass before an improvement is found, as displayed by the corresponding optimization path in Figure 5.24a. A smaller population will naturally lead to a reduction of solution diversity, which means it becomes less likely that beneficial adjustments are present in the population. In the case of scenario 1, only three of the four adjustments required to obtain the optimal solution are made before the optimization is halted due to 20 iterations without improvement. For scenario 2 (Figure 5.24b), the larger amount of required charge adjustments helps the algorithm to progress, despite the smaller population. It then highlights its positive aspect, which is the improved computation time per generation; in this case, the very best 'optimal solution' is actually reached, and about twice as fast compared to using population size 20.

Conversely, choosing a larger population size increases the computation time of each generation. However, since it benefits the solution diversity, chances increase that the very best solution is eventually reached, and it might do so within a smaller number of iterations. This is especially helpful for blast patterns that require few charge adjustments, like scenario 1 (Figure 5.24c). For scenario 2, on the other hand, a larger population mostly increases the computation time (Figure 5.24d). These examples show that for optimal performance of the GA, optimization parameters should be tweaked based on the blast patterns' particular requirements.

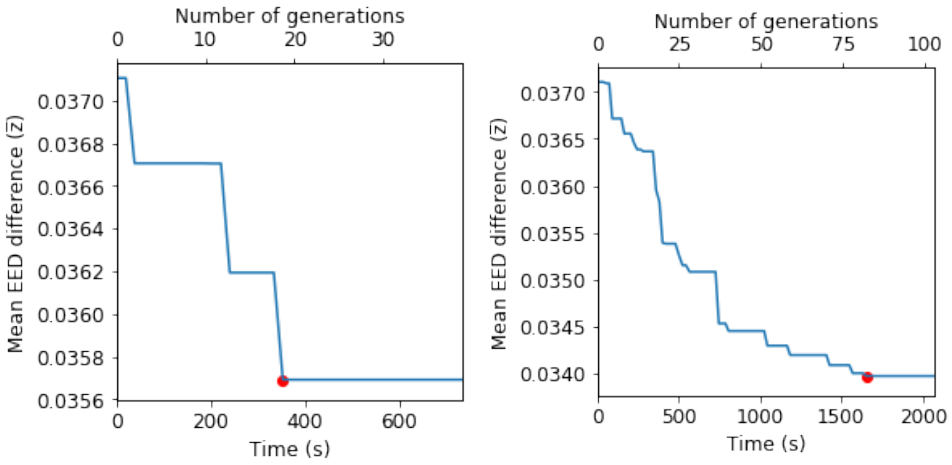

(a) GA scenario 1, population size = 10.

(b) GA scenario 2, population size = 10.

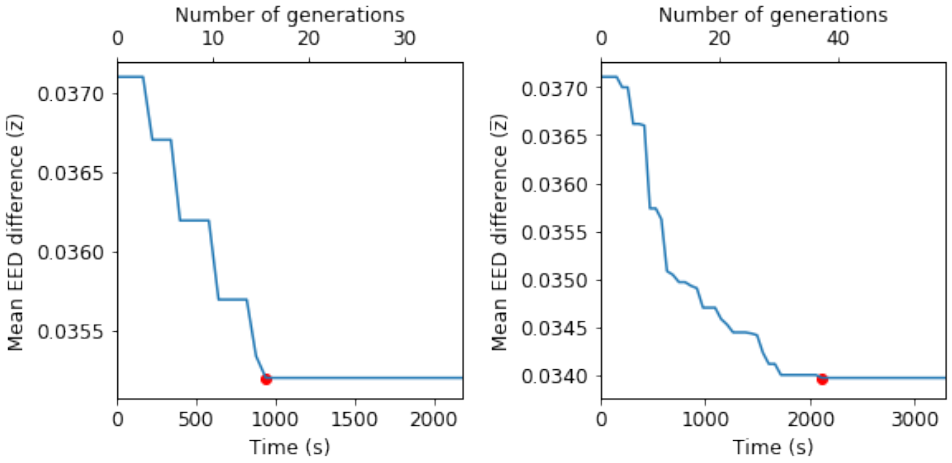

(c) GA scenario 1, population size = 30.

(d) GA scenario 2, population size = 30.

Figure 5.24: Influence of population size on GA optimization paths for scenarios 1 and 2.

This can also be illustrated by varying the mutation probability. Although it acts similarly for one part by introducing more solution diversity, selecting very high values for this parameter can also hinder optimization; if too many genes are mutated, this might reduce the effectiveness of tournament selection of parent solutions and their crossover, due to excessive alteration of offspring. Therefore, a higher mutation probability can either increase or decrease computation times, as shown in Figure 5.25c and Figure 5.25d.

In the current configuration, initial solutions for the GA are generated from random adjustments of one charge segment length up or down. Whenever some holes require multiple adjustments to reach the optimal solution, which is the case for scenario 2, this can rely more heavily on random mutations. As observed in Figure 5.25b and Figure 5.25d, the effect on the second half of the optimization path is limited. Although the mutation probability is higher for Figure 5.25d, it is still struggling to find the last couple of beneficial charge adjustments. A difference that can also be spotted between Figure 5.25a and Figure 5.25c, is that the optimization paths corresponding to a lower mutation probability seem to become somewhat more stretched out, due to more iterations without improvement early on.

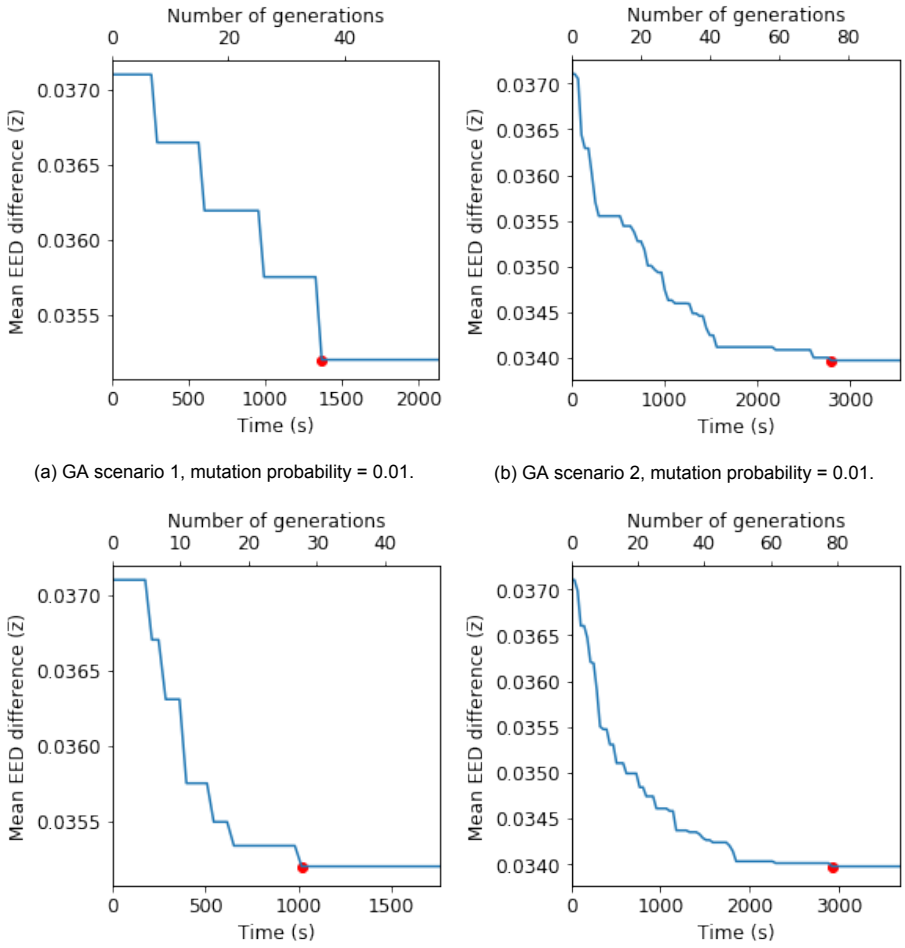

(a) GA scenario 1, mutation probability = 0.01.

(b) GA scenario 2, mutation probability = 0.01.

(c) GA scenario 1, mutation probability = 0.05.

(d) GA scenario 2, mutation probability = 0.05.

Figure 5.25: Influence of mutation probability on GA optimization paths for scenarios 1 and 2.

The higher mutation probability, on the other hand, results in a more parabolic optimization path, in which the first improvements are achieved relatively quickly. If the small number of required adjustments for the optimal solution of scenario 1 can not be easily obtained from the initial population, evidently mutation can play an important role here too. Moreover, this particular optimization path for scenario 1 is characterized by six distinct improvements to arrive at the optimal solution, compared to the usual four. This is most likely due to the increased mutation probability. Hence, an increased mutation probability might contribute to a more gradual optimization path, and could thereby reduce the chances of preemptively triggering the stopping criterion.

Clearly, the relationships between the GA optimization parameters and the resulting optimization paths are complex, and may strongly depend on the blast pattern and characteristics of its optimal charge adjustments solution. Keeping this in mind, an appropriate selection of these parameters is important for efficient optimization of the Nevada 1 and Nevada 2 datasets, but the very best settings are difficult to determine due to randomization effects. Overall, Tabu Search seems more effective at finding the very best solution, at least for this 5 by 5 test pattern. For full-scale blasts, GA may be useful to provide a better starting point for Tabu Search in case many charge adjustments are necessary to obtain the optimal solution. In the 5 by 5 test pattern, however, the number of charge adjustments would clearly not be large enough to improve computation time compared to simply using Tabu Search directly.

5.1.5. Explosive Energy Distribution

Because an appropriate EED cap percentile can not yet be defined using only the 5 by 5 test pattern data, this section will examine the block model and EED values corresponding to an arbitrary EED cap percentile of 50% as an example. The other control parameters are set to the appropriate values as defined before; a search radius of 5 m, block size of 0.2 m, and charge segment length of 0.3 m. This setup is the same as the one used to obtain the charge adjustments solution of Figure 5.21c, and also corresponds to scenario 1 of Section 5.1.4.

A cross-section of the block model's planned EED values, through drillholes number 5 to 9 as in Figure 4.7, is shown in Figure 5.26. Similarly, the real EED is displayed in Figure 5.27. Optimization by either TS or GA results in the expected charge adjustments in blastholes 6, 8, 16, and 18, and a visualization of the resulting optimized EED can be found in Figure 5.28. The absolute difference between the planned EED and real EED represents the initial state of the optimization objective and is given in Figure 5.29. The final state of the optimization objective is reached once these block-to-block differences are minimized. This situation is displayed in Figure 5.30, obtained from the absolute difference between the optimized EED and planned EED. For a visualization of the effect of optimization, Figure 5.31 shows how the block-to-block differences have changed between the initial state and the optimized state.

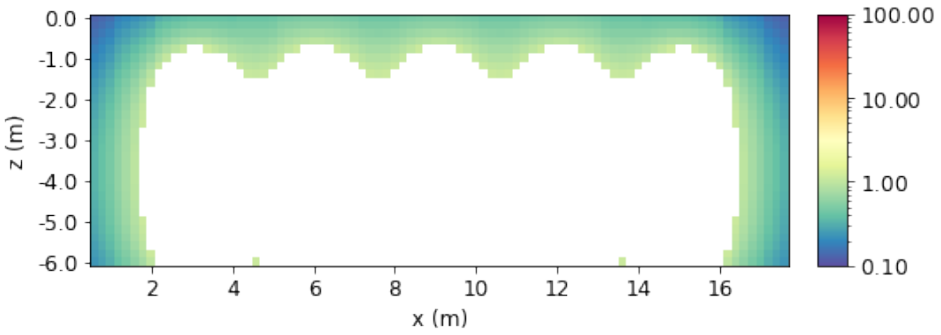

Figure 5.26: Cross-section of planned EED for 5 by 5 test pattern.

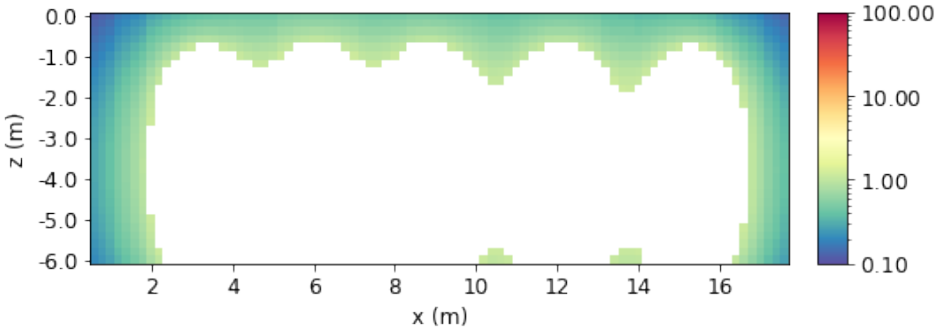

Figure 5.27: Cross-section of real EED for 5 by 5 test pattern.

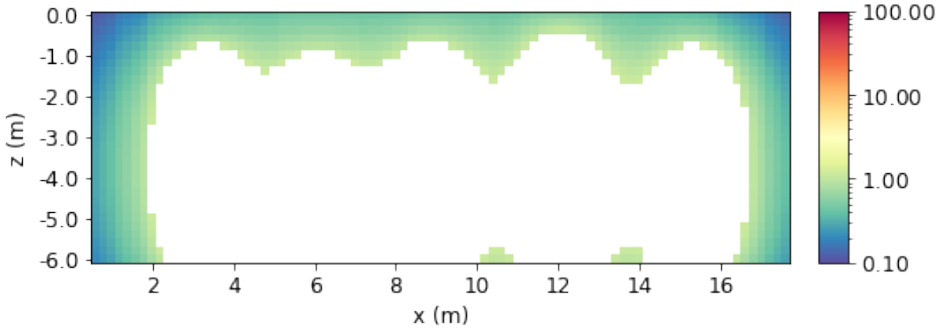

Figure 5.28: Cross-section of optimized EED for 5 by 5 test pattern.

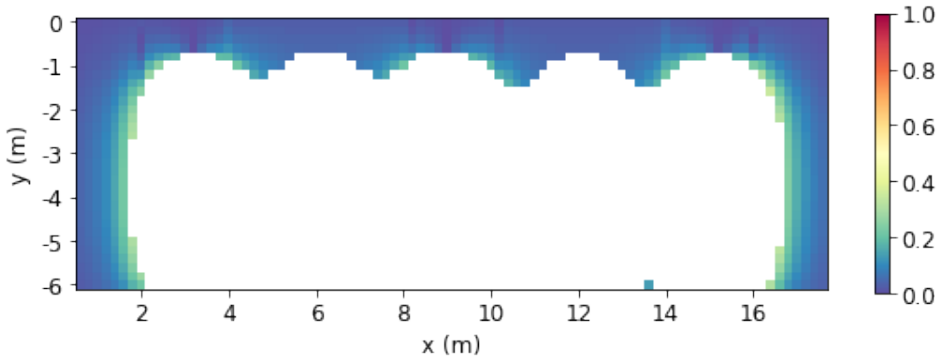

Figure 5.29: Cross-section of the difference between planned and real EED for 5 by 5 test pattern (initial state).

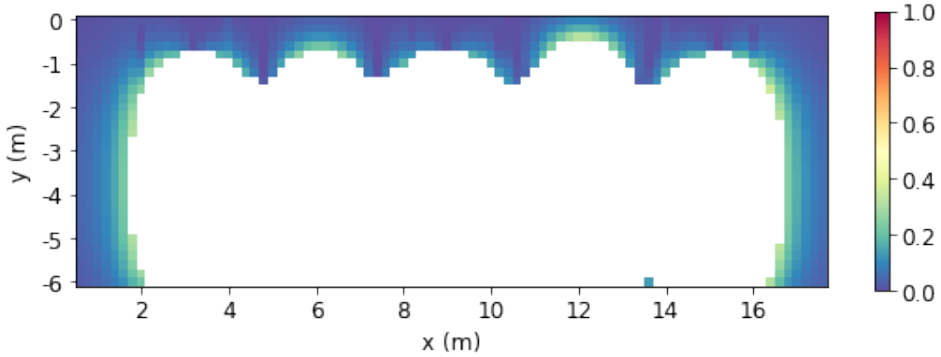

Figure 5.30: Cross-section of the difference between planned and optimized EED for 5 by 5 test pattern (optimized state).

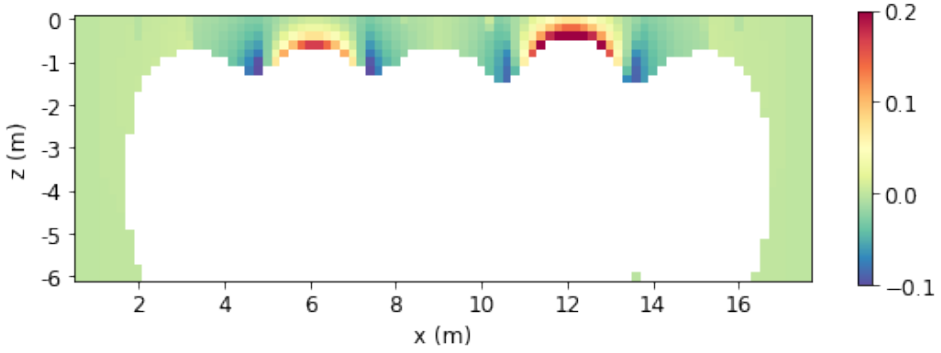

Figure 5.31: Cross-section of the difference between initial and optimized state of EED differences, for 5 by 5 test pattern.

It is evident that most of the EED values within the lower 50% percentile are located at the outer boundaries of the blasted area. Although some of the rocks may not receive sufficient energy for breakage already in the planned configuration, it is important to recognize the importance of breaking the rock mass appropriately at the intended limits, which may be affected by changes in the explosive energy distribution, especially in those parts. By discarding the highest values in the center of the blast, the focus is shifted towards such zones that are not set to receive a lot of explosive energy in the first place. Any changes in EED values here are most likely to affect fragmentation.

Optimization is therefore aimed towards minimizing the differences in explosive energy in these areas where it matters most. In Figure 5.27 it can be observed that due to the deviation of holes 7 and 9 away from hole 8, the area of discarded EED values is altered around blasthole 8 because some blocks now receive less explosive energy. The optimized EED in Figure 5.28 shows even more differences, caused by the adjustments of the explosive column height in blastholes 6 and 8. Since block-to-block differences can only be calculated in blocks that hold EED values in both configurations, Figure 5.29 and Figure 5.30 combine the 'masks' of discarded values for the planned EED en real EED, and planned EED and optimized EED respectively.

Although there are some differences found in between the other drillholes, Figure 5.29 shows that the largest differences are found around the deviated holes number 5 and 9. In Figure 5.30 it can be observed that the charge decrease in hole number 6 and increase in hole number 8 lead to reductions of the EED differences in the areas between these holes and holes 5, 7, and 9, in the upper part of the blast. However, these charge adjustments also introduce new differences directly above blastholes 6 and 8. By comparing the original differences of Figure 5.29 with the differences after optimization of Figure 5.30, Figure 5.31 is obtained. This figure is a more convenient representation of the effect of optimization on the EED differences and illustrates what was described before. What is especially striking, is the magnitude of the added differences related to the charge increase in blasthole 8 compared to those related to the charge decrease in hole 6; adjustments in opposite directions evidently have a different effect on the EED differences.

When the block model is examined from a top-down point of view, one can get a better overview of the low EED zones. Besides near the surface and at the outer vertical boundaries, low EED blocks can also be found near the bottom of the core of the blast, as illustrated in Figure 5.32a. Similarly, the low EED zone found in the upper section of the blast also extends a bit further down in the areas furthest away from the blastholes, as shown in Figure 5.32b. Although changes to the EED in these areas are of course still considered during optimization, the EED differences are more clearly visible at elevations closer to the surface, which contain more low-valued blocks.

In Figure 5.33, the explosive energy distribution at z = -1.0 m is displayed for the various configurations. It should be noted that for the planned EED, real EED, and optimized EED, in Figure 5.33a, Figure 5.33b, and Figure 5.33c respectively, the EED scale is changed compared to Figure 5.32a and Figure 5.32b for a more detailed view. The figures then show that the real EED values near blastholes 6 and 18 are higher compared to the planned EED, while the neighborhood of holes 8 and 16 see a decrease. This is caused by deviation of nearby holes away from numbers 8 and 16, and towards numbers 6 and 18. By increasing the height of the explosive column in holes 8 and 16, and reducing it in holes 6 and 18, these undesired changes to the EED are somewhat mitigated in the optimized EED.

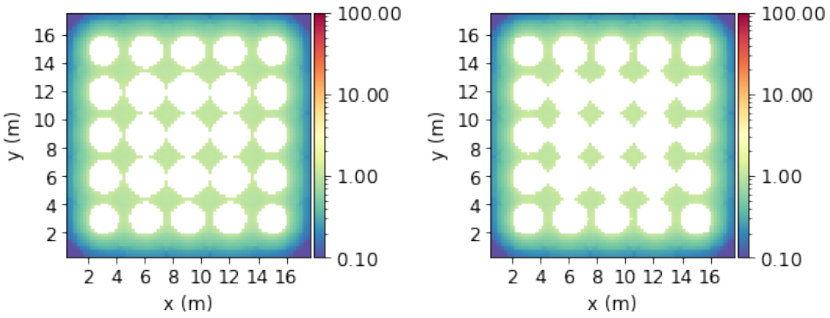

(a) z = -6.0 m. (b) z = - 1.6 m.

Figure 5.32: Top-down view of planned EED at z = -6.0 m and z = -1.6 m.

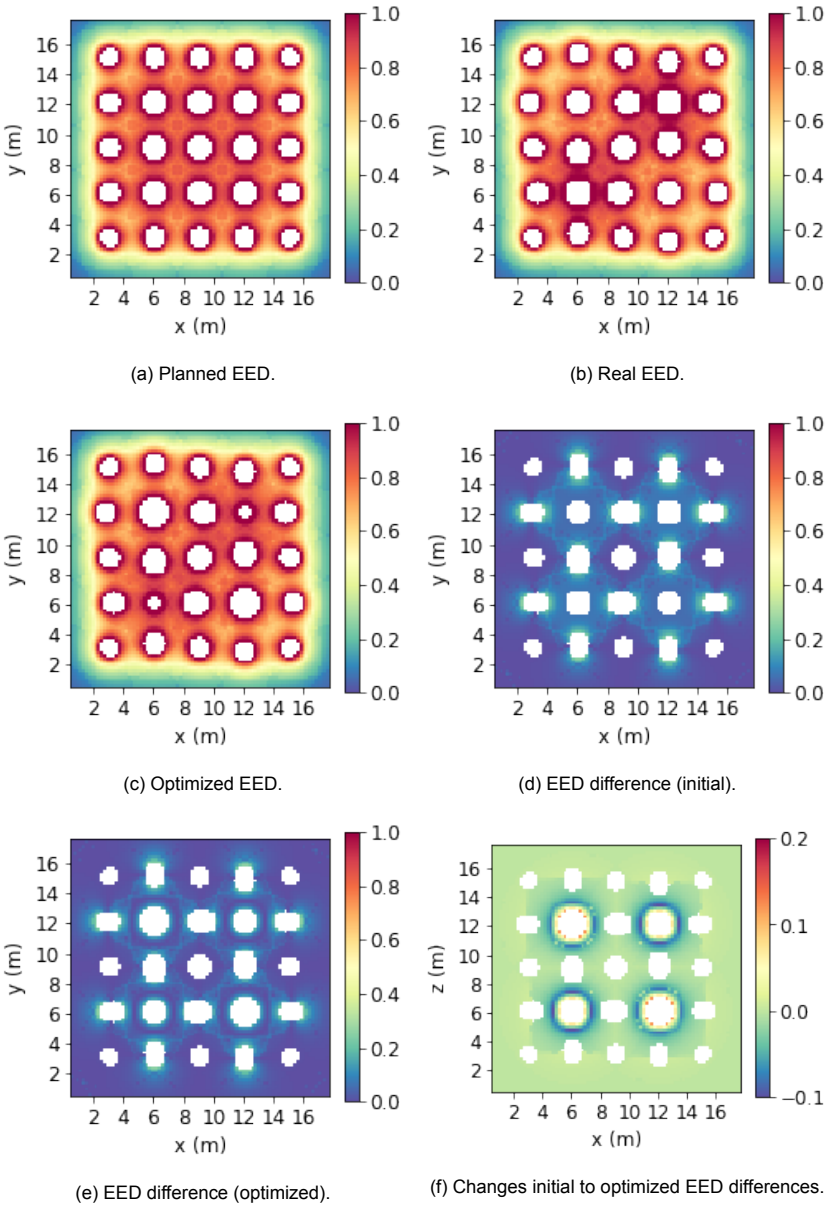

(a) Planned EED.

(b) Real EED.

(c) Optimized EED.

(d) EED difference (initial).

(e) EED difference (optimized).

(f) Changes initial to optimized EED differences.

Figure 5.33: Top-down view of the various EED configurations and their differences at z = -1.0 m.

As can be seen in Figure 5.33d, EED differences are not only found around blastholes 6, 8, 16, 18, and at areas in between these and the deviated holes; relatively large differences also occur near the deviated drillholes themselves. The difference between the planned EED and the optimized EED (Figure 5.33e) shows that the latter remain mostly unchanged, as optimization focuses on decreasing EED differences in areas in between drillholes. The effect of optimization on the EED differences in Figure 5.33f reaffirms what was already deduced from Figure 5.31; EED differences are indeed reduced effectively in blocks that lie in the middle of multiple (deviated) drillholes, but this is achieved at the cost of introducing new differences closer to the holes in which the charge adjustments are made. Once again, greater differences seem to be added by the charge increases in blastholes 8 and 16 compared to the reductions in holes 6 and 18. Moreover, the charge reductions lead to more decreases of EED differences, at least at this elevation.

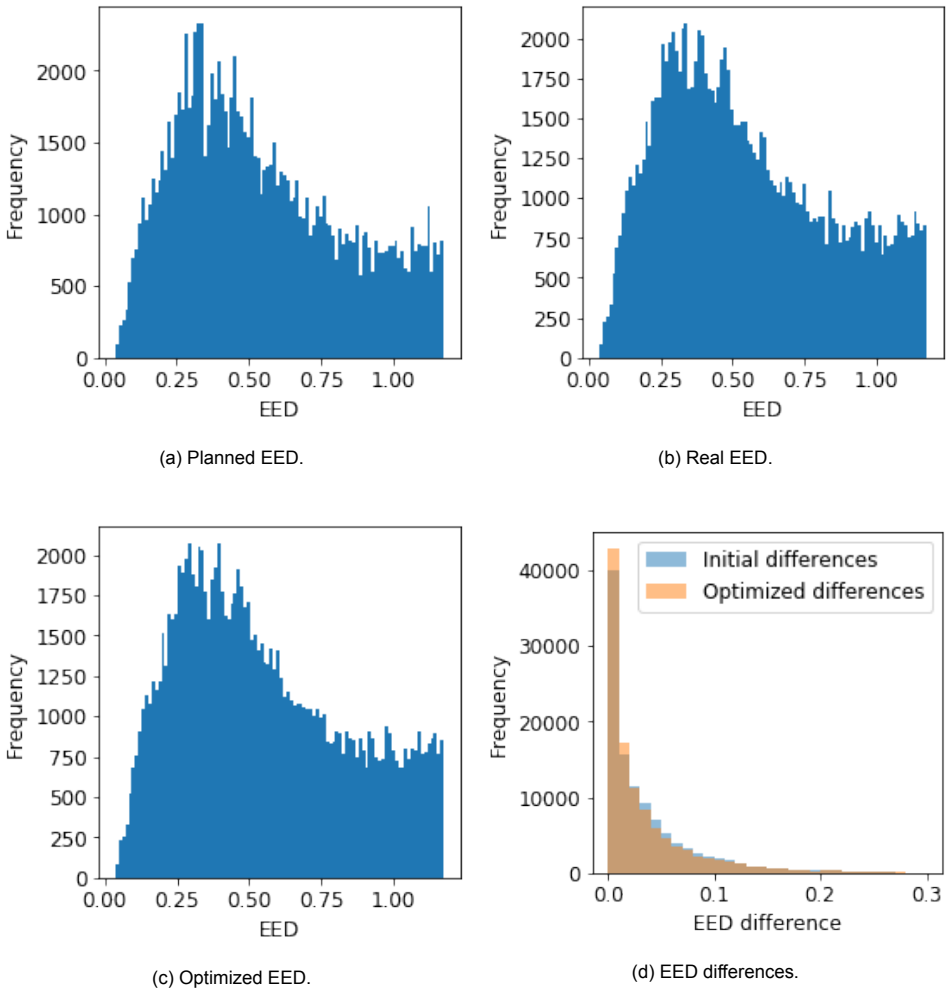

(a) Planned EED.

(b) Real EED.

(c) Optimized EED.

(d) EED differences.

Figure 5.34: Frequency distributions of the various EED configurations and their differences, for the block model of the 5 by 5 test pattern using EED cap percentile 50%.

The frequency distributions of the EED values found in the block model for each configuration are given in Figure 5.34. Because of the EED cap percentile of 50%, all values above ~1.2 are removed, and therefore only the lowest values remain. The planned EED shows the highest frequency for EED values of around 0.3, while the real and optimized EED contain more values that are slightly higher than this. Of course, there are other minor differences, but the consequences of drillhole deviation and charge adjustments do not have extreme impacts on the frequency distribution of EED values. A bit more detail can be found in frequency distributions of the EED differences. The block-to-block differences between the planned EED and real EED, labeled as 'initial differences' in figure d, and the block-to-block differences between the planned EED and optimized EED, labeled as 'optimized differences', are plotted in one figure to illustrate, once again, the effect of optimization. The lower frequency of EED differences between 0.03 and 0.1 for the optimized case indicates that most improvements attributed to optimization are found in this range. However, this comes at the cost of more EED differences of smaller magnitude (0.01-0.02).

Evidently, this leads to a net improvement of the objective value, the mean EED difference, of 5.15%. In Table 5.8, this value is listed among the improvements resulting from optimization of the 5 by 5 test pattern using other EED cap percentiles. The reader is reminded that not all of the EED cap percentiles lead to the same charge adjustment solutions, as found in Section 5.1.3. Naturally, a higher EED cap percentile leaves higher EED values in the block model, and therefore the mean EED rises as well. The higher EED values clearly lead to larger EED differences, which become increasingly difficult to mitigate by adjusting the height of explosive columns through optimization, as indicated by the decreasing improvement. In combination with the retrieved charging adjustment solutions found in Section 5.1.3, choosing an appropriate EED cap percentile becomes mostly a consideration about which minimal portion of EED data is still representative for the blast; low EED cap percentiles result in much higher improvements, but they only represent a small part of the data.

Table 5.8: Initial and optimized objective values for each EED cap percentile, and the corresponding improvements obtained with charge segment length 0.3 m.

EED cap percentile	**Mean planned EED**	**Mean initial EED difference ($\overline{Z}$)**	**Mean optimized EED difference ($\overline{Z}$)**	**Improvement of EED difference**
10%	0.1952	0.0081	0.0047	41.85%
20%	0.2718	0.0141	0.0107	24.14%
30%	0.3465	0.0194	0.0166	14.33%
40%	0.4348	0.0266	0.0250	6.07%
50%	0.5485	0.0371	0.0352	5.15%
60%	0.6792	0.0499	0.0476	4.66%
70%	0.8124	0.0633	0.0608	4.03%
80%	0.9552	0.0816	0.0787	3.55%
90%	1.1705	0.1195	0.1177	1.49%
100%	2.8531	0.6410	0.6410	0.00%

5.2. Nevada 1 Dataset

After examining the explosive energy distribution optimization system on a test scale, it will now be applied to the first full-size dataset Nevada 1. As described in Section 4.1, this dataset only contains the planned drillhole locations. To simulate deviations for the real drillhole setup, their x- and y-coordinates are randomly adjusted by values selected from a uniform distribution. As described in Section 4.3, two scenarios are considered; the first scenario uses a uniform distribution ranging from -0.5 to 0.5 m to produce a mean deviation in the xy-plane of 0.37 m, while the second is characterized by a mean deviation of 0.19 m obtained through a uniform distribution ranging from -0.25 to 0.25 m. These figures correspond to the first randomization (R1) as listed in Table 4.4.

In Section 5.2.1, the charge adjustment solutions resulting from optimization with the different EED cap percentiles are first evaluated to select the most appropriate option. Based on these findings, the subsequent sections will continue using only the most suitable EED cap percentiles with both scenarios. The performance of the Genetic Algorithm and Tabu Search optimization methods is then compared in Section 5.2.2, and finally, Section 5.2.3 will present the explosive energy distribution as calculated in the block model for the various drillhole setups and charging configurations to illustrate the beneficial effects of this optimization.

5.2.1. Charge Adjustments

This section will start with a comparison of the charging adjustments suggested by the solutions obtained from optimization (Tabu Search, with tabu tenure 3) of scenario 1, using the different EED cap percentiles. The relationship between charge increases and charge reductions changes depending on this variable, as discussed in Section 5.1.3, and therefore it affects the total number of adjustments made in each direction. Because it is desirable that the total amount of explosives used in the blast does not change too much from the planned quantity, it is assumed that this relationship is in balance when optimization results in an equal amount of charge increases and reductions. The adjustments obtained from optimization ran with the different EED cap percentiles are shown in Table 5.9.

Table 5.9: Number of charge reductions and increases by segment length 0.3 m for Nevada 1 dataset with random deviations picked from a uniform distribution between -0.5 and 0.5 m (scenario 1).

EED cap percentile	Charge reductions	Charge increases	Balance
10%	65	47	-18
20%	67	144	+77
30%	51	63	+12
40%	38	41	+3
50%	40	41	+1
60%	43	39	-4
70%	49	31	-18
80%	54	26	-28
90%	58	8	-50
100%	557	1	-556

Besides the odd outcome for the EED cap percentile of 10%, which supposedly leaves too little data for a representative outcome, there is a clear trend visible in the balance of charge increases and reductions; the lower EED cap percentiles produce a positive bias, and more and more charge reductions are made as it is increased. When the full 100% of the EED values is considered, this leads to an enormous number of reductions. In most blastholes, the top of the explosive column is lowered all the way down to the enforced limit, while only one charge increase is made.

The most promising EED cap percentiles are 40%, 50%, and 60%, which result in a nearly constant amount of explosives compared to the planned blasthole configuration, though still include around 80 adjustments in total. To assess the validity of this approach, as well as make a final choice for the most suitable EED cap percentile, the three candidate percentiles are tested using the different randomizations as listed in Table 4.4. The corresponding charge adjustment balances obtained through optimization can be found in Table 5.10.

Table 5.10: Charge adjustment balances for various randomizations of scenarios 1 and 2, with EED cap percentiles 40-60%.

Scenario 1			**Scenario 2**		
40%	**50%**	**60%**	**40%**	**50%**	**60%**
+3	+1	-4	-4	-4	0
-1	0	-1	0	-3	-2
-4	-5	-15	0	-1	-3
+10	+8	+3	2	-1	1
0	+1	-3	5	3	3

Examination of Table 5.9 and Table 5.10 leads to believe that even though the various deviation randomization might seem quite similar at first sight in terms of statistics, their effect on optimization is not necessarily the same. This can of course be attributed to the interaction between the drillholes, and in particular to which direction they have deviated in relation to each other. The trend of more charge increases at lower EED cap percentiles and more reductions at higher ones clearly remains. However, closing in on the zero-balance does not always seem to happen in the 40-60% range; for scenario 1, this may occur at a lower EED cap percentile for the 3rd randomization, or at a higher one for the 4th randomization. Although some of the differences are smaller in scenario 2, possibly related to the smaller deviations, its 5th randomization might achieve the zero-balance at a higher EED cap percentile too.

Nevertheless, when these results are combined, the average balance achieved with an EED cap percentile of 50% is -1, while the 40% option gives an average balance of +11, and 60% gives -21. Overall, using the lower 50% percentile of EED values, therefore, seems the most appropriate choice. Although this appears to be the best way to balance the charge reductions and increases, these results do indicate that it is not a fail-safe method to obtain an exactly equal amount of explosives as used in the planned configuration. Therefore, the quantity of the explosive will still be constrained to prevent alteration of the blast's overall powder factor, as discussed in Section 3.3, by enabling the constraints of Equation (3.9) and Equation (3.10).

When these constraints are applied to the 1st randomization of scenario 1, using an EED cap percentile of 50%, the result of Tabu Search optimization is the charge adjustment solution as illustrated in Figure 5.35. A first observation is that the final height of the explosive column is adjusted more than once in only one blasthole. Because the deviations are quite large, especially considering the drillhole diameter is only 0.125 m, a relatively large amount of charge adjustments is made; this optimal solution results in 40 charge increases and 40 reductions of segment length 0.3 m. Since the total number of drillholes in this blast is 243, nearly a third of these would see an alteration of the planned charging instructions.

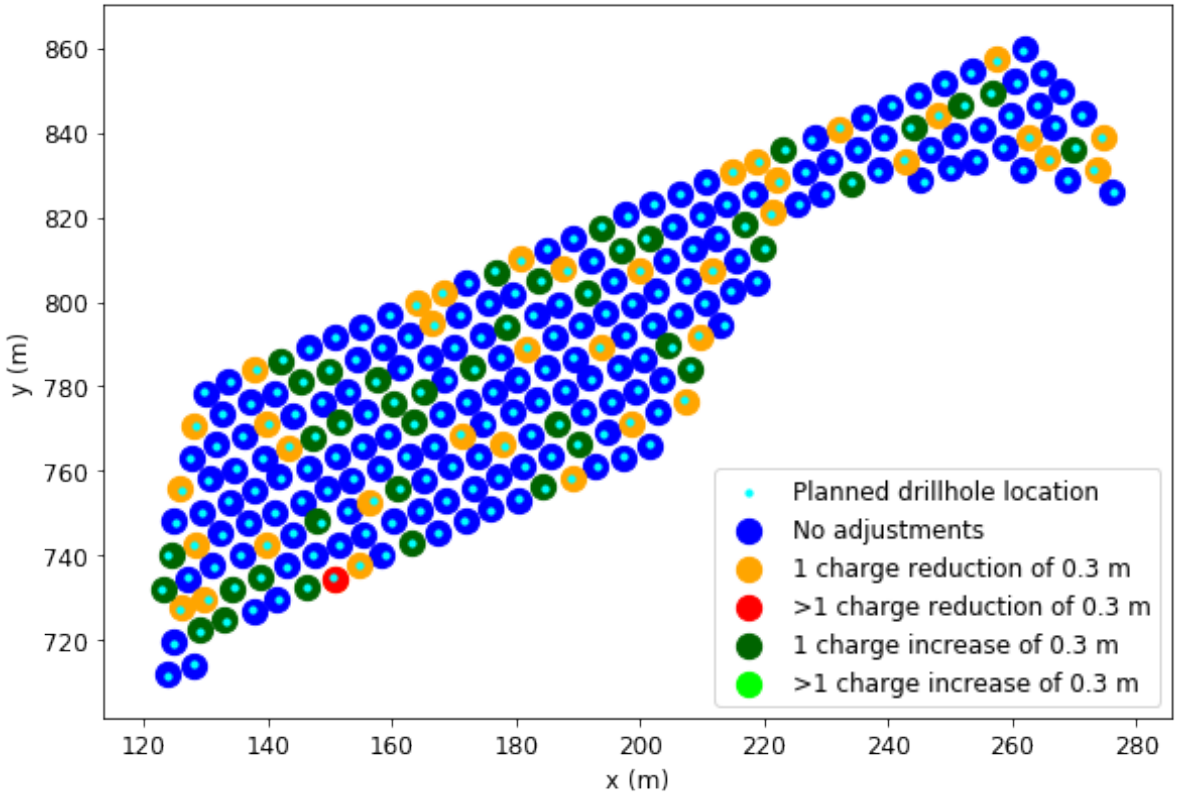

Figure 5.35: Visualization of Nevada 1 (scenario 1) optimized solution.

Although a number of adjustments are isolated, they are often found in groups. Clusters of both charge increases and reductions can be recognized, as well as combinations of the two. This emphasizes the interaction between adjustments in nearby drillholes, as the contribution of one adjustment to the EED values in surrounding blocks clearly influences adjustments in neighboring holes. If, for example, a charge increase in one blasthole does not sufficiently reduce the EED differences caused by the deviations, another increase in one of the neighboring holes may be helpful. This clearly seems favored over larger adjustments in a single hole. Conversely, if one charge increase results in a surplus of explosive energy in the surrounding area, the charge height may be reduced in neighboring holes to compensate for this. It should also be noted that for various drillholes that have been significantly deviated, this solution does not suggest any alteration of the explosive column height. This is likely due to charge adjustments in nearby holes that already (partly) compensate for the EED differences. At the same time, more adjustments could introduce too many new differences around neighboring blastholes to result in an improvement of the objective value.

An identical approach for the second scenario using the Nevada 1 dataset leads to the charge adjustment solution displayed in Figure 5.36. Because here the mean deviation in the xy-plane is only 0.19 m, as opposed to 0.37 m for scenario 1, the total number of adjustments is greatly reduced; only 10 charge increases and decreases are recommended by the optimal solution, for a total of 20 adjusted holes out of the 243. All holes are adjusted by only one charge segment length. Apart from a cluster in the top-right corner of the blast, most adjustments are made independent of each other. This indicates that there is little interaction between individual adjustments, and the effect of the tabu-mechanism may be limited.

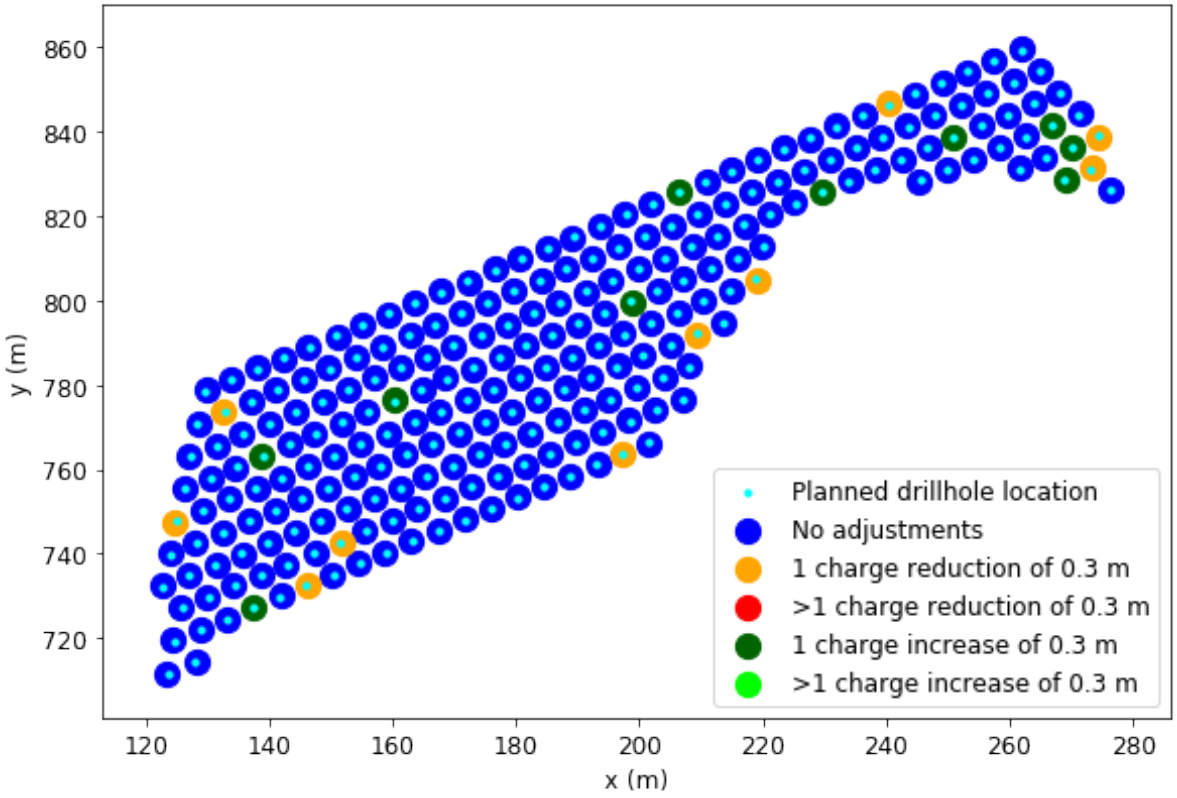

Figure 5.36: Visualization of Nevada 1 (scenario 2) optimized solution.

A notable observation in Figure 5.36 is that most charge adjustments are made in drillholes at the outer boundaries of the blast pattern, especially the reductions. Out of the 10 charge reductions, 8 are found in the outermost holes, with the other two located just one row inwards. Because blastholes at the boundaries of the blast have one 'open' side to which there are no other blastholes to compensate for small increases or decreases in EED, this could lead to larger differences than in areas where this is not the case and thereby increase the need for charge adjustments. Another factor may be the EED cap percentile of 50%. As observed in Section 5.1.5 for the 5 by 5 test pattern, the low EED values that remain are found mostly in the upper part of the blast and at the vertical boundaries, which could explain the focus on blastholes at the boundaries of the blast. The EED block model for the Nevada 1 dataset will be examined in Section 5.2.3.

5.2.2. Optimization

Similar to the approach in Section 5.1.4, the optimization paths for Tabu Search and Genetic Algorithm can be plotted for scenarios 1 and 2 of the Nevada 1 dataset to compare the performance of these optimization methods. The results can be found in Figure 5.37 and Figure 5.38. An important difference with the 5 by 5 test pattern is incorporation of a starting boost for the Tabu Search algorithm to reduce the duration of optimization. As described in Section 3.3, this mechanism performs the three best charge adjustments at once, without recalculation of the EED block model, until this procedure does not result in an overall improvement of the objective value anymore.

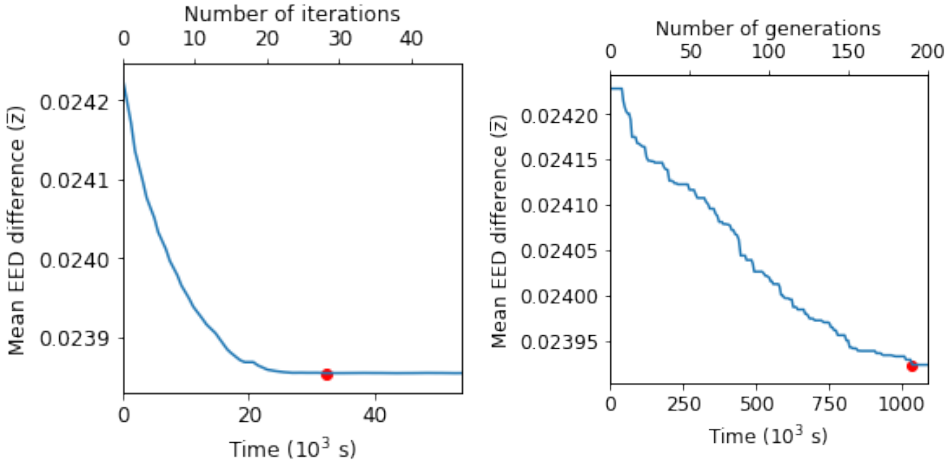

(a) Tabu Search.

(b) Genetic Algorithm.

Figure 5.37: TS and GA optimization paths for scenario 1.

For scenario 1 (Figure 5.37), this point is clearly reached after about 20,000 seconds, where the optimization path initially flattens out. Once the Tabu Search returns to optimization by making adjustments one by one including recalculation of the explosive energy distribution for each adjustment, the solution is further improved. For scenario 1, charge adjustments are often made in blastholes that are in close vicinity of each other, as illustrated previously in Figure 5.35, and switching to one adjustment at a time evidently has a positive impact on the final solution. Without the starting boost, however, the largest improvements in the initial stages of optimization would take approximately three times as long.

Despite the relatively large number of charge adjustments, the Genetic Algorithm (figure b) shows no benefit over Tabu Search, even in the first couple of generations. Using a mutation probability of 0.005 and population size of 20, it took almost 44,600 seconds to produce the first marginal improvement, which is close to the total computation time of the Tabu Search method. The stopping criterion was changed to 10 iterations without any improvement to prevent the time-consuming process of finding the last couple of beneficial charge adjustments. The computation time for this configuration was already 12.6 days, and the obtained solution is slightly worse than the one obtained using TS. The solutions generated by GA seem to be too random to compete with the more heuristic approach of Tabu Search. Using GA to generate a better initial solution for TS would only increase computation times, so simply using TS directly is still more efficient than such a hybrid method. Because of the vast difference in computational efficiency in the scenario that should be most suitable for the Genetic Algorithm, this method will not be examined any further.

The optimization path for scenario 2, displayed in Figure 5.38a, shows the optimal solution is achieved right at the end of the starting boost since the objective value does not increase or plateau at an intermediary level. Although scenario 2 mostly consists of charge adjustments in independent blastholes, this indicates that the program is capable of dealing with some clustering of adjusted holes already during the starting boost. If the total explosives quantity constraint is released, a nice example of the tabu mechanism arises in Figure 5.38b. After roughly 10,000 seconds, Tabu Search forces an unfavorable charge adjustment, which allows optimization to move away from the local optimum to find a better solution.

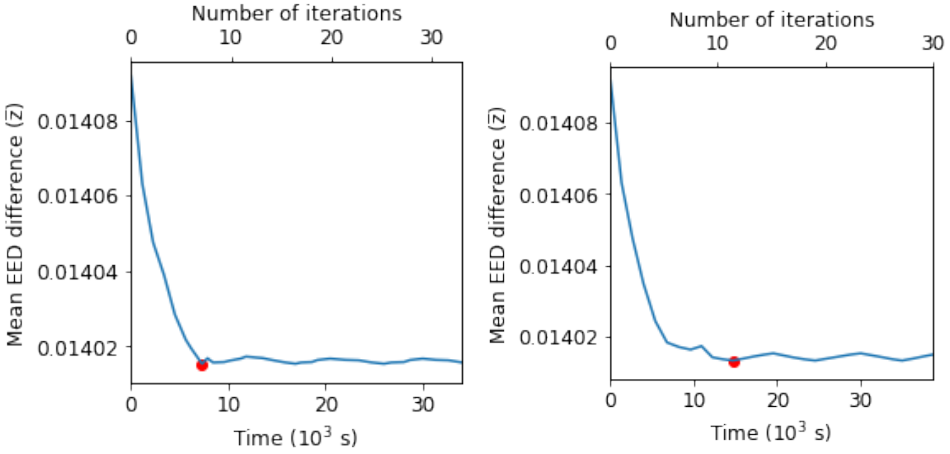

(a) Constrained.

(b) Unconstrained.

Figure 5.38: TS optimization paths for scenario 2.

5.2.3. Explosive Energy Distribution

In this section, information derived from the EED block model corresponding to the different drillhole and charging configurations will be presented. This was obtained using the previously specified control parameters; a search radius of 5 m, block size of 0.2 m, charge segment length of 0.3 m, EED cap percentile of 50%, and application of the total explosives quantity constraint. The optimized solutions correspond to the two scenarios already described in Section 4.3, and as illustrated in Figure 5.35 and Figure 5.36. First, cross-sectional views of the block model will give a general idea of which blocks are above the EED cap threshold and are therefore discarded, and in which areas the remaining blocks can be found that are used for optimization. By comparing EED values of the blocks corresponding to the different configurations, the effect of optimization on the explosive energy distribution is demonstrated.

Because of the larger deviations and the consequently greater amount of charge adjustments, the real and optimized EED corresponding to scenario 1 are used. These cross-sections are taken at y = 779.87 m, and only span part of the blast. The planned EED, real EED, and optimized EED throughout this slice of the block model are displayed in Figure 5.39, Figure 5.40, and Figure 5.41 respectively. In Figure 5.42, the absolute differences between the planned EED and real EED are shown, representing the starting point for optimization. Similarly, Figure 5.43 illustrates the differences between the planned EED and optimized EED, which is directly connected with the best objective value. Finally, the beneficial effect of optimization is demonstrated in Figure 5.44 through the difference between the initial and optimized state of the EED differences.

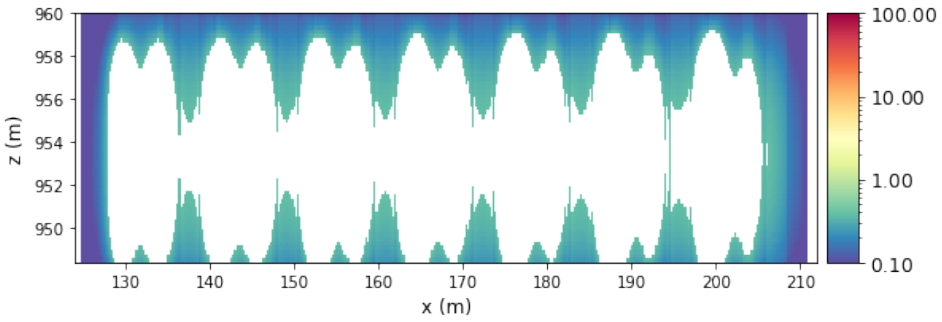

Figure 5.39: Cross-section of planned EED for dataset Nevada 1, at y = 779.87 m.

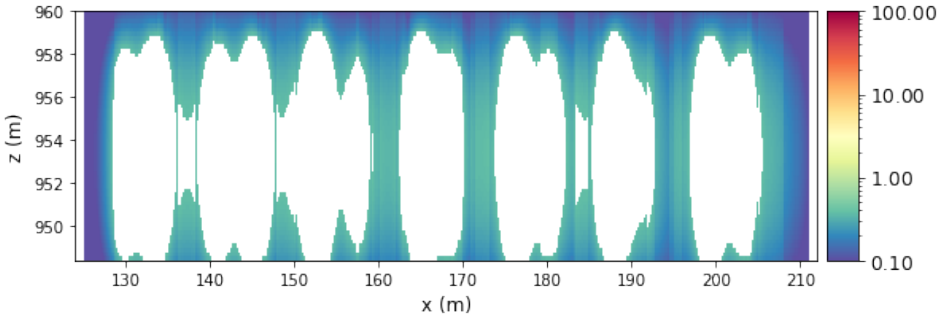

Figure 5.40: Cross-section of real EED for dataset Nevada 1, at y = 779.87 m.

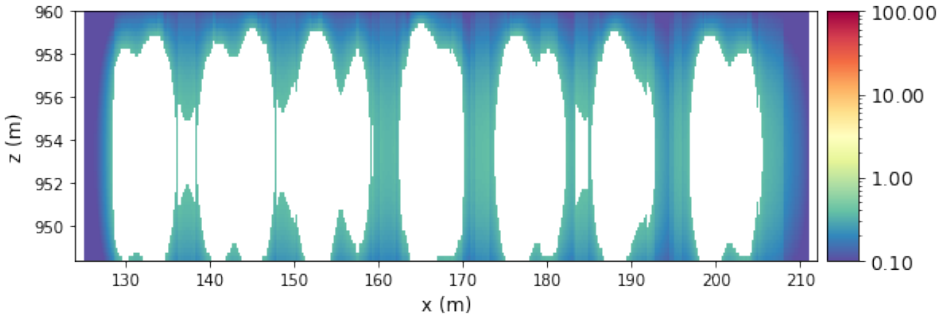

Figure 5.41: Cross-section of optimized EED for dataset Nevada 1, at y = 779.87 m.

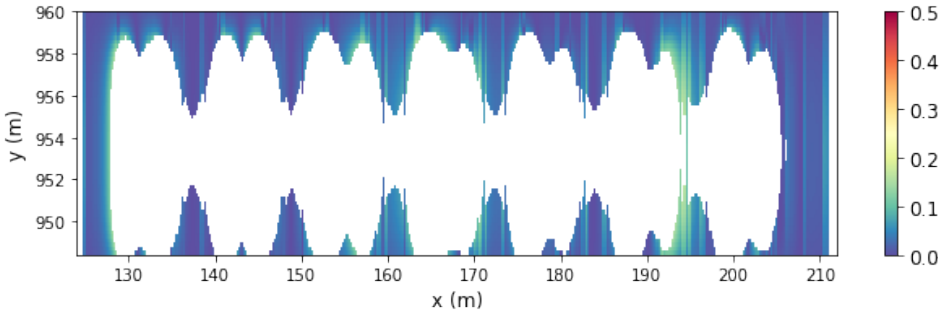

Figure 5.42: Cross-section of the difference between planned and real EED for dataset Nevada 1, scenario 1 (initial state of the objective), at y = 779.87 m.

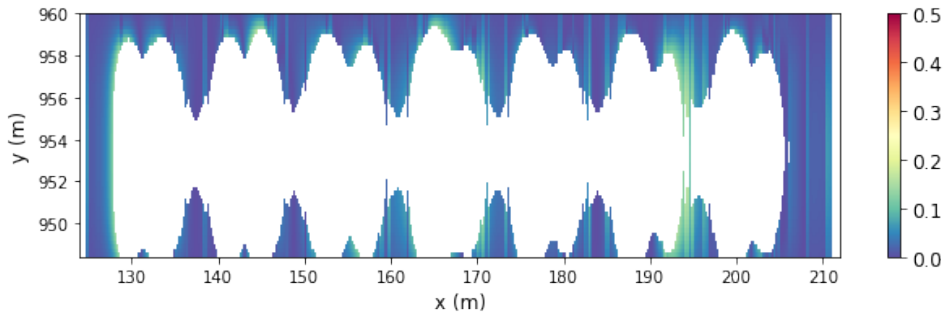

Figure 5.43: Cross-section of the difference between planned and optimized EED for dataset Nevada 1, scenario 1 (optimized state of the objective), at y = 779.87 m.

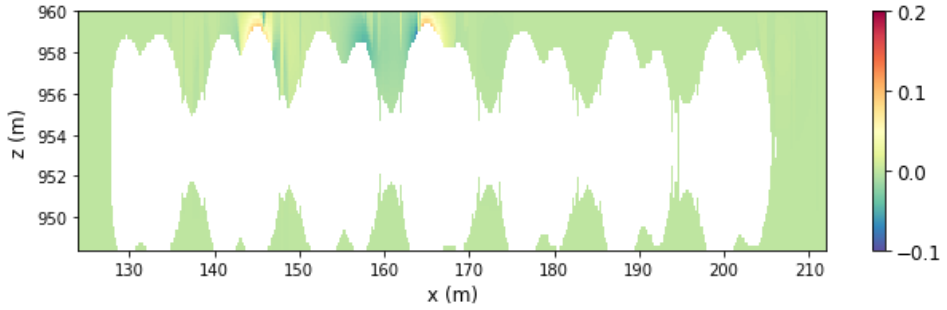

Figure 5.44: Cross-section of the difference between initial and optimized state of EED differences, for dataset Nevada 1, scenario 1, at y = 779.87 m.

It should come as no surprise that most remaining blocks with EED values below the EED cap threshold are found at the boundaries of the block model, similar to what was observed in the 5 by 5 test pattern in Section 5.1.5. Because the cross-section is not taken parallel to the blast pattern rows, these figures also illustrate the situation in between the drillholes; even in the center of the blast, relatively low EED value blocks can be found until a depth of z = 956 m, and up to z = 952 m connecting to the bottom of the blast. As a result of the significant drillhole deviations for scenario 1, the real and optimized EED in Figure 5.40 and Figure 5.41 even show multiple low EED areas passing all the way from the top to the bottom of the block model. Although at first sight the real EED looks almost identical to the optimized EED, small dissimilarities can be found in their differences with the planned EED.

In Figure 5.42 and Figure 5.43 it can be observed that differences in EED are quite spread out through the block model, due to the relatively large drillhole deviations. Although there is an obvious large zone around x = 195 m as one of the exceptions, many deviations are found directly above the 'drillhole shadow' of discarded blocks, in the upper part of the blast. This can likely be directly attributed to the movement of the drillholes with respect to the planned setup. Smaller differences are also found in the areas in between these areas of discarded blocks, at lower elevations. The effect of the charge adjustments, however, is most prominent in their direct vicinity. This is where some of the differences between Figure 5.42 and Figure 5.43 may be observed. For a more convenient representation, the difference between this initial and optimized state of the objective is presented in Figure 5.44. Although it can be challenging to observe the effect from this cross-section because it is not taken parallel to the blasthole rows, it seems like the same phenomenon is observed as in Figure 5.31; directly above the drillhole, charge adjustments lead to new EED differences. This is an undesired effect of providing the required alteration of EED values in blocks further away and in between blastholes.

For a more complete overview of the blast, top-down views of the planned EED, real EED, and optimized EED at z = 959 m are given in Figure 5.45, Figure 5.46, and Figure 5.47 respectively. These correspond to the first scenario with deviations in both the x- and y-direction picked from a uniform distribution ranging from -0.5 m to 0.5 m. The differences between the planned and real EED form once again the initial state of the objective, illustrated in Figure 5.48, and the difference between the planned and optimized EED, shown in Figure 5.49, represents its optimized state. The difference between these states is displayed in Figure 5.50.

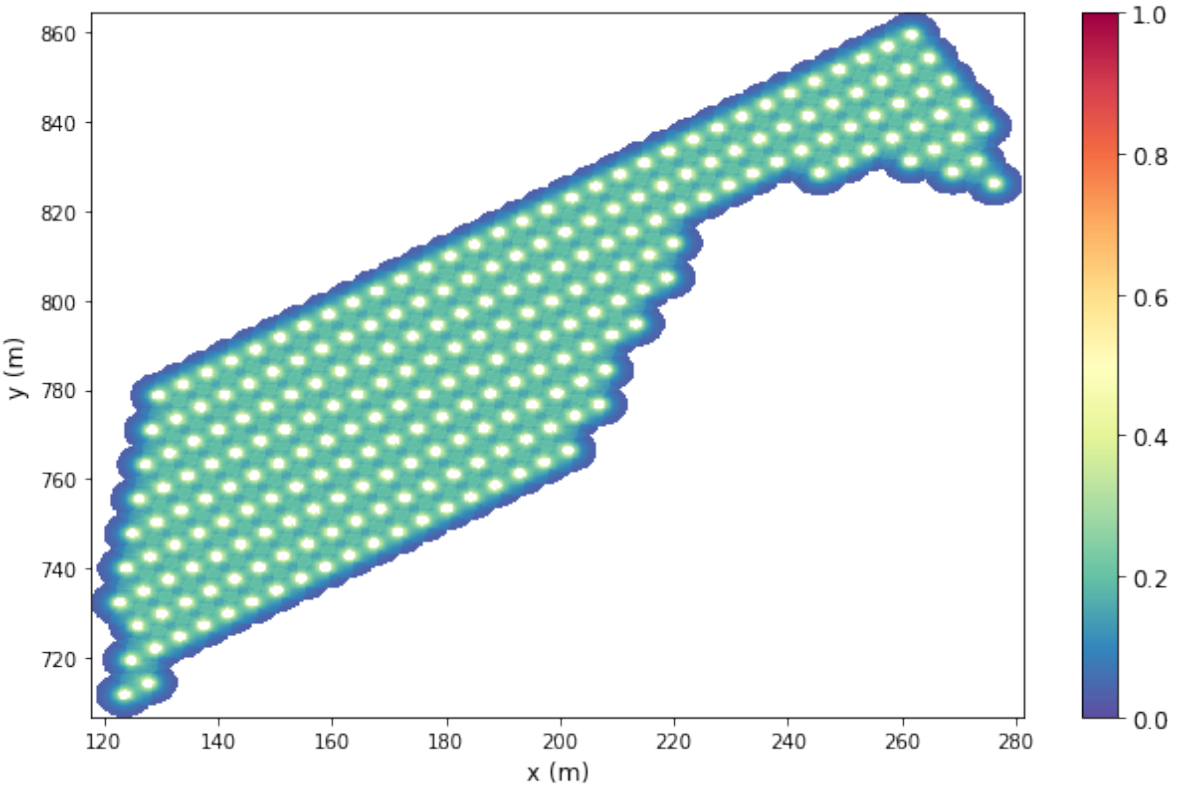

Figure 5.45: Top-down view of planned EED for dataset Nevada 1, at z = 959 m.

The first observation that can be made in these figures is that the lowest values are generally found at the boundaries of the blast. This is of course partly caused by the 5-meter search radius around each blasthole, of which the contours can be clearly identified. It should be noted that not all blocks at these boundaries for which the EED is calculated must necessarily result in broken rock. However, to ensure that the rock mass is broken and fragmented as intended, which is especially important in these areas of the blast, the real or optimized EED should still be as close as possible to the planned EED. Because these EED values are relatively low and only receive energy from one or two blastholes, deviation of holes at these boundaries can have a significant impact. Although the planned EED in Figure 5.45 shows of course a very consistent EED pattern throughout the block model because the spacing and burden is kept constant. The real EED for scenario 1 in Figure 5.46, however, is clearly not as continuous; the large deviations in drillhole locations cause changes to the EED in many areas of the blast, where zones of relatively elevated EED values alternate with areas of lower values.

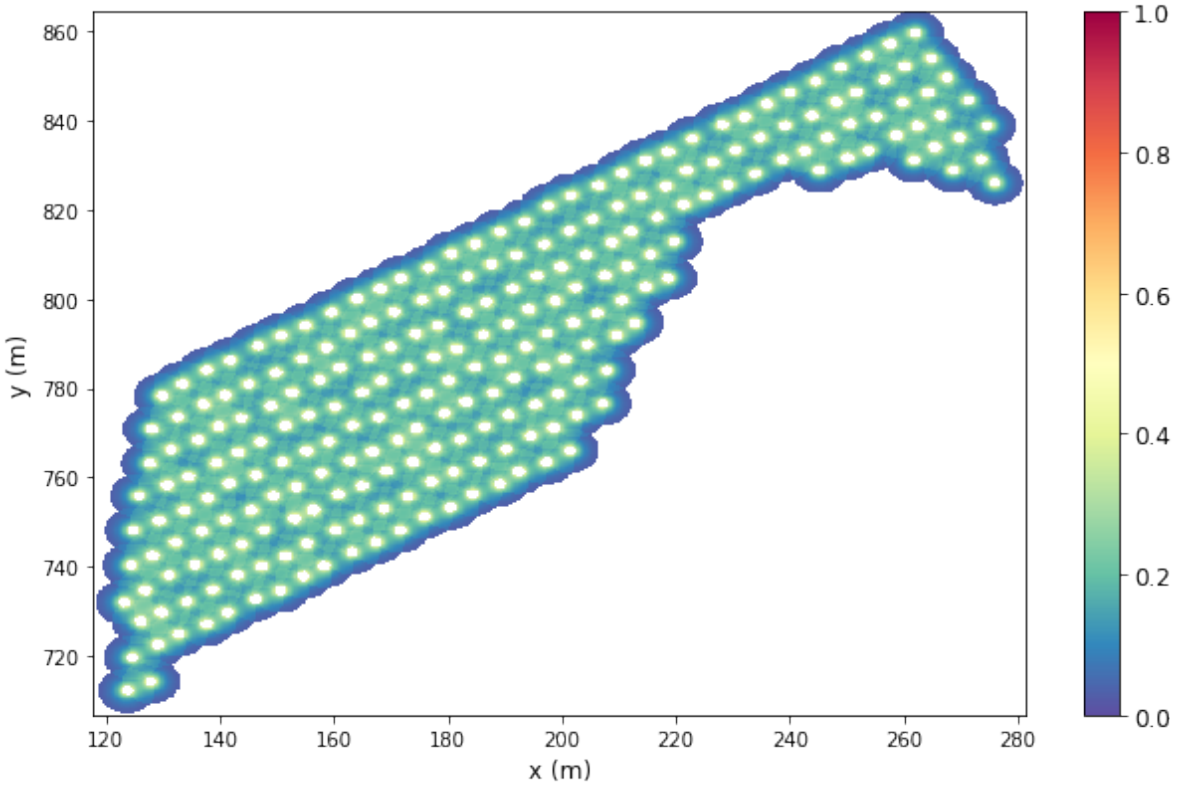

Figure 5.46: Top-down view of real EED for dataset Nevada 1, scenario 1, at z = 959 m.

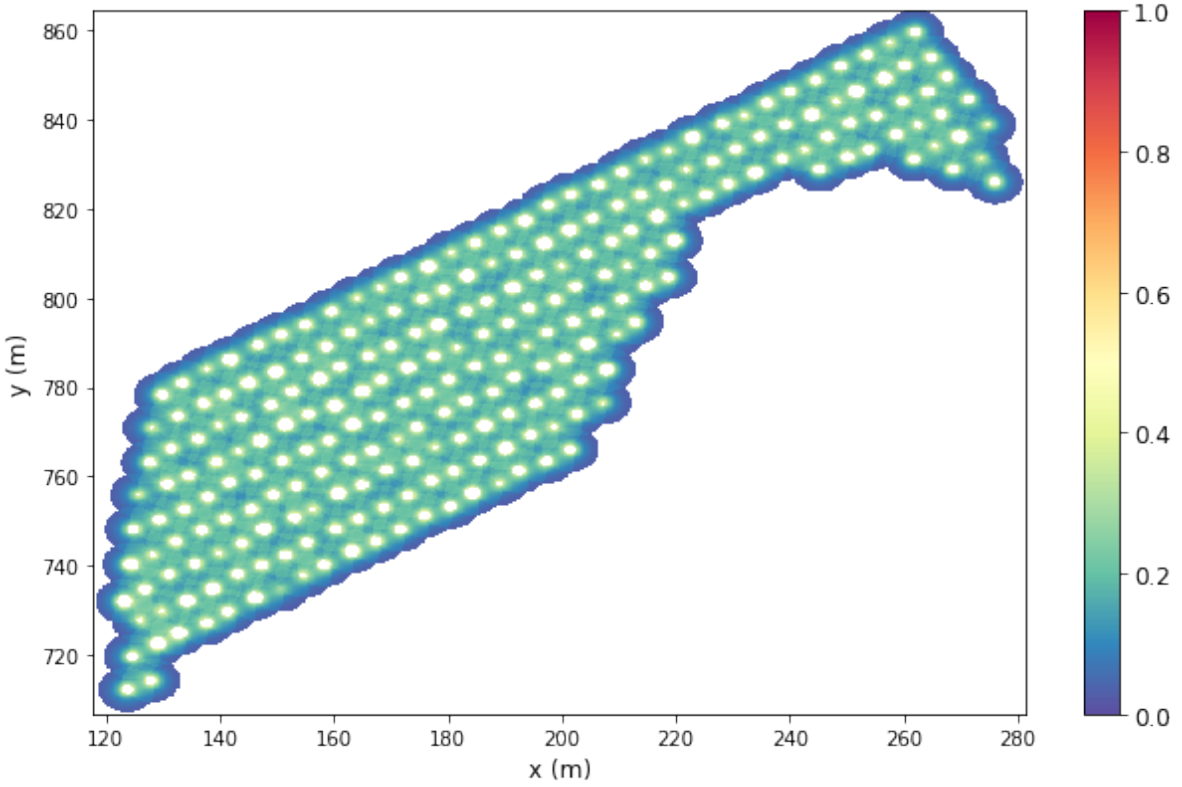

Figure 5.47: Top-down view of optimized EED for dataset Nevada 1, scenario 1, at z = 959 m.

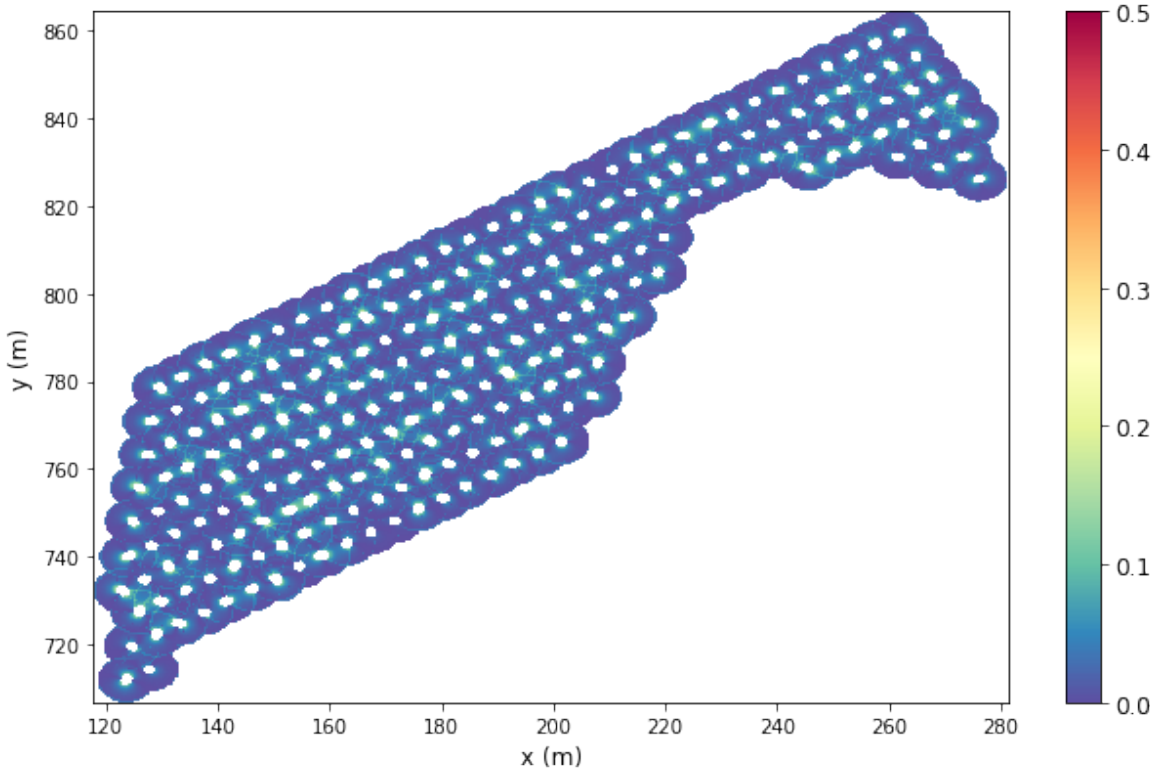

Figure 5.48: Top-down view of the difference between planned and real EED for dataset Nevada 1, scenario 1 (initial state of the objective), at z = 959 m.

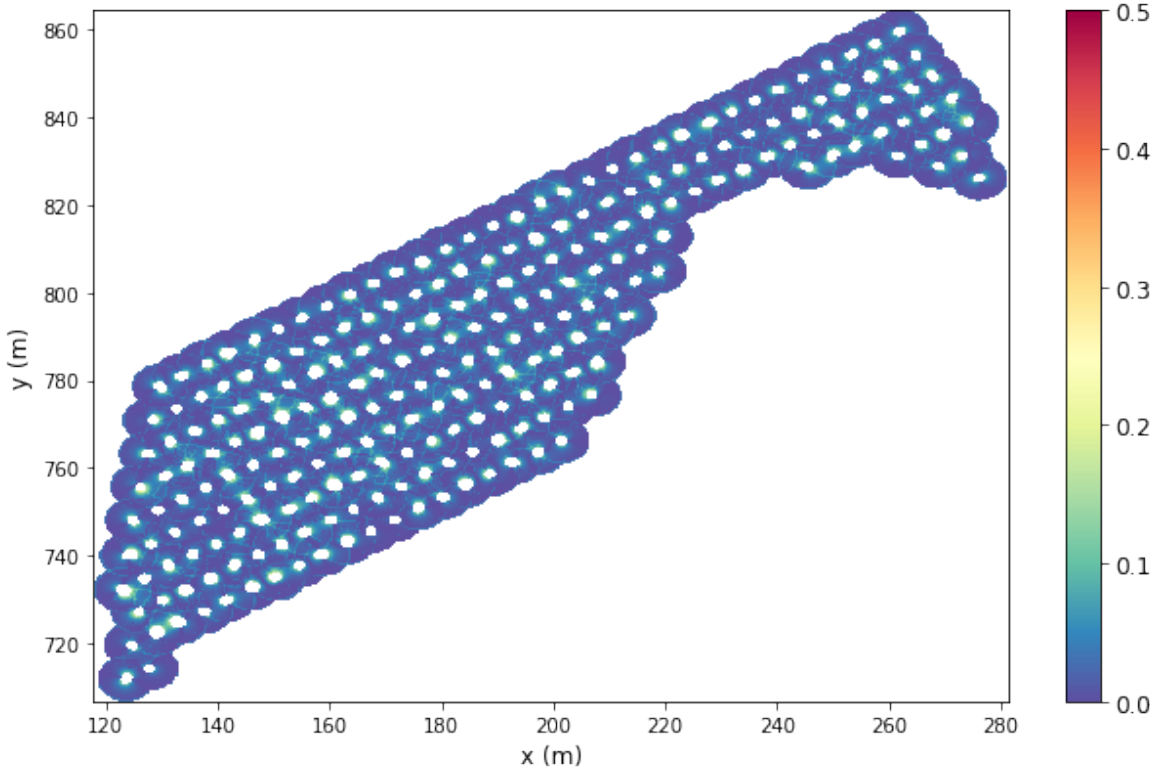

Figure 5.49: Top-down view of the difference between planned and optimized EED for dataset Nevada 1, scenario 1 (optimized state of the objective), at z = 959 m.

Due to the applied EED cap, the largest differences generally occur in between multiple deviated drillholes, as expected. This can be observed clearly in Figure 5.48. This figure also shows that many differences occur at search radius circles around blastholes. If a hole has deviated, this means that the area of the block model that lies within the search radius is also changed. Blocks that previously did not lie within range and did therefore not receive any explosive energy from a particular blasthole, may receive some in case the hole is moved towards them in the real drillhole configuration, and vice versa. Although the contribution of explosive charges was found to be negligible at a search radius of 5 meters in Section 5.1.1, Figure 5.48 indicates that interactions around the search radius could still be of influence to EED differences.

Although at this scale it is challenging to identify areas in Figure 5.49 that show improvement compared to Figure 5.48, a striking difference is the size of some of the discarded areas around blastholes. As a result of the charge adjustments, which can be found in Figure 5.35 for reference, these areas around adjusted blastholes become larger or smaller depending on the direction of the adjustment; a charge increase will lead to quite a strong increase in EED values in blocks directly above the charge, and therefore a larger area is discarded. Conversely, if the top of the explosive column is lowered, EED values in nearby blocks above the blasthole will receive significantly less explosive energy, which means more blocks get below the EED cap threshold.

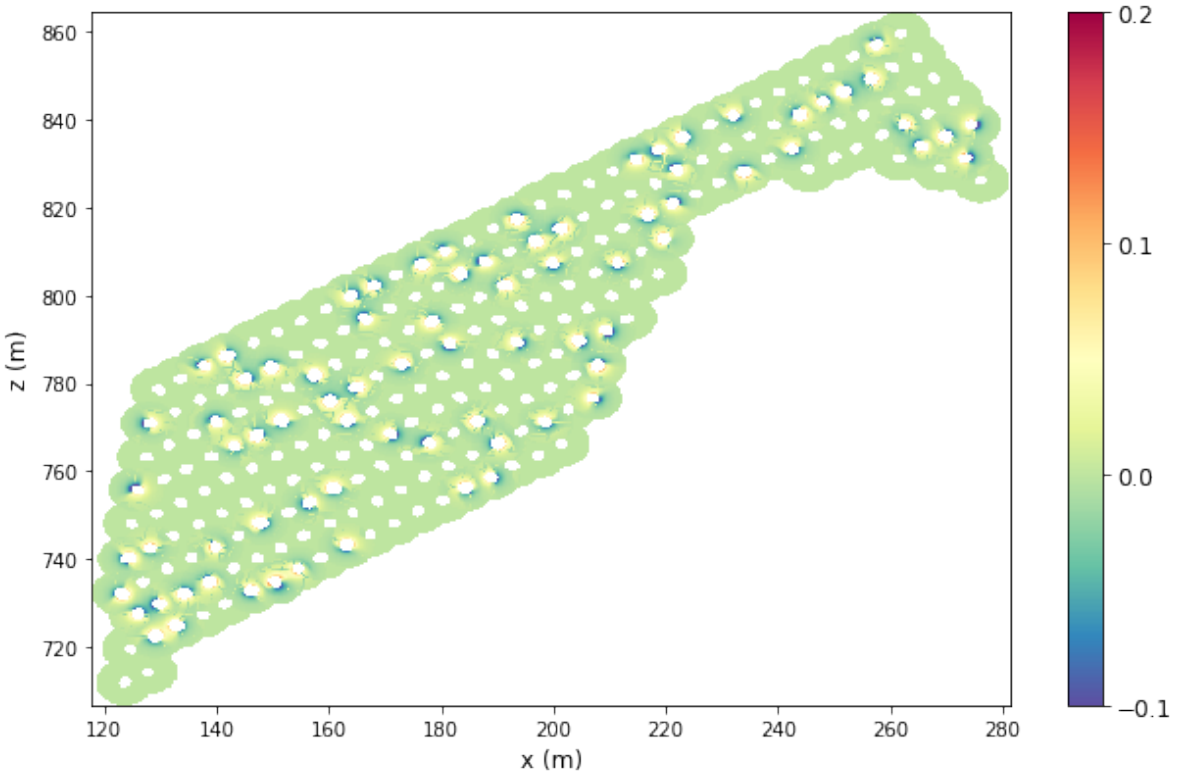

Figure 5.50: Top-down view of the difference between initial and optimized state of EED differences, for dataset Nevada 1, scenario 1, at z = 959 m.

Finally, Figure 5.50 illustrates the effect of optimization on the objective by comparing its initial state to the optimized state. Although the 5 by 5 blast pattern test showed that charge adjustments generally introduce new EED differences in the direct vicinity of its location, but lead to lower EED differences further away (Figure 5.33f), this is not always the case for the Nevada 1 dataset with scenario 1 random deviations, at least at this elevation. Due to the random nature of the deviations, as opposed to predefined ones that make multiple holes collectively move away from or towards another drillhole, a different dynamic is found. Instead of being divisible in inner and outer rings of negative/positive alterations to EED differences, here the effect appears to be more of a split between two sides; at one side of the blasthole the differences in EED are lowered, while at the other side they increase. This can be observed in numerous drillholes at the boundaries of the blast, but also emphasizes the cooperating effect of clusters of adjusted blastholes.

The same procedure can be applied to the second scenario, which has taken random deviations in from a uniform distribution between -0.25 m and 0.25 m. The planned EED will of course remain the same, but due to the different drillhole locations in the real EED setup, all other EED values will also change since this is a different optimization case, corresponding to the solution as presented in Section 5.2.1 (Figure 5.36). The real EED corresponding to this setup is displayed in Figure 5.51, followed by the optimized EED in Figure 5.52. The difference between the planned EED and real EED represents the initial state of optimization and is given in Figure 5.53. Similarly, Figure 5.54 provides the difference between the planned EED and optimized EED, which is analogous to the optimized state of the objective. The last top-down view demonstrates the effect of optimization on the explosive energy distribution by comparing the initial state of the objective to the optimized one, in Figure 5.55.

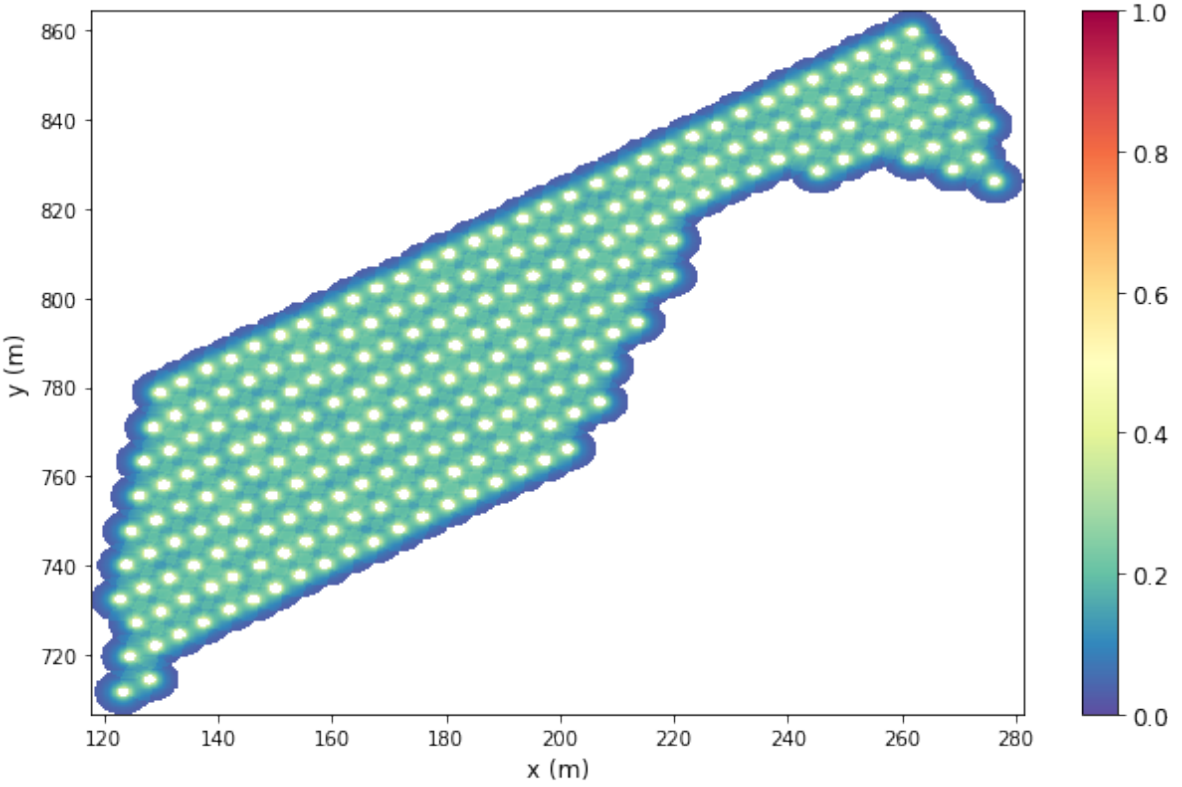

Figure 5.51: Top-down view of real EED for dataset Nevada 1, scenario 2, at z = 959 m.

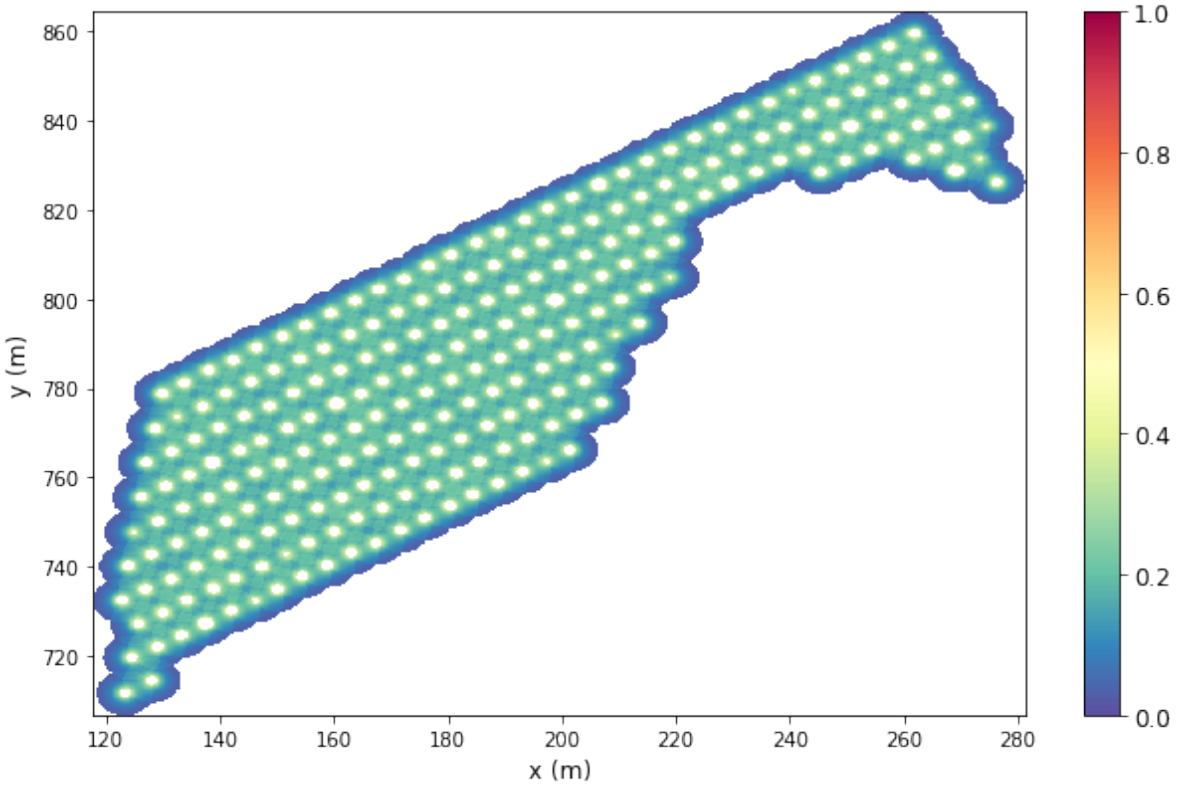

Figure 5.52: Top-down view of optimized EED for dataset Nevada 1, scenario 2, at z = 959 m.

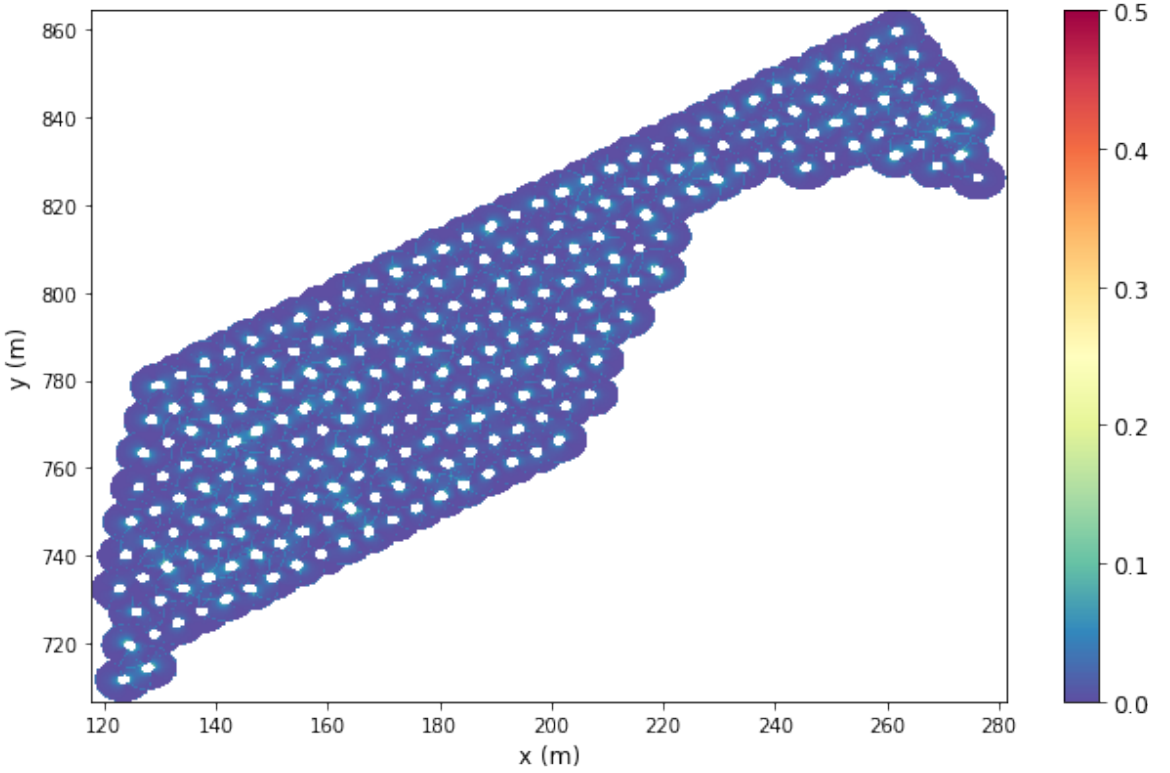

Figure 5.53: Top-down view of the difference between planned and real EED for dataset Nevada 1, scenario 2 (initial state of the objective), at z = 959 m.

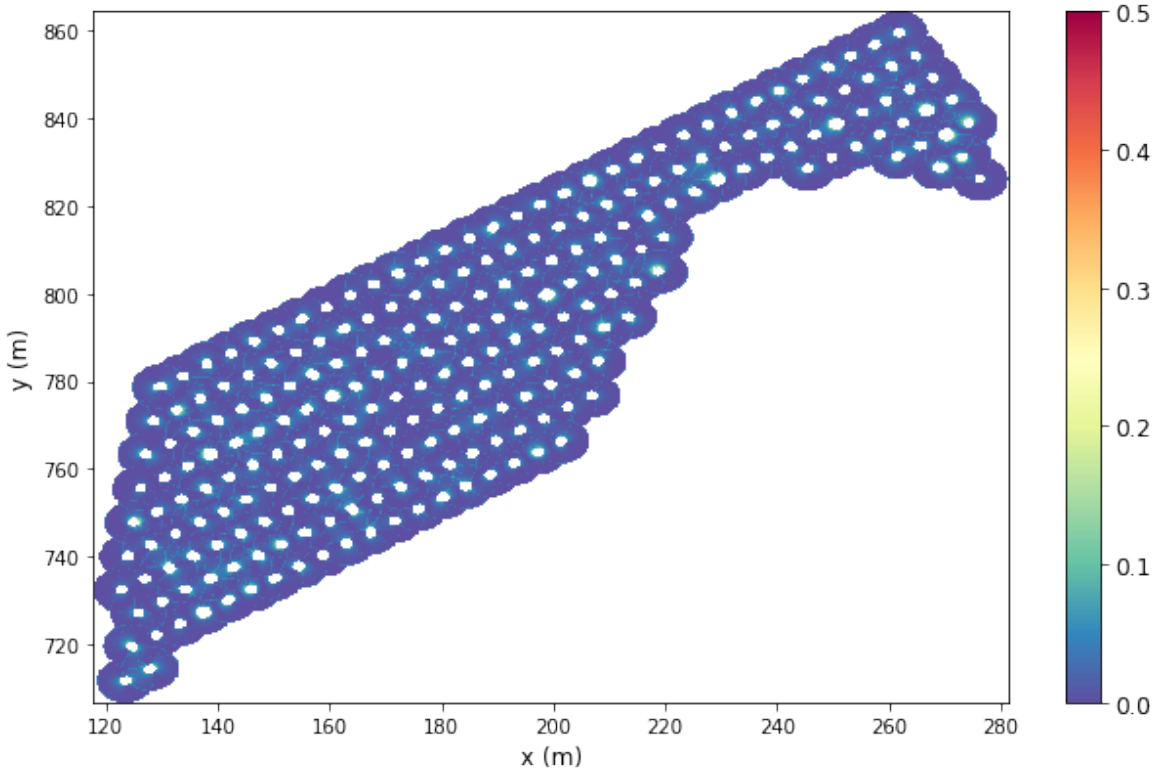

Figure 5.54: Top-down view of the difference between planned and optimized EED for dataset Nevada 1, scenario 2 (optimized state of the objective), at z = 959 m.

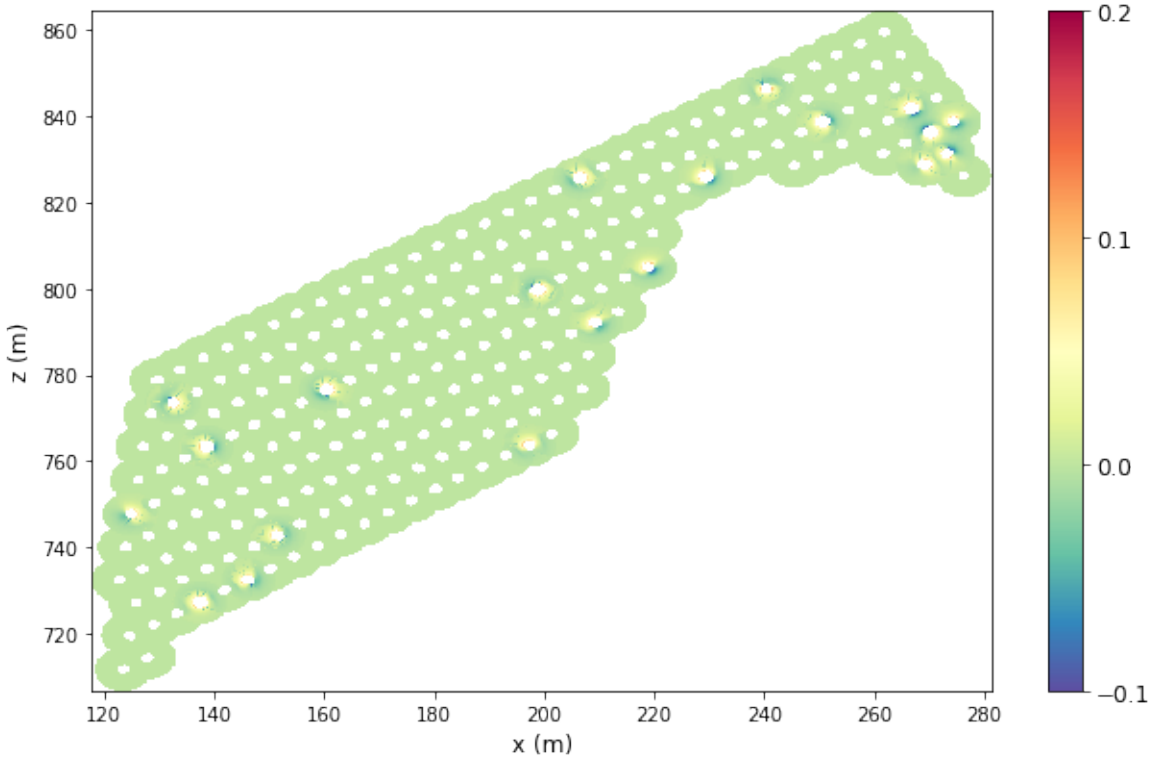

Figure 5.55: Top-down view of the difference between initial and optimized state of EED differences, for dataset Nevada 1, scenario 2, at z = 959 m.

The real EED for scenario 2, shown in Figure 5.51, looks a lot more consistent throughout the block model than the real EED corresponding to scenario 1 (Figure 5.46). Although there are still some areas that receive a little less or more explosive energy than intended, EED values are generally more in line with the planned EED (Figure 5.45), as should logically be expected due to the smaller deviations. It is no coincidence that optimization of this second scenario results in less charge adjustments than scenario 1. Nevertheless, the small number of adjustments can still be identified in the optimized EED (Figure 5.52) by the altered size of the discarded EED data around the adjusted blastholes.

In Figure 5.53 and Figure 5.54, the EED differences corresponding to the initial and optimized state of the objective respectively are clearly of a different magnitude than those observed in scenario 1. Although the EED differences are still often found in somewhat larger zones, apparently they are not high enough to warrant the clustered adjustment of multiple blastholes. As can be confirmed in Figure 5.36, some adjustments are made in such areas, but the majority consists of single isolated adjustments. Evidently, adjusting multiple holes in close vicinity of each other would compensate for more explosive energy than required, and has therefore become unfavorable. Only in the top-right corner of the blast, there is one cluster of adjusted blastholes where the EED differences caused by drillhole deviations are large enough.

Although the two-way split between the reduction and increase of EED differences around the adjusted blastholes can still be observed in Figure 5.55, the deteriorating component often seems to extend further than the improving component, at least at the examined elevation of z = 959 m. This can again be attributed to the smaller EED differences; when these differences are relatively small, their reduction is naturally more limited, while overcompensation by 0.3 m charge adjustments, on the other hand, becomes more likely.

The frequency distributions corresponding to the various EED configurations can be found in Figure 5.56 for scenario 1, and Figure 5.57 for scenario 2. For both cases, the frequency distributions are cut off at 0.391, which corresponds to the EED cap percentile of 50%. In the distributions for the planned EED, real EED, and optimized EED, at least two peaks can be clearly observed around 0.06 and 0.14, and possibly a third around 0.39. Because the remaining data is discarded, it is difficult to tell whether the top of this peak is reached within this window. A striking difference between the planned EED and real EED is the smoothening of the frequency distribution; apparently the random deviations contribute to a somewhat more continuous distribution of EED values, compared to the planned EED which is quite irregular, especially between 0.1 and 0.25.

For scenario 1, the real EED also smoothens the higher frequency values between 0.25 and 0.3. This also occurs for scenario 2, but the effect is not large enough to completely remove it here. Inspection of the real EED and optimized EED do not reveal very large differences, suggesting that the overall effect of the optimization on the EED frequency distribution is limited. The effect of optimization is illustrated in more detail by Figure 5.56d, which compares the frequency distributions of the EED difference calculated from the planned EED and real EED (initial differences) to those calculated from the planned EED and optimized EED (optimized differences). In this figure, the same effect is observed as in Figure 5.34d; optimization reduces the number of overall differences between 0.01 and 0.06, at the cost of introducing more differences smaller than 0.01. Although this trend is still visible in scenario 2, the small amount of adjustments makes these changes barely visible anymore.

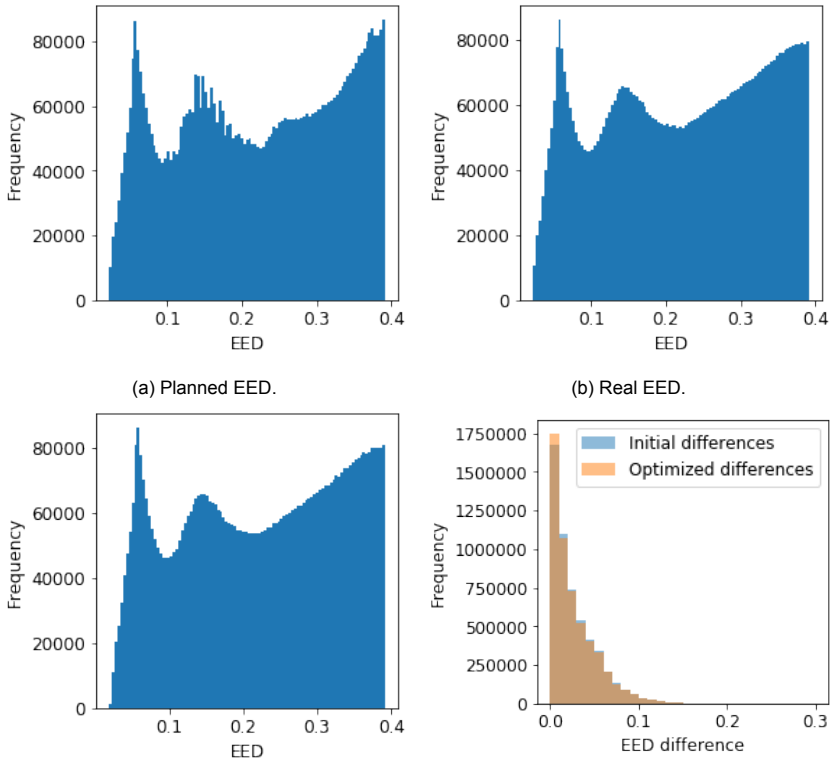

(a) Planned EED.

(b) Real EED.

(c) Optimized EED.

(d) EED differences.

Figure 5.56: Frequency distributions of the various EED configurations and their differences, for dataset Nevada 1, scenario 1.

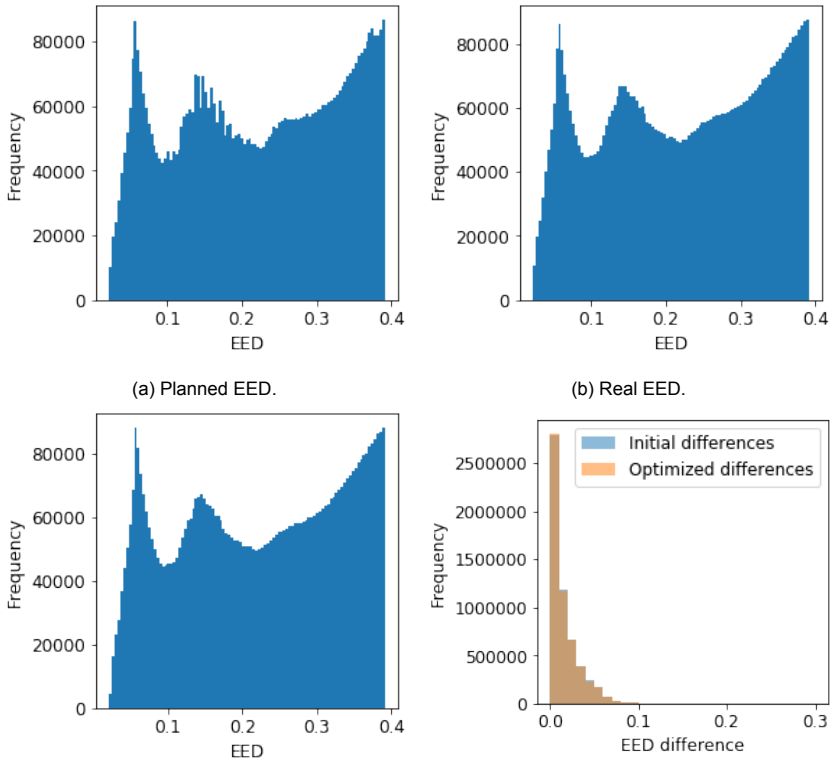

(a) Planned EED.

(b) Real EED.

(c) Optimized EED.

(d) EED differences.

Figure 5.57: Frequency distributions of the various EED configurations and their differences, for dataset Nevada 1, scenario 2.

Finally, the initial and optimized objective values calculated from the EED block models are listed in Table 5.11, along with the corresponding improvement expressed as percentages. Although these improvements are not enormous, it should be noted that the objective value is calculated from the differences throughout the entire block model. Because the charges in most drillholes remain unaltered, much of the EED differences are not addressed. In areas where many drillholes are adjusted, local improvements may therefore be much higher. Despite its smaller improvement, the adjustments made in scenario 2 could be seen as more effective; the 0.53% improvement was achieved by making a total of 20 charge adjustments, while scenario 1's improvement of 1.54% required 80 adjustments.

Table 5.11: Initial and optimized objective values for scenarios 1 and 2 of dataset Nevada 1, and corresponding improvements.

	Mean planned EED	**Mean initial EED difference ($\overline{Z}$)**	**Mean optimized EED difference ($\overline{Z}$)**	**Improvement of EED difference**
Scenario 1	0.1987	0.0242	0.0239	1.54%
Scenario 2	0.1987	0.0141	0.0140	0.53%

However, one should take note of the fact that only a portion of the block model is affected by the charge adjustments. If only these blocks are considered, the calculated improvements are larger. Table 5.12 lists this portion of blocks whose EED difference is altered due to optimization, and the improvement calculated from just these blocks. Especially the improvement for scenario 2 becomes a lot larger in this manner, due to the relatively small percentage of affected blocks, which is of course related to the smaller number of adjusted blastholes.

Table 5.12: Number of blocks affected by optimization and improvements for scenarios 1 and 2 of dataset Nevada 1.

	Total number of blocks in optimized EED	**Blocks affected by optimization**	**Improvement of EED difference in affected blocks**
Scenario 1	6,648,445	2,934,202 (44.1%)	2.31%
Scenario 2	6,539,128	1,024,052 (15.7%)	2.14%

5.3. Nevada 2 Dataset

The explosive energy distribution optimization program has been successfully applied to the Nevada 1 dataset in combination with random drillhole deviations. Now that this approach has produced satisfying results, and is found reasonably consistent with different magnitudes of drillhole deviation as well as numerous randomizations, the next step is to assess its functioning using the Nevada 2 dataset. Contrary to the Nevada 1 data, this one comes with both planned and actual drillhole locations, meaning the real EED, and thereby also the optimization of charge heights, will be based on real data instead of randomly fabricated drillhole deviations.

To start off, Section 5.3.1 will present the charge adjustment solutions for the Nevada 2 dataset, obtained using the same control parameters as previously applied in the optimization of the Nevada 1 dataset. For evaluation of the consistency of the approach that has been developed in Section 5.1 and Section 5.2 using the 5 by 5 test blast pattern and the Nevada 1 dataset, it is important to examine the results of optimization both with and without the explosives quantity constraint. The remaining sections of this chapter only consider the former option. The performance of the optimization methods will be briefly discussed in Section 5.3.2, followed by an overview of the EED data derived from the block model for the various drillhole location and charging configurations in Section 5.3.3.

5.3.1. Charge Adjustments

Contrary to the broad investigation of charge adjustment solutions in the similar Section 5.2.1 for the Nevada 1 dataset to determine an appropriate EED cap percentile, this section will be more targeted at validation of the selected 50% EED cap percentile and presenting the optimal solution obtained through this method. As a brief reminder, this particular setting was chosen because it resulted in the most evenly distributed number of charge reductions and increases before the explosives quantity constraint was applied to enforce this. Although the optimal solution for the Nevada 2 dataset will also be subjected to this constraint, it is important to verify whether this criterion can be approximated without it, as this would indicate a certain degree of consistency in the applied procedure. The charge adjustment solution obtained by Tabu Search, without constraining the total amount of explosives used, is visualized in Figure 5.58. Like before, the other control parameters are set as following; a search radius of 5 m, block size of 0.2 m, charge segment length of 0.3 m, and EED cap percentile of 50%. The tabu tenure is still set to three iterations, and optimization is boosted at the start to reduce the overall computation time.

Without constraining the total amount of explosives, optimization of the Nevada 2 dataset results in a total of 9 charge reductions and 6 increases. Although these numbers do not represent a perfect balance of the explosives quantity compared to the planned figures, they do indicate that optimization using the identified optimal settings is relatively consistent with the findings of the Nevada 1 dataset. One could argue that 50% more charge reductions are made relative to the number of charge increases, but this is of course influenced by the low number of total adjustments made for this dataset. When the number of overall charge adjustments is considered, a balance of -3 fits in well with the outcomes of the different randomizations for dataset Nevada 1, as listed in Table 5.10. Therefore, the complex relationships between improvements of the objective value, drillhole deviations, and the EED cap percentile, that were examined in Section 5.1.3 for the 5 by 5 test pattern and in Section 5.2.1 for the Nevada 1 dataset, also seem applicable to the Nevada 2 data using actual drillhole deviations.

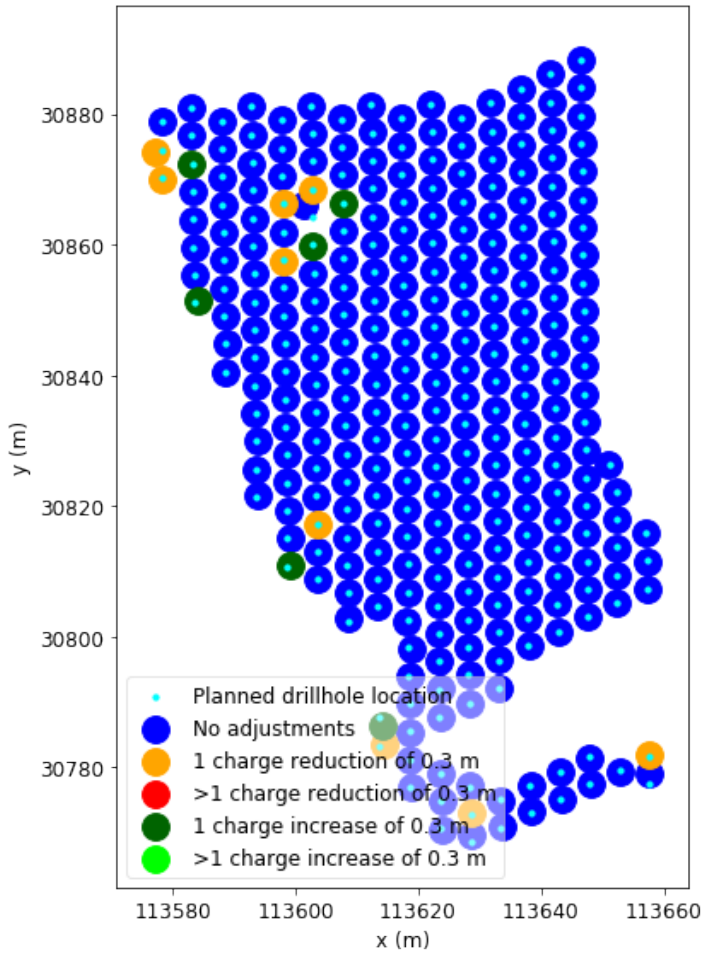

Figure 5.58: Visualization of Nevada 2 optimized solution (without total explosives quantity constraint).

After confirmation of the reliability of the chosen approach to produce a solution featuring a reasonably balanced number of charge reductions and increases for the Nevada 2 dataset without constraining the total amount of explosives, optimization is then performed with this constraint activated. The resulting charge adjustment solution is displayed in Figure 5.59. Although most adjustments remain, forcing the zero-balance of charge reductions and increases naturally leads to some differences. Compared to the unconstrained setup, two charge reductions are missing, and one increase is added for a total of 14 adjustments.

It should be noted that most of the adjustments are found at the boundaries of the blast, where at least one side is relatively unaffected by other blastholes. This could mean that charge adjustments in holes at the pattern boundaries cause less excessive or lacking EED contributions than those in the center of the blast, and are therefore more easily adjusted, as observed in Section 5.2 for the Nevada 1 dataset. However, due to irregular drilling at the western and southern end of the blast, many strongly deviated drillholes are found in exactly these boundary areas of the blast, and these holes are often the ones that are adjusted. Therefore, the magnitude of deviations seems to be the most important factor to cause charge adjustments, and not just the positioning of a drillhole at the edge of the blast pattern.

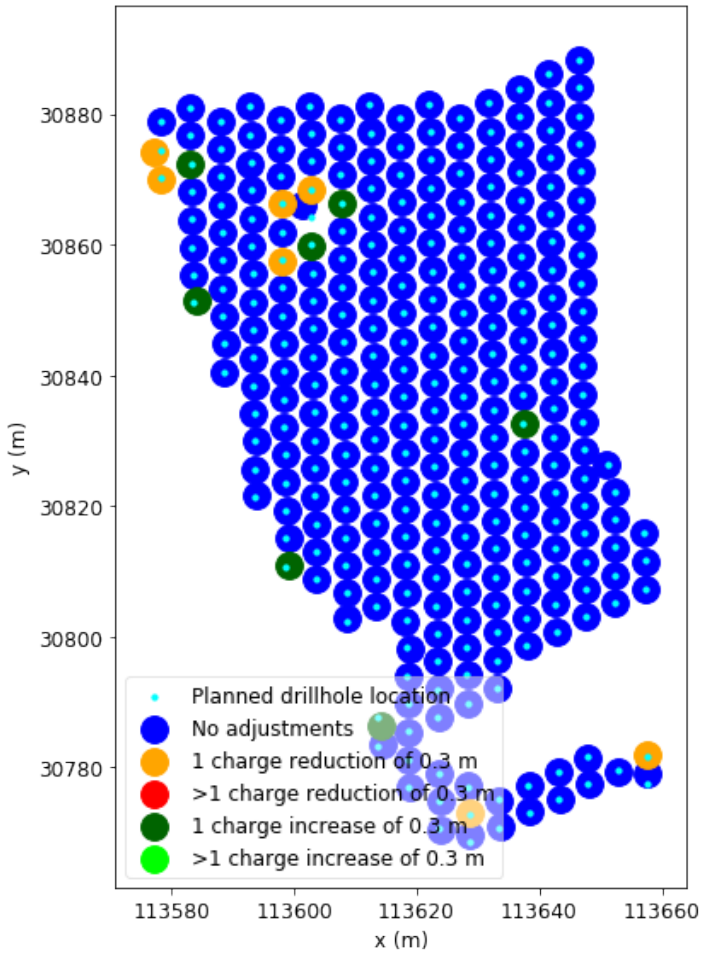

Figure 5.59: Visualization of Nevada 2 optimized solution (with total explosives quantity constraint).

Examination of the drillholes that have deviations of one drillhole diameter or larger, as identified in Table 4.3, shows that charge increases are made in holes number 6264, 6330, and 6184, and decreases are made in holes number 6275, 6341, and 6342. Evidently, charge adjustments are not simply performed in the most deviated drillholes; out of the 26 holes for which the deviation exceeds the threshold of one drillhole diameter, 0.200 m in this case, charge adjustments were made in only 6 cases. This indicates that large deviations by themselves are not necessarily compensated by charge adjustments, since this is also dependent on the position of nearby drillholes. The opposite is also true; large deviations are not a prerequisite for charge adjustments. 8 out of the 14 adjustments are made in drillholes with deviations smaller than one drillhole diameter. The cluster of adjustments in the core of the blast pattern is a good example of this; here, one very deviated drillhole leads to both charge increases and decreases in surrounding holes that are positioned relatively accurately.

5.3.2. Optimization

Because the total number of drillholes where the explosive column is adjusted is not significantly higher for the optimal solution of Nevada 2 compared to Nevada 1, it appears redundant to consider optimization using the Genetic Algorithm method due to its exorbitant computation times. Therefore, this section only provides the optimization path corresponding to the explosives quantity constrained Tabu Search with a tabu tenure of three iterations and starting boost activated, which is illustrated in Figure 5.60.

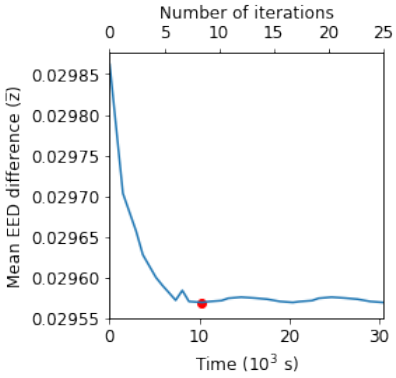

Figure 5.60: Tabu Search optimization path of Nevada 2 dataset, with explosives quantity constraint.

This optimization path once again nicely visualizes the effect of the tabu tenure mechanism; before reaching the lowest objective value, the solution is momentarily deteriorated to a slightly higher objective value. By placing previously adjusted holes on the tabu list, optimization is forced to search beyond the current optimal solution. Clearly, the solution reached before the increase of the objective value represented a local optimum. Because the latest adjusted drillhole was temporarily placed on the tabu list, a different adjustment became the most viable and led to the departure from the local optimum.

Comparing the optimization path for the Nevada 2 dataset with the one for scenario 2 of the Nevada 1 dataset (Figure 5.38a) shows they are very similar. Although the elapsed time per iteration seems slightly greater for Nevada 2, which is most likely due to the greater drillhole length leading to a larger block model, the overall computation times do not differ much. Moreover, the general structure of these optimization paths also shows a lot of resemblances. The starting boost initially causes a steep drop of the objective value in both cases, followed directly by a slight deterioration. Although the constrained version of the Nevada 1 optimization path does not subsequently reach a better solution, the unconstrained one (Figure 5.38b) does. Then, further adjustments quickly start looping the objective value, causing optimization to halt after around three times the duration it took to reach the optimal solution.

5.3.3. Explosive Energy Distribution

The block model holding the various EED values that is utilized by optimization to come to the charge adjustment solution presented in Section 5.3.1 will in this section be examined in more detail. This allows for a better understanding of how the charge adjustments affect the objective value, and also the explosive energy distribution throughout the blast. An identical approach will be taken as in Section 5.2.3 with the Nevada 1 dataset, except for the Nevada 2 dataset there is only one scenario for the real drillhole configuration. Once again, cross-sections of the block model for the planned EED, real EED, and optimized EED are produced to give an indication which areas of the block model are above the EED cap threshold and discarded, and which data remains to be used for optimization.

These cross-sections are taken at y = 30862.54 m and are displayed in Figure 5.61, Figure 5.62, and Figure 5.63 respectively. In Figure 5.64, the absolute differences between the planned EED and real EED are displayed, which represents the initial state of optimization. Similarly, Figure 5.65 presents the differences between the planned EED and optimized EED, which is analogous to the optimized state of the optimization objective. Finally, the beneficial effects of optimization are illustrated in Figure 5.66 as the difference between the initial and optimized state of the EED differences.

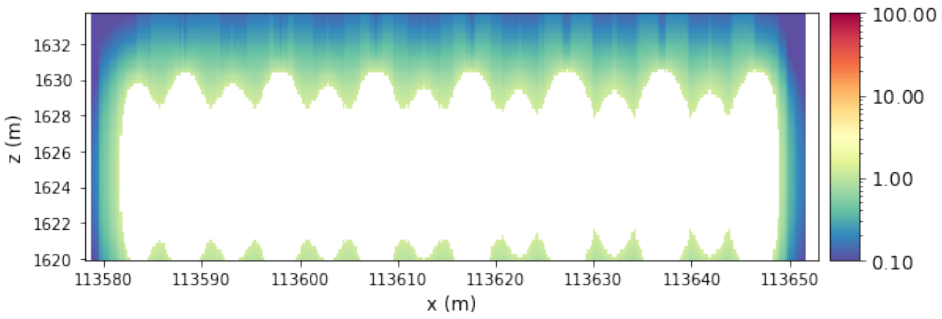

Figure 5.61: Cross-section of planned EED for dataset Nevada 2, at y = 30862.54 m.

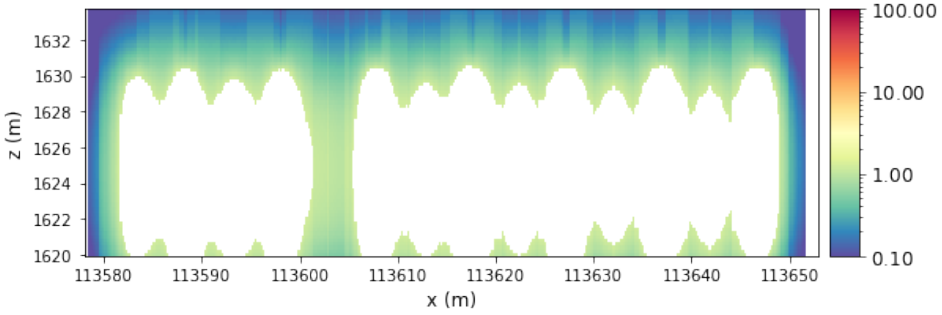

Figure 5.62: Cross-section of real EED for dataset Nevada 2, at y = 30862.54 m.

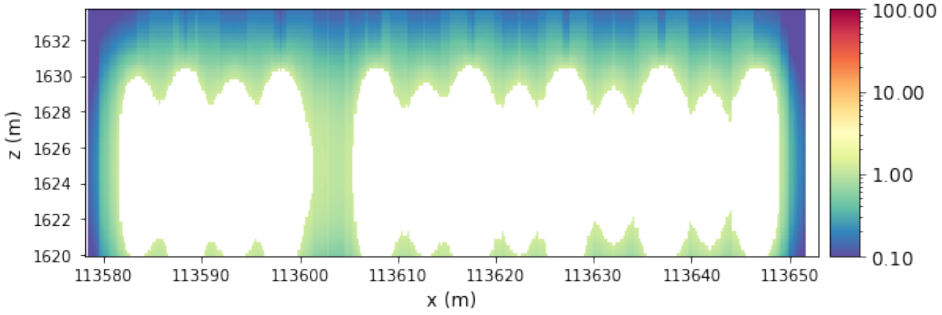

Figure 5.63: Cross-section of optimized EED for dataset Nevada 2, at y = 30862.54 m.

The first observation in the planned, real, and optimized EED (Figure 5.61, Figure 5.62, and Figure 5.63) is that the values that remain in the block model are a bit higher than those found in the block model corresponding to the Nevada 1 dataset. This can be attributed to the difference in blast design. The most important factor is presumably the drillhole diameter, which is 0.200 meter for the Nevada 2 dataset and only 0.125 m for the Nevada 1 dataset. Because more explosive energy is introduced into the bench, and equivalently into the block model, the EED values found in this block model are generally higher. From this, it follows naturally that the EED cap at the 50th percentile of the data also corresponds to a higher value. This demonstrates the benefit of selecting the EED cap using data percentiles as opposed to applying a cap at a predetermined value to all blast patterns equally. Moreover, due to the increased stemming height of 4.27 m compared to 1.5 m for the Nevada 1 blast design, the area of low-valued blocks above the explosive charges has increased significantly in size.

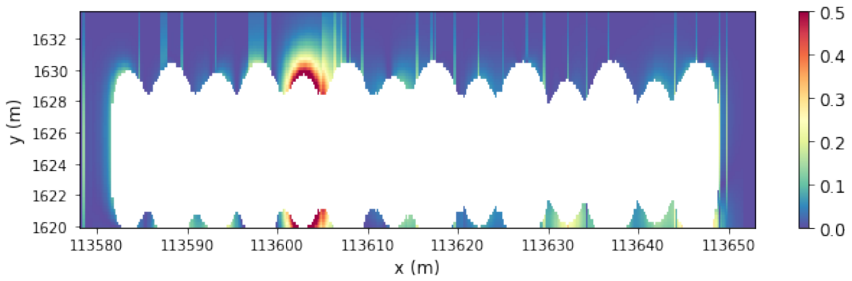

Figure 5.64: Cross-section of the difference between planned and real EED for dataset Nevada 2 (initial state of the objective), at y = 30862.54 m.

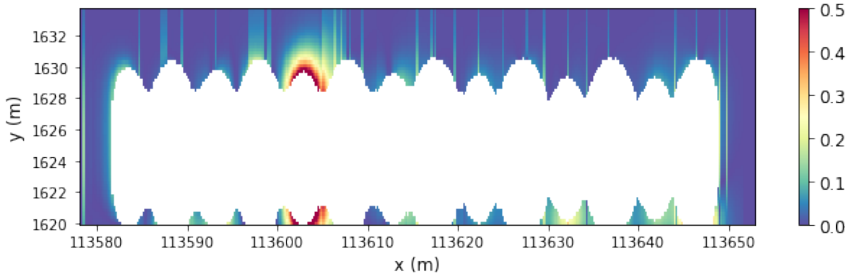

Figure 5.65: Cross-section of the difference between planned and optimized EED for dataset Nevada 2 (optimized state of the objective), at y = 30862.54 m.

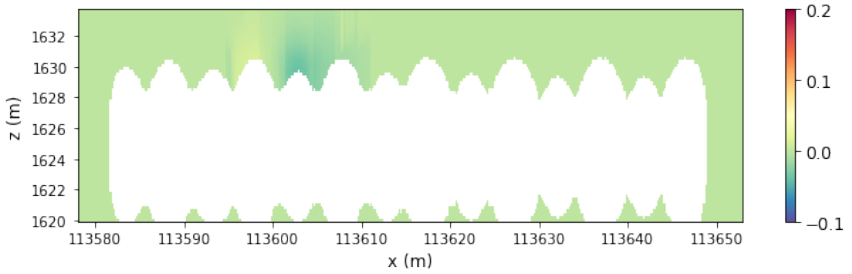

Figure 5.66: Cross-section of the difference between initial and optimized state of EED differences, for dataset Nevada 2, at y = 30862.54 m.

Since the cross-section is taken at a slice of the block model that is strongly affected by one of the large deviations near x = 113605 m, the consequences for the real EED and optimized EED are also large; the ‘shadow’ of discarded EED values around the deviated blasthole is not found in the real and optimized EED. Naturally, when the EED values in the planned configuration are discarded because they are above the EED cap threshold, and this is not the case in the other configurations, large EED differences follow, as shown in Figure 5.64 and Figure 5.65. Although the effect of charge adjustments in the neighboring holes is clearly visible in their direct vicinity, it seems impossible for such adjustments to account for EED differences as large as those caused by deviations of this magnitude.

In Figure 5.66, there is a clear vertical division visible between blocks whose EED differences have been reduced, and others that are increased. As expected, the area where the largest differences are found is characterized by small improvements, while EED differences around some of the adjusted neighboring holes are slightly increased to achieve this. The transition between these areas appears as a sharp, vertical line, which might be related to the search radius of 5 m around a nearby blasthole.

Top-down views of the block model will provide a broader perspective of the planned EED, real EED, and optimized EED, and are depicted in Figure 5.67, Figure 5.68, and Figure 5.69 respectively. These slices of the block model have been taken at the elevation of z = 1630.73 m, which is 1.27 m above the planned top of the explosive columns and 3.0 m below the surface. Following this, are Figure 5.70 and Figure 5.71, which show the difference between the planned EED and real EED, corresponding to the initial state of the objective, and the difference between the planned EED and optimized EED, corresponding to the optimized state of the objective. Finally, the differences between these initial and optimal states of the objective are illustrated in Figure 5.72 to visualize the effect of the charge adjustments on EED differences. Note that these images have been rotated by 90 degrees with respect to previous visualizations of the Nevada 2 data for more convenient formatting.

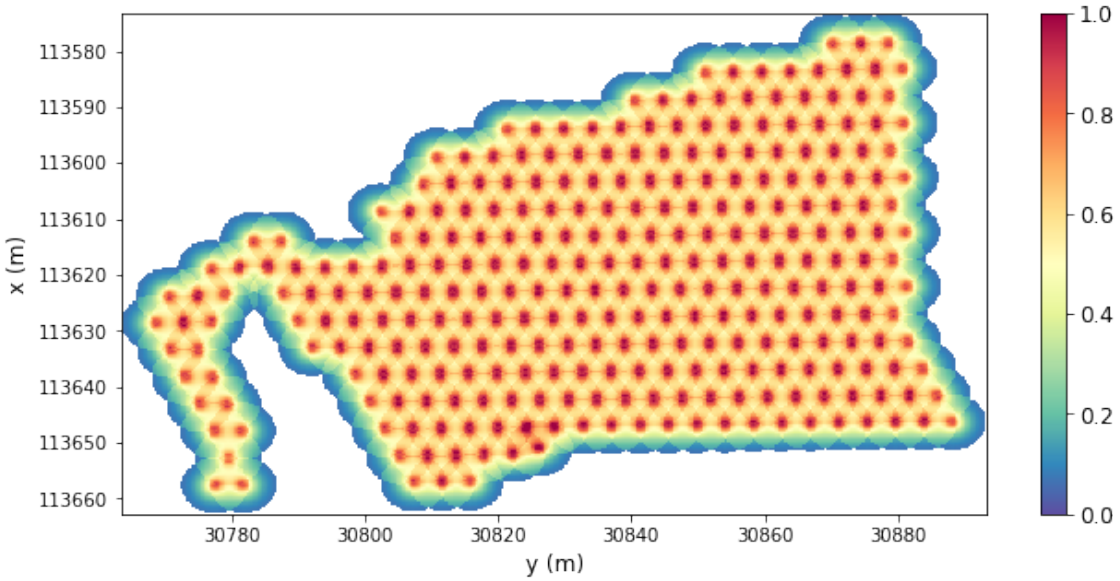

Figure 5.67: Top-down view of planned EED for dataset Nevada 2, at z = 1630.73 m.

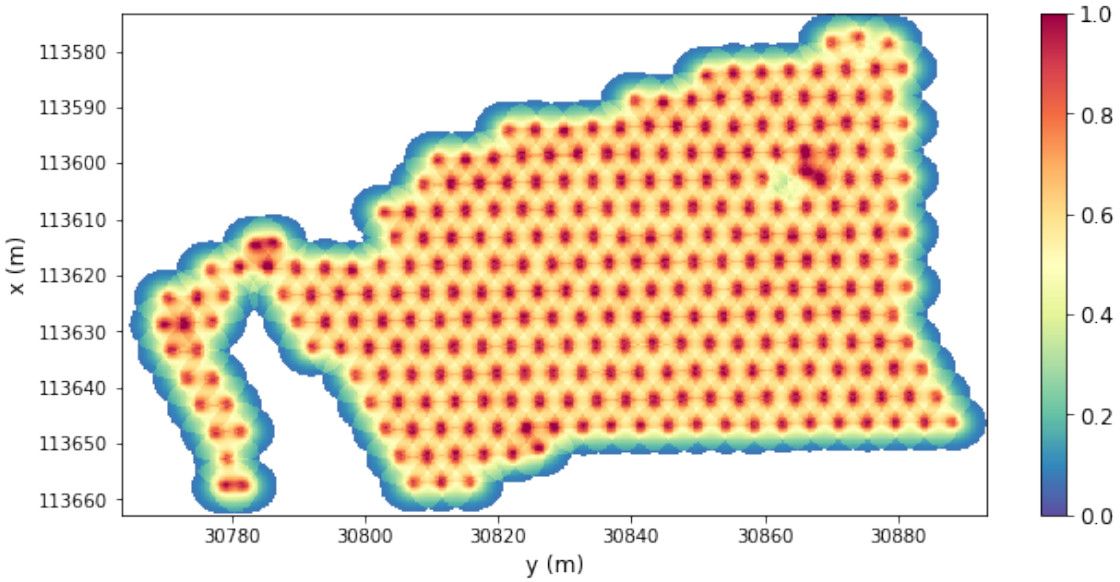

Figure 5.68: Top-down view of real EED for dataset Nevada 2, at z = 1630.73 m.

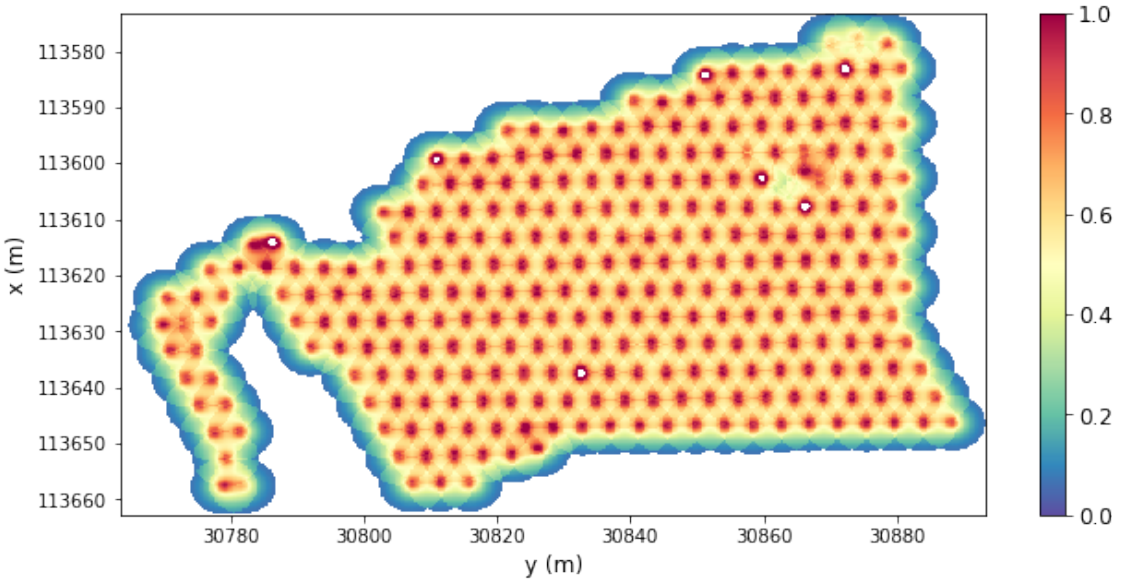

Figure 5.69: Top-down view of optimized EED for dataset Nevada 2, at z = 1630.73 m.

Like mentioned previously, the EED values found in the planned, real, and optimized configuration (Figure 5.67, Figure 5.68, and Figure 5.69) are higher than those encountered in the Nevada 1 block model. In these top-down overviews, it can be clearly observed that the number of blocks that approximate zero are very limited, even at the boundaries of the blast pattern. This is quite a contrast with the top-down views of the Nevada 1 block models that were examined in Section 5.2.3. Although it was found in Section 5.1.1 that the EED value at a search radius of 5 m is only 0.65% of the EED value found at 0.5 m away from a blasthole, compared to 0.71% for Nevada 1 blastholes, contributions to the EED that lie outside of the search radius and are therefore not considered are most likely larger in magnitude compared to the ones in the Nevada 1 blast design.

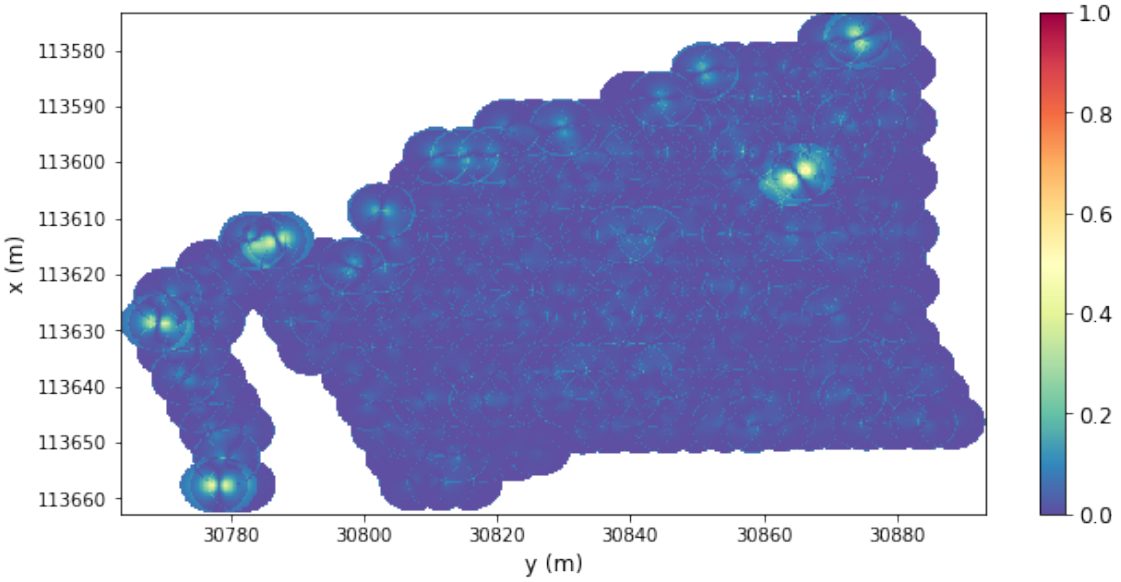

Figure 5.70: Top-down view of the difference between planned and real EED for dataset Nevada 2 (initial state of the objective), at z = 1630.73 m.

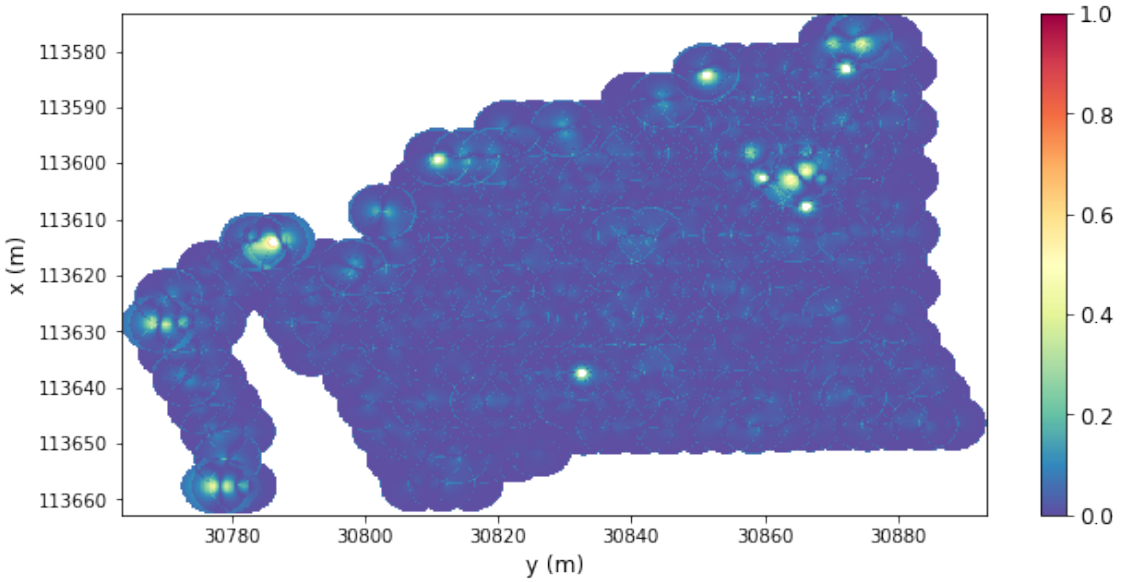

Figure 5.71: Top-down view of the difference between planned and optimized EED for dataset Nevada 2 (optimized state of the objective), at z = 1630.73 m.

Although most of the core of the blast pattern seems unaffected by the drillhole deviations of the real EED configuration, the EED values are significantly altered in a couple of deviation 'hotspots'. Besides the obvious alterations around x = 113605 m, y = 30865 m, most changes in EED can be found along the western and southern boundaries. This is confirmed by the EED differences observed in Figure 5.70. However, small differences are found throughout the blast pattern at the limits of search radii due to slight drillhole deviations, judging by the large amount of circle-shaped deviation zones. The optimized state of the EED differences in Figure 5.71 shows that a couple of large differences are introduced by the charge adjustments, at least at this elevation, while some existing differences are clearly reduced.

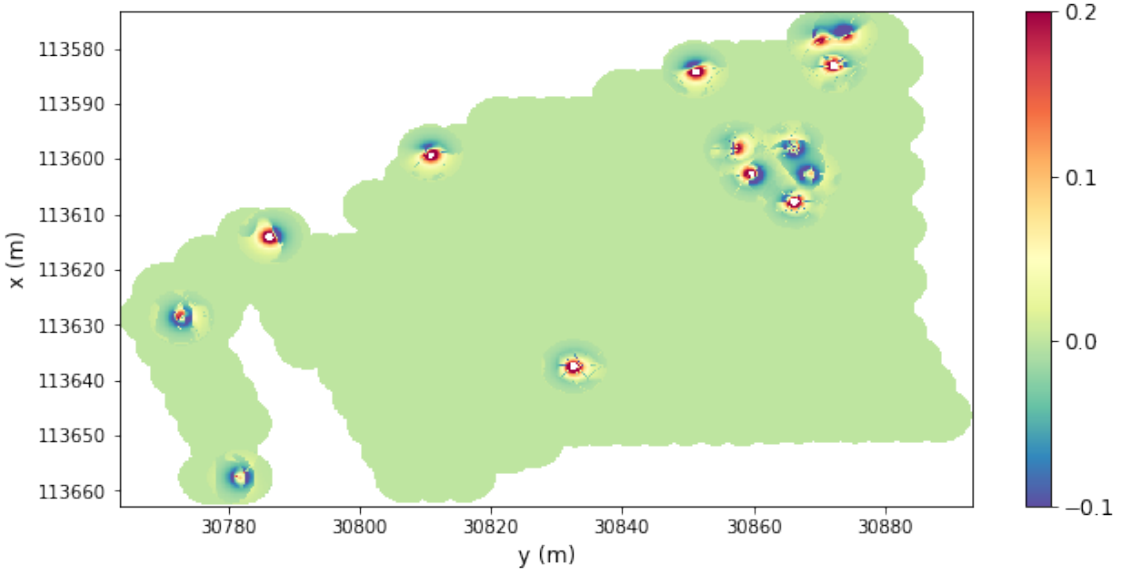

Figure 5.72: Top-down view of the difference between initial and optimized state of EED differences, for dataset Nevada 2, at z = 1630.73 m.

This is even more clearly illustrated in Figure 5.72. The cluster of adjusted drillholes at the previously specified coordinates seems to be quite effective at reducing the differences caused by the disproportionate deviation of one drillhole, and additional improvements are made along the western and southern boundaries of the blast pattern. In this plan view of the block model, both the radial and two-directional transitions between negative and positive changes to the EED difference can be observed. The magnitude of the newly introduced differences is in general relatively large in comparison to the reductions. At this elevation, the optimized EED even passes the EED cap threshold in some blocks closest to the altered explosive columns, which are therefore discarded. Although these new differences can be quite large, they typically do not span large areas. Reductions of EED differences are often found to extend further. Because this occurs of course in 3D, they apparently still outweigh the new differences that come with the charge adjustments to lead to overall improvements.

In Figure 5.73, the frequency distributions are given for the planned EED, real EED, optimized EED, as well as the initial and optimized EED differences. The most important observation is that they are vastly different from those retrieved from the Nevada 1 block model. Not only is the EED cap placed at a much higher value of 1.27, but the frequency distributions show just a single peak around 0.2, as opposed to the multimodal distribution of the Nevada 1 data (Figure 5.56, Figure 5.57). Although the EED values are in both cases of course calculated with the same EED formula, the distinctive properties are most likely rooted in the differences in blast design.

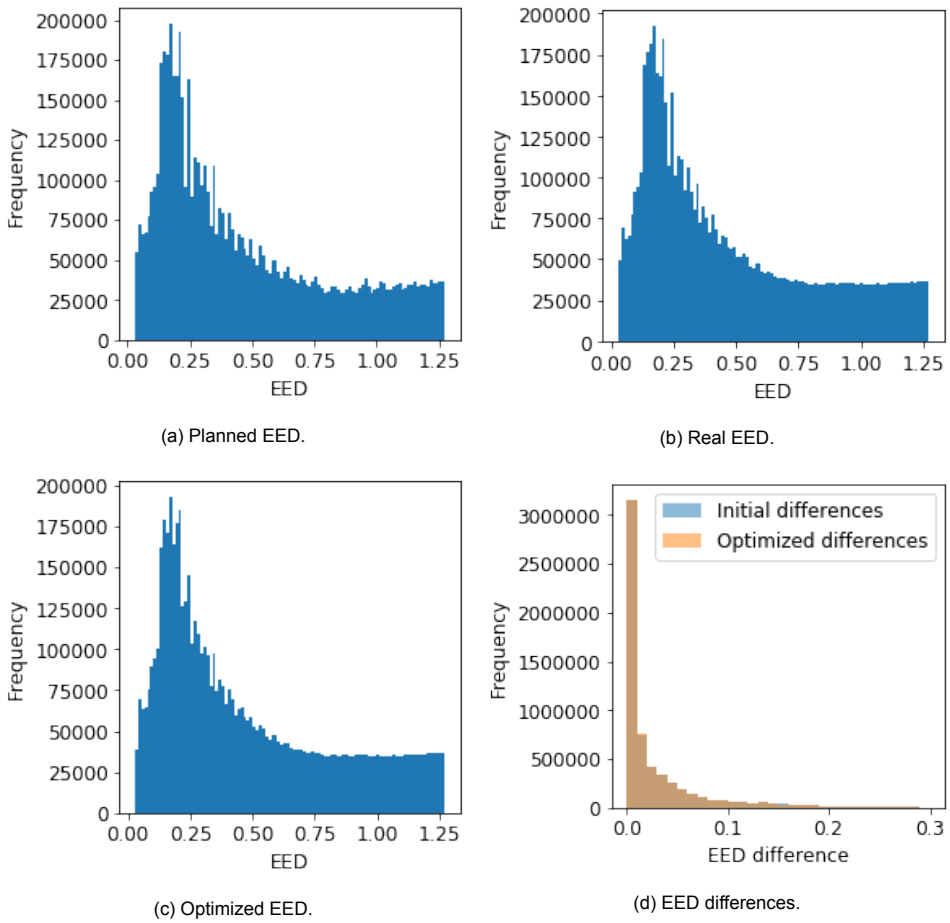

(a) Planned EED.

(b) Real EED.

(c) Optimized EED.

(d) EED differences.

Figure 5.73: Frequency distributions of the various EED configurations and their differences, for dataset Nevada 2.

By comparing the planned EED to the real EED, one can again conclude that the drillhole deviation has a somewhat smoothening effect on the EED frequency distribution. This seems to be even more prevalent in the optimized EED, although differences with the real EED seem minimal. This is reflected in the comparison between the initial and optimized EED differences. Whereas the frequency distributions of the Nevada 1 block model showed a slight increase in EED differences between 0 and 0.01, and slight decreases between 0.01 and 0.06, the changes in the Nevada 2 block model are too small to observe. However, the inspection of the data indicates that the same trend is found; the number of EED differences between 0.04 and 0.13 are reduced, at the expense of more EED differences below 0.04.

Last but not least, the overall improvement of the EED difference, or the objective value, resulting from optimization of the Nevada 2 dataset is 0.96%, which is derived from a mean initial EED difference of 0.0299 and mean optimized EED difference of 0.0296. To provide some perspective, the mean planned EED of the block model is 0.4369. Although an improvement of 0.96% might seem small, one should take into account that the majority of the block model remains unaffected by the 14 recommended charge adjustments. Out of the 6.76 million non-zero blocks in the optimized configuration, the EED difference was altered in only 742,788 of these or 11.0%. If only these blocks that are affected by optimization are considered, the calculated improvement becomes 3.94%.

6

Discussion

Although the mining industry generally recognizes drillhole deviation as an everyday problem, the potential consequences it has on blast performance are often simply accepted as a margin of error. Despite technological advancements in GPS-positioning and automation, complete elimination of this issue has proven to be difficult. Instead of focussing on the sources of drillhole deviation, it may be helpful to search for mitigating solutions too. By making adjustments to other properties of a blasthole pattern containing deviated drillholes, blast performance should become more consistent with expectations based on the original design. Due to the cascading effect of fragmentation on subsequent processes in a mining operation, this could lead to great benefits in terms of efficiency and costs.

The approach of this thesis has been to gauge the expected blast performance by comparing the spatial explosive energy distribution throughout a blockmodel encompassing a blast with deviated drillholes to the ideal situation with all holes in their planned location. In order to bring this 'real' explosive energy distribution more in line with the planned configuration, adjustments are made to blastholes' height of the explosive column to reduce block-to-block differences, which are optimized using Tabu Search or Genetic Algorithm. Because the block-to-block differences close to deviated blastholes become unreasonably high, satisfying results can only be obtained by applying a cap to the EED values such that focus shifts to the differences in low-valued blocks. Application of the developed optimization program on real Nevada blast pattern data, with both fabricated and actual drillhole deviations, has demonstrated its ability to successfully improve the explosive energy distribution of such blasts. However, the improvements with respect to the unaltered explosive charges were found to be small; partly due to the introduction of new EED differences caused by the charge adjustments, the achieved reduction of block-to-block differences relative to the planned blast design is likely not very significant given the inherent inconsistency of blast performance due to e.g. rock mass variability.

The design choice to minimize block-to-block differences in EED values between the planned and real drillhole configuration as the objective of optimization has made this project more challenging than expected. One of the major reasons for this decision is the lack of knowledge available on the behavior of explosive energy within a blast and its effect on the rock mass. Although the EED formula by [49] provides a useful estimation of the energy supplied at each discretization point, the significance of its magnitude in relation to blast performance remains unclear. Because no generalized approach exists to connect the obtained EED values with expectations for fragmentation, a simple value-based approach has no merit. The EED values encountered in the real drillhole configuration can therefore only be evaluated through comparison with the planned EED. This implies the assumption that the explosive energy distribution corresponding to the planned drillhole locations and explosive charges is ideal. Although it is generally a good starting point, it should be noted that the original blast design may in fact not be optimal, since it is often established by trial-and-error instead of theoretical analysis. Using the block-to-block comparison as optimization objective was quickly deemed more effective than other options; the mean block value seems to increase rather than decrease with deviated drillholes (a phenomenon that is also dependent on block size), and optimization based on frequency distributions generally disregards drillhole deviation altogether.

An unwelcome consequence of the block-to-block approach is that deviation of drillholes causes differences in blocks close to both the planned and real drillhole location, while the overall frequency distribution of EED values does not necessarily change. Although the largest differences are dealt with by the implementation of the EED cap, it may still affect the remaining lower values. In case all drillholes would be shifted in the same direction by an equal distance, for example, the overall energy supplied throughout the blast should not be affected, except at its designed boundaries. The block-by-block approach, however, does not allow any block values to be interchanged and would instead register many differences, which are to be minimized through optimization. Although the individual block values at blast pattern boundaries should remain constant to ensure the rock mass is broken at the designed perimeter, interchangement of block values further towards the center of the blast likely has a little significant impact on overall blast performance. Since the current setup nonetheless regards this as deterioration of the objective, the true improvements to the explosive energy distribution may be larger than calculated.

Despite the possibility of adjusting the bottom coordinates of the explosive columns within the developed optimization program, all optimization results have been obtained with this option turned off. The reasoning behind this is that the obtained improvements are too insignificant to warrant the additional practicality issues. Although the improvements from adjustments to the top of the explosive column are not very large either, they can most likely be achieved with relatively little effort because the procedure of explosives loading is not really altered except for the required quantity to be loaded. Adjustment of the bottom of the explosive column, however, requires the insertion of stemming material or some kind of plug into the drillholes before loading of explosives can commence. This would mean a significant change to the overall blasting cycle at the expense of additional time and costs, which is unlikely to be worthwhile given the small benefits for the blast as a whole. Moreover, it would likely increase the duration of optimization by at least one third due to the additional options that are considered. Nevertheless, alteration of explosive columns' bottom coordinate might aid in creating more even benches by compensating for the observed variation in drillhole depth.

The explosives quantity constraint was implemented in addition to the EED cap to suppress any remaining charge adjustment biases. Although it could be argued that a small variation in the used amount of explosives compared to the original blast design could be beneficial to the blast performance, a decision was made to focus on the most effective use of the explosives quantity as originally designed for the blast. After all, moving away from this exact quantity would influence the blast's overall powder factor. This figure has been carefully determined during blast design to fit the requirements for appropriate fragmentation, and is typically not altered. This means that some optimality of the obtained solution is discarded in favor of real-life decision-making. One might find better solutions using a dynamic $c_{allowance}$.

On the topic of optimality, the significance of the chosen EED cap percentile should not be underestimated either. As demonstrated in the results, choosing different values for this control parameter, which's use is a direct consequence of the block-to-block comparison approach, produces vastly different charge adjustment solutions. While the selection of the appropriate percentile of data considered for optimization was governed by its solution's resemblance of the planned explosives quantity to reduce any biases in charge adjustment, it is difficult to tell whether it results in truly optimal solutions. An affirmative argument to this question is the consistency that is found in optimization results of the Nevada 1 and Nevada 2 datasets, with both fabricated drillhole deviations of different magnitude as well as actual ones. In all of these investigated cases, the behavior of optimization was more or less as expected, meaning the 50% percentile EED cap did not result in excessive changes to the explosives quantity used in the obtained solutions. It should be noted, though, that the exact EED cap value might be influenced by block size; smaller block sizes lead to higher mean EED values, which could have an effect on the portion that lies within the lower 50% percentile. This is just one example of the complexities that arise due to the interconnection of various control parameters.

Although tests performed on the 5 by 5 blast pattern provided helpful insight into these relationships, not all of it translates well to full-scale problems where different aspects are introduced and excessive computation times impair the ability to test extensively. One of the most important factors for the high computational requirements is the block size. Because analysis in the results section has shown that a block size of 0.2 m is the smallest of the selected options to discretize the explosive energy distribution well enough for the desired accuracy of the chosen optimization objective, the reliability of the results would be greatly reduced by switching to a larger block size to improve computation times. Since suitability of the block sizes was assessed specifically using its effect on the objective value, other applications of an EED block model may require different block sizes.

Another major component is the search radius around blastholes. While the magnitude of EED values encountered at a distance of 5.0 m away from a blasthole was found to be less than 1% of those at 0.5 m, which might leave room for a decrease of the search radius in favor of lower computation times, results of the Nevada 1 and Nevada 2 datasets have brought another issue to light; the suitability of the 5.0 m search radius was determined at the depths of blastholes corresponding to the maximum EED output in the horizontal direction, whereas the relationship between the respective values at depths above the explosive column seems to be much less optimistic. This is particularly problematic due to the focus on this upper part of the blast as a result of capping high EED values in the core of the blast. Hence, re-evaluation of the appropriate search radius at various depths would be advisable for increased confidence in the results.

Similar to the EED cap, the selected charge segment length of 0.3 m plays an important role in reducing any biases in charge adjustments before application of the explosives quantity constraint, simply because it raises the threshold of required EED differences to make the adjustments beneficial. However, the reduction of this sensitivity compared to a charge segment length of 0.1 m is once again a trade-off with a degree of optimality; the current setup will always result in a slightly worse objective value than can be achieved with a smaller charge segment length. Another decisive consideration in this is the practicality of the chosen charge segment length. While the accuracy of 0.1 m could be challenging to achieve during explosives loading, 0.3 m should be a lot easier to differentiate for operators. It is especially convenient that this height is roughly equivalent to 1 foot, the preferred measurement unit in the United States.

In most Tabu Search optimization tests on the 5 by 5 test pattern, it was found that the effect of the tabu tenure on the final solution was limited. Although a few exceptions were encountered, generally the same solution was eventually obtained with a number of different choices for this optimization variable. The greatest difference is that Tabu Search with a larger tabu tenure searches further away from local optima, but in doing so simply takes longer to reach the stopping criterion and accept a solution as optimal. In most cases, no better solutions are found after reaching the initial optimum, and if so, it is usually found within a couple of iterations. Although the tabu tenure can still affect optimization in earlier stages and thus remains useful, it now appears redundant to continue searching for other optima until a loop in objective values is detected. Therefore, the stopping criterion could be adjusted to further reduce the duration of Tabu Search optimization. Still, the overall computation time of multiple hours remains an inconvenience. The retrieved optimization paths indicate that the tabu mechanism would provide some advantage over a simpler hill-climbing algorithm, but the benefits to the objective value are likely not staggering. Although its effect before reaching the initial optimum might be underestimated, individual charge adjustments performed during optimization seem less interconnected than expected.

Performance of the Genetic Algorithm has turned out to be inferior to Tabu Search in all cases. Due to its more randomized, global approach, EED values throughout the block model must be recalculated many times while resulting in only small improvements to the objective value. It has not been able to come up with better solutions than the Tabu Search competitor and takes many times the duration to achieve the same result. The only effect of changing its control parameters is on the optimization time. If the stopping criterion of 20 generations without improvement is disregarded, random mutation ensures that the optimal solution will eventually always be reached. To improve performance, a dynamic mutation probability could be helpful. Computation times might be further reduced by implementing the same ‘EED copy-paste’ method used by Tabu Search to calculate the effect of charge adjustments individually instead of recalculation of the entire block model, but the straightforward application of Tabu Search would still be much faster. The idea that the Genetic Algorithm can make many adjustments in one generation does not function efficiently enough to compensate for its excessive computation time, even as a kick-start in a hypothetical hybrid solution.

A striking observation that can be made in the solutions of both the Nevada 1 and Nevada 2 dataset, is that the majority of the charge adjustments are made in drillholes located at the boundary of the blast pattern. For the Nevada 2 dataset, this can be partly explained by the fact that most of the strongly deviated drillholes are simply positioned in these areas. However, this does not hold true for the random deviations applied to the Nevada 1 drillholes. This phenomenon may be related to the lower EED values that are encountered at the boundaries of the blast pattern that could, in addition to the reduced influence of nearby blastholes, make charge adjustments more effective. Moreover, when these drillholes have deviated outward, part of the EED values within their search radius could be shifted towards blocks that do not contain any values in the planned configuration, which are therefore ignored. This reduces the detrimental effect of charge adjustments at the outer boundary of the blast pattern, while the benefits are still obtained at the 'inner side' of the blasthole. When a hole in the middle of the pattern has deviated, it is surrounded on all sides by EED contributions from neighboring holes, and this situation does not apply.

From cross-sections of the various EED block models, it is clear that most improvements of the objective value are due to the reduction of EED differences in the upper part of the blast. Naturally, this occurs in the areas that are relatively close to the adjusted explosive charges. Although the EED calculation is based on the entire length of the explosive columns for all discretization points, the effect of adjustments to its top coordinate is much more apparent in blocks near this point compared to the ones at the bottom of the blast. Because the largest benefits are evidently obtained in the upper section (when only the top coordinates of explosive columns are adjusted), computational requirements could be reduced by evaluating just this portion of the block model instead of the complete vertical range, thereby focussing on the significant data only. More investigation is needed to determine at what depth the effect of charge adjustments loses its relevance, which of course depends on the magnitude of the adjustments made. Nevada 1 and Nevada 2 solutions contain only a single blasthole that has the height of its explosive column adjusted by more than one charge segment length of 0.3 m. Thus, the constraint that limits the maximum charge adjustment to half the stemming height is rarely applicable, which can mostly be attributed to the selected EED cap percentile of 50%. Nevertheless, these charge increases still cause the quantity of explosives in a single blasthole to exceed the original design specifications, while reducing the stemming height. The safety implications of the resulting increase in explosive energy in some of the most shallow parts of the blast should be carefully assessed, with special attention to the risk of flyrock. Because of its dependence on blast design and rock mass characteristics, this will differ on a case-by-case basis.

In addition to improvements of the EED differences, the charge adjustments also cause a fair portion of new differences in the blocks nearby. While the surrounding area as a whole evidently benefits from the alteration, the amount of energy that some blocks close to the explosive column receive can change dramatically due to these adjustments. Another approach to compensate for an altered explosive energy distribution might be to allow variation in the explosive density instead of the height of the explosive column. This would translate to the use of a selection of different explosives types if this option is available at the mine site. Instead of mainly influencing the area surrounding charge height adjustments, this could improve the EED along the entire length of the blasthole. An added benefit is that the impact of such adjustments on the most shallow part of the blast are likely smaller than alterations of the explosive column and stemming height, and thereby have a lesser effect on flyrock.

Like mentioned before, some of the encountered issues in this project can be ascribed to the approach of minimizing the block-to-block differences in EED. Although the application of the EED cap appears an acceptable way of mitigating these and facilitates optimization towards good, sensible results, it limits the confidence in whether the obtained solutions are in fact truly optimal. It seems like the EED cap can only be avoided by changing the optimization objective to a broader method than the block-to-block comparison. An alternative approach could be to divide the blast pattern into regions spanning a number of blastholes, assigning mean EED values to each of them based on the individual block values that it contains. If these regions can be chosen such that there are no high EED areas displaced across their borders due to drillhole deviation, the regions' EED values should only change slightly, providing manageable differences. The clear challenge in this is to find a suitable configuration that includes each block within a region for which the mean EED does not change too dramatically due to inclusion or exclusion of high EED zones as a result of drillhole deviation. While this method does take away some level of detail compared to the block-to-block comparison, it would no longer treat the interchangement of EED values between blocks (within a region) as detrimental to the objective.

The charge adjustment solutions of Nevada 1 and Nevada 2 have demonstrated that optimization of the explosive charges in a blast pattern can not simply be based on the magnitude of drillhole deviation alone. While some of the recommended charge adjustments are clearly found in strongly deviated holes, it is certainly not a requirement; the deviation of one drillhole does not always need to be particularly large to warrant adjustment of its explosive column height. The results show there can be a strong interaction between multiple less deviated, neighboring drillholes, which can cause equally significant EED differences. Although it could definitely be helpful to first consider potential adjustments in an area surrounding very deviated holes instead of the straightforward method of calculating the effect of all possible adjustments in the pattern, as in the current Tabu Search algorithm, the lesser deviated drillholes should not be ignored.

The actual drillhole locations included in the Nevada 2 dataset have provided a useful sample of real drillhole deviations, but an important component is still missing; the coordinates are retrieved from the GPS receiver on the drill rig, which means that errors in GPS positioning could still have an effect on the exact location of the drillholes. In addition to this, insufficient GPS coverage may be the reason for a 'gap' in the reported drillhole locations in the Nevada 2 pattern. To prevent these kinds of situations and register the actual drillhole deviations with higher accuracy, the optimization system should be combined with research done by [5] on the use of Unmanned Aerial Vehicles and photogrammetry for this purpose.

Due to the particular requirements for blasting in Nevada and its differences in blast design compared to many other places in the world, the developed optimization program might not be applicable elsewhere, or could require adjustment of the control parameters. One should also remember that, while some may be useful, all models are wrong and remain a simplification of reality. Because of the inability to accurately measure explosive energy in mining blasts and its poorly understood relationship with blast performance, it is difficult to verify the real-life value of the optimization program without collecting a large amount of fragmentation data and attempt to distinguish its effect from rock mass variability, which is already a challenging task for the purpose of original blast design, let alone slight alterations in a number of blastholes.

7

Conclusion

Although deviations in the location of rock blasting drillholes are a common occurrence in surface mining operations, little action is taken to reduce its adverse effects on blast performance. Recent technological advancements have greatly reduced its magnitude, but this thesis has demonstrated that the remaining inaccuracies relative to planned drillhole design can still have a pronounced effect on the explosive energy distribution throughout a blast, as drillholes are moved closer together or further apart.

The most important sources for external drillhole deviation found in literature consist of human error and GPS accuracy, which are influenced by operator experience, drill site topography, equipment state, tropospheric delay, satellite availability, and multipath. By altering the explosive energy distribution, it affects fragmentation and may require additional blasting or secondary breakage, causing production delays and increased costs. Excess boulders lower the efficiency of all subsequent operations, and control on ore loss and dilution can be reduced. Because it changes how the rock mass is broken, it can also lead to slope instability, uneven benches, and increased risk of flyrock.

Through development of an explosive energy distribution optimization system it has been demonstrated that the alteration of explosive energy due to drillhole deviation can be mitigated by adjusting the length of explosive charges. Optimization of full-scale case study blast patterns using the developed program provides small improvements of 0.53-1.54%, or 2.14-3.94% if the portion outside the influence of recommended charge adjustments is omitted. The applied methodology produces consistent results for two blast patterns with varying design characteristics, using both random and actual drillhole deviations.

This research has also reasonably satisfied some of the other objectives set; by keeping the amount of used explosives constant in the obtained solutions, the developed program theoretically leads to more effective use of the explosive substances. Adjustment of the height of explosive columns appears practically achievable within standard drilling and blasting procedures; the number of changes to the original blasting plan is limited, and the designed minimum adjustment length of 0.3 m (or roughly 1 foot) should be sufficiently differentiable for operators. The required computation time is a potential issue; although the Tabu Search algorithm reaches an optimal solution much quicker than the Genetic Algorithm approach, its runtime of multiple hours remains an inconvenience.

For further advancement on this topic, the following recommendations are made:

- Alternative methods to the block-to-block comparison of EED values should be examined as optimization objective for a more fitting representation of the improvements to the explosive energy distribution.
- Computation times could be further reduced by, for example, evaluating only the upper part of the blast, easing the Tabu Search stopping criterion, or first considering adjustments in drillholes near the most deviated ones only.
- This work should be combined with the research done by [5] to include any GPS-related inaccuracies in actual drillhole locations.
- Assessment of the safety implications of increasing the height of explosive columns at the expense of stemming, in particular the risk of flyrock, is essential before real-life applications can be considered.
- General knowledge on the behavior of explosive energy in surface mining blasts should be improved for a better understanding of its effect on fragmentation, to allow verification of the real benefits of adjusting charges to account for deviated drillholes.

Bibliography

[1] C.J. Konya and E.J. Walter. *Surface Blast Design*. Prentice Hall, 1990.

[2] G. Hollister-Short. “The use of gunpowder in Mining: A Document of 1627”. In: *History of Technology: Volume 8* (1983). Ed. by N. Smith, pp. 111–116.

[3] D. Gleeson. “Beyond blasting”. In: *International Mining* (Aug. 2019), pp. 32–42.

[4] W. A. Hustrulid. *Blasting principles for open pit mining (Volume 1)*. A.A. Balkema, 1999.

[5] J. Valencia et al. *Enhancement of explosive energy distribution using UAVs and machine learning*. 2019.

[6] R.L. Ash. “The mechanics of rock breakage (part 2) - Standards for blasting design”. In: *Pit Quarry* 56 (3 1963), pp. 118–122.

[7] W.C. Burkle. “Geology and its effect on blasting”. In: *Proceedings of the Annual Conference on Explosives and Blasting Technique* (Feb. 1979), pp. 105–120.

[8] AECI Explosive and Chemicals Limited. “Blasthole drilling and initiation patterns in surface blasting.” In: *Explosives Today* 2 (12 June 1978).

[9] I.R. Firth and P. Mousset-Jones. “Drilling and blasting practices in Nevada’s openpit mines”. In: *Mining Engineering* 55 (2003), pp. 33–38.

[10] P. Darling. *SME Mining Engineering Handbook*. Ed. by Peter Darling. 3rd ed. Society for Mining, Metallurgy, and Exploration (U.S.), 2011.

[11] T.N. Hagan. “Initiation sequence: Vital element of open pit blast design. Design Methods in Rock Mechanics.” In: *Proceedings of the 16th US Symposium on Rock Mechanics* (1975), pp. 345–355.

[12] T.N. Hagan. “The effects of blast geometry and initiation sequence on blasting results”. In: *Australian Mineral Foundation’s ’Drilling and Blasting Technology’ Course* (May 1977), p. 55.

[13] T.N. Hagan. “The influence of controllable blast parameters on fragmentation and mining costs”. In: *Proceedings of the 1st International Symposium on Rock Fragmentation by Blasting* (1983), pp. 31–52.

[14] T.N. Hagan and J.K. Mercer. *Safe and Efficient Blasting in Open Pit Mines*. Nov. 1983.

[15] W.A. Crosby and M.E. Pinco. “When to use aluminium in bulk explosives”. In: *Journal of Explosives Engineers* 9 (2 1989), pp. 30–34.

[16] W.A. Crosby and M.E. Pinco. “Review of the use of aluminium in bulk explosives for the mining industry”. In: *Engineering Mining Journal* 7 (3 1989), pp. 34–37.

[17] J.M. Wilson and N.T. Moxon. “The development of a low shock energy ammonium nitrate based explosive”. In: *Proceedings of the Explosives in Mining Workshop, AusIMM* (Nov. 1988), pp. 27–31.

[18] R.A. Dick. *The Impact of Blasting Agents and Slurries on Explosives Technology*. USBM IC 8560, 1972, p. 44.

[19] W.B. Sudweeks. “Physical and chemical proprties of eindustrial slurry explosives”. In: *Industrial Engineering Chemistry Product Research and Development* 124 (3 1985), pp. 432–436.

[20] W.B. Evans and D.P. Taylor. “Blended ANFO-based explosives”. In: *CIM Bulletin* 80 (905 1987), pp. 60–64.

[21] A. Konya and C.J. Konya. *Blasting mechanics: Material properties and powder factor*. Apr. 2019.

[22] U.S. Department of the Interior: Bureau of Reclamation. “Blast Design”. In: *Engineering Geology Field Manual Volume II* (2001), pp. 209–298.

[23] Dyno Nobel. *Surface Mining Products, Services and Reference Guide*. 2016.

[24] H.S. Marshall et al. “GPS Applications at Optimum Colliery”. In: *The Journal of The South African Institute of Mining and Metallurgy* 98 (3 1998), pp. 127–134.

[25] A. Y. Obregón. “GPS Drill Navigation and Data Collection in a Mining Environment”. In: *Proceedings of the 13th International Technical Meeting of the Satellite Division of The Institute of Navigation (ION GPS 2000)* (2000), pp. 1002–1006.

[26] U.S. Office of Surface Mining Reclamation and Enforcement. “Blasthole Drilling”. In: *Blaster’s Training Modules* (n.d.).

[27] M. B. Revuelta. *Mineral Resources: From Exploration to Sustainability Assessment*. Springer International Publishing, 2017.

[28] J. B. Segui and M. Higgins. “Blast design using measurement while drilling parameters”. In: *Fragblast* 6 (3-4 Sept. 2002), pp. 287–299.

[29] Australian Explosives Industry and Safety Group. *On-Bench Practices for Open Cut Mines and Quarries*. 2015.

[30] U.S. Office of Surface Mining Reclamation and Enforcement. “Blasthole Loading”. In: *Blaster’s Training Modules* (n.d.).

[31] A. Almgren and K. Klippmark. “Aspects of hole deviation in sublevel stoping”. In: *Proceedings of design and operation of caving and sublevel stoping mines, AIME* (1981), pp. 559–573.

[32] S.P. Singh, M. Ladouceur, and F. Rouhi. “Sources, implications, and control of blasthole deviation.” In: *Mine Planning and Equipment Selection* (1998), pp. 391–398.

[33] B. Adebayo and J. M. Akande. *Effects of blast hole deviation on drilling and muck-pile loading costs*. 2015, pp. 64–73.

[34] T. Pirinen et al. “Automatic Positioning and Alignment for Hole Navigation in Surface Drilling”. In: *The 31st International Symposium on Automation and Robotics in Construction and Mining (ISARC 2014)* (2014), pp. 88–94.

[35] A.M. Neale. “Blast optimization at Kriel Colliery”. In: *The Journal of The Southern African Institute of Mining and Metallurgy* 110 (2010), pp. 161–168.

[36] Caterpillar. *Specalog for Cat Terrain for Drilling AEHQ6176-03*. 2013.

[37] Caterpillar. *The Journey to Autonomous Drilling*. 2016.

[38] Caterpillar. *Automating Drills for Site-wide Benefits*. Caterpillar’s newest drill rig can be programmed to drill single rows autonomously with a high level of accuracy. 2020. URL: https://www.cat.com/en_US/articles/customer-stories/mining/viewpoint/autonomous-drilling-delivers-benefits.html.

[39] Rio Tinto. *Rio Tinto to almost double its autonomous drilling fleet in a drive to further improve safety and productivity*. 2018. URL: https://www.riotinto.com/en/news/releases/Autonomous-drilling-fleet-almost-doubled.

[40] Mining Technology. *Mining robots: Rio Tinto doubles down on autonomous drilling*. 2018. URL: https://www.mining-technology.com/features/mining-robots-rio-tinto-doubles-autonomous-drilling/.

[41] D. Kim et al. “Local deformation monitoring using GPS in an open pit mine: initial study”. In: *GPS Solutions* 7 (3 Dec. 2003), pp. 176–185.

[42] Modular Mining Systems. *Modular Introduces Next Generation High-Precision GNSS Positioning Technology for Increased Constellation Access and Availability - Modular Mining*. 2018.

[43] Applanix. *GNSS for Autonomous Haulage Systems (AHS) in Deep Open Pit Mines*. 2020. URL: https://www.applanix.com/news/blog-gnss-for-autonomous-haulage-systems-ahs-in-deep-open-pit-mines/.

[44] J. M. Stone et al. “GPS Pseudolite Transceivers and their Applications”. In: *Proceedings of the ION National Technical Meeting* (1999).

[45] Z.-Y. Shan, H.-Z. Han, and K. Jiang. “Optimization model of GNSS/pseudolites structure design for open-pit mine positioning”. In: *Transactions of Nonferrous Metals Society of China* 23 (2013), pp. 2201–2208.

[46] Y. Chen and X. He. “Contribution of Pseudolite Observations to GPS Precise Surveys”. In: *KSCE Journal of Civil Engineering* 12 (1 2008), pp. 31–36.

[47] B. Adebayo and B. Mutandwa. “Correlation of Blast-hole Deviation and Area of Block with Fragment Size and Fragmentation Cost”. In: *International Research Journal of Engineering and Technology* 2 (2015), pp. 402–406.

[48] R. C. Okeke. “Blasting and Mining”. In: *Explosives Engineering* (March/April 2015), pp. 8–13.

[49] T. Kleine, P. Townson, and K. Riihioja. “Assessment and computer automated blast design”. In: *Proceedings of the 24th International Symposium on the Application of Computers and Operations Research in the Mineral Industries* (1993), pp. 353–360.

[50] B. Lusk and J.J. Silva. “Energy distribution in the blast fragmentation process”. In: *Green Energy and Technology* (2018), pp. 11–30.

[51] A.T. Spathis. “On the Energy Efficiency of Blasting”. In: *Proceedings of the 6th international symposium on rock fragmentation by blasting* (1999), pp. 81–90.

[52] J. A. Sanchidrián, P. Segarra, and L. M. López. “Energy components in rock blasting”. In: *International Journal of Rock Mechanics and Mining Sciences* 44 (Jan. 2007), pp. 130–147.

[53] F. Ouchterlony, U. Nyberg, and M. Olsson. “The energy balance of production blasts at Norkalk’s Klinthagen quarry”. In: *Proceedings of the second world conference on explosives and blasting, Prague, 10-12 september* (2003). Ed. by R. Holmberg, pp. 193–203.

[54] Z.-X. Zhang. *Rock Fracture and Blasting; Theory and Applications*. Butterworth-Heinemann, 2016.

[55] W. A. Hustrulid. *Blasting principles for open pit mining (Volume 2)*. A.A. Balkema, 1999.

[56] R. Holmberg and P.-A. Persson. “The Swedish approach to contour blasting”. In: *Proceedings of the 4th Conference on Explosives and Blasting Technique* (1978), pp. 113–127.

[57] W.A Hustrulid et al. “A new method for predicting the extent of blast damage zone”. In: *Proceedings of Blasting Conference* (1992), paper no. 3.

[58] J.P. Savely. “Designing a final blast to improve stability”. In: *Proceedings of the SME Annual Meeting* (1986), pp. 80–86.

[59] K. Hino. *Fragmentation of rock through blasting and shock wave theory of blasting*. Quarterly report of the Colorado School of Mines, 1956.

[60] JKTech. *Blast simulation evaluation and management User Manual*. 1998.

[61] C. Blum and A. Roli. “Metaheuristics in Combinatorial Optimization: Overview and Conceptual Comparison”. In: *ACM Computing Surveys* 35 (3 Sept. 2003), pp. 268–308.

[62] C. García-Martínez, F. J. Rodriguez, and M. Lozano. “Genetic algorithms”. In: *Handbook of Heuristics* 1-2 (2018). Ed. by R. Martí, P. M. Pardalos, and M. G. C. Resende, pp. 431–464.

[63] M. Laguna. “Tabu Search”. In: *Handbook of Heuristics* (2018). Ed. by R. Martí, P. M. Pardalos, and M. G. C. Resende, pp. 742–758.

[64] Nevada Division of Minerals. *Total Mineral Production by Commodity 2019*. 2020.

[65] Nevada Division of Minerals. *Metallic Production by Producer 2019*. 2020.

[66] USGS National Minerals Information Center. *Mineral Commodity Summary Gold 2019*. 2020.

[67] D. Michaud. *Carlin Type Gold Deposit*. 2015. URL: `https://www.911metallurgist.com/blog/carlin-type-gold-deposit`.

[68] G.E.P. Box. “Science and statistics”. In: *Journal of the American Statistical Association* 71 (356 1976), pp. 791–799.

A

Effect of Block Size on Improvements with Different Charge Segment Lengths

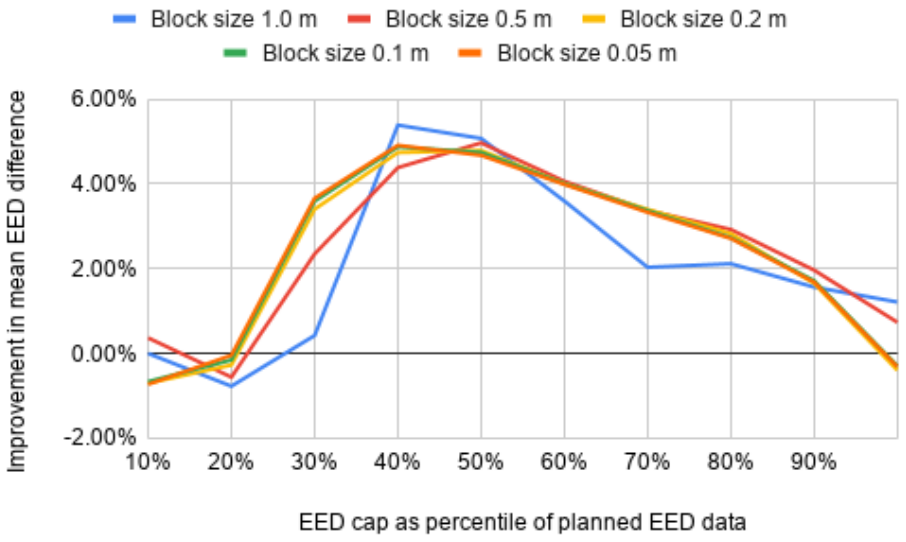

Figure A.1: Comparison of improvement in EED difference for different block sizes, for manual adjustments to the explosivecolumn by charge segment length 0.1 m.

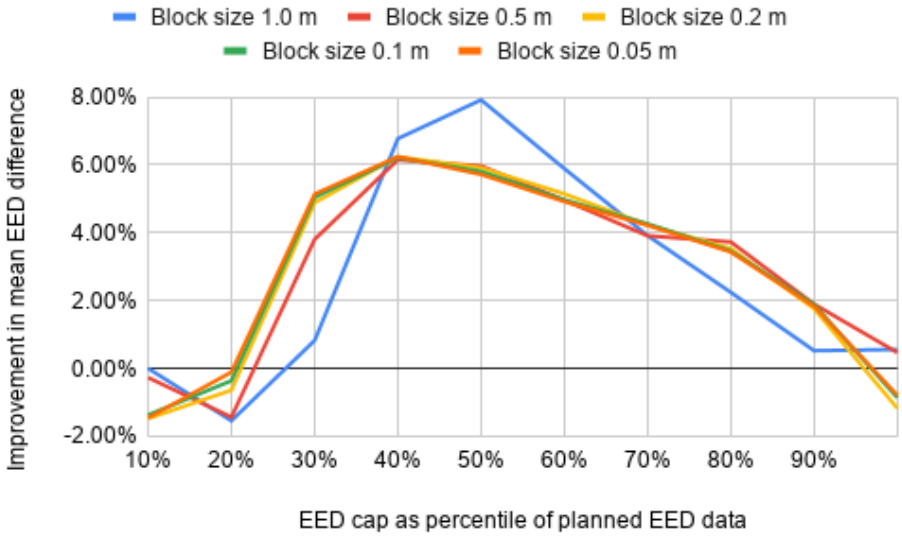

Figure A.2: Comparison of improvement in EED difference for different block sizes, for manual adjustments to the explosivecolumn by charge segment length 0.2 m.

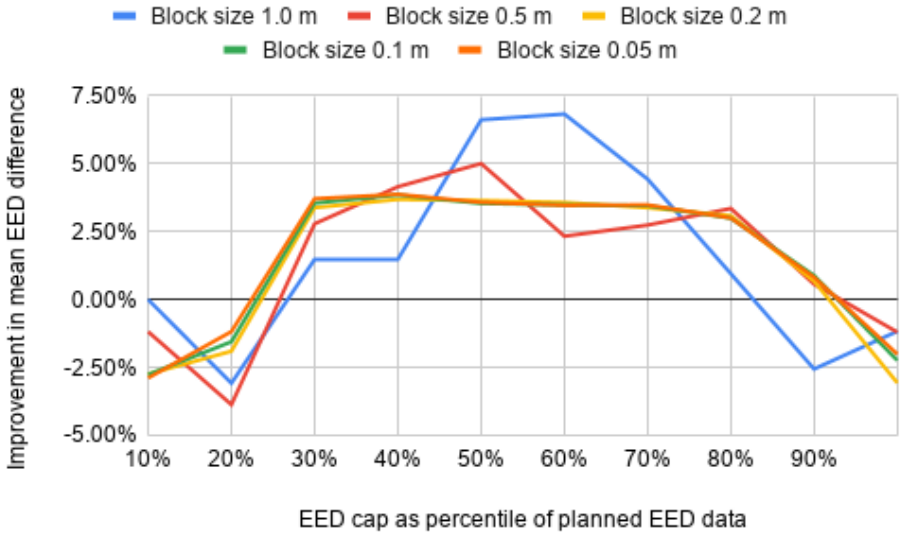

Figure A.3: Comparison of improvement in EED difference for different block sizes, for manual adjustments to the explosivecolumn by charge segment length 0.4 m.

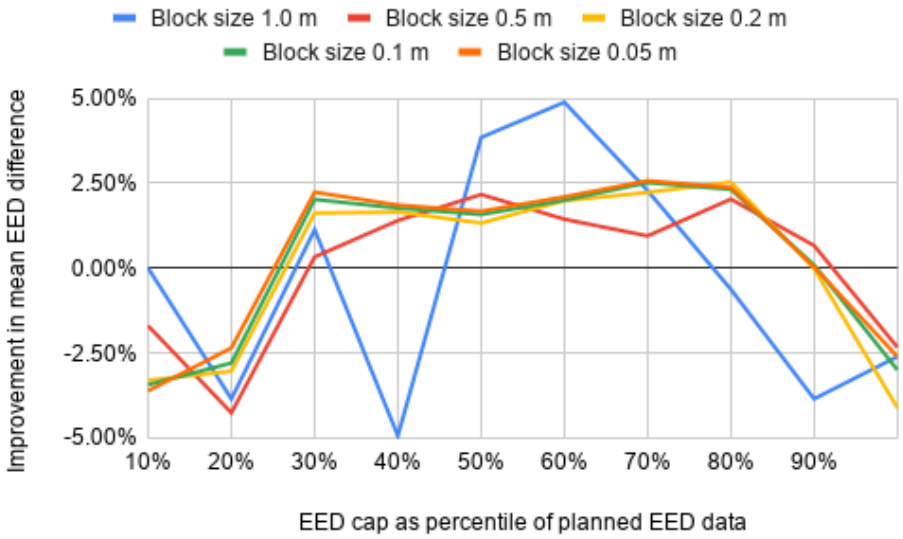

Figure A.4: Comparison of improvement in EED difference for different block sizes, for manual adjustments to the explosivecolumn by charge segment length 0.5 m.

B

Improvements of Expected Adjustments with Different Charge Segment Lengths

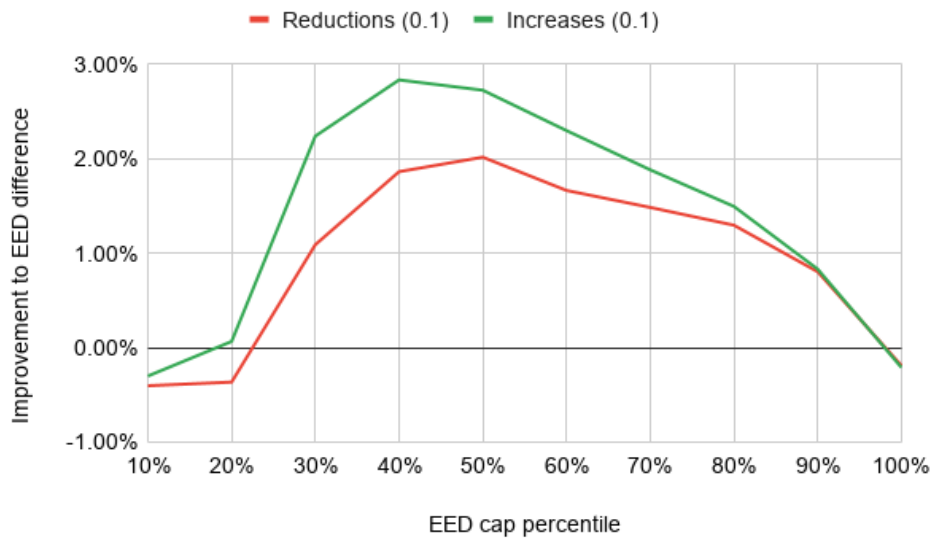

Figure B.1: Comparison of improvements from expected charge reductions and increases by charge segment length 0.1 m.

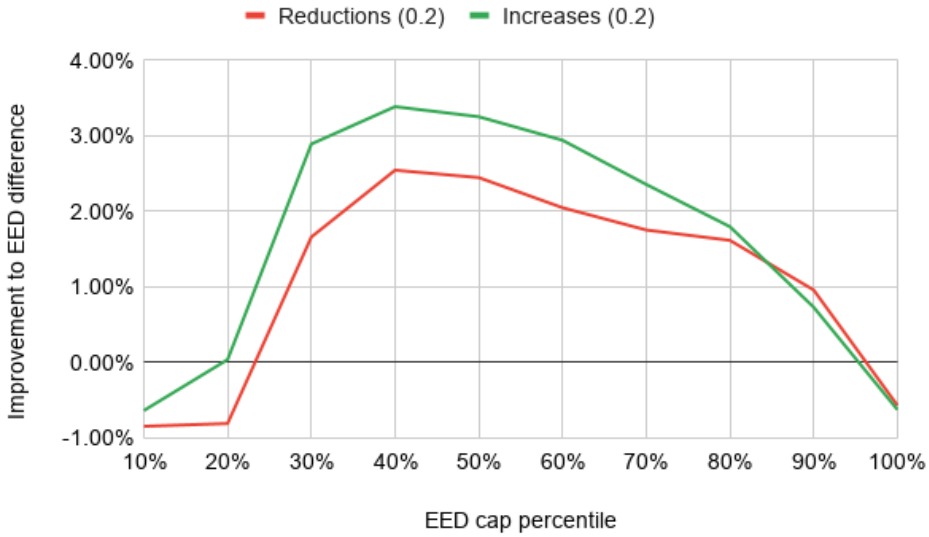

Figure B.2: Comparison of improvements from expected charge reductions and increases by charge segment length 0.2 m.

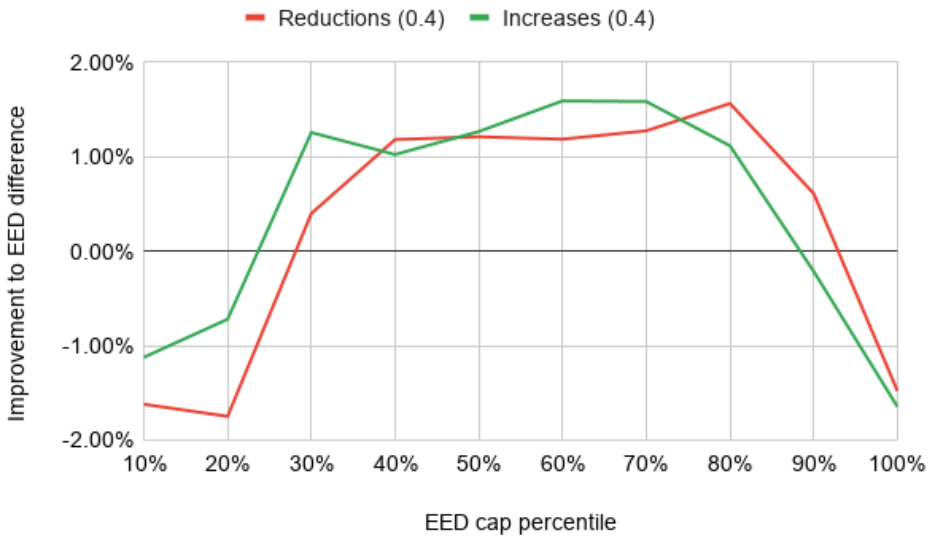

Figure B.3: Comparison of improvements from expected charge reductions and increases by charge segment length 0.4 m.

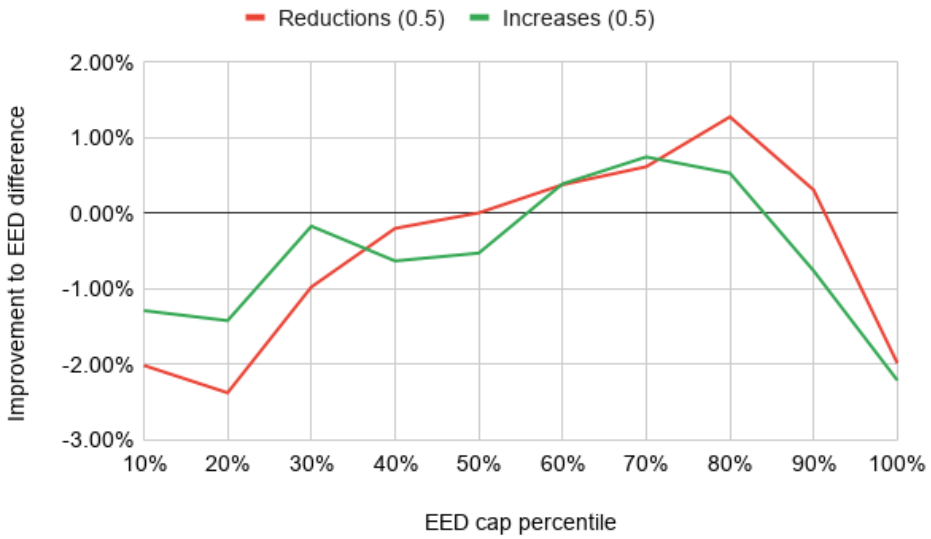

Figure B.4: Comparison of improvements from expected charge reductions and increases by charge segment length 0.5 m.

C

5 by 5 Test Pattern Solutions with Different Charge Segment Lengths

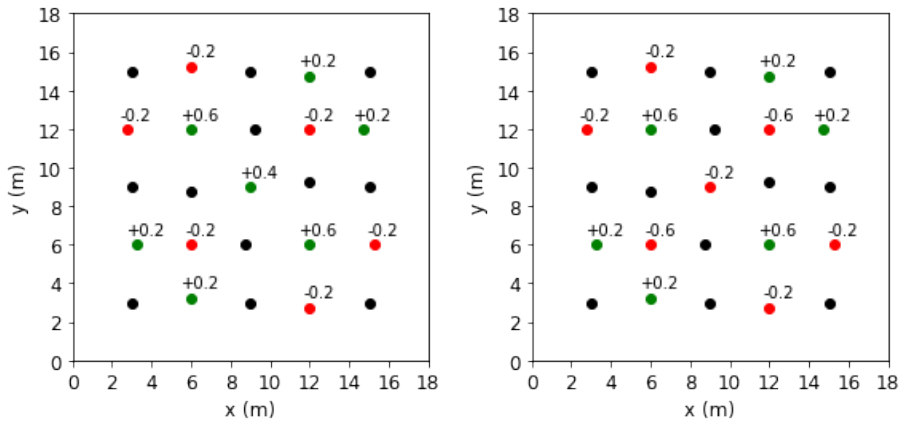

(a) Solution for 10% percentile.

(b) Solution for 20% percentile.

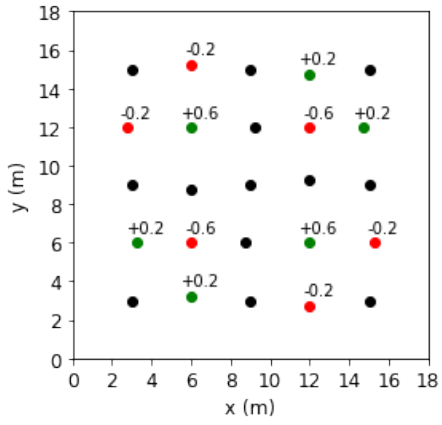

(c) Solution for 30% percentile.

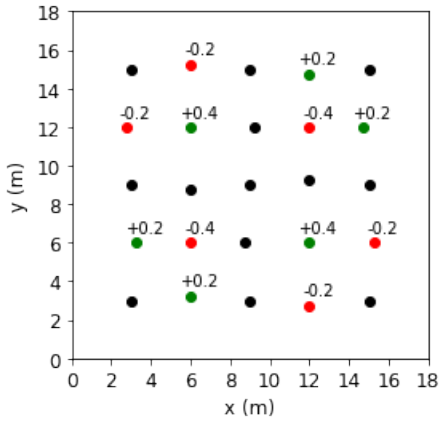

(d) Solution for 40% percentile.

Figure C.1: Charging adjustment solutions obtained using charge segment length 0.2 m, for 10-40% percentiles.

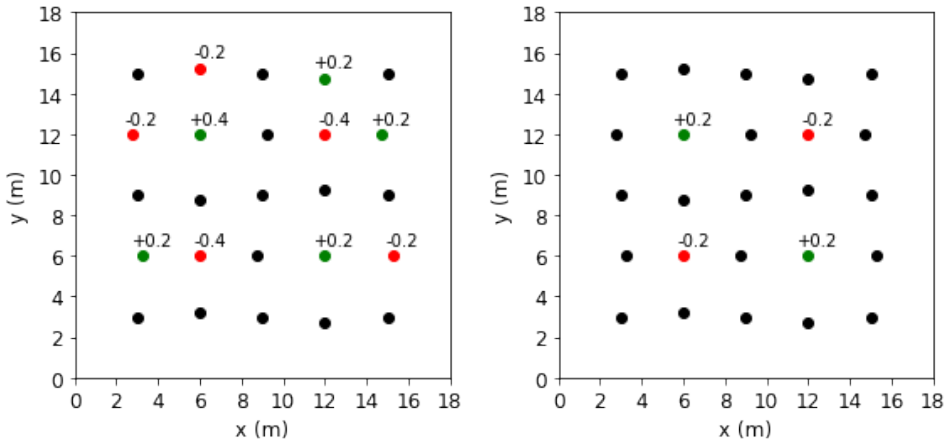

(a) Solution for 50% percentile.

(b) Solution for 60-90% percentile.

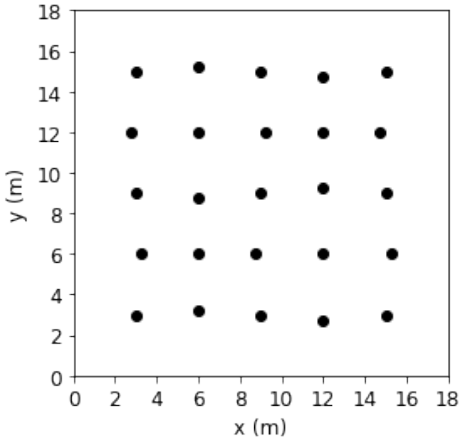

(c) Solution for 100% percentile.

Figure C.2: Charging adjustment solutions obtained using charge segment length 0.2 m, for 50-100% percentiles.

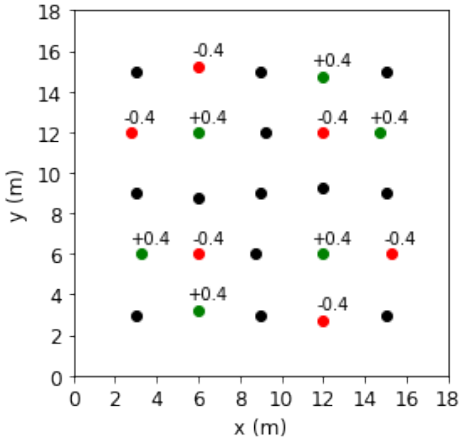

(a) Solution for 10% percentile.

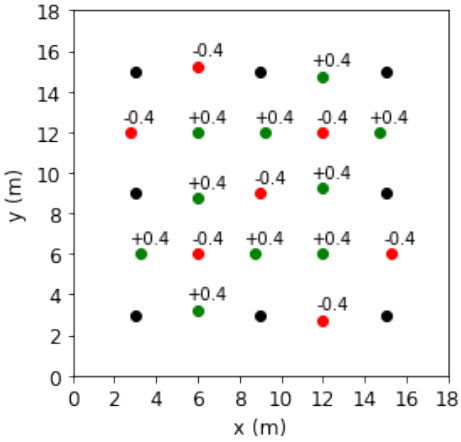

(b) Solution for 20% percentile.

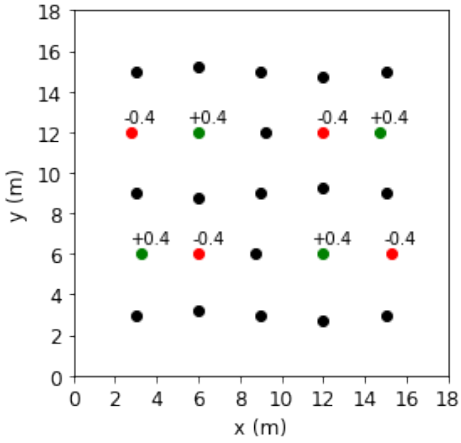

(c) Solution for 30% percentile.

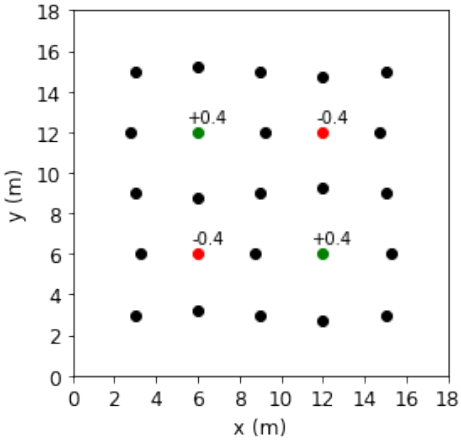

(d) Solution for 40-90% percentile.

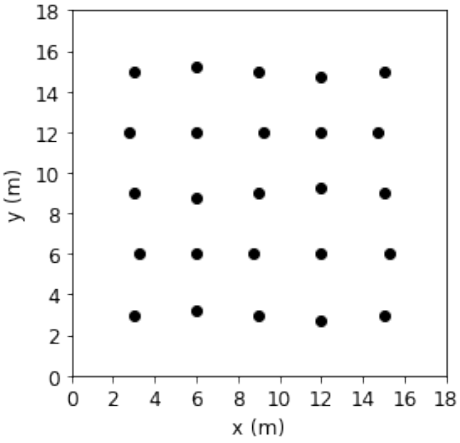

(e) Solution for 100% percentile.

Figure C.3: Charging adjustment solutions obtained using charge segment length 0.4 m, for all percentiles.

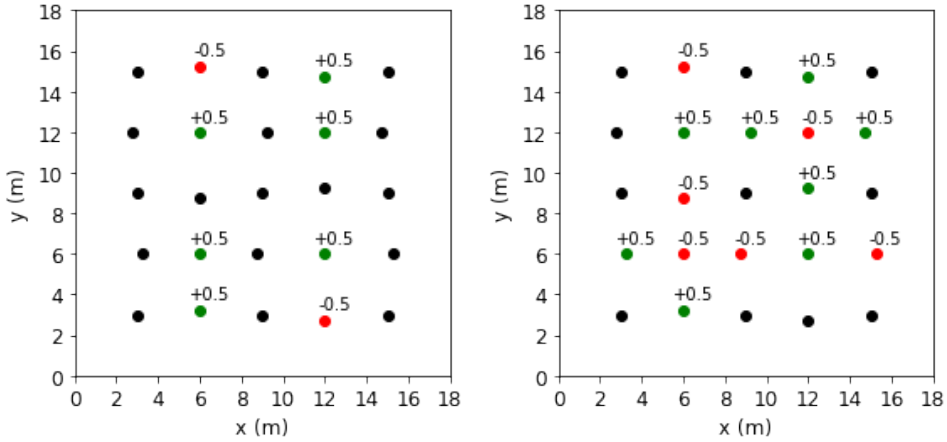

(a) Solution for 10% percentile.

(b) Solution for 20% percentile.

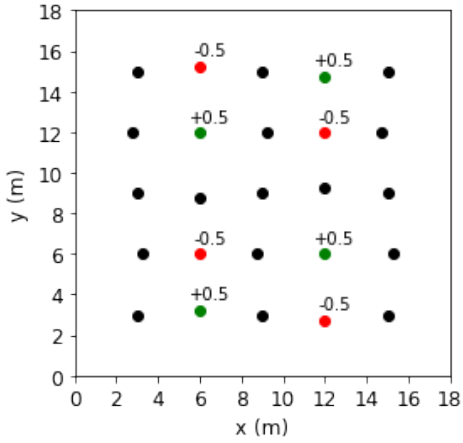

(c) Solution for 30% percentile.

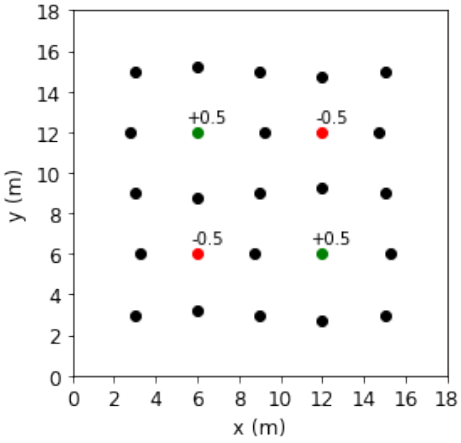

(d) Solution for 40-80% percentile.

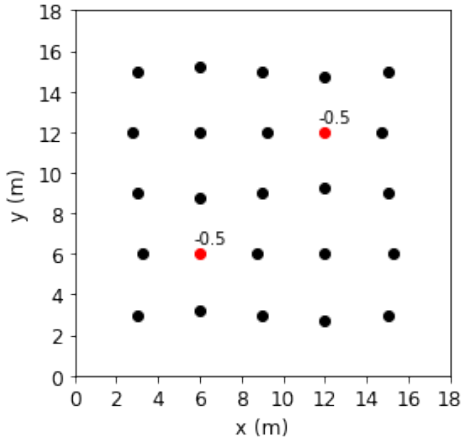

(e) Solution for 90% percentile.

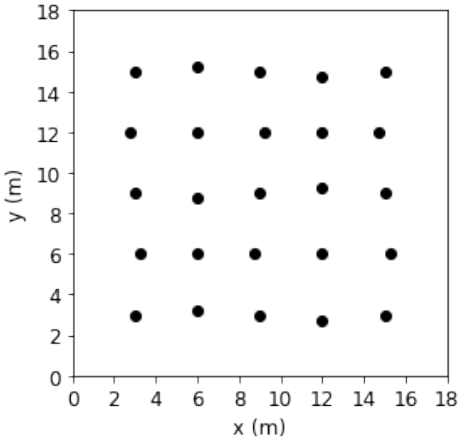

(f) Solution for 100% percentile.

Figure C.4: Charging adjustment solutions obtained using charge segment length 0.5 m, for all percentiles.